

**DISCOVERY OF A SELECTIVE BINDER OF PROTEASOMAL SUBUNIT  
RPN-6 AND ITS EFFECT ON PROTEASOME ACTIVITY**

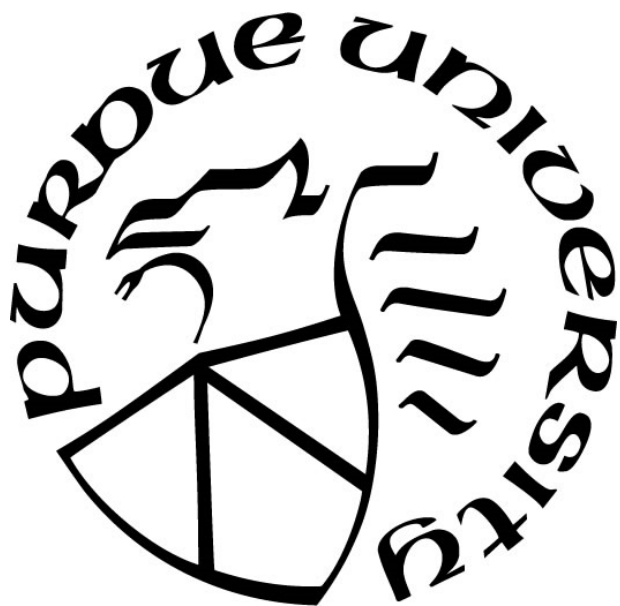
by  
**Wenzhi Tian**

**A Dissertation**

*Submitted to the Faculty of Purdue University*

*In Partial Fulfillment of the Requirements for the degree of*

**Doctor of Philosophy**



Department of Medicinal Chemistry and Molecular Pharmacology

West Lafayette, Indiana

August 2021

**THE PURDUE UNIVERSITY GRADUATE SCHOOL**  
**STATEMENT OF COMMITTEE APPROVAL**

**Dr. Darci J. Trader, Chair**

Department of Medicinal Chemistry and Molecular Pharmacology

**Dr. Daniel P. Flaherty**

Department of Medicinal Chemistry and Molecular Pharmacology

**Dr. Zhong-Yin Zhang**

Department of Medicinal Chemistry and Molecular Pharmacology

**Dr. Herman O. Sintim**

Department of Chemistry

**Approved by:**

Dr. Andy Hudmon

*This work would not have been done without the support from my family. Thank you, my mom, my dad, my uncle, my aunt and my amazing sisters. Your support was my greatest power to pursue for my degree. I am also extremely thankful to my girlfriend, Panyue. Thank you for being with me to push me to the best I can be.*

## **ACKNOWLEDGMENTS**

I would like to thank my advisor, Dr. Darci J. Trader, for her advice, support, suggestions and inspirations during my graduate study. I feel extremely fortunate to have Dr. Trader as my advisor that her passions on science have deeply influenced my decisions for future career and she devoted greatly to support her students to success. I would like to thank Dr. Zhang for his guidance when I was a first-year graduate student. His suggestion helped me to find out my goal for graduate study. I would like to thank Dr. Flaherty for his patient instruction on instrument operation when I was a first-year graduate student. The experimental results from the instrument opened up my next four-year research. I would also like to thank Dr. Sintim for his suggestions and comments during my committee meeting which provide unique views on my research. I also want to greatly thank my lab mates, Christine Muli, Andres Salazar-Chaparro, Saayak Halder, Machenzie Clement, Dr. Rachel Coleman and Dr. Marianne Maresh. I have learned so many from you on both science and life. A special thanks to Dr. Breanna Zerfas, one of the best postdocs I have met, she contributed greatly to everyone's science in lab and she has been a great source of support.

## TABLE OF CONTENTS

LIST OF TABLES.....	12
LIST OF FIGURES .....	13
ABBREVIATIONS .....	21
ABSTRACT.....	22
CHAPTER 1. THE PROTEASOME AND ITS SMALL MOLECULE REGULATORS.....	24
1.1 Overview of the ubiquitin-proteasome system. ....	24
1.1.1 Introduction to the ubiquitin-proteasome system. ....	24
1.1.2 The UPS and the 26S proteasome. ....	25
1.1.3 The 19S and 11S RP.....	26
1.1.4 The 20S CP and 20S iCP. ....	27
1.2 Proteasome affects cell function. ....	29
1.2.1 Tumorigenesis and proteasome. ....	29
1.2.2 Aging, neurodegenerative diseases and failure of the proteasome system.....	30
1.3 Small molecule inhibitors of proteasome. ....	31
1.3.1 Discovery of 20S proteasome inhibitors for cancer treatment. ....	31
1.3.2 Discovery of 19S RP inhibitors. ....	34
1.4 Conclusion. ....	37
1.5 Reference. ....	39
CHAPTER 2. DISCOVERY OF TXS-8, A SELECTIVE BINDER OF PROTEASOMAL SUBUNIT RPN-6. ....	54
2.1 Introduction of proteasomal subunit Rpn-6. ....	54
2.2 Central hypothesis and rationale regarding the discovery of a small molecule binder of proteasomal subunit Rpn-6. ....	56
2.3 One-bead-one-compound library design and screening. ....	57
2.3.1 One-bead-one-compound library design. ....	57
2.3.2 One-bead-one-compound library screening via thermal shift assay.....	58
2.3.3 Thermal shift results and MALDI-TOF analysis.....	60
2.3.4 Compound sequence analysis and new compound design. ....	61
2.4 Discovery of TXS-8 and derivative studies. ....	62
2.4.1 Fluorescence polarization assay on the peptoids. ....	62
2.4.2 Discovery of TXS-8 and derivative designs. ....	63

2.4.3	TXS-13 – TXS-36 screening and results. ....	64
2.4.4	TXS-8 thermal shift assay on Rpn-6. ....	65
2.4.5	Screening TXS-8 with other proteins for specificity. ....	65
2.5	TXS-8 target identification. ....	66
2.5.1	Modification of TXS-8 for non-covalent pull-down study.....	66
2.5.2	Modification of TXS-8 for covalent pull-down study. ....	67
2.5.3	TXS-8 covalent pull-down with purified Rpn-6.....	68
2.5.4	TXS-14 covalent pull-down with purified Rpn-6.....	68
2.5.5	TXS-8 covalent pull-down in cell lysate with endogenous Rpn-6 and proteomic analysis. ....	69
2.6	Conclusion. ....	71
2.7	General methods and materials. ....	72
2.8	One bead one compound library. ....	73
2.8.1	Library synthesis.....	73
2.8.2	Rpn-6 Expression and purification. ....	74
2.8.3	Thermal shift assay (TSA) screening. ....	75
2.9	Fluorescent polarization assay (FP) on Rpn-6. ....	76
2.9.1	FP tag synthesis. ....	76
2.9.2	FP peptoid linker synthesis.....	77
2.9.3	FP peptoid synthesis. ....	77
2.9.4	Fluorescence polarization (FP) assay. ....	78
2.9.5	Fluorescent polarization (FP) assay with other proteins.....	78
2.10	Pull-down assay with diazirine biotin dual labeled TXS-8 on purified Rpn-6 in blocking buffer. ....	79
2.11	Pull-down assay with diazirine biotin dual labeled TXS-8/TXS-14 on cell lysates. ....	80
2.12	Proteomic analysis on BMCC-BDzn-TXS-8 target. ....	81
2.13	Reference.....	83
CHAPTER 3. TXS-8 TOXICITY IN HEMATOLOGICAL CANCER CELLS AND DEVELOPMENT OF A GENERAL WORKFLOW ON INVESTIGATING THE IMPACT OF A SMALL MOLECULE ON PROTEASOME.....		91
3.1	Introduction.....	91
3.2	Rpn-6 overexpression in hematological cancer cells.....	92
3.3	Toxicity Assay with TXS-8 and Several Cell Lines.....	92
3.4	Dual Dosing Using Bortezomib/KDT-11 and TXS-8. ....	93

3.5	Preliminary Study of the Impact of TXS-8 on Proteasome Activity.....	95
3.5.1	Establishing TXS-8 Induced Cell Stress Condition.....	95
3.5.2	Investigating the Impact of TXS-8 on Proteasome Activity with a Biochemical Assay. .....	96
3.5.3	Investigating the Impact ofTXS-8 on Proteasome Activity in Ramos B-cell Lysate Using Proteasome Probes. ....	97
3.5.4	Investigating TXS-8 Impact on Proteasome Activity with FRET Probe and K-48 Immunoblot.....	98
3.6	A Three-Step Workflow of Investigating the Impacts of Small Molecules on Proteasome Activity. ....	99
3.6.1	Testing Proteasome Activity Changes Using Proteasome Selective Probes in Normal and Rpn-6 Knocked Down Cells. ....	100
3.6.1.1	Target Protein Knockdown and Proteasome Activity Measurement. ....	100
3.6.1.2	Establishing dosing conditions using viability assay with varying concentration of TXS-8.....	101
3.6.1.3	Proteasome Activity Measurement in sRpn-6, cRpn-6, or No siRNA Treated Cells. .....	102
3.6.2	Monitoring Full-Length Protein Degradation in Rpn-6 Knockdown and Normal HEK- 293T Cells Dosed with TXS-8. ....	102
3.6.2.1	Protein Plasmid Preparation and Transfection and Viability Testing. ....	103
3.6.2.2	Full-Length Protein Degradation Assay in Knockdown and Normal Cells Dosed withTXS-8.....	104
3.6.3	Proteasome Activity Changes in a Primary Cell Line. ....	104
3.6.3.1	Rpn-6 expression and viability assay in AC16 cells. ....	105
3.6.3.2	Proteasome Activity Assay in a Primary Cell Line.....	105
3.6.4	Summary of the Workflow and Potential Application. ....	106
3.7	Conclusion. ....	106
3.8	General methods and materials. ....	107
3.9	General Cell Culture and TXS-8 Toxicity Experiments.....	109
3.9.1	Suspension Cell Culturing and Dosing.....	109
3.9.1.1	Suspension Cell Splitting Protocol.....	109
3.9.1.2	Suspension Cell Dosing Protocol. ....	109
3.9.2	Adherent Cell Culturing and Dosing. ....	110
3.9.2.1	Adherent Cell Splitting Protocol. ....	110
3.9.2.2	Adherent Cell Dosing Protocol. ....	110

3.10	Dual dosing of TXS-8 with KDT-11/bortezomib. ....	111
3.10.1	Dual Dosing of TXS-8 with KDT-11 in Ramos B-cells and Multiple Myeloma Cells. ....	111
3.10.2	Dual Dosing of TXS-8 with Bortezomib in Ramos B-cells and Multiple Myeloma Cells. ....	112
3.11	TXS-8 Induced Cell Stress Conditions.....	113
3.12	TXS-8 Impact on Proteasome Activity Using 26S Purified Proteasome and Ramos B-cell Lysate.....	114
3.12.1	Monitoring Proteasome Activity Changes with Purified 26S Proteasome. ....	114
3.12.2	Monitoring Proteasome Activity Changes with Ramos B-cell Lysate. ....	114
3.13	Impact of TXS-8 on Proteasome Activity with the FRET Probe and K-48 Immunoblot. . ....	115
3.13.1	TXS-8 impact on proteasome activity with FRET probe.....	115
3.13.2	TXS-8 Impact on Proteasome Activity Using K-48 Polyubiquitin Immunoblot..	116
3.14	HEK-293T Cell Rpn-6 Knockdown Experiment. ....	116
3.14.1	Cell culture of HEK-293T cells. ....	116
3.14.2	HEK-293T Cell Rpn-6 Knockdown Protocol. ....	117
3.14.3	Rpn-6 Expression Measurement in sRpn-6, cRpn-6, or No siRNA Treated HEK-293T Cells. ....	117
3.15	Cellular TAS-2 Assay in HEK-293T Cells. ....	118
3.15.1	Viability Assay.....	118
3.15.1.1	96-well Plate Preparation. ....	118
3.15.1.2	HEK-293T Cell Preparation for Viability Assay. ....	119
3.15.1.3	Cell Dosing and Viability Assay.....	119
3.15.2	TAS-2 Assay with HEK-293T Cells.....	120
3.15.2.1	HEK-293T Cell Preparation for TAS-2 Assay. ....	120
3.15.2.2	Cell Dosing and TAS-2 Assay. ....	121
3.16	Green Fluorescent protein (GFP) Degradation Assay.....	121
3.16.1	HEK-293T Cell GFP Transfection and Rpn-6 Knockdown. ....	121
3.16.2	12-well Plate and HEK-293T Cell Preparation.....	123
3.16.3	HEK-293T Cell Dosing and Western Blot Analysis of GFP Degradation Assay.	124
3.17	Dosing Cardiomyocytes with TXS-8. ....	125
3.17.1	Determining Rpn-6 Levels in AC16 Cells by Western Blot.....	125

3.17.2	Establishing Cell Viability with AC16 Cells in Response to Dosing with TXS-8. ....	126
3.17.3	Monitoring Proteasome Activity in Response to TXS-8 with TAS-2. ....	126
3.18	Reference.....	130
CHAPTER 4. TXS-8 PROTAC DEVELOPMENT/BINDING SITE STUDY AND PROTEASOME PROBE DEVELOPMENT. ....		135
4.1	Introduction.....	135
4.2	TXS-8 PROTAC development. ....	136
4.2.1	Using PROTAC to selectively degrade target protein and induce toxicity. ....	136
4.2.2	TXS-8 PROTAC development. ....	137
4.2.2.1	Thalidomide TXS-8 PROTAC development. ....	137
4.2.2.1.1	Thalidomide synthesis and TXS-8 PROTAC development. ....	137
4.2.2.1.2	Thalidomide TXS-8 PROTAC toxicity assay.....	138
4.2.2.2	Pomalidomide TXS-8 PROTAC development.....	139
4.2.2.2.1	Pomalidomide synthesis, PROTAC development and toxicity test.....	139
4.2.2.2.2	Rpn-6 degradation assay with TXS-8 PROTACs.....	140
4.2.3	Summary of TXS-8 PROTAC development. ....	140
4.3	TXS-8 binding site study. ....	141
4.3.1	Introduction to binding site study. ....	141
4.3.2	Approach one: Cross-linking, trypsin digestion and HPLC separation.....	141
4.3.2.1	Competitive binding on Rpn-6. ....	143
4.3.2.2	Cross-linking, trypsin digestion, HPLC separation, MALDI-TOF MS/MS. ....	143
4.3.3	Approach two: Cross-linking, trypsin digestion, click chemistry and enrichment..	144
4.3.4	Summary of TXS-8 binding site study on Rpn-6. ....	146
4.4	New rhodamine-based proteasome probe development. ....	146
4.4.1	Limitations of current commercially available proteasome probes and development of rhodamine-based probes to monitor proteasome's chymotrypsin-like activity.....	146
4.4.2	Synthesis of LLE-Rh, LLR-Rh probes and testing with 20S CP. ....	148
4.4.3	Comparison between the commercially available AMC probes and rhodamine-based probes. ....	149
4.4.4	Using proteasome inhibitors can significantly reduce the probe cleavage <i>in vitro</i> and <i>in cellulo</i> . ....	150
4.4.5	Summary of the development of the selective proteasome probes.....	151

4.5	Conclusion in TXS-8 PROTAC development, binding site study and proteasome probe development.....	152
4.6	General methods and materials.....	153
4.7	Thalidomide and thalidomide-based PROTAC TXS-8 synthesis.....	154
4.7.1	Thalidomide synthesis.....	154
4.7.2	Thalidomide-based TXS-8 PROTAC synthesis.....	154
4.7.3	Viability test of the thalidomide-based TXS-8 PROTACs.....	155
4.8	Pomalidomide and pomalidomide-based TXS-8 PROTAC synthesis.....	156
4.8.1	Pomalidomide synthesis.....	156
4.8.2	Thalidomide-based TXS-8 PROTAC synthesis.....	157
4.8.3	Viability test of the pomalidomide-based TXS-8 PROTACs.....	157
4.8.4	Rpn-6 degradation in Ramos B-cells treated with PROTACs.....	158
4.9	Cross-linking, trypsin digestion and HPLC separation.....	159
4.9.1	Dzn-TXS-8-FP synthesis.....	159
4.9.2	Rpn-6 expression and purification.....	160
4.9.3	Competitive binding on Rpn-6.....	161
4.9.4	Cross-linking.....	161
4.9.5	Trypsin digestion and HPLC separation.....	161
4.9.6	HPLC separation and MS analysis.....	162
4.10	Rhodamine probe synthesis and testing.....	162
4.10.1	Rhodamine LLE-Rh and LLR-Rh probes synthesis.....	162
4.10.2	Biochemical assay with rhodamine probes in 20S CP:.....	167
4.10.3	A549 cell culture and Rh probe testing:.....	167
4.10.4	Biochemical assay with rhodamine probes and AMC probes in 20S CP:.....	169
4.10.5	Biochemical assay with rhodamine probes in 20S CP and proteasome inhibitor MG-132:.....	169
4.10.6	Cellular experiments with rhodamine probes in A549 cells and proteasome inhibitor MG-132:.....	170
4.10.7	Cellular experiments with rhodamine probes in A549 cells and proteasome inhibitor bortezomib:.....	171
4.10.8	Viability assay in A549 cells treated with proteasome inhibitor MG-132 and bortezomib:.....	172
4.11	Reference.....	172
CHAPTER 5. CONCLUSION AND FUTURE DIRECTIONS.....		182

5.1	General conclusion.....	182
5.2	Future directions. ....	187
5.2.1	Future directions regarding TXS-8 toxicity evaluation. ....	187
5.2.2	Future directions regarding TXS-8 PROTAC development. ....	187
5.2.3	Future directions regarding TXS-8 binding site study. ....	188
5.3	Final conclusion. ....	189
5.4	Reference. ....	190
APPENDIX A. MASS SPEC DATA .....		201
APPENDIX B. COPYRIGHT PERMISSION .....		239
VITA.....		241
PUBLICATIONS.....		242

## LIST OF TABLES

<b>Table 2.1.</b> Summary of frequency of each amine on every position.....	61
<b>Table 2.2.</b> List of the peptides observed during proteomics, their location within the Rpn-6 sequence, and the corresponding LFQ intensity observed for each peptide.....	82
<b>Table 3.1.</b> Raw chemo-luminescence values for TXS-8 toxicity testing. Values were normalized to DMSO control to generate % viability. ....	113
<b>Table 3.2.</b> NIH NCI-60 single dose experiment.....	129

## LIST OF FIGURES

<b>Figure 1.1 The ubiquitin-proteasome system (UPS).</b> By a series transfers, E1, E2 and E3 ligase label the target protein with a ubiquitin protein. The process could be repeated several times until a minimum of four ubiquitins are attached to the target protein. The poly-ubiquitinated protein is recognized by the proteasome followed by poly-ubiquitin chain removal and the degradation of the target protein in peptide fragments. ....	24
<b>Figure 1.2 Isoforms of the Proteasome.</b> The proteasome exists in equilibrium mainly between two isoforms, the 26S and the 20S. The 26S is composed of the 19S regulatory particle (RP) and the 20S core particle (CP) where the 19S RP recognizes ubiquitinated protein and unfolds the protein to allow the 20S CP to degrade the target. PDB:5GJR .....	25
<b>Figure 1.3. Bottom view and side view of 19S RP.</b> The ATPase ring is labeled in red. Several subunits are also labeled on the structure. PDB:5GJR .....	26
<b>Figure 1.4 Bottom view and side view of 19S RP.</b> The ATPase ring is labeled in red. Several subunits are also labeled on the structure. PDB:5GJR .....	26
<b>Figure 1.5. The 20S CP. Left:</b> Bottom view on the $\beta$ ring ( $\alpha$ ring removed) and side view of 20S CP. <b>Right:</b> Side view of 20S CP, the $\beta 1$ , $\beta 2$ and $\beta 5$ subunits were colored orange, yellow and red, respectively. The gate of the $\alpha$ ring is around 9 Å diameter in closed gate form. PDB:5GJR .....	27
<b>Figure 1.6 The Immunoproteasome.</b> When encountering IFN- $\gamma$ , cells start producing new catalytic proteasomal subunits as $\beta 1i$ , $\beta 2i$ , and $\beta 5i$ and replace corresponding $\beta$ subunits to form the immunoproteasome (iCP). The iCP will degrade oxidatively damaged proteins more efficiently and produce C-termini/hydrophobic peptides to be presented at the MHC-I complex for immune response. Normal tissue cells produce iCP only at specific circumstances but some immune cells endogenously express iCP. ....	28
<b>Figure 1.7. <math>\alpha</math>-synuclein structure.</b> $\alpha$ -synuclein is a highly disordered protein that has been identified mainly expressed in neuron cells. The aggregation of $\alpha$ -synuclein contributes to the development of Parkinson's disease. PDB: 4BXL .....	30
<b>Figure 1.8. MG-132.</b> MG-132 was discovered as the first covalent inhibitor of the proteasome. The aldehyde group can be attached to the catalytic threonine of $\beta$ subunits.....	32
<b>Figure 1.9. Bortezomib.</b> Bortezomib was the first proteasome inhibitor approved by FDA for cancer treatment. ....	32
<b>Figure 1.10 Carfilzomib.</b> Carfilzomib was discovered as the second-generation proteasome inhibitor.....	33
<b>Figure 1.11. Ixazomib.</b> Ixazomib was the first orally available proteasome inhibitor on market. ....	33
<b>Figure 1.12. 19S base ATPase ring.</b> Bottom view of the 19S base ATPase ring. A heterohexameric complex responsible for target protein tertiary structure removal and gate opening of the 20S CP. ....	34

<b>Figure 1.13. p97 inhibitors. (A)</b> EerI was discovered in 2004. <b>(B)</b> DBeQ was discovered in 2011. ....	34
<b>Figure 1.14. Rpn-13 inhibitors. (A)</b> RA190 was discovered in 2013. <b>(B)</b> KDT-11 was discovered in 2015. ....	35
<b>Figure 1.15 F. Rpn-13 inhibitors. (A)</b> Structure of IU1 <b>(B)</b> Co-crystal structure of IU1 with USP14. ....	36
<b>Figure 1.16. Other USP14 and Rpn11 inhibitors. (A)</b> VLX1570 was discovered in 2008 <b>(B)</b> Capzimin was discovered in 2017. ....	37
<b>Figure 2.1. Extracted structure of Rpn-6 from 26S proteasome.</b> Rpn-6 makes multiple protein-protein interactions with other proteasome subunits and the relative position of these subunits are labeled. PDB:5GJR.....	54
<b>Figure 2.2. The interface between the <math>\alpha</math> ring and the ATPase ring.</b> The interaction between Rpt-6, Rpn-6 and $\alpha 2$ subunits tilts the ATPase ring on the $\alpha$ ring (shown by the angle between two planes) and provides space for mechanical movement of the subunits during target protein degradation.....	55
<b>Figure 2.3. General structure of peptoid and workflow of OBOC library screening. (A)</b> General structure of 3-mer peptoid. Peptoids could be viewed as <i>N</i> -substituted glycine <b>(B)</b> Workflow of testing the library with Rpn-6 using a thermal shift assay and identification of hit compounds. ....	58
<b>Figure 2.4. Example of thermal shift assay.</b> Green line shows Rpn-6 with DMSO as the control. Two ligands were included in the example as one of them did not alter the melting temperature of Rpn-6 at all while the other one increased the melting temperature, suggesting it stabilized the protein. ....	59
<b>Figure 2.5. Example of a potential hit molecule identified from MALDI.</b> The MS-MS profile of the molecule was analyzed to confirm the composition of the peptoid.....	60
<b>Figure 2.6. New peptoids for binding test.</b> 12 new peptoids generated from <b>Table 2.1</b> . A fluorescein is included for a fluorescence polarization assay to determine binding affinities. ....	61
<b>Figure 2.7. Binding curve of all 12 testing compounds.</b> Peptoid monomers observed frequently in <b>Table 2.1</b> were used to reconstruct 12 new peptoids to test for binding. Appended to the peptoid was a fluorescein moiety through a mini-PEG linker at the <i>C</i> -terminus. ....	62
<b>Figure 2.8.</b> Structure of TXS-8 .....	63
<b>Figure 2.9. Structure of TXS-8 derivatives.</b> TXS-13/14/15 for the <i>N</i> -methylamine scan. ....	63
<b>Figure 2.10. TXS-8 derivative FP assay.</b> FP results of TXS-13/14/15. Removing any of the amine moiety on TXS-8 completely diminished the binding of the derivatives to Rpn-6. ....	64
<b>Figure 2.11. FP assay with TXS-32 and TXS-33. (A)</b> Structure of TXS-32 and TXS-33, the insertion of linear amine moieties at the <i>C</i> -terminus of TXS-8. <b>(B)</b> FP result of TXS-32 and TXS-33 on Rpn-6, they showed similar binding affinity to Rpn-6 comparing to TXS-8. ....	64
<b>Figure 2.12.</b> Thermal shift assay of TXS-8/14 on Rpn-6.....	65

<b>Figure 2.13.</b> TXS-8 FP assay with other proteins. ....	65
<b>Figure 2.14. TXS-8 for non-covalent pull-down.</b> The thiol group will be immobilized to the resin after reacting with the iodo group on the resin. ....	66
<b>Figure 2.15. Modification of TXS-8 for covalent pull-down experiment. (A)</b> Mechanism of diazirine activation. The carbene ion could bind with amino side chains for covalent cross-linking. <b>(B)</b> Structure of BMCC-BDzn-TXS-8 for covalent pull-down. Diazirine moiety shown in red, biotin moiety shown in blue.....	67
<b>Figure 2.16. BMCC-BDzn-TXS-8 pull-down experiment with purified Rpn-6.</b> A band corresponded to Rpn-6 in the elution lane was observed indicating the capture of Rpn-6 from the solution with the probe. (Western blot, anti-Rpn-6) .....	68
<b>Figure 2.17. TXS-14 pull-down (A)</b> Structure of BMCC-BDzn-TXS-14. <b>(B)</b> Pull-down with purified Rpn-6. (Western blot, anti-Rpn-6) .....	68
<b>Figure 2.18. Rpn-6 expression in different cell lines.</b> Hematological cancer cells like Ramos B-cell and multiple myeloma cells express significantly more Rpn-6 comparing to HEK-293T cells. (Western blot, anti-Rpn-6) .....	69
<b>Figure 2.19. TXS-8 endogenous Rpn-6 pull-down in cell lysate. (A)</b> Coomassie stained gel of BMCC-BDzn-TXS-8 pull-down, a distinct band corresponding to Rpn-6 weight was observed around 50 kDa. <b>(B)</b> Western blot of BMCC-BDzn-TXS-8 pull-down, Rpn-6 was observed in the elution lane and indicated a success of the experiment. Rpn-2 was only observed in flow through indicating that TXS-8 was not binding to Rpn-2. ....	70
<b>Figure 2.20.</b> Colored map of identified sequence from endogenous Rpn-6 pull-down in cell lysate. Red regions stand for sequence identified during proteomic analysis.....	70
<b>Figure 2.21. (A)</b> SDS-PAGE for Rpn-6 purification. <b>(B)</b> Western blot for purified Rpn-6. ....	74
<b>Figure 2.22.</b> Fluorescein synthesis. ....	76
<b>Figure 2.23.</b> Pull-down assay of purified Rpn-6 diluted in blocking buffer using BMCC-BDzn-TXS-8.....	80
<b>Figure 2.24. TXS-14 pull-down experiment (A)</b> SDS-PAGE Coomassie stain and. <b>(B)</b> Western blot using BMCC-BDzn-TXS-14 for pull-down with Ramos B-cell lysate.....	81
<b>Figure 2.25.</b> Peptide fragments (highlighted in yellow) observed during gel band analysis by proteomics.....	82
<b>Figure 3.1 Rpn-6 expression in HEK-293T, Ramos B-cells and MM.1R cells.</b> Hematological cancer cells overly express Rpn-6.....	92
<b>Figure 3.2 TXS-8/14 toxicity assay (A)</b> Cell viability assay with HEK-293T cells, Ramos B-cells and MM.1R cells dosed with TXS-8. The IC <sub>50</sub> of TXS-8 in Ramos B-cells and MM.1R was 15 $\mu$ M. <b>3.2 (B)</b> TXS-14 showed no significant toxicity in all cell lines tested, even at 200 $\mu$ M. This result validates our previous conclusion that the all three amines of TXS-8 was essential for its binding towards Rpn-6.....	92

<b>Figure 3.3 TXS-8/bortezomib dual dosing.</b> Dual dosing of bortezomib/KDT-11 with TXS-8 on MM.1R cells. The viability of the cells was examined and plotted to obtain a curve.....	93
<b>Figure 3.4 TXS-8/KDT-11 dual dosing.</b> Dual dosing of bortezomib/KDT-11 with TXS-8 on Ramos B-cells cells. The viability of the cells was examined and plotted to obtain a curve. ....	94
<b>Figure 3.5 Viability of Ramos B-cell treated with constant concentration of TXS-8.</b> 20 $\mu$ M of TXS-8 was added to Ramos B-cells at given time period, the viability of the cells was investigated to find out when the cells started dying. ....	95
<b>Figure 3.6 Structure of Suc-LLVY-AMC probe.</b> the red marker represents the cleavage site of the compound by the chymotrypsin-like site. ....	96
<b>Figure 3.7 Rate of fluorescence signal comparison with purified 26S proteasome.</b> Rate ( $\Delta$ RFU/min) of TXS-8, bortezomib and DMSO. No significant inhibition of proteasome activity was observed with dosage of TXS-8. Error bars represent SEM and n=3, ****p<0.00005, ns=p>0.05. ....	96
<b>Figure 3.8 Rate of fluorescence signal comparison in Ramos B-cell lysate.</b> Rate ( $\Delta$ RFU/min) of TXS-8, bortezomib and DMSO. No significant inhibition of proteasome activity was observed with dosage of TXS-8. Error bars represent SEM and n=3, ****p<0.00005, ns=p>0.05.....	97
<b>Figure 3.9 Structure of the FRET probe designed by our lab.</b> The red marker indicates the cleavage site of the peptide. Edan is colored in blue and dabcyI is colored in red.....	98
<b>Figure 3.10 Rate of fluorescence signal comparison with purified 26S proteasome.</b> Rate ( $\Delta$ RFU/min) of TXS-8, TXS-14 and DMSO. Proteasome activity was significantly decreased with 50 $\mu$ M of TXS-8 but TXS-14 showed no impact on proteasome activity. Error bars represent SEM and n=3, **p<0.005, ns=p>0.05. ....	98
<b>Figure 3.11 K-48 polyubiquitin immunoblot in Ramos B-cells treated with TXS-8 or bortezomib and DMSO.</b> TXS-8 did not significantly induce ubiquitinated protein accumulation like positive control bortezomib. ....	99
<b>Figure 3.12</b> A three-step general workflow of investigating the impact of a small molecule on proteasome activity. Figure made by BioRender.com.....	99
<b>Figure 3.13 Rpn-6 knockdown in HEK-293T cells with sRpn-6. (A)</b> Immunoblot of Rpn-6 in knockdown/control and mock treated HEK-293T cells. <b>(B)</b> Relative Rpn-6 expression in knockdown/control and mock treated HEK-293T cells. Error bars represent SEM and n=3, *p<0.05, **p<0.005, ns=p>0.05 .....	100
<b>Figure 3.14 Structure of the TAS-2 probe.</b> It is recognized by the $\beta$ 5 subunit. The red marker represents the cleavage site. The compound is a hybrid of a peptide (blue) and a peptoid (red). Upon cleavage by the proteasome the release of the rhodamine will generate fluorescence for quantification. ....	100
<b>Figure 3.15 Rate of fluorescence signal comparison in sRpn-6, cRpn-6, or mock transected HEK-293T cells.</b> The sRpn-6 treated cells exhibited a 15% decrease. Error bars represent SEM and n=4, **p<0.005, ns=p>0.05. ....	101

<b>Figure 3.16 Viability of sRpn-6, cRpn-6, or no siRNA transfected HEK-293T cells.</b> A significant cell death was observed above 40 $\mu$ M. Error bars represent SEM and n=3, ***p<0.0005, ns=p>0.05. ....	101
<b>Figure 3.17. Rate of fluorescence signal comparison in sRpn-6, cRpn-6, or mock transected HEK-293T cells.</b> (A) TAS-2 cleavage rate in sRpn-6 treated HEK-293T cells, no significant proteasome activity changes were observed. (B) TAS-2 cleavage rate in cRpn-6 treated HEK-293T cells, no significant proteasome activity changes were observed. (C) TAS-2 cleavage rate in no siRNA treated HEK-293T cells, no significant proteasome activity changes were observed. Error bars represent SEM and n=4, ns=p>0.05. ....	102
<b>Figure 3.18.</b> GFP transfection in HEK-293T cells with various amount of GFP plasmid. ....	103
<b>Figure 3.19.</b> Viability result in GFP transfected sRpn-6 or no siRNA treated HEK-293T cells. Error bars represent SEM n=6, ns=p>0.05. ....	103
<b>Figure 3.20. GFP degradation in sRpn-6 and no siRNA treated HEK-293T cells.</b> (A) Immunoblot of Rpn-6, GAPDH and GFP in Rpn-6 knocked down HEK-293T cells. (B) Immunoblot of Rpn-6, GAPDH and GFP in Rpn-6 normal HEK-293T cells. (C) GFP/GAPDH relative ratio comparison between 30 $\mu$ M TXS-8 and DMSO treated cells. In both Rpn-6 knocked down and normal HEK-293T cells, no significant GFP degradation difference was observed. Error bars represent SEM n=4, ns=p>0.05. ....	104
<b>Figure 3.21. (A)</b> Immunoblot of AC16 cell lysate, Rpn-6 was detected. <b>(B)</b> Viability of TXS-8 in AC16 cells with various concentration. ....	105
<b>Figure 3.22. Rate of fluorescence signal comparison in AC16 cells.</b> TAS-2 cleavage rate in AC16 cells, no significant proteasome activity changes were observed in TXS-8 treated cells. The Proteasome inhibitor MG-132 significantly inhibited proteasome activity. Error bars represent SEM n=4, ***p<0.0005, ns=p>0.05. ....	106
<b>Figure 3.23.</b> FRET probe assay with 26S proteasome dosed with TXS-8/TXS-14/DMSO. ....	115
<b>Figure 3.24. Western blot analysis of sRpn-6, cRpn-6 and no siRNA treated HEK-293T cells.</b> The blot showed the expression level of Rpn-6 in different time period. The analyzed data was plotted by the ratio of Rpn-6/GAPDH among the cells in <b>Figure 3.13B</b> . ....	118
<b>Figure 3.25. Plate layout for the viability assay.</b> The white wells were intentionally left for an additional 2 wells of sRpn-6/cRpn-6/no siRNA treated cells as a backup. ....	119
<b>Figure 3.26. Plate layout for the TAS-2 assay.</b> The white wells were intentionally left for an additional 1 well of sRpn-6/cRpn-6/no siRNA treated cells as a backup. ....	120
<b>Figure 3.27(A)</b> Layout of the 96-well plate for viability assay. <b>(B)</b> The sRpn-6/no siRNA treated HEK-293T cells have the same 12-well plate layout. ....	123
<b>Figure 3.28.</b> Detailed workflow of investigating the impact of a small molecule on proteasome activity. ....	128
<b>Figure 4.1 Cellular process of how PROTAC works.</b> The addition of PROTAC will induce the co-recruitment of the target protein and E3 ligase. The target protein could be poly-ubiquitinated and eventually be degraded by the 26S proteasome. ....	136

<b>Figure 4.2. Synthesis route of thalidomide derivative.</b> This is a one-step synthesis. ....	137
<b>Figure 4.3 General structure of the PROTAC.</b> The linker is consisted of one or two PEG-2 moieties (n=1; TWT-1, n=2; TWT-2).....	138
<b>Figure 4.4 Synthesis route of pomalidomide derivative.</b> This is a one-step synthesis. ....	138
<b>Figure 4.5 Viability test of the PROTACs.</b> No significant cell death was observed with either thalidomide-based TXS-8 PROTACs.....	138
<b>Figure 4.6. General structure of the PROTAC.</b> The linker is consisted with various PEG moieties (n=0 named as TWT-3, 2 named as TWT-4, 3 named as TWT-5, 4 named as TWT-6). ....	139
<b>Figure 4.7. Viability test of the PROTACs.</b> No significant cell death was observed with all pomalidomide-based TXS-8 PROTACs.....	139
<b>Figure 4.8. Rpn-6 degradation with PROTACs.</b> No significant Rpn-6 degradation was observed in either TWT-4 or TWT-5 treated Ramos B-cells. Band intensity difference was caused by different amounts of primary antibody used for immunoblot.....	140
<b>Figure 4.9. Workflow of approach one.</b> The protein was first cross-linked with Dzn-TXS-8-FP, a trypsin digestion was performed on the protein to acquire a pool of peptides, and the mixture was subjected to HPLC. Peptide(s) carrying Dzn-TXS-8-FP would show unique fluorescence signal that could be collected. The fractions will then be analyzed by LC-MS/MS or MALDI-TOF MS/MS.....	142
<b>Figure 4.10.</b> Structure of Dzn-TXS-8 and Dzn-TXS-8-FP.....	143
<b>Figure 4.11. Rpn-6 competitive binding study.</b> Rpn-6 was pre-treated with Dzn-TXS-8 followed by cross-linking. It was then treated with Dzn-TXS-8-FP, followed by cross-linking again. The gel was directly scanned without staining. Distinct bands were observed on the gel indicating Dzn-TXS-8-FP being added to Rpn-6. ....	143
<b>Figure 4.12. Rpn-6 cross-linking with Dzn-TXS-8-FP.</b> Rpn-6 was treated with Dzn-TXS-8-FP followed by cross-linking. Multiple bands were cut from the gel for trypsin digestion.....	143
<b>Figure 4.13. HPLC chromatograph.</b> Distinct peaks were observed at 494 nm channel corresponding to fluorescein on Dzn-TXS-8-FP. ....	144
<b>Figure 4.14. alkyne-Dzn-TXS-8 and DADPS probes. (A)</b> TXS-8 was synthesized with an alkyne handle for click chemistry. <b>(B)</b> General structure of dialkoxy-diphenylsilane (DADPS) probes, the azide group on the probe can be attached to alkyne with click chemistry. The silyl group was acid sensitive and could be hydrolyzed with 10% formic acid rapidly. ....	145
<b>Figure 4.15. Workflow of peptide enrichment with DADPS probes.</b> Rpn-6 was first treated with alkyne-Dzn-TXS-8 followed by cross-linking. The protein was trypsin digested, and click chemistry was performed to append the DADPS probe to TXS-8. The peptide fragment carrying TXS-8 was enriched via a pull-down experiment and analyzed.....	145

<b>Figure 4.16.</b> Bottom view on the $\beta$ ring ( $\alpha$ ring removed) and side view of 20S CP. The $\beta$ 1, $\beta$ 2 and $\beta$ 5 subunits were colored orange, yellow and red, respectively. The gate of the $\alpha$ ring is around 9 Å diameter in closed gate form. ....	147
<b>Figure 4.17. Commercially available proteasome probes.</b> AMC in green, peptide in blue, protecting group in purple, cleavage site marked in red line. <b>(A)</b> Ac-GPLD-AMC, selective probe for the caspase-like $\beta$ 1 subunit. <b>(B)</b> Boc-LRR-AMC, selective probe for the trypsin-like $\beta$ 2 subunit. <b>(C)</b> Suc-LLVY-AMC, selective probe for the chymotrypsin-like $\beta$ 5 subunit. ....	147
<b>Figure 4.18. LLVY-Rh probe.</b> Peptoid region in red, rhodamine 110 showed in green, peptide region showed in blue. Cleavage site is marked in red line. ....	148
<b>Figure 4.19 (A)</b> GPLD-Rh probe (peptoid in red, rhodamine in green, peptide in blue). <b>(B)</b> LLR-Rh probe (peptoid in red, rhodamine in green, peptide in blue). <b>(C)</b> Z-LLE-AMC, selective probe for the caspase-like $\beta$ 1 subunit. <b>(D)</b> LLE-Rh probe (peptoid in red, rhodamine in green, peptide in blue). ....	148
<b>Figure 4.20. Rate of Rh probes with 20S CP.</b> The GPLD-Rh probe showed inconsistent hydrolysis profile during the assay and we decided to use LLE-Rh probe to replace the GPLD-Rh probe for monitoring caspase-like activity on the 20S CP. LLE-Rh, LLR-Rh and LLVY-Rh probes were all cleaved by the 20S CP. ....	149
<b>Figure 4.21.</b> Rate ( $\Delta$ RFU/min) comparison between AMC probes and Rh probes. AMC probes required a high concentration (30 $\mu$ M) to be observed with significant signal, but Rh probes showed better sensitivity comparing to the AMC probes even at low concentration (10 $\mu$ M). The result from indicated that Rh probes were useful tools to monitor proteasome activity changes. ....	149
<b>Figure 4.22. (A) Purified 20S CP:</b> Cleavage rate comparison with different proteasome probes when treated with MG-132 in 20S CP. A significant probe hydrolysis rate decrease was observed with all subunits. <b>(B) A549 cells:</b> Cleavage rate comparison with different proteasome probes when treated with bortezomib in A549 cells. A significant probe hydrolysis rate decrease was observed the chymotrypsin-like subunit. Error bars represent SEM and n=4, ****p<0.00005, ***p<0.0005, **p<0.005. ....	150
<b>Figure 4.23. Synthesis route of thalidomide derivative.</b> ....	154
<b>Figure 4.24. Synthesis route of pomalidomide derivative.</b> ....	156
<b>Figure 4.25.</b> LC-MS of GPLD-Rh probe. ....	164
<b>Figure 4.26.</b> LC-MS of LLR-Rh probe. Due to the low coupling efficiency of arg-pbf to rhodamine, some rhodamine may not be coupled after two trials and leu could be added to rhodamine. The extra peak was determined as LL-Rh. ....	164
<b>Figure 4.27.</b> LC-MS of LLR-Rh probe. Due to the low coupling efficiency of arg-pbf to rhodamine, some rhodamine may not be coupled after two trials and leu could be added to rhodamine. The extra peak was determined as LL-Rh. ....	165
<b>Figure 4.28.</b> LC-MS of LLVY-Rh probe. The extra peak was determined as LLV-Rh. ....	165
<b>Figure 4.29.</b> LC-MS of LLE-Rh probe. ....	166

<b>Figure 4.30.</b> LC-MS of LLE-Rh probe. ....	166
<b>Figure 4.31. Raw data of probes incubated with 20S CP.</b> The probes were incubated with the 20S CP at a final concentration of 10 $\mu$ M. The result showed that GPLD-Rh probe was not hydrolyzed significantly by the 20S CP. ....	167
<b>Figure 4.32:</b> Rate ( $\Delta$ RFU/min) comparison among three probes in A549 cells at 10 $\mu$ M of final concentration. Error bars represent SEM and n=3.....	168
<b>Figure 4.33. Raw data of rhodamine and AMC probes incubated with 20S CP. (A)</b> AMC probe raw data comparison. <b>(B)</b> Rh and AMC probe comparison with 10 and 30 $\mu$ M concentration on the caspase subunit. <b>(C)</b> Rh and AMC probe comparison with 10 and 30 $\mu$ M concentration on the trypsin subunit. (30 $\mu$ M LLR-Rh error bar decreased by the end of the experiment because the readings were above detecting limit) <b>(D)</b> Rh and AMC probe comparison with 10 and 30 $\mu$ M concentration on the chymotrypsin subunit. (30 $\mu$ M LLVY-Rh error bar decreased by the end of the experiment because the readings were above detecting limit, the data presented in <b>Figure 5</b> had last 20 mins removed) .....	169
<b>Figure 4.34.</b> Rate ( $\Delta$ RFU/min) comparison among three probes treated with MG-132. Significant proteasome activity inhibition was observed with all three catalytic activities. Error bars represent SEM and n=4. ****p<0.00005.....	170
<b>Figure 4.35.</b> Rate ( $\Delta$ RFU/min) comparison among three probes in A549 cells at 10 $\mu$ M of final concentration with 15 $\mu$ M of MG-132. Error bars represent SEM and n=4. ****p<0.00005, ns=p>0.05. ....	170
<b>Figure 4.36.</b> Rate ( $\Delta$ RFU/min) comparison among three probes in A549 cells at 10 $\mu$ M of final concentration with 15 $\mu$ M of bortezomib. Error bars represent SEM and n=4. **p<0.005, ***p<0.0005, ****p<0.00005.....	171
<b>Figure 4.37.</b> Viability assay in A549 cells treated with MG-132 or bortezomib. No significant cell death was observed after 2 hours of treatment. Error bars represent SEM and n=5. ns=p>0.05. ....	172

## ABBREVIATIONS

Fmoc	Fluorenylmethyloxycarbonyl protecting group.
DMF	Dimethyl formamide
DIC	<i>N,N'</i> -diisopropylcarbodiimide
HBTU	Tetramethyluronium hexafluorophosphate
DIPEA	Diisopropyl ethyl amine
DCM	Dichloromethane
COMU	(1-Cyano-2-ethoxy-2-oxoethylidenaminoxy)dimethylamino-morpholino-carbenium hexafluorophosphate
TFA	Trifluoroacetic acid
TIPS	Triisopropylsilane
THF	Tetrahydrofuran
DMSO	Dimethyl sulfoxide
ACN	Acetonitrile
BAA	Bromoacetic acid
<i>E. coli</i> :	<i>Escherichia coli</i>
EtOAC	Ethyl acetate
HMDS	Hexamethyldisilazane
MMt	Monomethoxytrityl
M-PER	M-PER <sup>TM</sup> mammalian protein extraction solution
PBS	Phosphate-buffered saline
TEA	Triethylamine

## ABSTRACT

The ubiquitin-proteasome system is responsible for cellular protein recycling, and it is a crucial system to maintain proper protein balances in cells. Proteasome is the main component of the system, and the system is tightly related to multiple cellular processes. Malfunction of the proteasome could lead to various diseases including cancer, neurodegenerative diseases and autoimmune diseases. As a result, researchers have been developing small molecules to target the proteasome to regulate its function. Currently, three small molecules have been approved by FDA as proteasome inhibitors to treat hematological cancer multiple myeloma. However, these small molecules inhibit the same enzymatic subunit on the proteasome and drug resistance has been observed among patients administrating these proteasome inhibitors. To develop new small molecules to target the proteasome, we started to investigate the 19S regulatory particle of the proteasome. In this work, we presented a workflow of discovering a small molecule selective binder, TXS-8, to 19S regulatory particle subunit Rpn-6. We also developed a series of assays to investigate the impact of small molecule on proteasome activity. At last, we introduced the binding site study of TXS-8, development of TXS-8-based PROTAC and new proteasome probe development.

We first developed a one-bead-one-compound (OBOC) library to screen with Rpn-6 to discover potential binders to Rpn-6. After careful evaluation and validation, TXS-8 was discovered as the best hit from the screening. Our covalent pull-down experiment with cell lysate later confirmed TXS-8 as a selective binder of Rpn-6 and proteomic analysis of the pulled down protein also validated Rpn-6 as the major target of TXS-8.

We then investigated the impact of TXS-8 in Rpn-6 overexpressed cancer cells like Ramos B-cell and multiple myeloma. TXS-8 was four-fold more toxic in these cells comparing to our control HEK-293T cells. To understand the cause of cell death when dosed with TXS-8, we began to investigate the impact of TXS-8 on proteasome activity, but some preliminary results were inconsistent. By the same time, there is also lack of a general workflow to investigate the impact of small molecules on proteasome activity. Therefore, we developed a three-step process to illustrate the general workflow using TXS-8 as an example. We first knocked down Rpn-6 in HEK-293T cells and monitored proteasome activity changes with a cell permeable probe our lab developed. We then transfected HEK-293T cells with a full-length foreign protein and knocked

down Rpn-6 in these cells. We later monitored the degradation of the foreign protein when dosed with TXS-8. In the last step, we monitored the proteasome activity changes in primary cell lines when dosed with TXS-8. From these three steps, we successfully demonstrated a general workflow to investigate if a small molecule can affect proteasome activity. We also concluded that TXS-8 was unable to affect proteasome activity at non-lethal concentration.

To further investigate TXS-8 and provide guidance for future structural optimization to improve potency, we proposed two methods on investigating the general binding site of TXS-8 on Rpn-6 using cross-linking techniques that is currently ongoing. We also modified TXS-8 into proteolysis targeting chimeras (PROTACs) to investigate if TXS-8-based PROTAC can improve toxicity and selectively induce Rpn-6 degradation in cells. However, no significant cell toxicity or Rpn-6 degradation was observed when dosed with TXS-8-based PROTACs.

Finally, Due to limitation of cell permeable probes, we were unable to investigate the impact of TXS-8 on the caspase-like  $\beta 1$  and trypsin-like  $\beta 2$  subunit of the proteasome in our previous studies. Although TXS-8 did not alter the chymotrypsin-like activity at non-lethal concentration, examining the effect of TXS-8 on the caspase-like and trypsin-like activity could still benefit our research. Besides, we also desire to expand our proteasome activity toolbox by developing more sensitive proteasome probes. Therefore, by analyzing and combing the commercially available proteasome probes and LLVY-Rh probes, we decided to develop selective proteasome probes for the  $\beta 1$  and  $\beta 2$  subunit to provide useful tools for future potential small molecule proteasome regulator characterization.

# CHAPTER 1. THE PROTEASOME AND ITS SMALL MOLECULE REGULATORS.

## 1.1 Overview of the ubiquitin-proteasome system.

### 1.1.1 Introduction to the ubiquitin-proteasome system.

Cells produce significant amount of proteins at any given time, but most of them are considered as short-life proteins and require rapid degradation and recycling once the protein has fulfilled its job.<sup>1,2</sup> This task is performed by the ubiquitin-proteasome system (UPS) where the target protein is poly-ubiquitinated by a repeated step involving multiple E1, E2 and E3 ligases (**Figure 1.1**). Ubiquitin is a multifaceted post-translational modification protein that can be involved in most eukaryotic biology.<sup>3,4</sup> Ubiquitin contains seven lysine residues in its sequence and a methionine at its N-terminal, where one or multiple ubiquitins can be further added to another ubiquitin on the above residues. By repeating the step multiple times, a polyubiquitin chain is formed. Among various polyubiquitin chains, the Lys48 (K48) polyubiquitin chain on the target protein can be specifically recognized by the proteasome and the chain will be removed and

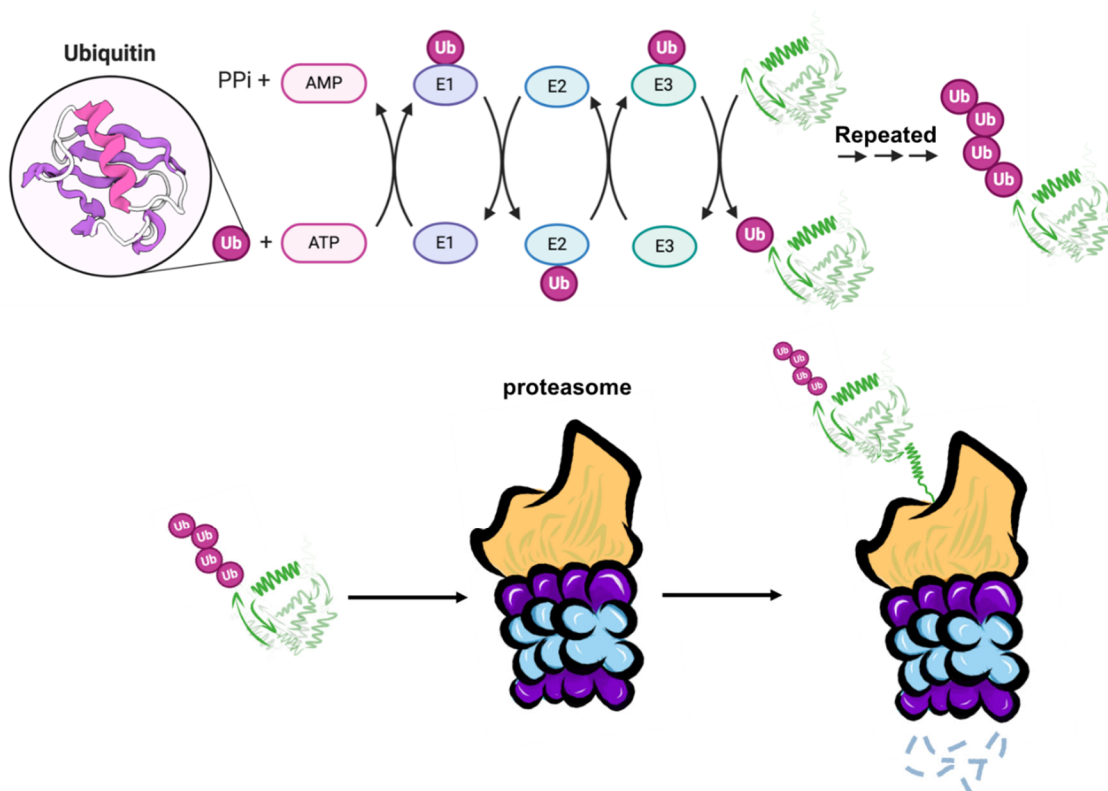


**Figure 1.1 The ubiquitin-proteasome system (UPS).** By a series transfers, E1, E2 and E3 ligase label the target protein with a ubiquitin protein. The process could be repeated several times until a minimum of four ubiquitins are attached to the target protein. The poly-ubiquitinated protein is recognized by the proteasome followed by poly-ubiquitin chain removal and the degradation of the target protein in peptide fragments.

recycled for labeling other proteins later.<sup>3–8</sup> The detailed mechanism of what determines if a protein will be poly-ubiquitinated is still under investigation, but research has shown that modifications on the polyubiquitin chain could potentially determine the fate of the protein.<sup>9,10</sup> On the other hand, the recognition of the poly-ubiquitinated protein by the proteasome will trigger a series of conformational changes on the proteasome, which will then remove the poly-ubiquitin chain as well as the tertiary structure on the target protein to allow for protein degradation.<sup>11–13</sup> The ubiquitin-proteasome system is crucial for the proliferation and survival of cells as more than 80% of cellular protein degradation is accomplished by the system.<sup>14,15</sup> The degradation of proteins is also related to immune response as some partially degraded peptide fragments will be presented on the cell surface forming major histocompatibility complex class I (MHC-I).<sup>16–18</sup> These MHC-I complexes are examined by immune cells like T-cells or macrophages. When pathogenic infection happens, the degradation of foreign protein by the proteasome will generate foreign antigenic peptide fragments presented on the MHC-I complexes and will be recognized by immune cells to trigger immune response.<sup>16,18–22</sup> Since ubiquitin-proteasome system plays crucial role to maintain proper protein balance in cells, further studies have been put forward to investigate its role regarding cell proliferation, DNA damage repair, cancer developments etc.<sup>23–27</sup> These researches have demonstrated the importance to better understand the ubiquitin-proteasome system and the possibility of utilizing the system for various disease treatments like neurodegenerative disease and cancer.<sup>28–31</sup>

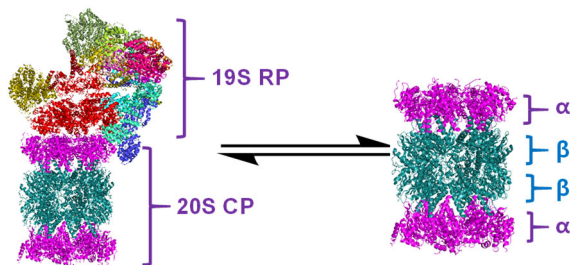


**Figure 1.2 Isoforms of the Proteasome.** The proteasome exists in equilibrium mainly between two isoforms, the 26S and the 20S. The 26S is composed of the 19S regulatory particle (RP) and the 20S core particle (CP) where the 19S RP recognizes ubiquitinated protein and unfolds the protein to allow the 20S CP to degrade the target. PDB:5GJR

### 1.1.2 The UPS and the 26S proteasome.

The main component of the UPS is the 26S proteasome which it is made up of a 20S core particle (20S CP) and a 19S regulatory particle (RP or known as PA700).<sup>12,15,32,33</sup> The 26S proteasome is normally referred as the standard proteasome or in some cases as the proteasome. The 19S RP on the 26S proteasome is responsible for recognizing the poly-ubiquitin chain from the target protein, removing the poly-ubiquitin chain and the tertiary structure of the

target protein, opening the gate of the 20S CP and translocating the polypeptide into the 20S CP for degradation.<sup>12,34–38</sup> The 20S CP is the catalytic portion of the 26S proteasome responsible for protein degradation. Since first discovered in 1970s, proteasome has gained great interest among researchers, as the proteasome has been found to be implicated in various cellular process including transcriptional regulation, cell differentiation, DNA damage repair etc.<sup>23–26,39,40</sup> As mentioned in **Chapter 1.1.1**, UPS is

responsible for more than 80% of protein degradation and recycling in cells which requires a significant amount of proteasome and regulating proteins to achieve the task. An estimation of around 2% of cellular proteins are related to UPS.<sup>41</sup>

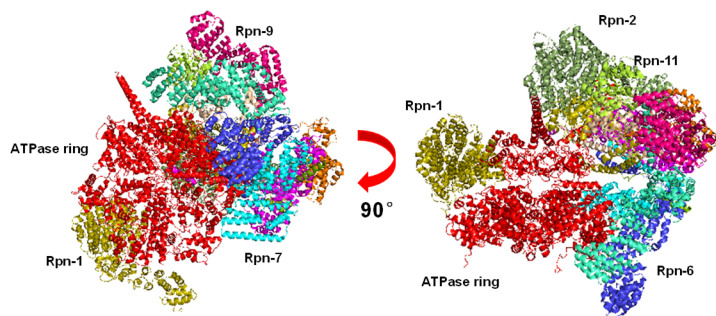


**Figure 1.3. Bottom view and side view of 19S RP.** The ATPase ring is labeled in red. Several subunits are also labeled on the structure. PDB:5GJR

### 1.1.3 The 19S and 11S RP.

The 19S RP is made up of 19 individual proteasome subunits that can be briefly separate into two groups, the 19S RP base subunits and the 19S lid subunits (**Figure 1.3**).<sup>35–37,42</sup> The base subunits include Rpt-1 to Rpt-6, these subunits belong to the AAA-ATPase protein family, utilizing ATP hydrolysis to adopt conformational

changes to open the gate of the 20S CP allowing the target polypeptide being translocated for degradation.<sup>43–47</sup> Rpn-1 and Rpn-2 are the two largest subunits on the 19S RP, and they provide protein-protein interactions scaffolds for other 19S RP subunits as well as ubiquitin processing platform. They also provide protein-protein interactions for other non-proteasome regulating proteins like Usp14 and they are also considered a part of the base of the 19S RP.<sup>48–52</sup> The remaining 11 subunits including Rpn3, Rpn-5 to Rpn-13 and Rpn-15 are considered as the lid subunits of the 19S RP.<sup>53–55</sup> Among them, Rpn-10 and Rpn-13 are recognized as the ubiquitin receptor and Rpn-11 is recognized as the deubiquitinating subunit (DUB).<sup>56–60</sup> To sum up, the lid of the 19S RP is responsible to bind with the poly-ubiquitinated protein and remove the ubiquitin from the target. The base of the 19S RP removes the tertiary structure of the protein making it into a linear polypeptide and opening the gate of the 20S CP for translocation.

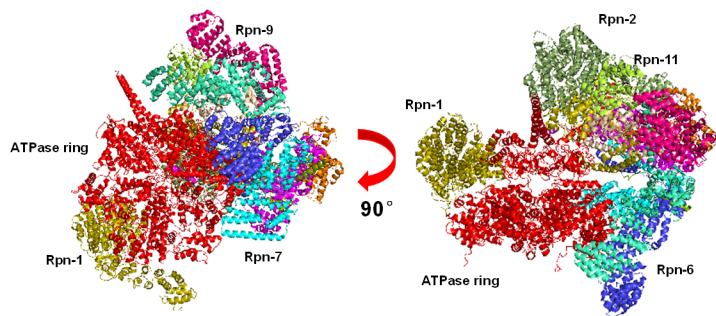


**Figure 1.4 Bottom view and side view of 19S RP.** The ATPase ring is labeled in red. Several subunits are also labeled on the structure. PDB:5GJR

Beside the 19S RP, another form of the regulatory particle 11S RP (or PA28) also exists in cells (**Figure 1.4**).<sup>42,61</sup> The 11S RP can promote the gate-opening of the 20S CP in a similar way as the 19S RP but structurally the 11S RP is a cone-shaped structure complex made of heteroheptameric  $\alpha$ ,  $\beta$  or homoheptameric  $\gamma$  subunits and 11S RP does not contain any ATPase subunits like the base of 19S

RP.<sup>62,63</sup> The PA 28 $\gamma$  is mainly located around the nucleus and is involved in cell apoptosis and proliferation, and some research has also suggested it may have additional functions related to DNA double-strand breaks. The PA 28 $\alpha\beta$  exists mostly in the cytoplasm and can be overexpressed when stimulated by cytokine interferon (IFN- $\gamma$ ). Researchers have shown that the activity of the PA 28 $\alpha\beta$  is linked with effective immune response with selectively upregulation in MHC-I complexes antigen presentation.<sup>64,65</sup> Both the PA28 and 19S RP can bind with the 20S CP to form various proteasomes complexes like PA28 $\alpha\beta$ -20S, PA28 $\gamma$ -20S and a hybrid version of the proteasome as PA28-20S-19S with different pattern of cleavage products. To sum up, both 11S RP and 19S RP are important components of the proteasome, although structurally different, they are involved in various cellular processes like protein degradation, antigen presentation.<sup>33,66</sup>

#### 1.1.4 The 20S CP and 20S iCP.

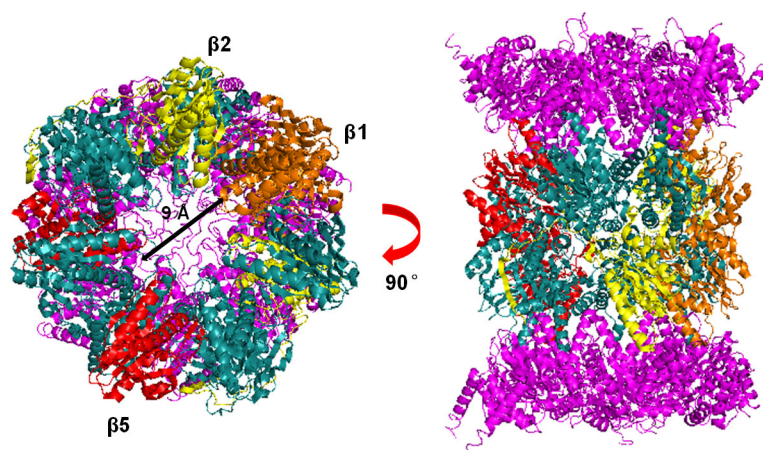


**Figure 1.5. The 20S CP.** Left: Bottom view on the  $\beta$  ring ( $\alpha$  ring removed) and side view of 20S CP. Right: Side view of 20S CP, the  $\beta 1$ ,  $\beta 2$  and  $\beta 5$  subunits were colored orange, yellow and red, respectively. The gate of the  $\alpha$  ring is around 9 Å diameter in closed gate form. PDB:5GJR

Multiple steps are involved for target protein degradation and these steps are accomplished with various proteasome subunits while polypeptide hydrolysis takes place in the 20S CP. The 20S CP (or the 20S proteasome) presents a barrel-like structure composed of four  $\alpha$ ,  $\beta$ ,  $\alpha$  stacked rings (**Figure 1.5**). Each of the  $\alpha$  and  $\beta$  rings is made up by seven subunits from  $\alpha 1$ - $\alpha 7$  and  $\beta 1$ - $\beta 7$ , respectively. The  $\alpha$  ring of

the 20S CP forms the gate of the 20S CP complex and exists mostly in closed form with an approximate diameter of 9 Å.<sup>15,42,67-70</sup> The closed form of the  $\alpha$  ring keeps most folded cellular proteins from entering the gate of the 20S CP. However, some proteins that are oxidatively damaged, or intrinsically disordered can still enter the gate of the 20S CP. These proteins are missing proper tertiary structure and are able to enter the gate of the 20S proteasome without being poly-ubiquitinated. Once these proteins enter the 20S CP, it can undergo ubiquitin independent degradation pathway to be hydrolyzed.<sup>71-73</sup>

The  $\beta$  ring of the 20S CP resides the protease-like catalytic  $\beta 1$ ,  $\beta 2$  and  $\beta 5$  subunits. These subunits use the *N*-terminal threonine as the nucleophilic warhead to attack and hydrolyze amide bonds from the target polypeptide. The  $\beta 1$ ,  $\beta 2$  and  $\beta 5$  subunits present caspase-like, trypsin-like and chymotrypsin-like activities, respectively. The above three subunits are responsible for the degradation for the target protein and producing various peptide fragments for further degradation or antigen presentation onto the MHC-I complexes.<sup>42,61,69</sup>

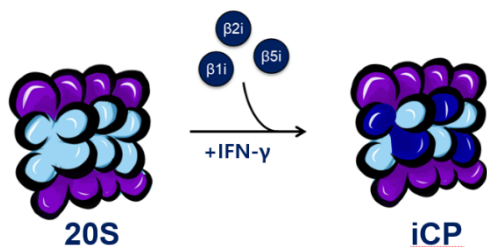


**Figure 1.6 The Immunoproteasome.** When encountering IFN- $\gamma$ , cells start producing new catalytic proteasomal subunits as  $\beta 1i$ ,  $\beta 2i$ , and  $\beta 5i$  and replace corresponding  $\beta$  subunits to form the immunoproteasome (iCP). The iCP will degrade oxidatively damaged proteins more efficiently and produce C-termini/hydrophobic peptides to be presented at the MHC-I complex for immune response. Normal tissue cells produce iCP only at specific circumstances but some immune cells endogenously express iCP.

When cells are under stress conditions like elevated reactive oxygen species (ROS) damage or pathogenic infection, the cell will express another isoform of the 20S CP called 20S immunoproteasome (iCP) upon encountering cytokines like IFN- $\gamma$  (**Figure 1.6**).<sup>74–76</sup> The  $\beta 1$ ,  $\beta 2$  and  $\beta 5$  subunits synthesis will be switched to  $\beta 1i$ ,  $\beta 2i$  and  $\beta 5i$  synthesis presenting lower caspase-like but higher trypsin-like and chymotrypsin-like activities compared to the 20S CP. These  $\beta$  subunits will be incorporated into the newly synthesized 20S iCP.<sup>77,78</sup> However, the incorporation and maturation of the  $\beta 1i$ ,  $\beta 2i$  subunits are dependent on the incorporation of  $\beta 5i$  while  $\beta 5i$  can be incorporated independently to the 20S iCP.

The 20S iCP can degrade oxidatively damaged or foreign proteins and produces basic C-termini or hydrophobic peptides which can be presented by the MHC-I complexes for antigen presentation.<sup>20,22,77,79</sup> The 20S iCP can form hybrid proteasome with either the 19SRP or the 11S RP except the PA 28 $\gamma$  and its function plays a crucial role in cell immune response.

Consistent expression of the immunoproteasome subunits are also observed in some immune cells like B cells and macrophages likely due to permanent activation of signaling pathways.<sup>20</sup> However, during some viral infections like human immunodeficiency virus (HIV), the virus produces proteins that downregulate the  $\beta 2i$  and  $\beta 5i$  subunits and inhibit the 20S iCP to prevent the degradation of the viral proteins and subsequent peptide fragment loading on to the MHC-I complex. HIV-1 Tat protein interacts with  $\beta 2i$  and  $\beta 5i$  of the 20S iCP and six  $\beta$  subunits of the 20S CP to decrease proteasome activity. Tat protein can also bind with the  $\alpha$  subunits to prevent the interaction between 20S CP or 20S iCP and regulatory particles. The interaction of the Tat protein

with the  $\alpha$  subunits also blocks the gate of the  $\alpha$  ring and prevents proteins from entering the proteasome.<sup>80–82</sup>

## **1.2 Proteasome affects cell function.**

### **1.2.1 Tumorigenesis and proteasome.**

Among the targets of proteasome, cell cycle related proteins are included like cyclins, p27, p53, mTOR, c-Myc. These proteins can significantly regulate various signaling pathways upon expression and eventually affect cell cycle and cellular differentiation.<sup>23,24,83</sup> Cell cycle progression requires sophisticated and precise protein expression/degradation. Environmental changes like encountering reactive oxygen species or gene mutation during replication can cause disruptions in proteostasis, leading to abnormal protein accumulation and subsequent increase in cell stress. Appropriately eliminating the cellular stress by increasing the amount of proteasome complexes may restore the cell. But cell apoptosis will also be observed if the cellular stress overwhelms the cell. Besides recovering or dying from the stress, some cells upregulate multiple transcription factor proteins like HIF-1 $\alpha$ , JNK that will lead to the expression of growth factors, cell cycle regulatory molecules etc.<sup>76,84,85</sup> Although proteasome is responsible for degrading these proteins, the production of these proteins may exceed the capacity of proteasome degradation, resulting in abnormal cell activity.

The cells that survive the harsh environment have lost control of general cycle regulation processes, resulting uncontrolled cell division and tumorigenesis. In response to elevated expression of transcriptional proteins, rapid degradation of these proteins is also required to avoid cell apoptosis. Therefore, some cancer cells significantly upregulate proteasome activity to avoid apoptosis caused by protein accumulation. Among them, hematological cancers like non-Hodgkin's lymphoma (NHL), multiple myeloma (MM), acute myeloid leukemia (AML) have shown strong relationship between proteasome activity and tumor survival/progression.<sup>86–88</sup> Taken B-cell lymphoma and multiple myeloma as examples, these cells belong to cancers of the blood and can affect different parts of the body. Multiple myeloma strikes the plasma cells where the normal cells secrete immunoglobulins to fight with pathogens but the disease cells will compete off the normal cells due to their fast proliferation rate. The disease cells will also produce abnormal immunoglobulins which will both impair the immune system and damage bones.<sup>89</sup> B-cell

lymphoma on the other hand, hits the lymphatic system where normally B cells mature and contribute to immune system. However, B-cell lymphoma patients will produce a large quantity of immature B cells that cannot secrete immunoglobulins and they can easily spread through the entire body by lymphatic system.<sup>90</sup> Since either these cells produces a large amount of proteins or replicate rapidly, they are extremely sensitive on proteasome activity for survival. Based on the high dependency on proteasome activity for cell survival, hypothesis on inhibition of proteasome activity to treat these types of cancer has been put forward.<sup>91-93</sup> Extensive research has been conducted on developing small molecules to inhibit proteasome activity which will be discussed in **Chapter 1.3.1**. To briefly summarize the development of proteasome inhibitors, researchers have demonstrated the inhibition of proteasome activities using small molecules is a plausible method for cancer treatment and apoptosis in cancer cells treated with proteasome inhibitors has been observed. Food and Drug Administration (FDA) has approved three proteasome inhibitors for multiple myeloma treatment indicating proteasome as a valued target for drug development.

### 1.2.2 Aging, neurodegenerative diseases and failure of the proteasome system.

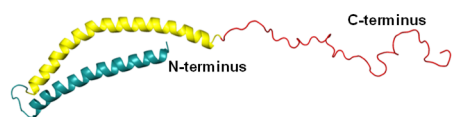


**Figure 1.7.  $\alpha$ -synuclein structure.**  $\alpha$ -synuclein is a highly disordered protein that has been identified mainly expressed in neuron cells. The aggregation of  $\alpha$ -synuclein contributes to the development of Parkinson's disease. PDB: 4BXL

Aging is an inevitable event for all living species and will significantly change the cellular processes and activities.<sup>94</sup> Several hypotheses have been proposed to provide feasible explanations for the phenomenon including accumulated oxidative damaged proteins, loss of proteostasis, telomere shortening or programmed aging etc.<sup>95</sup> Although the detailed mechanism of aging remains unclear, research has shown that there is a strong relationship between aging and decreased proteasome function as aged cells express less proteome activities. Besides, researchers have also demonstrated that the progressive decline in cellular proteostasis and accumulation of unwanted proteins is a hallmark of aging.<sup>96-98</sup> This has been proven in animal based studies where increased proteasome activity provides longer lifespan for animals like naked mole rat and giant clam comparing to other similar size mammals.<sup>99-102</sup> Tissue experiments from human and rat also demonstrate that the proteasome activity in younger donor cells are 2-6 fold higher comparing to older biopsies.<sup>95,103</sup> The impact of declined proteasome activity during aging is profound and lasting as protein accumulation in cells could potentially contribute to multiple neurodegenerative diseases such as Parkinson's disease

and Alzheimer's disease.<sup>29,104–106</sup> Taken Parkinson's disease as an example, decreased proteasome activity results in the aggregation of  $\alpha$ -synuclein to form various species of oligomers and fibrils in neuron cells (**Figure 1.7**). The primary biological function of  $\alpha$ -synuclein in cells is still under investigation, but it is relatively specifically expressed in neurons. Researches have shown  $\alpha$ -synuclein can bind to lipids in the plasma membrane and can interact with synaptic vesicles.<sup>104,107,108</sup>  $\alpha$ -synuclein is a highly disordered protein in unbound state and is prone to form aggregates by itself. Among different aggregates of  $\alpha$ -synuclein, the oligomers are considered as the toxic species that will impact various cellular pathways and result in neuronal cell death. Failure of the proteasome system in Parkinson's disease is supported by the presence of ubiquitinated protein, 11S RP and 19S RP in Lewy Bodies, which is the final form of protein aggregation, indicating the unsuccessful rescue from the cell to clear the aggregates.<sup>109,110</sup> To fight against decreased proteasome activity and aging, researchers have been developing new models for study and investigating small molecules that can restore proteasome activities, which will be discussed in **Chapter 1.4**. Yeast, as an example, has been used for aging studies as its proteasome is structurally similar to human's and yeast undergoes similar aging process as human cells.<sup>111–113</sup>

### **1.3 Small molecule inhibitors of proteasome.**

#### **1.3.1 Discovery of 20S proteasome inhibitors for cancer treatment.**

As mentioned in **Chapter 1.2.1** that the proteasome activity is crucial for cell survival and proliferation, cancer cells need to be more careful on maintaining the balance of protein synthesis and degradation than surrounding normal cells. Researchers have started to investigate using small molecules to inhibit the proteasome activity to treat cancer. It is hypothesized that inhibiting proteasome activities in cancer cells will induce protein accumulation and result more severe consequences like apoptosis. Currently, three small molecules have been approved by FDA for proteasome inhibition to treat multiple myeloma and they represent the development of novel chemotherapy molecules for cancer treatment.

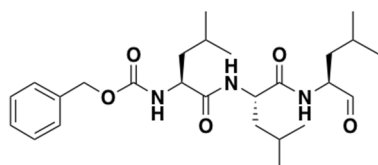


**Figure 1.8. MG-132.** MG-132 was discovered as the first covalent inhibitor of the proteasome. The aldehyde group can be attached to the catalytic threonine of  $\beta$  subunits.

After scientists better understood the NF- $\kappa$ B pathway in pathogenesis, the first proteasome inhibitor named, MG-132, was developed by modifying existing serine protease inhibitors (**Figure 1.8**).<sup>91,114,115</sup> It is a tripeptide aldehyde (carbobenzyl-leu-leu-leu-aldehyde) and is still the most widely used proteasome inhibitor in research because it is inexpensive, potent and quickly reversible. The molecule structure mimicked the preferred substrate of the chymotrypsin-like  $\beta 5$  subunit and the aldehyde group covalently inhibited the activity of the subunit by forming hemiacetal with the hydroxyl group of the active site *N*-terminal threonine. Given that the precursor of MG-132 regulated the NF- $\kappa$ B pathway in serine protease, researchers had also demonstrated that treatment of MG-132 blocked the activation of the NF- $\kappa$ B pathway by preventing the degradation of I $\kappa$ B and induced ER stress to cause NF- $\kappa$ B suppressors protein accumulation.<sup>114</sup> However, MG-132 still showed some limitations as aldehyde inhibitors had a relative short live-span and did not show activity in mice models.

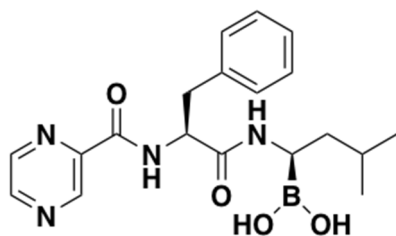


**Figure 1.9. Bortezomib.** Bortezomib was the first proteasome inhibitor approved by FDA for cancer treatment.

With the success of developing MG-132 as the first proteasome inhibitor, researchers started to investigate using other warheads for proteasome inhibitor development to acquire higher selective and bioavailability where peptide boronates were introduced. The first FDA approved small molecule proteasome inhibitor was bortezomib (Velcade) in 2003 in United States for multiple myeloma and mantle cell lymphoma treatment (**Figure 1.9**).<sup>92,116,117</sup> It was a dipeptide that presented a boronic acid warhead to bind with the  $\beta 5$  subunit of the proteasome. Unlike previously discovered aldehyde proteasome inhibitor MG-132 with a fast dissociation rate, bortezomib had a much slower dissociation rate, such that it could even be considered as an irreversible proteasome inhibitor in a period of time.<sup>118</sup> It was one of recommended treatments for multiple myeloma and research had shown bortezomib induced cell apoptosis in cancers. Similar to MG-132, bortezomib not only inhibited the NF- $\kappa$ B pathway, but it also prevented the degradation of cell cycle regulating proteins like p53. However, as the first generation proteasome inhibitor on market, bortezomib suffered off-target effects especially on other serine protease like HtrA2/Omi.<sup>119</sup> Heart related

damage after administrating bortezomib was also observed among patients indicating other potential off-target effects from bortezomib.<sup>120–122</sup> Bortezomib had also been reported to inhibit the caspase-like  $\beta 1$  subunit and trypsin-like  $\beta 2$  subunit at higher concentration of dosage.<sup>120–122</sup>

In addition to potential off-target induced side effects, some patients administrating bortezomib also acquired drug resistance. The exact mechanism of resistance development was still under investigation, but several phenomena were observed. Overexpression of the  $\beta 5$  and  $\beta 5$  mutant subunits with Ala49Thr were found in bortezomib resistant patients where researchers had hypothesized that these overexpressed  $\beta 5$  subunits were used as “decoys” to bind with bortezomib and attenuate inhibition effect.<sup>123–125</sup> These bortezomib-resistant cells also displayed significant resistance to other peptide-based proteasome inhibitors making them difficult to treat. It is likely that the resistance of bortezomib is acquired by a combined complex mechanism so more research is needed to further explain the detailed mechanism.

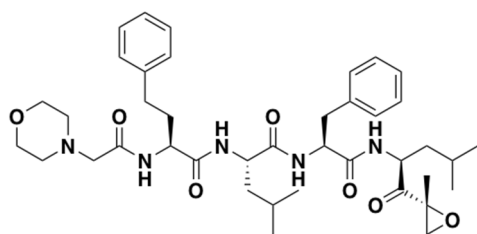


**Figure 1.10 Carfilzomib.** Carfilzomib was discovered as the second-generation proteasome inhibitor.

The off-target and drug resistance problem led some research groups to focus on developing second-generation proteasome inhibitors with better selectivity and potency where carfilzomib was discovered (**Figure 1.10**). Using an epoxyketone warhead, carfilzomib showed better selectivity and potency to proteasome inhibition. Unlike aldehyde and boronate proteasome inhibitors, the

epoxyketone warhead formed a morpholine ring when reacting with the active N-terminal threonine of the  $\beta 5$  subunit resulting in an irreversible proteasome activity inhibition. It was approved in 2012 by FDA for patients with multiple myeloma. Side effects have also been observed in patients as well as drug resistance of carfilzomib.<sup>119,126</sup>

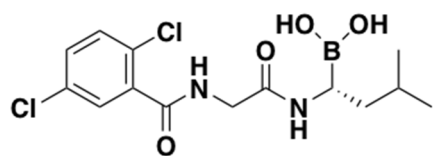


**Figure 1.11. Ixazomib.** Ixazomib was the first orally available proteasome inhibitor on market.

Finally, ixazomib was approved by FDA in 2015 to treat multiple myeloma as the third proteasome inhibitor (**Figure 1.11**). Ixazomib was a second-generation proteasome inhibitor and it was a boronic acid derivative just like bortezomib. It inhibited proteasome activity similarly to bortezomib but with a much faster dissociation rate than bortezomib. The biggest

advantage of applying ixazomib for multiple myeloma treatment was its oral availability as the previous two proteasome inhibitors had to be administrated through injection. The molecule was

made into a citrate prodrug where upon administration the citrate was hydrolyzed to release the ixazomib.<sup>127,128</sup> Ixazomib is friendly for elder or frail patients with limited access to frequent clinic appointments.

### 1.3.2 Discovery of 19S RP inhibitors.

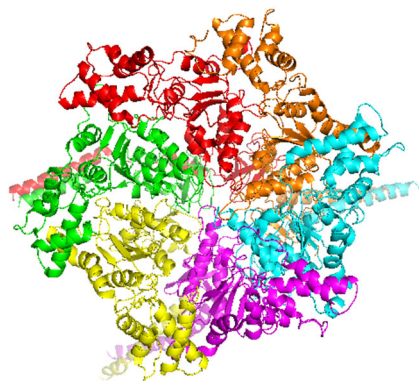


**Figure 1.12. 19S base ATPase ring.** Bottom view of the 19S base ATPase ring. A heterohexameric complex responsible for target protein tertiary structure removal and gate opening of the 20S CP.

As mentioned in **Chapter 1.3.1**, currently the FDA has approved proteasome inhibitors that only target the 20S CP, specifically the chymotrypsin-like  $\beta 5$  subunit. However, off-target effect and drug resistance effects have been observed among patients administrating these proteasome inhibitors.<sup>118,124</sup> Proteasome is a macromolecular protein complex with multiple subunits, and the 19S RP is an important component of the 26S proteasome as described in **Chapter 1.1.3** to recognize the ubiquitinated protein, unfold the target protein and translocate the target polypeptide into the 20S CP for degradation. Therefore, researchers have turned to focus on developing small molecule inhibitors to disrupt the 19S RP function and eventually affect the proteasome activity.

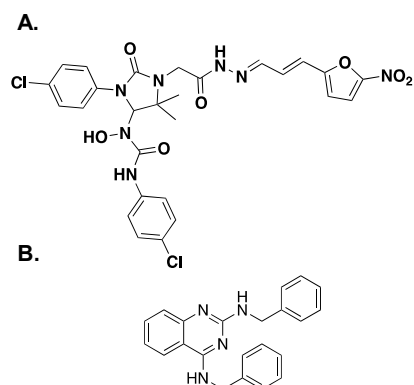


**Figure 1.13. p97 inhibitors.** (A) EerI was discovered in 2004. (B) DBE-Q was discovered in 2011.

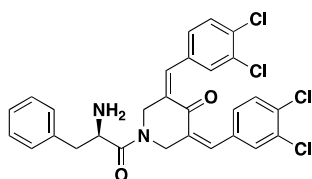
The 19S RP can be divided into the lid and the base parts where the base is composed of Rpt-1 to Rpt-6 ATPases and the lid is composed of other 19S RP subunits (**Figure 1.12**). The ATPases of the base are classified as the AAA ATPase and the proteins in this family are highly conserved from archaeal to eukaryotic cells.<sup>43,44</sup> The Rpt-1 through Rpt-6 form a heterohexameric ring-like structure sitting on top of the  $\alpha$  ring. Currently, there was only one known compound, RIP-1, screened from a one-bead-one-compound library that targeted Rpt-4.<sup>129</sup> However, further research of the compound is needed

to determine if the compound really inhibits Rpt-4 function and contribute to observed cell toxicity.

Other than the Rpt ATPase ring incorporated into the 26S proteasome, p97 is another ATPase complex that is highly involved in the UPS. However, p97 is not “fixed” onto proteasome

for its function. Instead, p97 complex is considered as the transportation protein that “carries” the ubiquitinated protein to the proteasome.<sup>130–132</sup> Unlike ATPase ring on the 19S RP made of six different subunits, p97 forms a homohexameric structure consists of a N-terminal domain, two ATPase domains and a C-terminal domain.<sup>133</sup> Research of investigating p97 inhibitors had been more successful comparing to the Rpt subunit inhibitor study.<sup>134</sup> Eeyarestatin I (EerI) was discovered in 2004 that showed the ability to trigger MHC-I turnover and recruited p97 to interact with ER (**Figure 1.13A**). Cell death observed when treated with EerI was similar to that caused by bortezomib.<sup>135–137</sup> DBeQ was discovered later in 2011 during competitive ATP inhibition assay (**Figure 1.13B**). This molecule was found to be selective towards p97. Several analogs of DBeQ had been reported that were orally bioavailable and can selectively inhibit the ATPase domain of p97 to induce proteotoxic stress.<sup>138</sup>

**A.**



**B.**

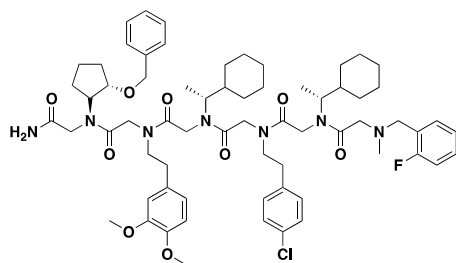


**Figure 1.14. Rpn-13 inhibitors.** (A) RA190 was discovered in 2013. (B) KDT-11 was discovered in 2015.

The lid of the 19S RP contains all other non-ATPase subunits, and inhibitors of several Rpn subunits have been discovered. The 26S proteasome has two ubiquitin receptors: Rpn-10 and Rpn-13. These two subunits facilitate the 19S RP function as they recognize the poly-ubiquitin chain on the target protein. Despite the existence of two ubiquitin receptors, Rpn-10 is an essential subunit where mutation of Rpn-10's ubiquitin-interacting-motifs result in lethal consequences in mouse studies.<sup>58,139,140</sup> Although Rpn-13 is nonessential for cell survival in normal cells, Rpn-13

knockdown by small interfering RNA still significantly decrease the viability in multiple myeloma cells highlighting the possibility of inhibiting Rpn-13 function as potential cancer treatment.<sup>57</sup> Earlier research has shown that Rpn-10 undergoes Rsp-5 mediated mono-ubiquitination resulting in subunit deactivation. Subsequently de-ubiquitination of Rpn-10 will then result in subunit activation. It is hypothesized that the target protein either binds to Rpn-10 first then Rpn-13 or binds cooperatively to both subunits.<sup>59,139</sup> However, Rpn-10 inhibitor research tends to be difficult since Rpn-10 is an essential subunit of the proteasome and inhibiting Rpn-10 could lead to severe consequences to healthy cells. On the other hand, there are two inhibitors of Rpn-13 discovered. RA190 was discovered in 2013 and it is a covalent inhibitor of Rpn-13. It

covalently bound to Cys88 on the PRU domain of Rpn-13 via Michael addition (**Figure 1.14A**). It was observed to induce ubiquitinated protein accumulation and eventually triggered apoptosis in multiple myeloma cells. RA190 had shown promising anticancer activity in multiple myeloma and can overcome bortezomib-resistance.<sup>56</sup>

Another noncovalent reversible inhibitor of Rpn-13 was KDT-11 discovered in 2015 through a one-bead-one-compound peptoid library screening (**Figure 1.14B**). It was also observed to induce ubiquitinated protein accumulation in multiple myeloma cells and resulted in cell apoptosis. Although the binding site of KDT-11 remains unknown, research had shown that it did not bind to the same surface as RA190 or Lys48-linked ubiquitin chains. Due to the fact that KDT-11 is a 6-mer peptoid with poor solubility in water, further improvement on physical properties of KDT-11 is required for future *in vivo* studies.<sup>141</sup>

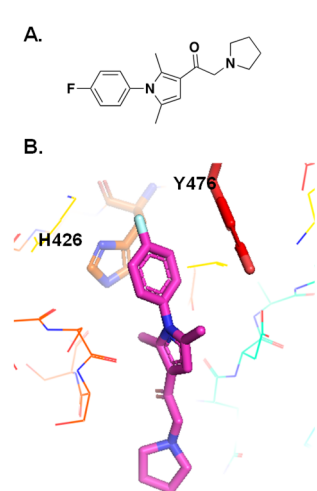


**Figure 1.15 F. Rpn-13 inhibitors.** (A) Structure of IU1 (B) Co-crystal structure of IU1 with USP14.

Rpn-10 and Rpn-13 are the ubiquitin receptor proteins of the 19S RP, other proteins are required for de-ubiquitination of the target protein. Three de-ubiquitinases (DUB) are involved in the process including USP14, Uch37 and Rpn-11 where both Uch37 and USP14 are thiol protease recruited to the 19S RP and released after de-ubiquitination while Rpn-11 is an intrinsic 19S RP subunit. Although all three proteins function as DUBs, they act differently to remove the ubiquitin chain from the target protein. The Uch37 is activated when binding to Rpn-13 and is only capable of trimming small adduct from ubiquitin. USP14 binds to the Rpn-1 subunit and can remove di and tri or the entire ubiquitin chain from the target protein. Rpn-11 is different from both USP14 and Uch37 as research has shown that the early removal of the ubiquitin chain from the target protein will weaken the binding of the substrate to the 19S RP. Rpn-11 removes at the proximal end of the poly-ubiquitin chain and is proposed that the de-ubiquitination by Rpn-11 is started after the target protein is committed to degradation when the 19S RP ATPase ring has engaged with 20S CP gate opening and the substrate translocation.<sup>11,49,142–145</sup>

IU1 was discovered from a fluorescence assay screening where it was found to preferentially bind USP14 (**Figure 1.15**). Recent research demonstrated the inhibition mechanism of IU1 using co-crystal structure of IU1 with the catalytic domain of USP14 where the small molecule bound

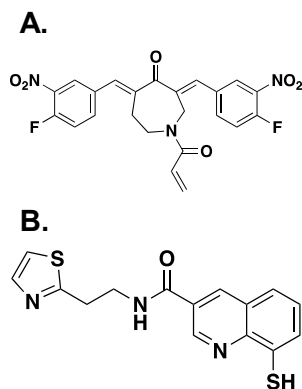


Figure 1.16. **Other USP14 and Rpn11 inhibitors.** (A) VLX1570 was discovered in 2008 (B) Capzimin was discovered in 2017.

to the catalytic cysteine residue of the USP14 and blocked ubiquitin binding.<sup>146–150</sup> The co-crystal structure also facilitated the optimization of IU1 to IU1-248 which showed a ten-fold improvement in potency. Other USP14 inhibitor had also been developed like VLX1570, using  $\alpha$ ,  $\beta$ -unsaturated ketone as Michael acceptor for catalytic cysteine binding, similar to the binding mechanism of RA190 onto Rpn-13 (**Figure 1.16A**).<sup>151</sup> Uch37 currently has no selective inhibitors discovered. The precursor of VLX1570, b-AP15 was discovered as a dual inhibitor of both Uch37 and USP14.<sup>152</sup> Understanding the mechanism of current non-selective Uch37 inhibitors is necessary to advance future studies into selective Uch37 inhibitor.

Quinoline-8-thiol (8TQ) was discovered during a fragment-based drug screening of Rpn-11 binder.<sup>60</sup> Structural optimization of 8TQ to increase selectivity and potency led to the discovery of capzimin (**Figure 1.16B**). Treatment of capzimin was shown to induce ubiquitinated protein accumulation and the expression levels of HIF-1 $\alpha$  and p53.<sup>153,154</sup> However, further *in vivo* studies on capzimin is required to evaluate the impact of the small molecule.

## 1.4 Conclusion.

Proteasome is a crucial protein complex in cells to maintain the proteostasis and regulate various cellular process.<sup>1,2</sup> Composed by a 20S CP and a 19S RP, the proteasome utilize the 19S RP to recognize the poly-ubiquitinated protein and the 20S CP degrades the protein into peptide fragments.<sup>11–13</sup> The activity of proteasome is strictly regulated to keep the cells healthy and sustainable. Therefore, proteasome malfunction could lead to serious consequences including tumorigenesis, cancer progression, aging and neurodegenerative diseases.<sup>96–98</sup> To combat with various proteasome dysfunction induced diseases, scientists have devoted tremendous amount of effort in understanding the UPS and how proteasome works.

In some cancer cell lines, proteasome activity is significantly increased to satisfy the unlimited demand for cell metabolism and proliferation. Inhibiting 20S CP activity becomes a potential therapeutic method of treating these cancers. The approval of bortezomib, carfilzomib and ixozomib by FDA have demonstrated the success in developing small molecule covalent

inhibitors of the 20S CP that can significantly interfere with cellular proteostasis and induce cancer cell apoptosis.<sup>91,114,115</sup> However, drug resistance has also been observed among patients administrating these proteasome inhibitors, raising the demand for novel proteasome inhibitor discovery and development.

19S RP on the other hand, has gained more attention in recent research for inhibitor development. Although 19S RP does not degrade protein, it is still considered as a vital component of the proteasome for its assistant function on the 20S CP. Multiple inhibitors of 19S RP has been discovered targeting either the base or the lid subunits. However, none of the inhibitors has been approved by FDA for cancer treatment. Further investigation into the 19S RP is required to fully understand the role of each subunit of the 19S RP for future drug discovery.

When cell ages, the proteasome activity also decrease accordingly and could potentially result in neurodegenerative diseases. Various mechanisms have been proposed to explain the deterioration of proteasome function but a comprehensive theory is still missing. Restoring the proteasome activity with small molecules is a promising therapeutic approach to alleviate the impact of proteasome function decrease. Gating opening small molecules like SDS, TCH-165 have been discovered to increase all three protease-like activities on the proteasome.<sup>155</sup> Other small molecule stimulators like MMk-886, AM-404 and miconazole are also discovered using newly developed proteasome probes and some have shown promising stimulation effect on proteasome activities.<sup>156,157</sup> However, stimulating proteasome activity is still a relative underexplored field. Multiple questions remain to be answered: (1) Can these small molecules induce protein degradation *in vivo*. (2) Will increasing proteasome activity benefit proteasome activity decreased neuron cells but deprave normal tissue cells. (3) Will increasing proteasome activity break the balance among tumor suppressor proteins and result in tumorigenesis etc. It is important to have multiple proteasome stimulators with various stimulating ability to be used as tools for cross checking and future stimulator evaluation.

The development of proteasome inhibitors and stimulators have demonstrated proteasome as a highly potential candidate for small molecule development. Either to inhibit or stimulate the proteasome depends on the circumstance and the goal to achieve. With advanced understanding of the proteasome, drug discovery and development will take place in a more convenient and efficient way.

## 1.5 Reference.

- (1) Fuertes, G.; Villarroya, A.; Knecht, E. Role of Proteasomes in the Degradation of Short-Lived Proteins in Human Fibroblasts under Various Growth Conditions. *The International Journal of Biochemistry & Cell Biology* **2003**, *35* (5), 651–664. [https://doi.org/10.1016/S1357-2725\(02\)00382-5](https://doi.org/10.1016/S1357-2725(02)00382-5).
- (2) Ciechanover, A.; Schwartz, A. L. The Ubiquitin-Proteasome Pathway: The Complexity and Myriad Functions of Proteins Death. *Proceedings of the National Academy of Sciences* **1998**, *95* (6), 2727–2730. <https://doi.org/10.1073/pnas.95.6.2727>.
- (3) Swatek, K. N.; Komander, D. Ubiquitin Modifications. *Cell Research* **2016**, *26* (4), 399–422. <https://doi.org/10.1038/cr.2016.39>.
- (4) Strous, G. J.; Govers, R. The Ubiquitin-Proteasome System and Endocytosis. *7*.
- (5) Scheffner, M.; Nuber, U.; Huibregtse, J. M. Protein Ubiquitination Involving an E1–E2–E3 Enzyme Ubiquitin Thioester Cascade. *Nature* **1995**, *373* (6509), 81–83. <https://doi.org/10.1038/373081a0>.
- (6) Lecker, S. H.; Goldberg, A. L.; Mitch, W. E. Protein Degradation by the Ubiquitin–Proteasome Pathway in Normal and Disease States. *JASN* **2006**, *17* (7), 1807–1819. <https://doi.org/10.1681/ASN.2006010083>.
- (7) Churcher, I. Protac-Induced Protein Degradation in Drug Discovery: Breaking the Rules or Just Making New Ones? *Journal of Medicinal Chemistry* **2018**, *61* (2), 444–452. <https://doi.org/10.1021/acs.jmedchem.7b01272>.
- (8) Ottis, P.; Toure, M.; Cromm, P. M.; Ko, E.; Gustafson, J. L.; Crews, C. M. Assessing Different E3 Ligases for Small Molecule Induced Protein Ubiquitination and Degradation. *ACS Chemical Biology* **2017**, *12* (10), 2570–2578. <https://doi.org/10.1021/acscchembio.7b00485>.
- (9) Ikeda, F.; Crosetto, N.; Dikic, I. What Determines the Specificity and Outcomes of Ubiquitin Signaling? *Cell* **2010**, *143* (5), 677–681. <https://doi.org/10.1016/j.cell.2010.10.026>.
- (10) Deol, K. K.; Lorenz, S.; Strieter, E. R. Enzymatic Logic of Ubiquitin Chain Assembly. *Front. Physiol.* **2019**, *10*, 835. <https://doi.org/10.3389/fphys.2019.00835>.
- (11) Amerik, A. Y.; Hochstrasser, M. Mechanism and Function of Deubiquitinating Enzymes. *Biochimica et Biophysica Acta (BBA) - Molecular Cell Research* **2004**, *1695* (1–3), 189–207. <https://doi.org/10.1016/j.bbamcr.2004.10.003>.
- (12) Chen, S.; Wu, J.; Lu, Y.; Ma, Y.-B.; Lee, B.-H.; Yu, Z.; Ouyang, Q.; Finley, D. J.; Kirschner, M. W.; Mao, Y. Structural Basis for Dynamic Regulation of the Human 26S Proteasome. *Proceedings of the National Academy of Sciences* **2016**, *113* (46), 12991–12996. <https://doi.org/10.1073/pnas.1614614113>.

- (13) Ding, Z.; Xu, C.; Sahu, I.; Wang, Y.; Fu, Z.; Huang, M.; Wong, C. C. L.; Glickman, M. H.; Cong, Y. Structural Snapshots of 26S Proteasome Reveal Tetraubiquitin-Induced Conformations. *Molecular Cell* **2019**, *73* (6), 1150–1161.e6. <https://doi.org/10.1016/j.molcel.2019.01.018>.
- (14) Ciechanover, A. The Ubiquitin-Proteasome Proteolytic Pathway. *Cell* **1994**, *79* (1), 13–21. [https://doi.org/10.1016/0092-8674\(94\)90396-4](https://doi.org/10.1016/0092-8674(94)90396-4).
- (15) Bedford, L.; Paine, S.; Sheppard, P. W.; Mayer, R. J.; Roelofs, J. Assembly, Structure, and Function of the 26S Proteasome. *Trends in Cell Biology* **2010**, *20* (7), 391–401. <https://doi.org/10.1016/j.tcb.2010.03.007>.
- (16) Kloetzel, P.-M. The Proteasome and MHC Class I Antigen Processing. *Biochimica et Biophysica Acta (BBA) - Molecular Cell Research* **2004**, *1695* (1–3), 225–233. <https://doi.org/10.1016/j.bbamcr.2004.10.004>.
- (17) Leone, P.; Shin, E.-C.; Perosa, F.; Vacca, A.; Dammacco, F.; Racanelli, V. MHC Class I Antigen Processing and Presenting Machinery: Organization, Function, and Defects in Tumor Cells. *JNCI Journal of the National Cancer Institute* **2013**, *105* (16), 1172–1187. <https://doi.org/10.1093/jnci/djt184>.
- (18) Sijts, E. J. A. M.; Kloetzel, P.-M. The Role of the Proteasome in the Generation of MHC Class I Ligands and Immune Responses. *Cell. Mol. Life Sci.* **2011**, *68* (9), 1491–1502. <https://doi.org/10.1007/s00018-011-0657-y>.
- (19) Kloetzel, P.-M. Antigen Processing by the Proteasome. *Nature Reviews Molecular Cell Biology* **2001**, *2* (3), 179–188. <https://doi.org/10.1038/35056572>.
- (20) McCarthy, M. K.; Weinberg, J. B. The Immunoproteasome and Viral Infection: A Complex Regulator of Inflammation. *Front. Microbiol.* **2015**, *6*. <https://doi.org/10.3389/fmicb.2015.00021>.
- (21) Lázaro, S.; Gamarra, D.; Del Val, M. Proteolytic Enzymes Involved in MHC Class I Antigen Processing: A Guerrilla Army That Partners with the Proteasome. *Molecular Immunology* **2015**, *68* (2), 72–76. <https://doi.org/10.1016/j.molimm.2015.04.014>.
- (22) Loureiro, J.; Ploegh, H. L. Antigen Presentation and the Ubiquitin-Proteasome System in Host–Pathogen Interactions. In *Advances in Immunology*; Elsevier, 2006; Vol. 92, pp 225–305. [https://doi.org/10.1016/S0065-2776\(06\)92006-9](https://doi.org/10.1016/S0065-2776(06)92006-9).
- (23) Adams, J. The Proteasome in Cell-Cycle Regulation. In *Proteasome Inhibitors in Cancer Therapy*; Adams, J., Ed.; Humana Press: Totowa, NJ, 2004; pp 77–84. [https://doi.org/10.1007/978-1-59259-794-9\\_6](https://doi.org/10.1007/978-1-59259-794-9_6).
- (24) Bassermann, F.; Eichner, R.; Pagano, M. The Ubiquitin Proteasome System — Implications for Cell Cycle Control and the Targeted Treatment of Cancer. *Biochimica et Biophysica Acta (BBA) - Molecular Cell Research* **2014**, *1843* (1), 150–162. <https://doi.org/10.1016/j.bbamcr.2013.02.028>.

- (25) Karpov, D. S.; Spasskaya, D. S.; Tutyaeva, V. V.; Mironov, A. S.; Karpov, V. L. Proteasome Inhibition Enhances Resistance to DNA Damage via Upregulation of Rpn4-Dependent DNA Repair Genes. *FEBS Letters* **2013**, 587 (18), 3108–3114. <https://doi.org/10.1016/j.febslet.2013.08.007>.
- (26) Moiseeva, T. N.; Bottrill, A.; Melino, G.; Barlev, N. A. DNA Damage-Induced Ubiquitylation of Proteasome Controls Its Proteolytic Activity. *Oncotarget* **2013**, 4 (9), 1338–1348. <https://doi.org/10.18632/oncotarget.1060>.
- (27) Salceda, S.; Caro, J. Hypoxia-Inducible Factor 1 $\alpha$  (HIF-1 $\alpha$ ) Protein Is Rapidly Degraded by the Ubiquitin-Proteasome System under Normoxic Conditions. *Journal of Biological Chemistry* **1997**, 272 (36), 22642–22647. <https://doi.org/10.1074/jbc.272.36.22642>.
- (28) Almond, J.; Cohen, G. The Proteasome: A Novel Target for Cancer Chemotherapy. *Leukemia* **2002**, 16 (4), 433–443. <https://doi.org/10.1038/sj.leu.2402417>.
- (29) Dantuma, N. P.; Bott, L. C. The Ubiquitin-Proteasome System in Neurodegenerative Diseases: Precipitating Factor, yet Part of the Solution. *Frontiers in Molecular Neuroscience* **2014**, 7. <https://doi.org/10.3389/fnmol.2014.00070>.
- (30) Gong, B.; Radulovic, M.; Figueiredo-Pereira, M. E.; Cardozo, C. The Ubiquitin-Proteasome System: Potential Therapeutic Targets for Alzheimer's Disease and Spinal Cord Injury. *Front. Mol. Neurosci.* **2016**, 9. <https://doi.org/10.3389/fnmol.2016.00004>.
- (31) Deng, L.; Meng, T.; Chen, L.; Wei, W.; Wang, P. The Role of Ubiquitination in Tumorigenesis and Targeted Drug Discovery. *Sig Transduct Target Ther* **2020**, 5 (1), 11. <https://doi.org/10.1038/s41392-020-0107-0>.
- (32) Coux, O.; Tanaka, K.; Goldberg, A. L. STRUCTURE AND FUNCTIONS OF THE 20S AND 26S PROTEASOMES. 49.
- (33) Tanaka, K. The Proteasome: Overview of Structure and Functions. *Proceedings of the Japan Academy, Series B* **2009**, 85 (1), 12–36. <https://doi.org/10.2183/pjab.85.12>.
- (34) Hoffman, L.; Rechsteiner, M. Nucleotidase Activities of the 26 S Proteasome and Its Regulatory Complex. *Journal of Biological Chemistry* **1996**, 271 (51), 32538–32545. <https://doi.org/10.1074/jbc.271.51.32538>.
- (35) Lander, G. C.; Martin, A.; Nogales, E. The Proteasome under the Microscope: The Regulatory Particle in Focus. *Current Opinion in Structural Biology* **2013**, 23 (2), 243–251. <https://doi.org/10.1016/j.sbi.2013.02.004>.
- (36) Rosenzweig, R.; Osmulski, P. A.; Gaczynska, M.; Glickman, M. H. The Central Unit within the 19S Regulatory Particle of the Proteasome. *Nat Struct Mol Biol* **2008**, 15 (6), 573–580. <https://doi.org/10.1038/nsmb.1427>.

- (37) Ehlinger, A.; Walters, K. J. Structural Insights into Proteasome Activation by the 19S Regulatory Particle. *Biochemistry* **2013**, *52* (21), 3618–3628. <https://doi.org/10.1021/bi400417a>.
- (38) Dong, Y.; Zhang, S.; Wu, Z.; Li, X.; Wang, W. L.; Zhu, Y.; Stoilova-McPhie, S.; Lu, Y.; Finley, D.; Mao, Y. Cryo-EM Structures and Dynamics of Substrate-Engaged Human 26S Proteasome. *Nature* **2018**. <https://doi.org/10.1038/s41586-018-0736-4>.
- (39) Motosugi, R.; Murata, S. Dynamic Regulation of Proteasome Expression. *Front. Mol. Biosci.* **2019**, *6*, 30. <https://doi.org/10.3389/fmolb.2019.00030>.
- (40) Auld, K. L.; Silver, P. A. Transcriptional Regulation by the Proteasome as a Mechanism for Cellular Protein. *Cell Cycle* **2006**, *5* (14), 1503–1505. <https://doi.org/10.4161/cc.5.14.2979>.
- (41) Thibaut, T. A.; Smith, D. M. A Practical Review of Proteasome Pharmacology. *Pharmacol Rev* **2019**, *71* (2), 170–197. <https://doi.org/10.1124/pr.117.015370>.
- (42) Tanaka, K. The Proteasome: Overview of Structure and Functions. *Proceedings of the Japan Academy, Series B* **2009**, *85* (1), 12–36. <https://doi.org/10.2183/pjab.85.12>.
- (43) Bar-Nun, S.; Glickman, M. H. Proteasomal AAA-ATPases: Structure and Function. *Biochimica et Biophysica Acta (BBA) - Molecular Cell Research* **2012**, *1823* (1), 67–82. <https://doi.org/10.1016/j.bbamcr.2011.07.009>.
- (44) Beyer, A. Sequence Analysis of the AAA Protein Family. *Protein Science* **2008**, *6* (10), 2043–2058. <https://doi.org/10.1002/pro.5560061001>.
- (45) Snider, J.; Thibault, G.; Houry, W. A. The AAA+ Superfamily of Functionally Diverse Proteins. *Genome Biology* **2008**, *9* (4), 216. <https://doi.org/10.1186/gb-2008-9-4-216>.
- (46) Iyer, L. M.; Leipe, D. D.; Koonin, E. V.; Aravind, L. Evolutionary History and Higher Order Classification of AAA+ ATPases. *Journal of Structural Biology* **2004**, *146* (1–2), 11–31. <https://doi.org/10.1016/j.jsb.2003.10.010>.
- (47) Ehlinger, A.; Park, S.; Fahmy, A.; Lary, J. W.; Cole, J. L.; Finley, D.; Walters, K. J. Conformational Dynamics of the Rpt6 ATPase in Proteasome Assembly and Rpn14 Binding. *Structure* **2013**, *21* (5), 753–765. <https://doi.org/10.1016/j.str.2013.02.021>.
- (48) Liu, X.; Xiao, W.; Zhang, Y.; Wiley, S. E.; Zuo, T.; Zheng, Y.; Chen, N.; Chen, L.; Wang, X.; Zheng, Y.; Huang, L.; Lin, S.; Murphy, A. N.; Dixon, J. E.; Xu, P.; Guo, X. Reversible Phosphorylation of Rpn1 Regulates 26S Proteasome Assembly and Function. *Proc Natl Acad Sci USA* **2020**, *117* (1), 328–336. <https://doi.org/10.1073/pnas.1912531117>.
- (49) Shi, Y.; Chen, X.; Elsasser, S.; Stocks, B. B.; Tian, G.; Lee, B.-H.; Shi, Y.; Zhang, N.; de Poot, S. A. H.; Tuebing, F.; Sun, S.; Vannoy, J.; Tarasov, S. G.; Engen, J. R.; Finley, D.; Walters, K. J. Rpn1 Provides Adjacent Receptor Sites for Substrate Binding and

- Deubiquitination by the Proteasome. *Science* **2016**, *351* (6275), aad9421–aad9421. <https://doi.org/10.1126/science.aad9421>.
- (50) Rosenzweig, R.; Bronner, V.; Zhang, D.; Fushman, D.; Glickman, M. H. Rpn1 and Rpn2 Coordinate Ubiquitin Processing Factors at Proteasome\*. *Journal of Biological Chemistry* **2012**, *287* (18), 14659–14671. <https://doi.org/10.1074/jbc.M111.316323>.
  - (51) Zhang, W.; Zhao, C.; Hu, Y.; Jin, C. NMR <sup>1</sup>H, <sup>13</sup>C, <sup>15</sup>N Backbone and Side Chain Resonance Assignment of the N-Terminal Domain of Yeast Proteasome Lid Subunit Rpn5. *Biomol NMR Assign* **2019**, *13* (1), 1–4. <https://doi.org/10.1007/s12104-018-9840-5>.
  - (52) Kim, H. T.; Goldberg, A. L. UBL Domain of Usp14 and Other Proteins Stimulates Proteasome Activities and Protein Degradation in Cells. *Proc Natl Acad Sci USA* **2018**, *115* (50), E11642–E11650. <https://doi.org/10.1073/pnas.1808731115>.
  - (53) Estrin, E.; Lopez-Blanco, J. R.; Chacón, P.; Martin, A. Formation of an Intricate Helical Bundle Dictates the Assembly of the 26S Proteasome Lid. *Structure* **2013**, *21* (9), 1624–1635. <https://doi.org/10.1016/j.str.2013.06.023>.
  - (54) Bai, M.; Zhao, X.; Sahara, K.; Ohte, Y.; Hirano, Y.; Kaneko, T.; Yashiroda, H.; Murata, S. In-Depth Analysis of the Lid Subunits Assembly Mechanism in Mammals. *Biomolecules* **2019**, *9* (6), 213. <https://doi.org/10.3390/biom9060213>.
  - (55) Sharon, M.; Taverner, T.; Ambroggio, X. I.; Deshaies, R. J.; Robinson, C. V. Structural Organization of the 19S Proteasome Lid: Insights from MS of Intact Complexes. *PLoS Biology* **2006**, *4* (8), e267. <https://doi.org/10.1371/journal.pbio.0040267>.
  - (56) Anchoori, R. K.; Karanam, B.; Peng, S.; Wang, J. W.; Jiang, R.; Tanno, T.; Orłowski, R. Z.; Matsui, W.; Zhao, M.; Rudek, M. A.; Hung, C.; Chen, X.; Walters, K. J.; Roden, R. B. S. A Bis-Benzylidene Piperidone Targeting Proteasome Ubiquitin Receptor RPN13/ADRM1 as a Therapy for Cancer. *Cancer Cell* **2013**, *24* (6), 791–805. <https://doi.org/10.1016/j.ccr.2013.11.001>.
  - (57) Husnjak, K.; Elsasser, S.; Zhang, N.; Chen, X.; Randles, L.; Shi, Y.; Hofmann, K.; Walters, K. J.; Finley, D.; Dikic, I. Proteasome Subunit Rpn13 Is a Novel Ubiquitin Receptor. *Nature* **2008**, *453* (7194), 481–488. <https://doi.org/10.1038/nature06926>.
  - (58) Smalle, J.; Kurepa, J.; Yang, P.; Emborg, T. J.; Babiychuk, E.; Kushnir, S.; Vierstra, R. D. The Pleiotropic Role of the 26S Proteasome Subunit RPN10 in Arabidopsis Growth and Development Supports a Substrate-Specific Function in Abscissic Acid Signaling. *The Plant Cell* **2003**, *15* (4), 965–980. <https://doi.org/10.1105/tpc.009217>.
  - (59) Isasa, M.; Katz, E. J.; Kim, W.; Yugo, V.; González, S.; Kirkpatrick, D. S.; Thomson, T. M.; Finley, D.; Gygi, S. P.; Crosas, B. Monoubiquitination of RPN10 Regulates Substrate Recruitment to the Proteasome. *Molecular Cell* **2010**, *38* (5), 733–745. <https://doi.org/10.1016/j.molcel.2010.05.001>.

- (60) Perez, C.; Li, J.; Parlati, F.; Rouffet, M.; Ma, Y.; Mackinnon, A. L.; Chou, T.-F.; Deshaies, R. J.; Cohen, S. M. Discovery of an Inhibitor of the Proteasome Subunit Rpn11. *Journal of Medicinal Chemistry* **2017**, *60* (4), 1343–1361. <https://doi.org/10.1021/acs.jmedchem.6b01379>.
- (61) Livneh, I.; Cohen-Kaplan, V.; Cohen-Rosenzweig, C.; Avni, N.; Ciechanover, A. The Life Cycle of the 26S Proteasome: From Birth, through Regulation and Function, and onto Its Death. *Cell Research* **2016**, *26* (8), 869–885. <https://doi.org/10.1038/cr.2016.86>.
- (62) The Proteasome Regulator PA28 $\alpha/\beta$  Can Enhance Antigen Presentation without Affecting 20S Proteasome Subunit Composition. *Eur. J. Immunol.* **8**.
- (63) Wójcik, C.; Tanaka, K.; Paweletz, N.; Naab, U.; Wilk, S. Proteasome Activator (PA28) Subunits,  $\alpha$ ,  $\beta$  and  $\gamma$  (Ki Antigen) in NT2 Neuronal Precursor Cells and HeLa S3 Cells. *European Journal of Cell Biology* **1998**, *77* (2), 151–160. [https://doi.org/10.1016/S0171-9335\(98\)80083-6](https://doi.org/10.1016/S0171-9335(98)80083-6).
- (64) de Graaf, N.; van Helden, M. J. G.; Textoris-Taube, K.; Chiba, T.; Topham, D. J.; Kloetzel, P.-M.; Zaiss, D. M. W.; Sijts, A. J. A. M. PA28 and the Proteasome Immunosubunits Play a Central and Independent Role in the Production of MHC Class I-Binding Peptides in Vivo. *Eur. J. Immunol.* **2011**, *41* (4), 926–935. <https://doi.org/10.1002/eji.201041040>.
- (65) Sijts, A.; Sun, Y.; Janek, K.; Kral, S.; Paschen, A.; Schadendorf, D.; Kloetzel, P.-M. The Role of the Proteasome Activator PA28 in MHC Class I Antigen Processing. *Molecular Immunology* **2002**, *39* (3–4), 165–169. [https://doi.org/10.1016/S0161-5890\(02\)00099-8](https://doi.org/10.1016/S0161-5890(02)00099-8).
- (66) Pick, E.; Berman, T. S. Formation of Alternative Proteasomes: Same Lady, Different Cap? *FEBS Letters* **2013**, *587* (5), 389–393. <https://doi.org/10.1016/j.febslet.2013.01.014>.
- (67) Latham, M. P.; Sekhar, A.; Kay, L. E. Understanding the Mechanism of Proteasome 20S Core Particle Gating. *Proceedings of the National Academy of Sciences* **2014**, *111* (15), 5532–5537. <https://doi.org/10.1073/pnas.1322079111>.
- (68) Kumar Deshmukh, F.; Yaffe, D.; Olshina, M.; Ben-Nissan, G.; Sharon, M. The Contribution of the 20S Proteasome to Proteostasis. *Biomolecules* **2019**, *9* (5), 190. <https://doi.org/10.3390/biom9050190>.
- (69) Kunjappu, M. J.; Hochstrasser, M. Assembly of the 20S Proteasome. *Biochimica et Biophysica Acta (BBA) - Molecular Cell Research* **2014**, *1843* (1), 2–12. <https://doi.org/10.1016/j.bbamcr.2013.03.008>.
- (70) Rabl, J.; Smith, D. M.; Yu, Y.; Chang, S.-C.; Goldberg, A. L.; Cheng, Y. Mechanism of Gate Opening in the 20S Proteasome by the Proteasomal ATPases. *Molecular Cell* **2008**, *30* (3), 360–368. <https://doi.org/10.1016/j.molcel.2008.03.004>.
- (71) Eralles, J.; Coffino, P. Ubiquitin-Independent Proteasomal Degradation. *Biochimica et Biophysica Acta (BBA) - Molecular Cell Research* **2014**, *1843* (1), 216–221. <https://doi.org/10.1016/j.bbamcr.2013.05.008>.

- (72) Tsvetkov, P.; Reuven, N.; Shaul, Y. Ubiquitin-Independent P53 Proteasomal Degradation. *Cell Death Differ* **2010**, *17* (1), 103–108. <https://doi.org/10.1038/cdd.2009.67>.
- (73) Kalejta, R. F.; Shenk, T. Proteasome-Dependent, Ubiquitin-Independent Degradation of the Rb Family of Tumor Suppressors by the Human Cytomegalovirus Pp71 Protein. *Proceedings of the National Academy of Sciences* **2003**, *100* (6), 3263–3268. <https://doi.org/10.1073/pnas.0538058100>.
- (74) Aiken, C. T.; Kaake, R. M.; Wang, X.; Huang, L. Oxidative Stress-Mediated Regulation of Proteasome Complexes. *Molecular & Cellular Proteomics* **2011**, R110.006924. <https://doi.org/10.1074/mcp.R110.006924>.
- (75) Lin, C.-F.; Chen, C.-L.; Chien, S.-Y.; Tseng, P.-C.; Wang, Y.-C.; Tsai, T.-T. Oxidative Stress Facilitates IFN- $\gamma$ -Induced Mimic Extracellular Trap Cell Death in A549 Lung Epithelial Cancer Cells. *PLoS ONE* **2016**, *11* (8), e0162157. <https://doi.org/10.1371/journal.pone.0162157>.
- (76) Klaunig, J. E.; Wang, Z. Oxidative Stress in Carcinogenesis. *Current Opinion in Toxicology* **2018**, *7*, 116–121. <https://doi.org/10.1016/j.cotox.2017.11.014>.
- (77) Ferrington, D. A.; Gregerson, D. S. Immunoproteasomes. In *Progress in Molecular Biology and Translational Science*; Elsevier, 2012; Vol. 109, pp 75–112. <https://doi.org/10.1016/B978-0-12-397863-9.00003-1>.
- (78) Kremer, M.; Henn, A.; Kolb, C.; Basler, M.; Moebius, J.; Guillaume, B.; Leist, M.; Van den Eynde, B. J.; Groettrup, M. Reduced Immunoproteasome Formation and Accumulation of Immunoproteasomal Precursors in the Brains of Lymphocytic Choriomeningitis Virus-Infected Mice. *J.I.* **2010**, *185* (9), 5549–5560. <https://doi.org/10.4049/jimmunol.1001517>.
- (79) Kimura, H.; Caturegli, P.; Takahashi, M.; Suzuki, K. New Insights into the Function of the Immunoproteasome in Immune and Nonimmune Cells. *Journal of Immunology Research* **2015**, *2015*, 1–8. <https://doi.org/10.1155/2015/541984>.
- (80) Gavioli, R.; Gallerani, E.; Fortini, C.; Fabris, M.; Bottoni, A.; Canella, A.; Bonaccorsi, A.; Marastoni, M.; Micheletti, F.; Cafaro, A.; Rimessi, P.; Caputo, A.; Ensoli, B. HIV-1 Tat Protein Modulates the Generation of Cytotoxic T Cell Epitopes by Modifying Proteasome Composition and Enzymatic Activity. *J Immunol* **2004**, *173* (6), 3838–3843. <https://doi.org/10.4049/jimmunol.173.6.3838>.
- (81) Huang, X.; Seifert, U.; Salzmann, U.; Henklein, P.; Preissner, R.; Henke, W.; Sijts, A. J.; Kloetzel, P.-M.; Dubiel, W. The RTP Site Shared by the HIV-1 Tat Protein and the 11S Regulator Subunit  $\alpha$  Is Crucial for Their Effects on Proteasome Function Including Antigen Processing. *Journal of Molecular Biology* **2002**, *323* (4), 771–782. [https://doi.org/10.1016/S0022-2836\(02\)00998-1](https://doi.org/10.1016/S0022-2836(02)00998-1).

- (82) Seeger, M.; Ferrell, K.; Frank, R.; Dubiel, W. HIV-1 Tat Inhibits the 20 S Proteasome and Its 11 S Regulator-Mediated Activation. *Journal of Biological Chemistry* **1997**, *272* (13), 8145–8148. <https://doi.org/10.1074/jbc.272.13.8145>.
- (83) Dang, F.; Nie, L.; Wei, W. Ubiquitin Signaling in Cell Cycle Control and Tumorigenesis. *Cell Death Differ* **2021**, *28* (2), 427–438. <https://doi.org/10.1038/s41418-020-00648-0>.
- (84) Haase, V. H. The VHL/HIF Oxygen-Sensing Pathway and Its Relevance to Kidney Disease. *Kidney International* **2006**, *69* (8), 1302–1307. <https://doi.org/10.1038/sj.ki.5000221>.
- (85) Reuter, S.; Gupta, S. C.; Chaturvedi, M. M.; Aggarwal, B. B. Oxidative Stress, Inflammation, and Cancer: How Are They Linked? *Free Radical Biology and Medicine* **2010**, *49* (11), 1603–1616. <https://doi.org/10.1016/j.freeradbiomed.2010.09.006>.
- (86) Suh, K. S.; Tanaka, T.; Sarojini, S.; Nightingale, G.; Gharbaran, R.; Pecora, A.; Goy, A. The Role of the Ubiquitin Proteasome System in Lymphoma. *Critical Reviews in Oncology/Hematology* **2013**, *87* (3), 306–322. <https://doi.org/10.1016/j.critrevonc.2013.02.005>.
- (87) Csizmar, C. M.; Kim, D.-H.; Sachs, Z. The Role of the Proteasome in AML. *Blood Cancer Journal* **2016**, *6* (12), e503–e503. <https://doi.org/10.1038/bcj.2016.112>.
- (88) Siegel, R. L.; Miller, K. D.; Jemal, A. Cancer Statistics, 2017. *CA: A Cancer Journal for Clinicians* **2017**, *67* (1), 7–30. <https://doi.org/10.3322/caac.21387>.
- (89) Rajkumar, S. V.; Kumar, S. Multiple Myeloma: Diagnosis and Treatment. *Mayo Clinic Proceedings* **2016**, *91* (1), 101–119. <https://doi.org/10.1016/j.mayocp.2015.11.007>.
- (90) Jaffe, E. S.; Pittaluga, S. Aggressive B-Cell Lymphomas: A Review of New and Old Entities in the WHO Classification. *Hematology* **2011**, *2011* (1), 506–514. <https://doi.org/10.1182/asheducation-2011.1.506>.
- (91) Kisselev, A. F.; van der Linden, W. A.; Overkleeft, H. S. Proteasome Inhibitors: An Expanding Army Attacking a Unique Target. *Chemistry & Biology* **2012**, *19* (1), 99–115. <https://doi.org/10.1016/j.chembiol.2012.01.003>.
- (92) Dou, Q.; Zonder, J. Overview of Proteasome Inhibitor-Based Anti-Cancer Therapies: Perspective on Bortezomib and Second Generation Proteasome Inhibitors versus Future Generation Inhibitors of Ubiquitin-Proteasome System. *Current Cancer Drug Targets* **2014**, *14* (6), 517–536. <https://doi.org/10.2174/1568009614666140804154511>.
- (93) Muli, C. S.; Tian, W.; Trader, D. J. Small-Molecule Inhibitors of the Proteasome's Regulatory Particle. *ChemBioChem* **2019**, *20*, cbic.201900017. <https://doi.org/10.1002/cbic.201900017>.

- (94) Vilchez, D.; Saez, I.; Dillin, A. The Role of Protein Clearance Mechanisms in Organismal Ageing and Age-Related Diseases. *Nat Commun* **2014**, *5* (1), 5659. <https://doi.org/10.1038/ncomms6659>.
- (95) Saez, I.; Vilchez, D. The Mechanistic Links Between Proteasome Activity, Aging and Age-related Diseases. *CG* **2014**, *15* (1), 38–51. <https://doi.org/10.2174/138920291501140306113344>.
- (96) Santra, M.; Dill, K. A.; de Graff, A. M. R. Proteostasis Collapse Is a Driver of Cell Aging and Death. *Proc Natl Acad Sci USA* **2019**, *116* (44), 22173–22178. <https://doi.org/10.1073/pnas.1906592116>.
- (97) Taylor, R. C.; Dillin, A. Aging as an Event of Proteostasis Collapse. *Cold Spring Harbor Perspectives in Biology* **2011**, *3* (5), a004440–a004440. <https://doi.org/10.1101/cshperspect.a004440>.
- (98) Labbadia, J.; Morimoto, R. I. The Biology of Proteostasis in Aging and Disease. *Annu. Rev. Biochem.* **2015**, *84* (1), 435–464. <https://doi.org/10.1146/annurev-biochem-060614-033955>.
- (99) Rodriguez, K. A.; Osmulski, P. A.; Pierce, A.; Weintraub, S. T.; Gaczynska, M.; Buffenstein, R. A Cytosolic Protein Factor from the Naked Mole-Rat Activates Proteasomes of Other Species and Protects These from Inhibition. *Biochimica et Biophysica Acta (BBA) - Molecular Basis of Disease* **2014**, *1842* (11), 2060–2072. <https://doi.org/10.1016/j.bbadis.2014.07.005>.
- (100) Rodriguez, K. A.; Edrey, Y. H.; Osmulski, P.; Gaczynska, M.; Buffenstein, R. Altered Composition of Liver Proteasome Assemblies Contributes to Enhanced Proteasome Activity in the Exceptionally Long-Lived Naked Mole-Rat. *PLoS ONE* **2012**, *7* (5), e35890. <https://doi.org/10.1371/journal.pone.0035890>.

- (101) Triplett, J. C.; Tramutola, A.; Swomley, A.; Kirk, J.; Grimes, K.; Lewis, K.; Orr, M.; Rodriguez, K.; Cai, J.; Klein, J. B.; Perluigi, M.; Buffenstein, R.; Butterfield, D. A. Age-Related Changes in the Proteostasis Network in the Brain of the Naked Mole-Rat: Implications Promoting Healthy Longevity. *Biochimica et Biophysica Acta (BBA) - Molecular Basis of Disease* **2015**, *1852* (10), 2213–2224. <https://doi.org/10.1016/j.bbadis.2015.08.002>.
- (102) Schmidt, M.; Finley, D. Regulation of Proteasome Activity in Health and Disease. *Biochimica et Biophysica Acta (BBA) - Molecular Cell Research* **2014**, *1843* (1), 13–25. <https://doi.org/10.1016/j.bbamcr.2013.08.012>.
- (103) Hayashi, T.; Goto, S. Age-Related Changes in the 20S and 26S Proteasome Activities in the Liver of Male F344 Rats. *Mechanisms of Ageing and Development* **1998**, *102* (1), 55–66. [https://doi.org/10.1016/S0047-6374\(98\)00011-6](https://doi.org/10.1016/S0047-6374(98)00011-6).
- (104) Thibaut, T. A.; Anderson, R. T.; Smith, D. M. A Common Mechanism of Proteasome Impairment by Neurodegenerative Disease-Associated Oligomers. *Nature Communications* **2018**, *9* (1). <https://doi.org/10.1038/s41467-018-03509-0>.
- (105) Scott, M. R.; Rubio, M. D.; Haroutunian, V.; Meador-Woodruff, J. H. Protein Expression of Proteasome Subunits in Elderly Patients with Schizophrenia. *Neuropsychopharmacol* **2016**, *41* (3), 896–905. <https://doi.org/10.1038/npp.2015.219>.
- (106) Im, E.; Chung, K. C. Precise Assembly and Regulation of 26S Proteasome and Correlation between Proteasome Dysfunction and Neurodegenerative Diseases. *BMB Reports* **2016**, *49* (9), 459–473. <https://doi.org/10.5483/BMBRep.2016.49.9.094>.
- (107) Cookson, M. R.  $\alpha$ -Synuclein and Neuronal Cell Death. *Mol Neurodegeneration* **2009**, *4* (1), 9. <https://doi.org/10.1186/1750-1326-4-9>.
- (108) Huang, M.; Wang, B.; Li, X.; Fu, C.; Wang, C.; Kang, X.  $\alpha$ -Synuclein: A Multifunctional Player in Exocytosis, Endocytosis, and Vesicle Recycling. *Front. Neurosci.* **2019**, *13*, 28. <https://doi.org/10.3389/fnins.2019.00028>.
- (109) McNaught, K. S. P.; Shashidharan, P.; Perl, D. P.; Jenner, P.; Olanow, C. W. Aggresome-Related Biogenesis of Lewy Bodies: Relationship between Aggresomes and Lewy Bodies. *European Journal of Neuroscience* **2002**, *16* (11), 2136–2148. <https://doi.org/10.1046/j.1460-9568.2002.02301.x>.
- (110) Xia, Q. Proteomic Identification of Novel Proteins Associated with Lewy Bodies. *Front Biosci* **2008**, *Volume* (13), 3850. <https://doi.org/10.2741/2973>.
- (111) Zimmermann, A.; Hofer, S.; Pendl, T.; Kainz, K.; Madeo, F.; Carmona-Gutierrez, D. Yeast as a Tool to Identify Anti-Aging Compounds. *FEMS Yeast Research* **2018**, *18* (6). <https://doi.org/10.1093/femsyr/foy020>.

- (112) Longo, V. D.; Shadel, G. S.; Kaerberlein, M.; Kennedy, B. Replicative and Chronological Aging in *Saccharomyces Cerevisiae*. *Cell Metabolism* **2012**, *16* (1), 18–31. <https://doi.org/10.1016/j.cmet.2012.06.002>.
- (113) Kaerberlein, M.; Burtner, C. R.; Kennedy, B. K. Recent Developments in Yeast Aging. *PLoS Genet* **2007**, *3* (5), e84. <https://doi.org/10.1371/journal.pgen.0030084>.
- (114) Nakajima, S.; Kato, H.; Takahashi, S.; Johno, H.; Kitamura, M. Inhibition of NF- $\kappa$ B by MG132 through ER Stress-Mediated Induction of LAP and LIP. *FEBS Letters* **2011**, *585* (14), 2249–2254. <https://doi.org/10.1016/j.febslet.2011.05.047>.
- (115) Crawford, L. J. A.; Walker, B.; Ovaa, H.; Chauhan, D.; Anderson, K. C.; Morris, T. C. M.; Irvine, A. E. Comparative Selectivity and Specificity of the Proteasome Inhibitors BzLLLCOCHO, PS-341, and MG-132. *Cancer Research* **2006**, *66* (12), 6379–6386. <https://doi.org/10.1158/0008-5472.CAN-06-0605>.
- (116) Selimovic, D.; Porzig, B. B. O. W.; El-Khattouti, A.; Badura, H. E.; Ahmad, M.; Ghanjati, F.; Santourlidis, S.; Haikel, Y.; Hassan, M. Bortezomib/Proteasome Inhibitor Triggers Both Apoptosis and Autophagy-Dependent Pathways in Melanoma Cells. *Cellular Signalling* **2013**, *25* (1), 308–318. <https://doi.org/10.1016/j.cellsig.2012.10.004>.
- (117) Chen, D.; Frezza, M.; Schmitt, S.; Kanwar, J.; P. Dou, Q. Bortezomib as the First Proteasome Inhibitor Anticancer Drug: Current Status and Future Perspectives. *Current Cancer Drug Targets* **2011**, *11* (3), 239–253. <https://doi.org/10.2174/156800911794519752>.
- (118) Accardi, F.; Toscani, D.; Bolzoni, M.; Dalla Palma, B.; Aversa, F.; Giuliani, N. Mechanism of Action of Bortezomib and the New Proteasome Inhibitors on Myeloma Cells and the Bone Microenvironment: Impact on Myeloma-Induced Alterations of Bone Remodeling. *BioMed Research International* **2015**, *2015*, 1–13. <https://doi.org/10.1155/2015/172458>.
- (119) Arastu-Kapur, S.; Anderl, J. L.; Kraus, M.; Parlati, F.; Shenk, K. D.; Lee, S. J.; Muchamuel, T.; Bennett, M. K.; Driessen, C.; Ball, A. J.; Kirk, C. J. Nonproteasomal Targets of the Proteasome Inhibitors Bortezomib and Carfilzomib: A Link to Clinical Adverse Events. *Clin Cancer Res* **2011**, *17* (9), 2734–2743. <https://doi.org/10.1158/1078-0432.CCR-10-1950>.
- (120) Hasinoff, B. B.; Patel, D.; Wu, X. Molecular Mechanisms of the Cardiotoxicity of the Proteasomal-Targeted Drugs Bortezomib and Carfilzomib. *Cardiovascular Toxicology* **2017**, *17* (3), 237–250. <https://doi.org/10.1007/s12012-016-9378-7>.
- (121) Jerkins, J. Bortezomib-Induced Severe Congestive Heart Failure. *Cardiol* **2010**. <https://doi.org/10.4021/cr105e>.
- (122) Orciuolo, E.; Buda, G.; Cecconi, N.; Galimberti, S.; Versari, D.; Cervetti, G.; Salvetti, A.; Petrini, M. Unexpected Cardiotoxicity in Haematological Bortezomib Treated Patients. *British Journal of Haematology* **2007**, *138* (3), 396–397. <https://doi.org/10.1111/j.1365-2141.2007.06659.x>.

- (123) Lü, S.; Wang, J. The Resistance Mechanisms of Proteasome Inhibitor Bortezomib. *Biomarker Research* **2013**, *1* (1). <https://doi.org/10.1186/2050-7771-1-13>.
- (124) Oerlemans, R.; Franke, N. E.; Assaraf, Y. G.; Cloos, J.; van Zantwijk, I.; Berkers, C. R.; Scheffer, G. L.; Debipersad, K.; Vojtekova, K.; Lemos, C.; van der Heijden, J. W.; Ylstra, B.; Peters, G. J.; Kaspers, G. L.; Dijkmans, B. A. C.; Scheper, R. J.; Jansen, G. Molecular Basis of Bortezomib Resistance: Proteasome Subunit B5 (PSMB5) Gene Mutation and Overexpression of PSMB5 Protein. *Blood* **2008**, *112* (6), 2489–2499. <https://doi.org/10.1182/blood-2007-08-104950>.
- (125) Yang, W.-C.; Lin, S.-F. Mechanisms of Drug Resistance in Relapse and Refractory Multiple Myeloma. *BioMed Research International* **2015**, *2015*, 1–17. <https://doi.org/10.1155/2015/341430>.
- (126) Berenson, J. R.; Hilger, J. D.; Yellin, O.; Dichmann, R.; Patel-Donnelly, D.; Boccia, R. V.; Bessudo, A.; Stampleman, L.; Gravenor, D.; Eshaghian, S.; Nassir, Y.; Swift, R. A.; Vescio, R. A. Replacement of Bortezomib with Carfilzomib for Multiple Myeloma Patients Progressing from Bortezomib Combination Therapy. *Leukemia* **2014**, *28* (7), 1529–1536. <https://doi.org/10.1038/leu.2014.27>.
- (127) Moreau, P.; Masszi, T.; Grzasko, N.; Bahlis, N. J.; Hansson, M.; Pour, L.; Sandhu, I.; Ganly, P.; Baker, B. W.; Jackson, S. R.; Stoppa, A.-M.; Simpson, D. R.; Gimsing, P.; Palumbo, A.; Garderet, L.; Cavo, M.; Kumar, S.; Touzeau, C.; Buadi, F. K.; Laubach, J. P.; Berg, D. T.; Lin, J.; Di Bacco, A.; Hui, A.-M.; van de Velde, H.; Richardson, P. G. Oral Ixazomib, Lenalidomide, and Dexamethasone for Multiple Myeloma. *New England Journal of Medicine* **2016**, *374* (17), 1621–1634. <https://doi.org/10.1056/NEJMoa1516282>.
- (128) Al-Salama, Z. T.; Garnock-Jones, K. P.; Scott, L. J. Ixazomib: A Review in Relapsed and/or Refractory Multiple Myeloma. *Targ Oncol* **2017**, *12* (4), 535–542. <https://doi.org/10.1007/s11523-017-0504-7>.
- (129) Lim, H.-S.; Cai, D.; Archer, C. T.; Kodadek, T. Periodate-Triggered Cross-Linking Reveals Sug2/Rpt4 as the Molecular Target of a Peptoid Inhibitor of the 19S Proteasome Regulatory Particle. *2*.
- (130) Xia, D.; Tang, W. K.; Ye, Y. Structure and Function of the AAA+ ATPase P97/Cdc48p. *Gene* **2016**, *583* (1), 64–77. <https://doi.org/10.1016/j.gene.2016.02.042>.
- (131) Jentsch, S.; Rumpf, S. Cdc48 (P97): A ‘Molecular Gearbox’ in the Ubiquitin Pathway? *Trends in Biochemical Sciences* **2007**, *32* (1), 6–11. <https://doi.org/10.1016/j.tibs.2006.11.005>.
- (132) Ye, Y.; Meyer, H. H.; Rapoport, T. A. The AAA ATPase Cdc48/P97 and Its Partners Transport Proteins from the ER into the Cytosol. *Nature* **2001**, *414* (6864), 652–656. <https://doi.org/10.1038/414652a>.

- (133) Niwa, H.; Ewens, C. A.; Tsang, C.; Yeung, H. O.; Zhang, X.; Freemont, P. S. The Role of the N-Domain in the ATPase Activity of the Mammalian AAA ATPase P97/VCP. *Journal of Biological Chemistry* **2012**, *287* (11), 8561–8570. <https://doi.org/10.1074/jbc.M111.302778>.
- (134) Anderson, D. J.; Le Moigne, R.; Djakovic, S.; Kumar, B.; Rice, J.; Wong, S.; Wang, J.; Yao, B.; Valle, E.; Kiss von Soly, S.; Madriaga, A.; Soriano, F.; Menon, M.-K.; Wu, Z. Y.; Kampmann, M.; Chen, Y.; Weissman, J. S.; Aftab, B. T.; Yakes, F. M.; Shawver, L.; Zhou, H.-J.; Wustrow, D.; Rolfe, M. Targeting the AAA ATPase P97 as an Approach to Treat Cancer through Disruption of Protein Homeostasis. *Cancer Cell* **2015**, *28* (5), 653–665. <https://doi.org/10.1016/j.ccell.2015.10.002>.
- (135) Wang, Q.; Shinkre, B. A.; Lee, J.; Weniger, M. A.; Liu, Y.; Chen, W.; Wiestner, A.; Trenkle, W. C.; Ye, Y. The ERAD Inhibitor Eeyarestatin I Is a Bifunctional Compound with a Membrane-Binding Domain and a P97/VCP Inhibitory Group. *PLoS ONE* **2010**, *5* (11), e15479. <https://doi.org/10.1371/journal.pone.0015479>.
- (136) Wang, Q.; Li, L.; Ye, Y. Inhibition of P97-Dependent Protein Degradation by Eeyarestatin I. *Journal of Biological Chemistry* **2008**, *283* (12), 7445–7454. <https://doi.org/10.1074/jbc.M708347200>.
- (137) Fiebigler, E.; Hirsch, C.; Vyas, J. M.; Gordon, E.; Ploegh, H. L.; Tortorella, D. Dissection of the Dislocation Pathway for Type I Membrane Proteins with a New Small Molecule Inhibitor, Eeyarestatin. *MBoC* **2004**, *15* (4), 1635–1646. <https://doi.org/10.1091/mbc.e03-07-0506>.
- (138) Chou, T.-F.; Brown, S. J.; Minond, D.; Nordin, B. E.; Li, K.; Jones, A. C.; Chase, P.; Porubsky, P. R.; Stoltz, B. M.; Schoenen, F. J.; Patricelli, M. P.; Hodder, P.; Rosen, H.; Deshaies, R. J. Reversible Inhibitor of P97, DBeQ, Impairs Both Ubiquitin-Dependent and Autophagic Protein Clearance Pathways. *Proceedings of the National Academy of Sciences* **2011**, *108* (12), 4834–4839. <https://doi.org/10.1073/pnas.1015312108>.
- (139) Keren-Kaplan, T.; Zeev Peters, L.; Levin-Kravets, O.; Attali, I.; Kleifeld, O.; Shohat, N.; Artzi, S.; Zucker, O.; Pilzer, I.; Reis, N.; Glickman, M. H.; Ben-Aroya, S.; Prag, G. Structure of Ubiquitylated-Rpn10 Provides Insight into Its Autoregulation Mechanism. *Nat Commun* **2016**, *7* (1), 12960. <https://doi.org/10.1038/ncomms12960>.
- (140) Hamazaki, J.; Sasaki, K.; Kawahara, H.; Hisanaga, S.; Tanaka, K.; Murata, S. Rpn10-Mediated Degradation of Ubiquitinated Proteins Is Essential for Mouse Development. *MCB* **2007**, *27* (19), 6629–6638. <https://doi.org/10.1128/MCB.00509-07>.
- (141) Trader, D. J.; Simanski, S.; Kodadek, T. A Reversible and Highly Selective Inhibitor of the Proteasomal Ubiquitin Receptor Rpn13 Is Toxic to Multiple Myeloma Cells. *Journal of the American Chemical Society* **2015**, *137* (19), 6312–6319. <https://doi.org/10.1021/jacs.5b02069>.

- (142) D'Arcy, P.; Brnjic, S.; Olofsson, M. H.; Fryknäs, M.; Lindsten, K.; De Cesare, M.; Perego, P.; Sadeghi, B.; Hassan, M.; Larsson, R.; Linder, S. Inhibition of Proteasome Deubiquitinating Activity as a New Cancer Therapy. *Nature Medicine* **2011**, *17* (12), 1636–1640. <https://doi.org/10.1038/nm.2536>.
- (143) Lee, M. J.; Lee, B.-H.; Hanna, J.; King, R. W.; Finley, D. Trimming of Ubiquitin Chains by Proteasome-Associated Deubiquitinating Enzymes. *Molecular & Cellular Proteomics* **2011**, *10* (5), R110.003871. <https://doi.org/10.1074/mcp.R110.003871>.
- (144) Reyes-Turcu, F. E.; Ventii, K. H.; Wilkinson, K. D. Regulation and Cellular Roles of Ubiquitin-Specific Deubiquitinating Enzymes. *Annual Review of Biochemistry* **2009**, *78* (1), 363–397. <https://doi.org/10.1146/annurev.biochem.78.082307.091526>.
- (145) Verma, R. Role of Rpn11 Metalloprotease in Deubiquitination and Degradation by the 26S Proteasome. *Science* **2002**, *298* (5593), 611–615. <https://doi.org/10.1126/science.1075898>.
- (146) Lee, B.-H.; Lee, M. J.; Park, S.; Oh, D.-C.; Elsasser, S.; Chen, P.-C.; Gartner, C.; Dimova, N.; Hanna, J.; Gygi, S. P.; Wilson, S. M.; King, R. W.; Finley, D. Enhancement of Proteasome Activity by a Small-Molecule Inhibitor of USP14. *Nature* **2010**, *467* (7312), 179–184. <https://doi.org/10.1038/nature09299>.
- (147) Boselli, M.; Lee, B.-H.; Robert, J.; Prado, M. A.; Min, S.-W.; Cheng, C.; Silva, M. C.; Seong, C.; Elsasser, S.; Hatle, K. M.; Gahman, T. C.; Gygi, S. P.; Haggarty, S. J.; Gan, L.; King, R. W.; Finley, D. An Inhibitor of the Proteasomal Deubiquitinating Enzyme USP14 Induces Tau Elimination in Cultured Neurons. *Journal of Biological Chemistry* **2017**, *292* (47), 19209–19225. <https://doi.org/10.1074/jbc.M117.815126>.
- (148) Kiprowska, M. J.; Stepanova, A.; Todaro, D. R.; Galkin, A.; Haas, A.; Wilson, S. M.; Figueiredo-Pereira, M. E. Neurotoxic Mechanisms by Which the USP14 Inhibitor IU1 Depletes Ubiquitinated Proteins and Tau in Rat Cerebral Cortical Neurons: Relevance to Alzheimer's Disease. *Biochimica et Biophysica Acta (BBA) - Molecular Basis of Disease* **2017**, *1863* (6), 1157–1170. <https://doi.org/10.1016/j.bbadis.2017.03.017>.
- (149) Tian, Z.; D'Arcy, P.; Wang, X.; Ray, A.; Tai, Y.-T.; Hu, Y.; Carrasco, R. D.; Richardson, P.; Linder, S.; Chauhan, D.; Anderson, K. C. A Novel Small Molecule Inhibitor of Deubiquitylating Enzyme USP14 and UCHL5 Induces Apoptosis in Multiple Myeloma and Overcomes Bortezomib Resistance. *Blood* **2014**, *123* (5), 706–716. <https://doi.org/10.1182/blood-2013-05-500033>.
- (150) Wang, Y.; Jiang, Y.; Ding, S.; Li, J.; Song, N.; Ren, Y.; Hong, D.; Wu, C.; Li, B.; Wang, F.; He, W.; Wang, J.; Mei, Z. Small Molecule Inhibitors Reveal Allosteric Regulation of USP14 via Steric Blockade. *Cell Research* **2018**, *28* (12), 1186–1194. <https://doi.org/10.1038/s41422-018-0091-x>.

- (151) Wang, X.; Mazurkiewicz, M.; Hillert, E.-K.; Olofsson, M. H.; Pierrou, S.; Hillertz, P.; Gullbo, J.; Selvaraju, K.; Paulus, A.; Akhtar, S.; Bossler, F.; Khan, A. C.; Linder, S.; D'Arcy, P. The Proteasome Deubiquitinase Inhibitor VLX1570 Shows Selectivity for Ubiquitin-Specific Protease-14 and Induces Apoptosis of Multiple Myeloma Cells. *Scientific Reports* **2016**, *6* (1). <https://doi.org/10.1038/srep26979>.
- (152) Wang, X.; D'Arcy, P.; Caulfield, T. R.; Paulus, A.; Chitta, K.; Mohanty, C.; Gullbo, J.; Chanan-Khan, A.; Linder, S. Synthesis and Evaluation of Derivatives of the Proteasome Deubiquitinase Inhibitor B-AP15. *Chemical Biology & Drug Design* **2015**, *86* (5), 1036–1048. <https://doi.org/10.1111/cbdd.12571>.
- (153) Li, J.; Yakushi, T.; Parlati, F.; Mackinnon, A. L.; Perez, C.; Ma, Y.; Carter, K. P.; Colayco, S.; Magnuson, G.; Brown, B.; Nguyen, K.; Vasile, S.; Suyama, E.; Smith, L. H.; Sergienko, E.; Pinkerton, A. B.; Chung, T. D. Y.; Palmer, A. E.; Pass, I.; Hess, S.; Cohen, S. M.; Deshaies, R. J. Capzimin Is a Potent and Specific Inhibitor of Proteasome Isopeptidase Rpn11. *Nature Chemical Biology* **2017**, *13* (5), 486–493. <https://doi.org/10.1038/nchembio.2326>.
- (154) Holmqvist, A. Inhibitory Effect on the Proteasome Regulatory Subunit, RPN11/POH1, with the Use of Capzimin-PROTAC to Trigger Apoptosis in Cancer Cells. 30.
- (155) Jones, C. L.; Njomen, E.; Sjögren, B.; Dexheimer, T. S.; Tepe, J. J. Small Molecule Enhancement of 20S Proteasome Activity Targets Intrinsically Disordered Proteins. *ACS Chem. Biol.* **2017**, *12* (9), 2240–2247. <https://doi.org/10.1021/acscchembio.7b00489>.
- (156) Trader, D. J.; Simanski, S.; Dickson, P.; Kodadek, T. Establishment of a Suite of Assays That Support the Discovery of Proteasome Stimulators. *Biochimica et Biophysica Acta (BBA) - General Subjects* **2017**, *1861* (4), 892–899. <https://doi.org/10.1016/j.bbagen.2017.01.003>.
- (157) Coleman, R. A.; Muli, C. S.; Zhao, Y.; Bhardwaj, A.; Newhouse, T. R.; Trader, D. J. Analysis of Chain Length, Substitution Patterns, and Unsaturation of AM-404 Derivatives as 20S Proteasome Stimulators. *Bioorganic & Medicinal Chemistry Letters* **2019**, *29* (3), 420–423. <https://doi.org/10.1016/j.bmcl.2018.12.030>.

## CHAPTER 2. DISCOVERY OF TXS-8, A SELECTIVE BINDER OF PROTEASOMAL SUBUNIT RPN-6.

### 2.1 Introduction of proteasomal subunit Rpn-6.

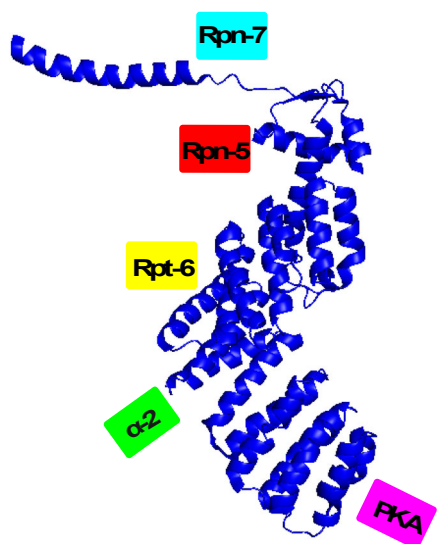


**Figure 2.1.** Extracted structure of Rpn-6 from 26S proteasome. Rpn-6 makes multiple protein-protein interactions with other proteasome subunits and the relative position of these subunits are labeled. PDB:5GJR

Rpn-6 (PSMD-11) is a subunit of the 19S RP and is considered a part of the 19S RP lid (**Figure 2.1**). It is a 47 kDa protein made of 422 amino acids. The protein presents an  $\alpha$ -solenoid horseshoe shaped N-terminal domain while the C-terminal of Rpn-6 contains the proteasome-CSN-eIF3 (PCI) domain.<sup>1,2</sup> According to reported crystal structure of Rpn-6 from *Drosophila melanogaster* (*D. melanogaster*), the protein presents a right-handed super-helical turn made of five double-helix repeats structurally similar to tetratricopeptide repeats (TPR).<sup>3-5</sup> The C-terminal region of Rpn-6 consists of a PCI domain with three antiparallel  $\beta$ -sheets.<sup>6</sup> Structural similarities are shared among other RP non-ATPase subunits of the 19S lid, including Rpn-3, Rpn-5 and Rpn-7.<sup>7-10</sup>

Although no crystal structure of human Rpn-6 alone has been solved, putative comparisons to other species can be drawn as the proteasome is a highly conserved protein complex through evolution.<sup>11-14</sup> The human 26S proteasome shares structural similarities with the *D. melanogaster* 26S proteasome, making it reasonable to speculate that Rpn-6 also shares similarities across the two. Besides being a part of the 19S RP, Rpn-6 has a recognition helix in the canonical winged-helix region which can be placed in the major groove of DNA.<sup>3,7</sup> Considering that the proteasome plays a role in DNA double-strand repair, we can reasonably speculate that Rpn-6 may bind with DNA to allow physical contact between the 26S proteasome and DNA.<sup>15-19</sup> Further investigation is required to fully understand how the 26S proteasome is involved with DNA damage repair and if there are physical contacts between them.

With the development of cryogenic electron microscopy (cryo-EM) technology, the 26S proteasome has been resolved at higher resolution in the past several years.<sup>20-23</sup> Some of these resolved structures have reached atomic level and revealed a detailed structural composition of the 26S proteasome. These exciting discoveries not only help researchers to understand the formation

of the 26S proteasome, but also demonstrate the dynamic movement of the 26S proteasome during target protein translocation and degradation. Although a human Rpn-6 crystal structure has not been resolved yet, the extracted Rpn-6 from these cryo-EM structures indicate strong structural similarity compared to previous *D. melanogaster* Rpn-6.

As some researchers have pointed out, the interaction between Rpn-6 and other proteasome subunits are crucial and maintain the structural integrity of the 26S proteasome. Rpn-6 is also identified as the molecular clamp, holding the 19S RP and 20S CP together by presenting critical protein-protein interactions.<sup>1-3,24</sup>

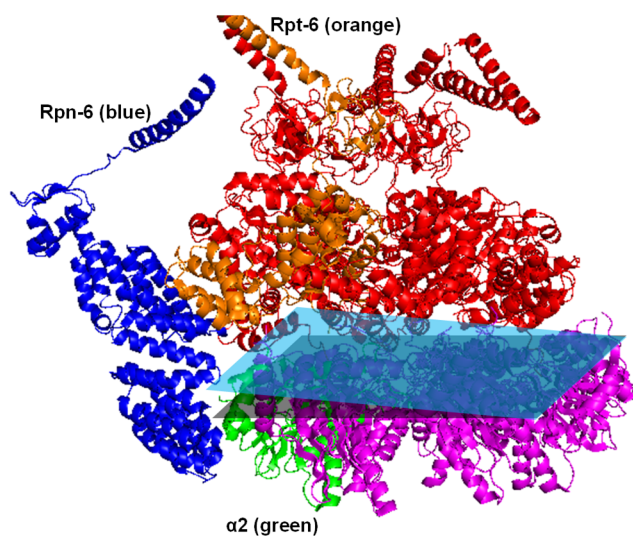


**Figure 2.2. The interface between the  $\alpha$  ring and the ATPase ring.** The interaction between Rpt-6, Rpn-6 and  $\alpha 2$  subunits tilts the ATPase ring on the  $\alpha$  ring (shown by the angle between two planes) and provides space for mechanical movement of the subunits during target protein degradation.

During the assembly of the 19S RP lid, the interaction between Rpn-6 and Rpn-7 at the PCI domain connects the Rpn-3/Rpn-7/Rpn-15 protein complex with the Rpn-6/Rpn-5/Rpn-8/Rpn-9 protein complex via a stable coil-coil interaction at the C-terminal PCI domains of these subunits. Rpn-6 is not only a vital subunit that participates in the assembly of the 19S RP lid, but it also interacts with both Rpt-6 and Rpt-3 on the ATPase ring of 19S RP base and the  $\alpha 2$  subunit on the 20S CP.<sup>3,25-28</sup> Structurally, six ATPase subunits asymmetrically interact with seven  $\alpha$  ring subunits, resulting in each

ATPase subunit “sitting” on the interface between two  $\alpha$  subunits. During the assembly of the 19S RP, the tail of Rpt-6 is inserted into the  $\alpha 2$ - $\alpha 3$  pocket with high specificity and affinity, but this interaction is attenuated in mature 26S proteasomes, where the tail of Rpt-6 is placed away from the pocket, causing a decrease in structural stability. However, the decreased interaction between Rpt-6 and the  $\alpha$  subunit is compensated by the interactions among Rpt-6/Rpn-6/ $\alpha 2$  subunits where Rpn-6 connects Rpt-6 and  $\alpha 2$  by using itself as a bridge. The weakened interaction between the tail of Rpt-6 and  $\alpha 2$ - $\alpha 3$  subunit pockets creates a cavity between the ATPase ring and the  $\alpha$  ring, resulting in the ATPase ring tilting on top of the  $\alpha$  ring (**Figure 2.2**).<sup>29-31</sup> This cavity provides some space for conformational changes but additional spaces are provided during target protein

degradation where the interactions between Rpn-5/Rpt-3 and Rpn-7/Rpt-2 disappear to allow drastic conformational changes in both the ATPase ring and  $\alpha$  ring.<sup>9</sup> However, the interaction between Rpn-6 and Rpt-6 remains, highlighting Rpn-6 as a crucial subunit to hold the 19S RP and 20S CP together. Meanwhile, the C-terminal tails of other ATPase subunits including Rpt2, Rpt-3 and Rpt-5 are inserted into the  $\alpha$  subunit pockets; recent cryo-EM based dynamic studies have demonstrated that the insertion of the ATPase subunit tails into the  $\alpha$  subunit pockets upon ATP hydrolysis could be the major driving force of the gate opening of the 20S CP.<sup>32–34</sup> To summarize, during the gate opening process, multiple protein-protein interactions between 19S RP subunits diminish to allow conformational changes on the 19S RP and 20S CP. Rpn-6 serves as the anchor to connect the lid and base of the 19S RP with the  $\alpha$  ring of the 20S CP to maintain the structural integrity of the 26S proteasome. The low-resolved N-terminal  $\alpha$ -solenoid region of Rpn-6 in the proteasome cryo-EM based dynamic study also demonstrated the drastic conformational change of the protein through the recruitment, irreversible commitment and substrate processing steps as about half of the N-terminal region of Rpn-6 remains unsolved.<sup>20,35,36</sup>

Rpn-6 can also be phosphorylated at Ser14 by protein kinase A (PKA) near the N-terminal region.<sup>37,38</sup> Researches have shown that the phosphorylation of Ser14 enhances proteasome activity in human stem cells and *Caenorhabditis. elegans* (*C. elegans*).<sup>39</sup> The phosphorylation of Rpn-6 also promotes the formation of doubly capped 30S proteasomes that can clear short-lived proteins more rapidly than the 26S proteasome. REF here for this statement A mutagenesis study confirmed the proteasome activity enhancement upon Ser14 phosphorylation: mutating Ser14 into phosphomimic Asp14 still maintained proteasome activity enhancement but mutation into Ala14 decreases proteasome activity and clearance of aggregated proteins in cells. As mentioned in **Chapter 1.2.1**, some cancers, such as hematological cancers, significantly upregulated proteasome activity for survival.<sup>40–42</sup> It is not surprising to observe that Ser14 phosphorylation of Rpn-6 is also upregulated in cancer cells, which again stresses the importance of the function of Rpn-6 in cellular processes.<sup>38</sup>

## **2.2 Central hypothesis and rationale regarding the discovery of a small molecule binder of proteasomal subunit Rpn-6.**

Rpn-6 is a subunit of the 26S proteasome which maintains the structural integrity of the 26S proteasome during the translocation of the target peptide. Phosphorylation of Ser14 on Rpn-6

boosts proteasome activity by enhancing the formation of the 30S proteasome to clear short-lived proteins. Rpn-6 is also upregulated in some cancer cells, making Rpn-6 a potential target for drug development. As previously mentioned in **Chapter 1.3**, all current FDA approved proteasome inhibitors target the same enzymatic region on the 20S CP. Drug resistance and cancer relapse has been observed among patients having been treated with these proteasome inhibitors. Therefore, it is urgent to discover other proteasome inhibitors targeting different regions on the proteasome to overcome drug resistance with current proteasome inhibitors. We and other researchers have turned our attention to the 19S RP of the 26S proteasome. We concluded Rpn-6 is a crucial component of the 26S proteasome and by binding Rpn-6, we would be capable of interfering with 26S proteasome hydrolysis activity therefore significantly affecting cellular processes in cancer cells. Since Rpn-6 makes multiple protein-protein interactions with other proteasomal subunits, we hypothesized that using a small molecule binder of Rpn-6 could disrupt the protein-protein interaction of Rpn-6 with other subunits and decrease proteasome activity. We anticipate a proteasome activity decrease could be harmful or even fatal for some cancer cells over expressing Rpn-6. Combined with the current proteasome inhibitors, our Rpn-6 binder could be used to provide an alternative strategy to treat proteasome inhibitor resistant cancer patients and serve as a tool to further understand the assembly of the 19S lid.

## **2.3 One-bead-one-compound library design and screening.**

### **2.3.1 One-bead-one-compound library design.**

To test Rpn-6 with more compounds, we decided to generate an one-bead-one-compound (OBOC) peptoid library for Rpn-6 and screen the library via differential scanning fluorimetry (also known as thermal shift assay). An OBOC library utilizes the split-and-pool method to create a library in a short amount of time.<sup>43–45</sup> Specifically, we performed solid-phase synthesis on Rink-amide resin by first functionalizing with bromo-acetic acid. Then the resin was separated into different reaction vessels for amine coupling. After coupling, the resin fractions were then combined for bromo-acetic acid coupling and the splitting process was repeated. The peptoid compounds were designed as a 3-mer peptoids with seven potential amines at each position (**Figure 2.3A**). In total, we designed a library of  $7*7*7=343$  compounds to maximize the number of peptoids for testing and screening. After the library was synthesized, a small portion of the resin

beads were placed individually in a well of a 96-well plate and the peptoid was cleaved using trifluoroacetic acid (TFA) cocktail.<sup>47</sup> The cleaved product was analyzed by matrix-assisted laser desorption/ionization (MALDI) for sequence identification. The purpose of the step was to examine the synthesis efficiency of the OBOC library, with the library quality only being considered sufficient for screening if 80% of the sequences could be identified. After analyzing all the sequences, we acquired from MALDI, we were able to determine 88% of the sequences analyzed and moved forward to use for screening for Rpn-6 binding.

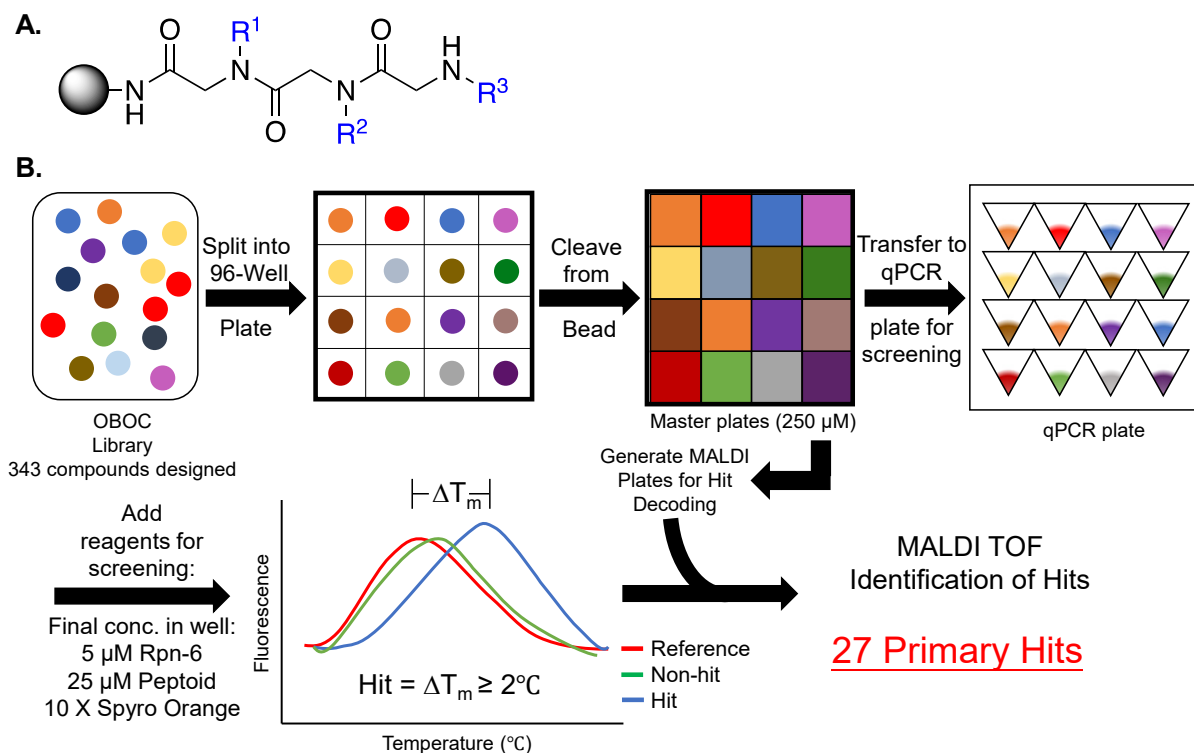


**Figure 2.3. General structure of peptoid and workflow of OBOC library screening.** (A) General structure of 3-mer peptoid. Peptoids could be viewed as *N*-substituted glycine (B) Workflow of testing the library with Rpn-6 using a thermal shift assay and identification of hit compounds.

### 2.3.2 One-bead-one-compound library screening via thermal shift assay.

To generate a master plate for library screening, we transferred 420 beads into seven 96-well plates. The excess 22% beads compared to the 343 designed compounds were meant to compensate for the 12% loss of the synthesis efficiency and to cover all compounds we synthesized so we could test them at least once. The beads were cleaved by TFA cocktail and dried under vacuum. A stock solution of 250  $\mu\text{M}$  in dimethyl sulfoxide (DMSO) was prepared for screening. Since Rpn-6 does not exhibit enzymatic function like the  $\beta 5$  subunit on the 20S CP, we screened

for Rpn-6 ligands by utilizing differential scanning fluorimetry, or more commonly referred to as a thermal shift assay (**Figure 2.3B**).<sup>48–51</sup> This screening method has previously been used to discover a BET inhibitor and is commonly used in small molecule or fragment-based library screening.<sup>52–55</sup> Briefly, the target protein is mixed with a hydrophobic dye and the mixture is slowly heated to allow the protein to unfold, thus exposing its hydrophobic core for dye binding. The binding of the protein with dye will generate an increase in fluorescence signal, followed by signal decrease as protein starts to aggregate, burying the dye into the aggregate (**Figure 2.4**). By analyzing the signal increase and decrease, the melting temperature of the target protein can be calculated. When investigating small molecules, the ligand will be mixed with the target protein and the hydrophobic dye. Upon heating, the protein will start to unfold and expose its hydrophobic core as described above. However, if the small molecule binds to the target protein, it could alter the structural integrity of the target protein such that stabilizing molecules will increase the melting temperature of the target protein (**Figure 2.4**). This approach for discovering the protein-ligand interactions can be high throughput and it requires relatively less protein compared to other screening methods. Recent developments in this technology has even allowed for thermal shift assay in living cells for ligand screening.<sup>56,57</sup>

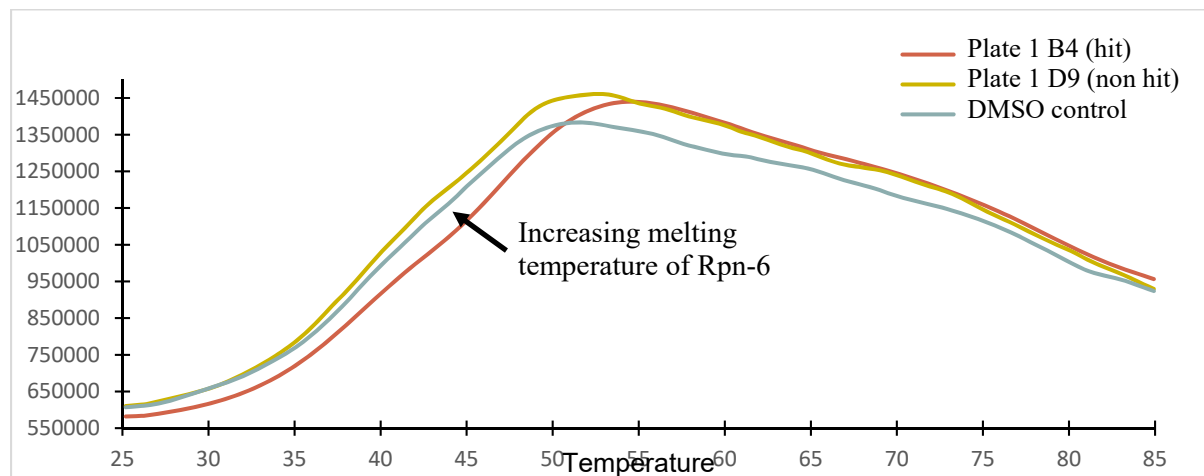
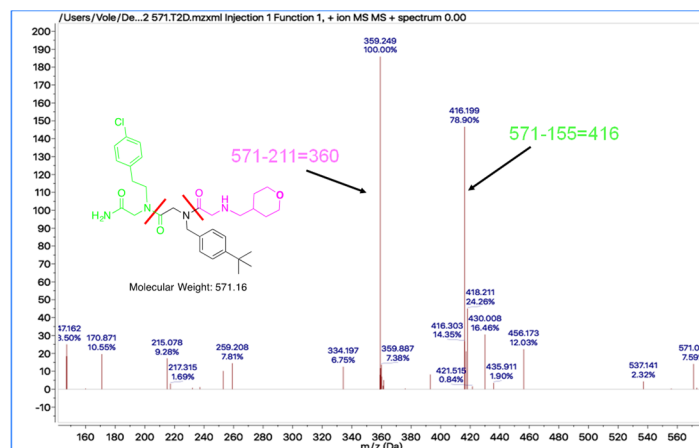


**Figure 2.4. Example of thermal shift assay.** Green line shows Rpn-6 with DMSO as the control. Two ligands were included in the example as one of them did not alter the melting temperature of Rpn-6 at all while the other one increased the melting temperature, suggesting it stabilized the protein.

The qPCR plate for the thermal shift assay was prepared by mixing Rpn-6 with the hydrophobic dye (Spiro Orange) and an aliquoted peptoid from the master plate to reach a final concentration of 10  $\mu$ M. The plate was heated over time and fluorescent signal from the dye was monitored at excitation of 490 nm and emission of 594 nm. The melting point for Rpn-6 in each

well was determined, and after the assay was finished any well which showed a melting temperature shift of 2 °C or more was considered a primary hit from the library. The peptoid was transferred from the corresponded well on the master plate onto a MALDI plate for MALDI-TOF analysis. 36 compounds were identified as initial hits from the thermal shift assay with Rpn-6.

### 2.3.3 Thermal shift results and MALDI-TOF analysis.

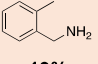
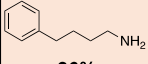
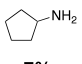
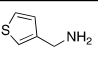
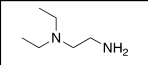
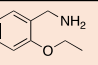
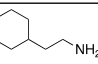
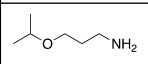
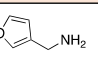
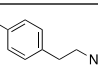
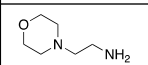
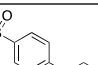
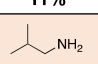
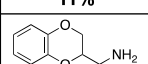
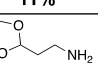
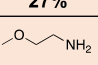
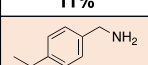
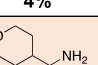
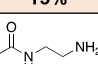
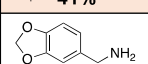
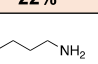


**Figure 2.5. Example of a potential hit molecule identified from MALDI.** The MS-MS profile of the molecule was analyzed to confirm the composition of the peptoid.

The MALDI plate was sent to the Purdue Proteomics Facility (PPF) for analysis. The MS of each potential hit was identified, and MS-MS was also performed on these compounds for peptoid sequencing. We listed all possible ligand masses and cross-checked the data from MALDI with our list to reconstruct the compound based on the MALDI mass.<sup>58</sup> However, multiple compounds on the list exhibited identical

masses, requiring MS-MS from MALDI to analyze the composition of the compound and to determine the structure of the peptoid (**Figure 2.5**). MS-MS based peptoid structure reconstruction was also applied for hit compounds with unique masses to validate the MS result. In total, we were able to identify the composition of 27 compounds from 36 initial hit compounds and the hit percentage from the 420-compound library was calculated as 6%.

**Table 2.1.** Summary of frequency of each amine on every position.

Position 1	Position 2	Position 3
 19%	 26%	 7%
 8%	 4%	 41%
 12%	 7%	 11%
 11%	 11%	 11%
 27%	 11%	 4%
 15%	 41%	 22%
 8%	 0%	 4%

### 2.3.4 Compound sequence analysis and new compound design.

After obtaining the structures of 27 hits from the previous step, we summarized the frequency of each amine from each hit and generated a list of amine frequency for comparison. Peptoids are essentially modular compounds, where each module is composed of various *N*-substituted glycine moieties (**Figure 2.3A**).<sup>59</sup> We hypothesized that the position of the specific amines was crucial to the ligand's ability to bind with Rpn-6. As shown in **Table 2.1**, certain amine moieties appeared more frequently than others at specific positions, indicating the possibility of designing new compounds for further testing. Therefore, instead of resynthesizing the identified hits, we chose to

build new testing molecules based on the frequency of amines at each position. For position one, no significant preference was observed among the top three amines, so we decided to include all three for new compound designs. For the second and third position, two amines showed up more frequently among the hits. Therefore, the first along with the second most observed amines were included in both positions. Eventually, we constructed 3\*2\*2=12 compounds for further testing

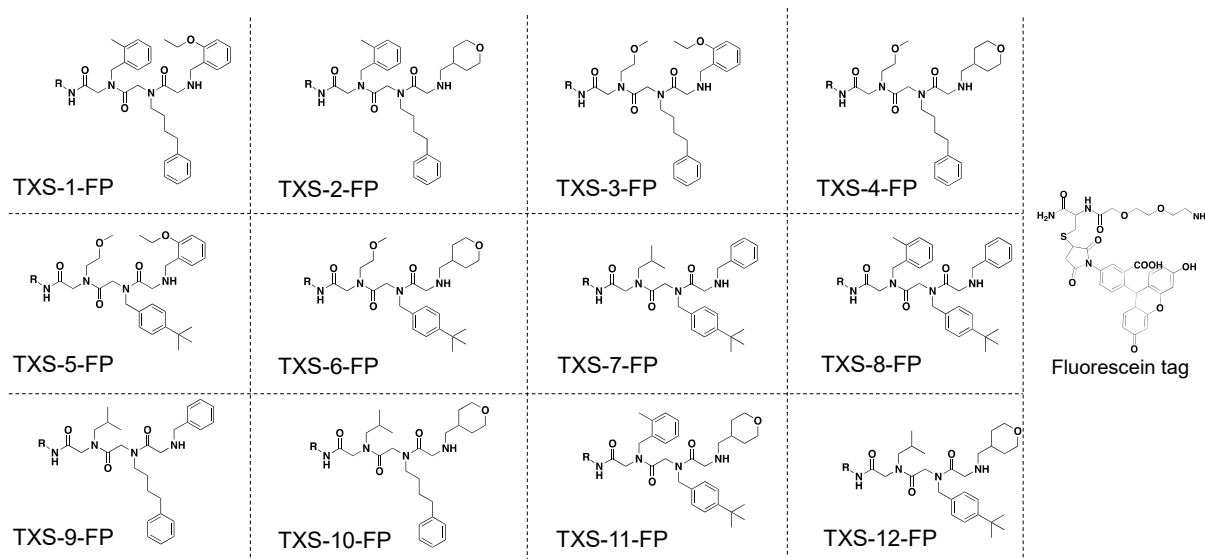


**Figure 2.6.** New peptoids for binding test. 12 new peptoids generated from **Table 2.1**. A fluorescein is included for a fluorescence polarization assay to determine binding affinities.

(Figure 2.6). To evaluate the exact binding affinity of each compound towards Rpn-6, a fluorescein was incorporated on each molecule to allow us to perform a fluorescence polarization assay later. These 12 peptoids were resynthesized by solid-phase synthesis and purified by HPLC.

## 2.4 Discovery of TXS-8 and derivative studies.

### 2.4.1 Fluorescence polarization assay on the peptoids.

To evaluate the binding affinity of each peptoid with Rpn-6, we performed a fluorescence polarization assay (FP assay). Fluorescence polarization is a traditional method of monitoring the binding affinity of a substrate to a protein.<sup>60–63</sup> Briefly, fluorescence is the radiation emitted by a substance due to incident radiation of a shorter wavelength. In this experiment, the signal is generated by the fluorescein moiety on the peptoid. Polarization stands for the restriction of a transverse wave wholly or partially to one direction. Generally, the sample is first excited with polarized light. Then, the sample would emit the absorbed light in both the parallel and perpendicular directions which the intensity of the light could be recorded. In the case of unbound small molecules, the rotation of the ligand itself would be rapid, causing light to be emitted in all directions and resulting in a low polarization. However, when a ligand binds with a protein like

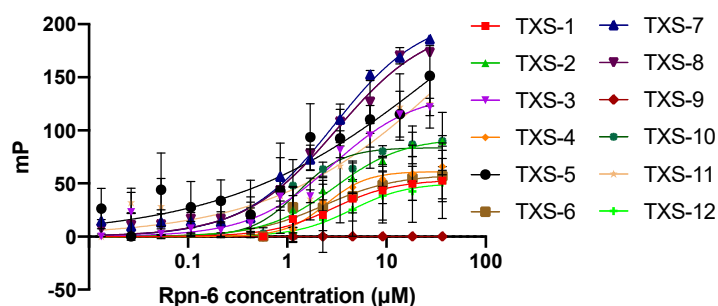
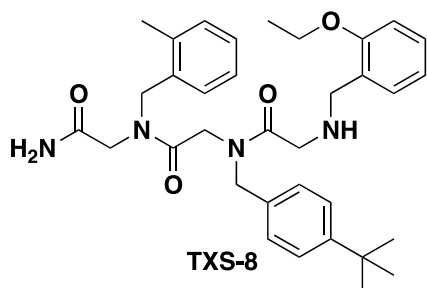


**Figure 2.7. Binding curve of all 12 testing compounds.** Peptoid monomers observed frequently in Table 2.1 were used to reconstruct 12 new peptoids to test for binding. Appended to the peptoid was a fluorescein moiety through a mini-PEG linker at the C-terminus.

Rpn-6, the relatively larger size of the protein makes the protein-ligand complex rotate slower as compared to unbound ligand and resulting in a high polarization. The tighter the binding is, the higher the polarization reading is observed. By using FP a assay, all 12 compounds were tested with the same batch of Rpn-6 and the result of the

experiment was analyzed and graphed to calculate a  $K_d$  of each compound (Figure 2.7). The experiment was repeated with another batch of freshly made Rpn-6 to validate the previous result. The assay results indicated various binding affinities of different peptods to Rpn-6 and controls were performed to exclude the possibility of the fluorescein moiety binding to Rpn-6. We

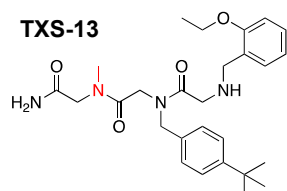
concluded this because peptoid 9 (TXS-9) showed no polarization reading at all and indicated neither fluorescein nor peptoid 9 bound to Rpn-6 during the experiment.



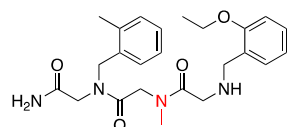
## 2.4.2 Discovery of TXS-8 and derivative designs.

Among all 12 peptoids, we discovered that TXS-8 showed the best binding affinity towards Rpn-6 in triplicate (**Figure 2.8**). TXS-7 showed the second-best binding affinity towards Rpn-6 in the first test, but the second test results were inconsistent and we decided to exclude TXS-7 from further

**Figure 2.8.** Structure of TXS-8



**TXS-14**



**TXS-15**

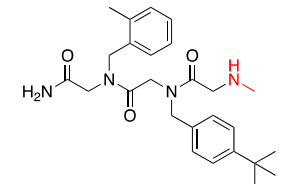


**Figure 2.9. Structure of TXS-8 derivatives.** TXS-13/14/15 for the *N*-methylamine scan.

study. Therefore, TXS-8 was identified as the best hit from the FP assay screening with a  $K_d$  of  $\sim 14 \mu\text{M}$ . The discovery of TXS-8 was an exciting result as our top hit was already in the low micromolar range for binding to Rpn-6.

As mentioned in **Chapter 2.3.4**, peptoids are module compounds composed with various *N*-substituted glycine moieties. We wanted to investigate if all three amines were essential for TXS-8 binding to Rpn-6. A *N*-methylamine scan was performed on TXS-8 where three additional peptoids were designed with each of the amine on TXS-8 replaced with *N*-methylamine; the experiment shares a similar concept to an alanine scan for peptide ligands. In an alanine scan, individual amino acids are replaced with an alanine to investigate whether the peptide ligand loses or maintains its binding affinity towards the target protein.<sup>64</sup> The alanine scan is meant to discover the essential amino acid(s) of the peptide ligand

responsible for binding for future investigations. To perform the *N*-methylamine scan on TXS-8, we designed three derivatives as TXS-13/14/15 (**Figure 2.9**). In addition to the *N*-methylamine scan, we also investigated if inserting additional amines at either *N*- or *C*-termini would increase the affinity of TXS-8 towards Rpn-6, as a previous protein binding peptoids utilized by our lab was a 6-mer peptoid.<sup>65</sup> TXS-16 to TXS-36 were designed for the insertion experiments. All

peptoids were designed to include the fluorescein for the FP assay, synthesized by solid-phase synthesis, purified by HPLC, and tested with Rpn-6 via the FP assay for binding affinity.

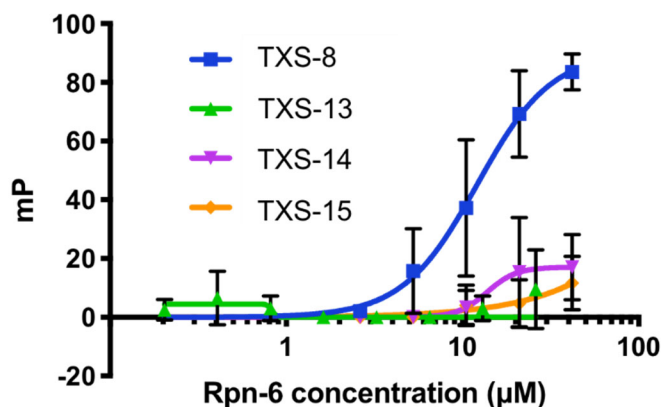


**Figure 2.10. TXS-8 derivative FP assay.** FP results of TXS-13/14/15. Removing any of the amine moiety on TXS-8 completely diminished the binding of the derivatives to Rpn-6.

#### 2.4.3 TXS-13 – TXS-36 screening and results.

Our FP assay results indicated that replacement of any of the three amine moieties of TXS-8 with an *N*-methylamine completely diminished its binding towards Rpn-6. The result also showed that all three amines were essential for TXS-8 binding to Rpn-6 (**Figure 2.10**). For insertion studies from

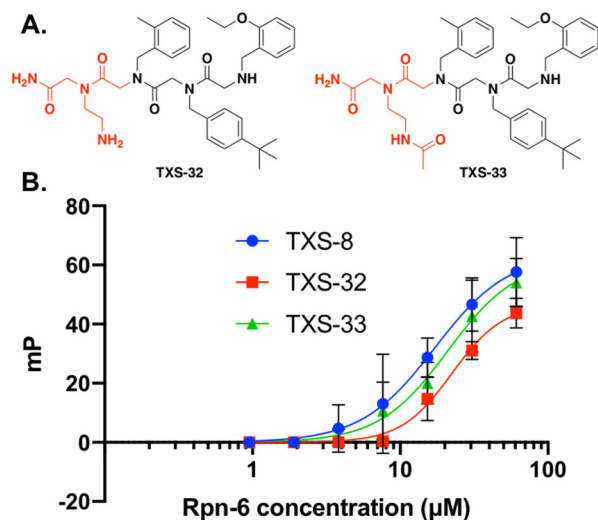


**Figure 2.11. FP assay with TXS-32 and TXS-33.** (A) Structure of TXS-32 and TXS-33, the insertion of linear amine moieties at the C-terminus of TXS-8. (B) FP result of TXS-32 and TXS-33 on Rpn-6, they showed similar binding affinity to Rpn-6 comparing to TXS-8.

TXS-16 to TXS-36, most of the derivatives we synthesized presented either no binding or significantly weakened binding to Rpn-6. Based on the results, we also concluded that adding an amine moiety at the *N*-terminus of TXS-8 would greatly decrease the binding of the peptoid to Rpn-6. However, modifications at the C-terminus were tolerated in certain conditions though the modification did not significantly improve the affinity of the derivative to Rpn-6 (**Figure 2.11A**).

Among all moieties we inserted at the C-terminus, amines with linear side chains like ethylenediamine or *N*-acetyl ethylenediamine were better tolerated than amines with bulky side

chains like cyclohexane or benzene. This observation provided us with a feasible method for future TXS-8 derivative design (**Figure 2.11B**). From the results of derivative screening, it was evident that the composition of TXS-8 was essential to bind with Rpn-6 and extending the 3-mer peptoid

at the C-terminus is tolerated with linear side chains, explaining why the mini-PEG linker is tolerated for the FP assay.

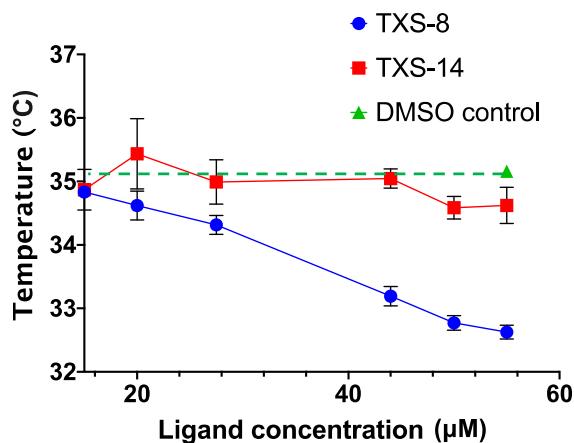


**Figure 2.12.** Thermal shift assay of TXS-8/14 on Rpn-6.

#### 2.4.4 TXS-8 thermal shift assay on Rpn-6.

After testing TXS-13/14/15 via the FP assay and confirming the necessity of all three amines for TXS-8 binding to Rpn-6, we also performed a thermal shift assay to investigate how TXS-8 affects the melting temperature of Rpn-6. TXS-14 was included in the experiment as a negative control since it did not show binding to Rpn-6 during the FP assay. We discovered that TXS-8

lowered the melting temperature of Rpn-6 in a dose-dependent manner while TXS-14 did not alter the Rpn-6 melting temperature at all, indicating that TXS-8 was a potential protein destabilizer of Rpn-6 (**Figure 2.12**). The result highlighted the feasibility of using a thermal shift assay for molecular screening and again emphasized the importance of all three amine moieties on TXS-8 for its interaction with Rpn-6.

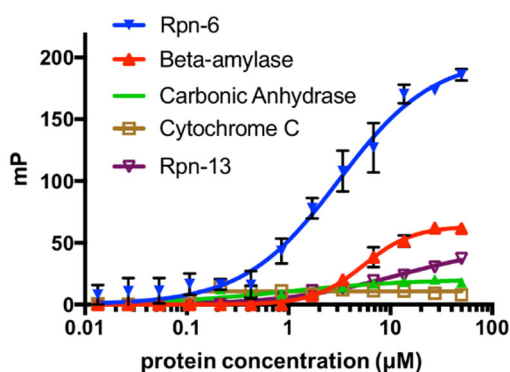


**Figure 2.13.** TXS-8 FP assay with other proteins.

#### 2.4.5 Screening TXS-8 with other proteins for specificity.

After completing the TXS-8 derivative screening with Rpn-6, we wanted to investigate the specificity of TXS-8 towards other proteins. Using various purified proteins that are commercially available, we wanted to test whether TXS-8 binds with these proteins during FP assay. Another

subunit of 19S RP, Rpn-13, was also included in this experiment. Rpn-13 was previously reported to bind with peptoids and we wanted to investigate if TXS-8 as a peptoid could also bind with Rpn-13.<sup>65</sup> The result from the FP assay showed no appreciable binding between TXS-8 and other proteins, including Rpn-13. Although beta-amylase showed moderate binding to TXS-8, we later discovered that the protein could also bind to other protein binders like flavonoid compounds. The

result from the experiment above highlighted the selectivity of TXS-8 to Rpn-6 as compared to other proteins (**Figure 2.13**).

## 2.5 TXS-8 target identification.

### 2.5.1 Modification of TXS-8 for non-covalent pull-down study.

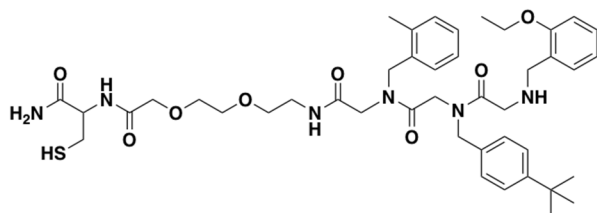


**Figure 2.14. TXS-8 for non-covalent pull-down.** The thiol group will be immobilized to the resin after reacting with the iodo group on the resin.

Knowing TXS-8 was initially selective towards Rpn-6 from **Chapter 2.4.5** provided potential value of using TXS-8 in future Rpn-6 studies. However, the screening from **Chapter**

**2.4.5** only included several foreign proteins and the result was not strongly persuasive. To further

explore if TXS-8 was selective to Rpn-6, we

wanted to modify TXS-8 for a pull-down experiment. However, TXS-8 presented neither nucleophilic or electrophilic components, nor does Rpn-6 have catalytic amino acids as an exploitable covalent handle. Therefore, we hypothesized that TXS-8 bound to Rpn-6 non-covalently and we decided to perform a non-covalent pull-down experiment. Using the SulfoLink Immobilization Kit from ThermoFisher, we immobilized TXS-8 to resin for non-covalent pull-down and began our experiment with purified Rpn-6 to investigate the pull-down efficiency (**Figure 2.14**). However, we were unable to discover any protein in our elution fraction after multiple trials with purified Rpn-6. Given that TXS-8 has around 14  $\mu$ M binding affinity over Rpn-6, it was likely that the interaction between TXS-8 and Rpn-6 was not strong enough to keep Rpn-6 bound on the resin during washing procedures. Therefore, an alternative strategy was needed to address the selectivity of TXS-8.

### 2.5.2 Modification of TXS-8 for covalent pull-down study.

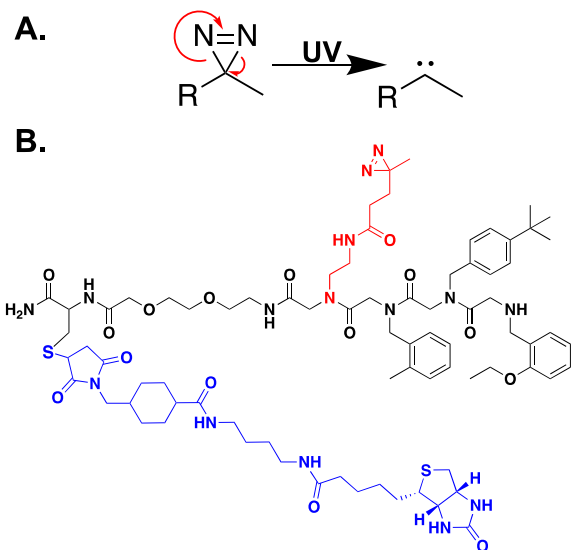


**Figure 2.15. Modification of TXS-8 for covalent pull-down experiment.** (A) Mechanism of diazirine activation. The carbene ion could bind with amino side chains for covalent cross-linking. (B) Structure of BMCC-BDzn-TXS-8 for covalent pull-down. Diazirine moiety shown in red, biotin moiety shown in blue.

Although we were unable to capture Rpn-6 using TXS-8 for a non-covalent pull-down experiment, we moved forward and investigated if performing a covalent pull-down is feasible. This required redesigning TXS-8 to include a covalent cross-linking group for use in a pull-down experiment. We chose to incorporate a diazirine moiety for covalent cross-linking.<sup>66–69</sup> Upon treatment of UV light, the diazirine undergoes an elimination reaction to generate a carbene ion by releasing dinitrogen. The carbene ion is highly reactive and can covalently bond with a peptide backbone or a side chain of amino acids (**Figure 2.15A**), which is beneficial as the binding pocket for TXS-8 is unknown and therefore we cannot target any specific amino acids. As we discovered

previously in **Chapter 2.4.3**, inserting an amine with linear side chains at the C-terminus of TXS-8 is tolerable, thus we decided to incorporate the diazirine moiety using a NHS-diazirine at the C-terminus of TXS-8. A biotin moiety was also included in the new compound for biotin-streptavidin pull-down as the interaction of biotin and streptavidin is one of the strongest non-covalent interactions (**Figure 2.15B**).<sup>70,71</sup> The biotin-streptavidin pull-down would allow us to enrich the cross-linked Rpn-6 regardless of TXS-8 potency or diazirine crosslinking efficiency. The BMCC-BDzn-TXS-8 was synthesized by solid-phase synthesis and purified by HPLC.

### 2.5.3 TXS-8 covalent pull-down with purified Rpn-6.

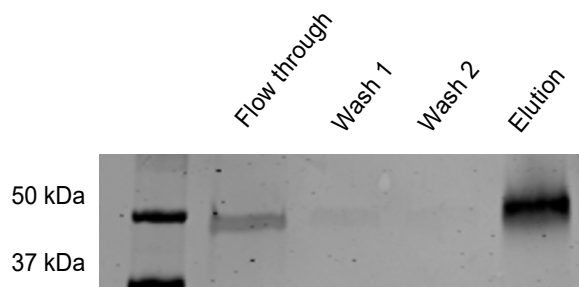


**Figure 2.16. BMCC-BDzn-TXS-8 pull-down experiment with purified Rpn-6.** A band corresponded to Rpn-6 in the elution lane was observed indicating the capture of Rpn-6 from the solution with the probe. (Western blot, anti-Rpn-6)

Similar to what we performed in the non-covalent Rpn-6 pull-down experiment; we started the covalent pull-down experiment with purified Rpn-6. A blocking buffer which includes a variety of proteins from cell lysate was added to Rpn-6 to mimic the cellular environment. The ligand was incubated with the purified Rpn-6 for one hour followed by UV activation and cross-linking for 30 mins. Magnetic streptavidin beads were added to the mixture for pull-down. The beads were washed

with phosphate buffer saline (PBS) with 1% Tween 20 and eluted with 0.1 M glycine solution at pH 2.0. A distinct band was observed in the elution lane on our western blot and the result indicated purified Rpn-6 was successfully captured in our covalent pull-down using the BMCC-BDzn-TXS-8 probe (**Figure 2.16**).

### 2.5.4 TXS-14 covalent pull-down with purified Rpn-6.

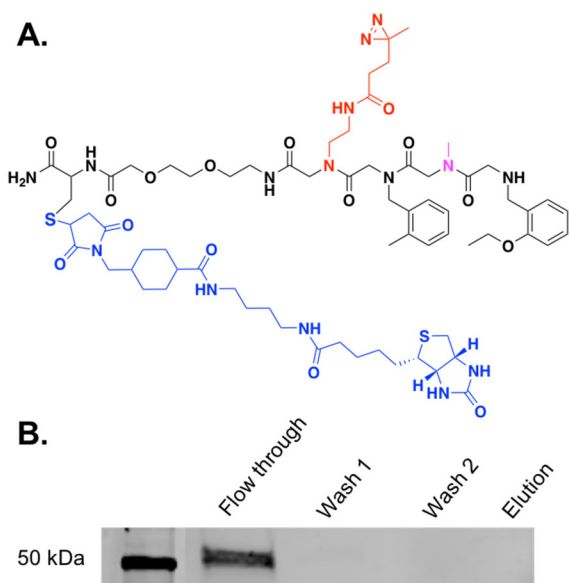


**Figure 2.17. TXS-14 pull-down (A) Structure of BMCC-BDzn-TXS-14. (B) Pull-down with purified Rpn-6.** (Western blot, anti-Rpn-6)

After successfully pulling down purified Rpn-6 with BMCC-BDzn-TXS-8, we modified TXS-14 for covalent pull-down experiment as a negative control. Previous FP and thermal shift assay results indicated TXS-14 does not bind with Rpn-6 and we wanted to validate the observations with the covalent pull-down experiment (**Figure 2.17A**). BMCC-BDzn-TXS-14 was synthesized via solid-phase synthesis and purified by HPLC. A pull-down experiment with BMCC-BDzn-TXS-14 was performed using the same conditions as BMCC-

BDzn-TXS-8. As hoped, no band was observed from the elution lane in both Coomassie stained gel and western blot (**Figure 2.17B**).

### 2.5.5 TXS-8 covalent pull-down in cell lysate with endogenous Rpn-6 and proteomic analysis.

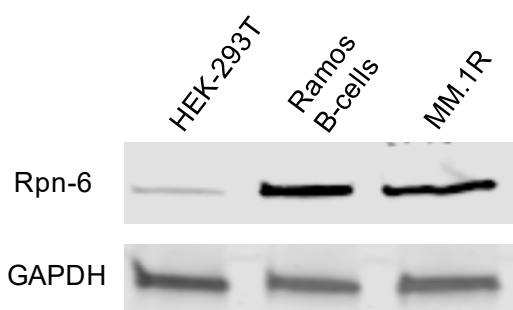


**Figure 2.18. Rpn-6 expression in different cell lines.** Hematological cancer cells like Ramos B-cell and multiple myeloma cells express significantly more Rpn-6 comparing to HEK-293T cells. (Western blot, anti-Rpn-6)

With the success on performing pull-down experiments with purified Rpn-6 and BMCC-BDzn-TXS-8, we were confident to move onto next step of TXS-8 target validation. To further explore the target of TXS-8 in cells, we decided to perform covalent pull-down experiments using BMCC-BDzn-TXS-8 in cell lysate. Before we performed the experiment, we first analyzed the relative Rpn-6 expression levels among several cell lines in our lab. This experiment provided us with both the best cell line for the covalent pull-down experiment and a prerequisite experiment for future cell-based studies which will be presented in **Chapter 3**. Among various cell lines, we discovered that Ramos B-cells and multiple myeloma cells expressed the highest amount of Rpn-6 as compared to other cells (**Figure 2.18**). Interestingly, Ramos B-cells and multiple myeloma cells are both hematological cancer cells and have shown to upregulate cellular proteasome activities for survival.<sup>86–88</sup> We chose Ramos B-cells for the covalent pull-down experiment. The cells were collected and lysed using mammalian protein extraction reagent (M-PER) according to the manufacturer's protocol. BMCC-BDzn-TXS-8 was added to the cell lysate to allow for binding. The mixture was then exposed to UV light followed by subsequent streptavidin pull-down. In the experiment, both Coomassie staining and western blot were performed to investigate the protein composition in each fraction. As hoped, Rpn-6 was observed in the elution lane in both the Coomassie stained gel and the western blot (**Figure 2.19**). The band around 50 kDa on the Coomassie stained gel was cut out and the sample was submitted to Purdue Proteomics Facility for liquid chromatography-mass spectrometry/mass spectrometry (LC-MS/MS) analysis. This sample was submitted to validate the observed band in the western blot as Rpn-6 and to provide guidance for future optimization of TXS-8 for binding site study. Rpn-6 was confirmed to be

present in the submitted sample as the major protein. However, not all peptides were identified from the proteomic analysis, two regions were missing during the analysis. These missing regions were the  $\alpha$ -solenoid region from amino acid 180-240 and the intersection between the  $\alpha$ -solenoid region and PCI domain from amino acid 300-330 (**Figure 2.20**).

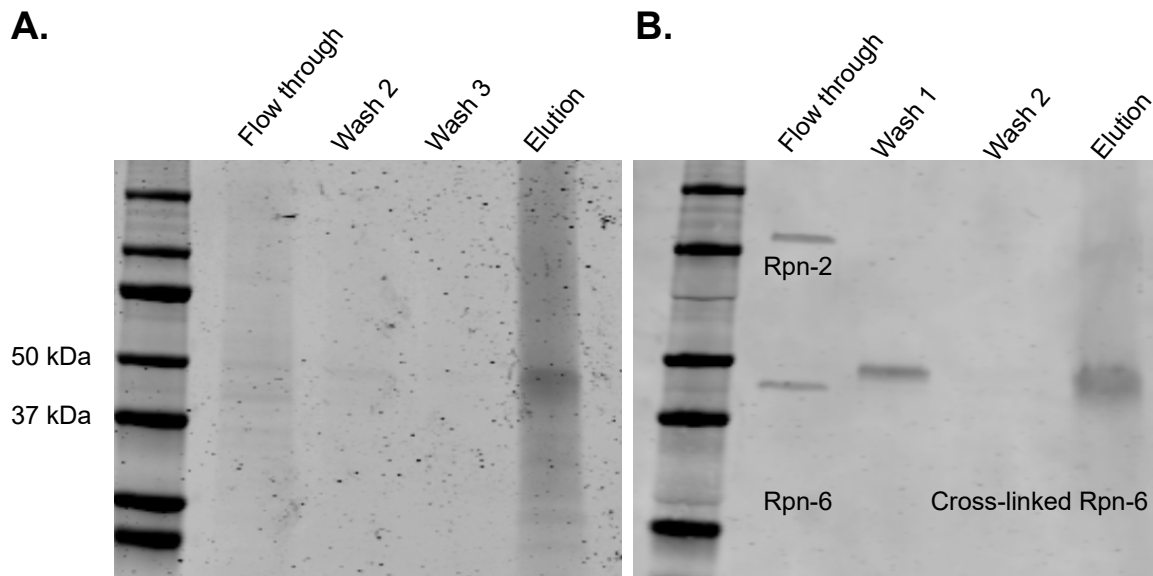


**Figure 2.19. TXS-8 endogenous Rpn-6 pull-down in cell lysate.** (A) Coomassie stained gel of BMCC-BDzn-TXS-8 pull-down, a distinct band corresponding to Rpn-6 weight was observed around 50 kDa. (B) Western blot of BMCC-BDzn-TXS-8 pull-down, Rpn-6 was observed in the elution lane and indicated a success of the experiment. Rpn-2 was only observed in flow through indicating that TXS-8 was not binding to Rpn-2.

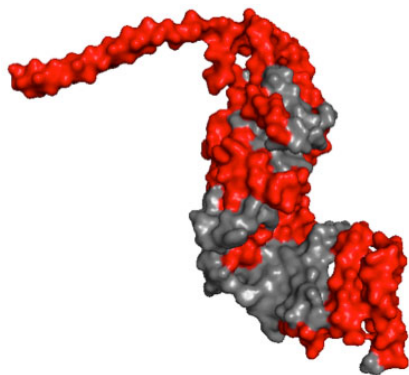


**Figure 2.20.** Colored map of identified sequence from endogenous Rpn-6 pull-down in cell lysate. Red regions stand for sequence identified during proteomic analysis.

This was an exciting discovery as we had shown Rpn-6 was the major protein in covalent TXS-8 pull-down experiments. The unidentified regions on Rpn-6 also provided us guides to possible binding site(s) of TXS-8 on Rpn-6; as the cross-linking of BMCC-BDzn-TXS-8 onto Rpn-6 brought unusual components and mass to the binding site peptide fragment, the analysis software would not be able to identify the cross-linked peptide fragment using an existing database and will result in the loss of sequence identification.

## 2.6 Conclusion.

Cancer is a debilitating condition that causes significant health related and economic burdens on patients and their families. As our understanding of cancer has been evolving for decades, we begin to realize that the proteasome, the “cell’s garbage disposal,” has significant effects on cancer survival, metastasis and proliferation.<sup>72–75</sup> The proteasome is a crucial protein complex that maintains proper cell proliferation and cellular function.<sup>15,16,76</sup> But abnormal proteasome activity increase in cells caused by stress conditions may lead to results in tumorigenesis.<sup>40–42</sup> Inhibiting proteasome activity using small molecules has shown to be effective against cancers with upregulated proteasome activity and several proteasome inhibitors have been developed and approved by the FDA for treatment of hematological cancers, such as multiple myeloma. Currently, the developed proteasome inhibitors all target the  $\beta 5$  subunit to inhibit its chymotrypsin-like function described in **Chapter 1.3.1**, resulting in protein accumulation and cell apoptosis.<sup>77–79</sup> However, due to the monistic inhibition mechanism, resistance against these proteasome inhibitors has been observed among patients, as cancer cells overexpress  $\beta 5$  subunits as “decoys” to attenuate the effect from proteasome inhibitors.<sup>80–82</sup> It is urgent that we study other 26S proteasome subunits, which are not in the  $\beta$  ring but present crucial functions to maintain proteasome activities, for novel inhibitor development. Rpn-6 is a subunit of the 19S RP and has been identified as an important subunit for maintaining proteasome structural integrity and boosting proteasome activity upon phosphorylation. Rpn-6 is also a crucial subunit for the proper formation of the 19S RP lid and the translocation of target protein into the catalytic barrel.<sup>1–3,24</sup> Although Rpn-6 displays no enzymatic-like function, in contrast to some  $\beta$  subunits, it exhibits multiple protein-protein interactions with other proteasome subunits on the 19S RP and the 20S CP. We hypothesized that developing a small molecule protein binder will disrupt the proper function of Rpn-6 and will lead to 26S proteasome malfunction, affecting cell survival.

We present here the discovery, development and characterization of a peptoid molecule TXS-8 as a selective binder of proteasomal subunit Rpn-6. The discovery process highlights the feasibility of utilizing one-bead-one-compound libraries for convenient and high-throughput screening. Combining an one-bead-one-compound library with thermal shift assay, we can easily identify small molecules bound to the target protein by monitoring changes in protein melting temperature. Using fluorescence polarization assay allows us to determine the binding affinity of

the hit from the screening to the target protein. TXS-8 is identified as the best hit from the assay with an  $K_d$  of  $\sim 14 \mu\text{M}$  to Rpn-6.

The structural study of TXS-8 reveals two important aspects of TXS-8. First, all three amines are essential for TXS-8 to bind with Rpn-6 and second the insertion of linear alkyl structure like ethylene group at the C-terminus of TXS-8 is accepted, although no increase of binding affinity has been observed with additional amines. TXS-8 is also selective towards Rpn-6 when other proteins are screened against TXS-8 including 19S RP subunit Rpn-13, which has previously been reported to bind with peptoid.

The structure of TXS-8 was further modified for use in a covalent pull-down experiment, where diazirine and biotin moieties are introduced to the molecule as functional handles. In both purified Rpn-6 and endogenous Rpn-6 from cell lysate experiments, Rpn-6 is observed as the major protein in the elution fraction. Additionally, negative control TXS-14 does not pull down any Rpn-6 in either experiment, demonstrating peptoid structure specificity. The result again highlights the importance of all three amines on TXS-8 for its binding. It also indicates that TXS-8 is a selective binder of Rpn-6.

With the increase in research on proteasomal subunits, the discovery of TXS-8 could potentially provide a breakthrough for other proteasome subunit binding studies. We can move to further investigate if this new small molecule of Rpn-6 will be relatively more toxic in cancer cells that overexpress Rpn-6 and how it will affect proteasome activity. We can also use TXS-8 to investigate its binding site on Rpn-6 for future optimization of the molecule to increase potency. Interestingly, it is currently unknown whether Rpn-6 also participates in different cellular functions aside from being a subunit of a proteasome and TXS-8 could be used as a tool for such studies.

## **2.7 General methods and materials.**

All chemicals were obtained from either Sigma-Aldrich, Acros Organic, Alfa Aesar or Fisher Scientific. The resin was obtained from Rapp Polymere GmbH (Polystyrene AM RAM, 0.65 mmol/g). The anhydrous DMF was obtained from Acros Organic. The 96-well plates were obtained from Fisher Scientific. The polypropylene syringe with frit was obtained from Fisher Scientific. The Opti-TOF<sup>TM</sup> 384 well insert for MALDI-TOF was obtained from AB Applied Biosystems. The Ultrapure CHCA MALDI Matrix was obtained from Protea Biosciences. The *E. coli* stock was obtained from Addgene (pQTEV-PSMD11). The Mini-Protean® TGX<sup>TM</sup> Gel and

the Precision Plus Protein <sup>TM</sup> Kaleidoscope <sup>TM</sup> protein ladder were obtained from BIO-RAD. Ampicillin (Amp) was obtained from Fisher Bio-reagents. Isopropyl  $\beta$ -D-1-thiogalactopyranoside (IPTG) was obtained from Sigma. HisPur Ni<sup>2+</sup>-NTA resin was obtained from Thermo-Scientific. The bacteria culture tube with dual-position caps were obtained from Fisher-Scientific. The dialysis tubes were obtained from Fisher Scientific (nominal MWCO 6000-8000). The gel running buffer was made from the 10X stock from BIO-RAD. The Coomassie Brilliant Blue R-250 solution was obtained from Bioscience. The 5000X Sypro <sup>TM</sup> Orange protein gel stain stock was obtained from Fisher Scientific. The MicroAmp<sup>®</sup> EnduraPlate <sup>TM</sup> optical 96-well fast clear reaction plate with barcode (referred as TSA plate) and MicroAmp <sup>TM</sup> optical adhesive film were both obtained from Applied Biosystems. The assay was carried out on a StepOne <sup>TM</sup> Real-time PCR system from Fisher Scientific. The Centrifugal filter units were obtained from Merck Milipore Ltd. The 384-well plate (round bottom, half volume) was obtained from Fisher Scientific. DMSO for molecular biology was obtained from Sigma-Aldrich. The Eppendorf tubes were obtained from Fisher Scientific. The BMCC-biotin, NHS-EZ-link-diazirine, Pierce<sup>TM</sup> streptavidin magnetic beads were all obtained from ThermoFisher Scientific. The pull-down assay protocol was modified from the protocol provided on the ThermoFisher website.

## **2.8 One bead one compound library.**

### **2.8.1 Library synthesis.**

100 mg of resin (100-200 mesh, 0.65 mmol/g, 300  $\mu$ m) was measured and suspended with DCM in the fritted syringe for 10 mins to allow the beads to expand. The DCM was drained and the Fmoc was removed by shaking with 20% piperidine in DMF twice with 15 mins each at RT. 4 mL of 2 M bromoacetic acid (BAA) solution (in anhydrous DMF) and 4 mL of 1 M *N,N'*-diisopropylcarbodiimide (DIC) (in anhydrous DMF) was mixed until a white precipitate appears. The mixture was added to the syringe and agitated at 37°C for 20 mins. The resin was rinsed with anhydrous DMF 3 times and was suspended in 3.5 mL of anhydrous DMF. Another 7 empty syringes were prepared and 0.5 mL of the resin/DMF solution was transferred to each syringe with a pipette. The DMF was removed and 1 mL of a 1 M amine solution (amine in anhydrous DMF) was added correspondingly to each syringe. The syringe was agitated at 37°C for one hour. The solution was removed and the resin was washed with anhydrous DMF 3 times. Then the resin was

combined into one syringe with another 8 mL of BAA and DIC mixture added. The syringe was agitated at 37°C for 20 mins. The DMF was removed and the resin was washed with anhydrous DMF 3 times. The above split and pool process was repeated for the remaining amines.

To generate master plates for screening, beads were suspended in ethanol. The beads were separated under a microscope with a 10 µL pipette tip and transferred to a well in a 96-well plate. It is important that there is only one bead per well and the wells on the edge of the plate were not used. 60 wells were available for each plate and B7, D10, E3 and G6 were left empty to be used as controls. The ethanol was removed by evaporation. The peptoid was cleaved from the bead with 50 µL of a solution of 95% TFA, 2.5% DCM, 2.5% TIPS for 40 mins. The TFA solution was removed via Centrивap and 7 µL of 1:1 H<sub>2</sub>O/AcCN (0.1% TFA) was added to each well. 1.2 µL of solution was removed from the plate onto a MALDI plate for future analysis. The water/acetonitrile solution was then removed via Centrивap. Next, 4 µL of DMSO was added to each well to dissolve the peptoid. 30 µL of PBS was added to each well to acquire a ligand concentration of 250 µM. The plate was covered with aluminum foil and stored at -80°C for future screening.

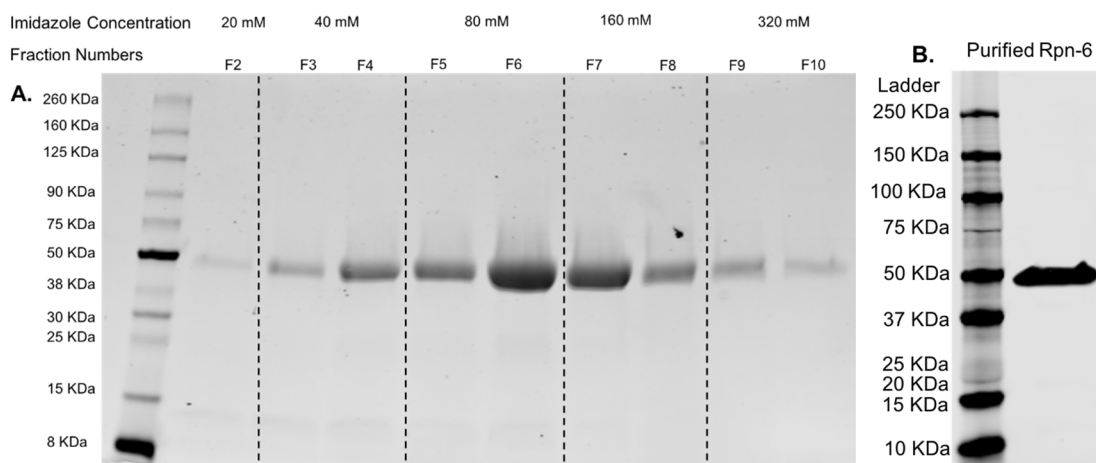


**Figure 2.21. (A) SDS-PAGE for Rpn-6 purification. (B) Western blot for purified Rpn-6.**

## 2.8.2 Rpn-6 Expression and purification.

The frozen *E. coli* stock was removed from the -80°C and was defrosted at RT. 8 mL of sterilized LB broth solution with Amp was added to a bacteria culture tube and 20 µL of the *E. coli* stock was suspended in the culture medium. The tube was incubated at 37°C for a minimum of 6 hours. 25 g of LB broth solid was added to a 2.8 L flask and was dissolved with 1L of Mili-Q

water. The LB broth solution was sterilized and it was cooled to room temperature. 100 mg of Amp was added to the flask before transferring the 8 mL pre-cultured *E. coli*. The flask was further incubated at 37°C until an OD of 0.6-0.8 was reached as measured by Nanodrop™ (Thermo Fisher). 119 mg of IPTG (final concentration 1mM) was added to the flask and the flask was further incubated at room temperature overnight. The cell media was transferred into a 1L flask and was spun down at 4700 rpm for 10 mins in a centrifuge (Thermo Scientific Legend™ XTR Centrifuge). The cell media was removed and the bacteria pellet was re-suspended in 20 mL of pre-cooled *E. coli* lysis buffer. The lysis buffer was collected and cells were further lysed by an ultrasonic disruptor with a pulse on for two seconds followed by pulse off for 5 seconds. The total time for pulse on was one minute and the process was repeated three times. The lysate was centrifuged at 13000 x g for 30 mins followed by Ni<sup>2+</sup> affinity chromatography in a 4°C fridge. 1 mg of imidazole (5mM) was added to the column before chromatography to limit non-specific binding. 5 mL of 20mM, 40 mM, 80 mM, 160 mM and 320 mM imidazole in PBS were prepared in duplicate and the solution was cooled to 4°C. The cell lysate was drained from the column and the resin was washed with cold PBS 3 times. The imidazole solution was added to elute the protein from the resin from low to high concentration. Gel loading buffer was added to a small amount of each elution fraction to reach a 1:4 ratio. The mixture was heated up for 3 mins to allow protein to fully denature. SDS-PAGE was applied to the above mixture and the gel was stained with Coomassie. The gel was checked by Li-Cor (**Figure 2.21**). Fractions with pure Rpn-6 were collected in a dialysis tube and the tube was stirred in 3 L of cold PBS overnight to remove the imidazole. The protein solution was transferred into a 50 mL falcon tube and was spun down at 13000xg for 10 mins to sediment any suspension in the solution. The protein solution was then transferred into another 50 mL falcon tube and was stored at 4°C fridge.

### **2.8.3 Thermal shift assay (TSA) screening.**

The OBOC plate was taken out from the -80°C fridge to warm up to room temperature. The protein solution was added to a centrifugal filter unit and was concentrated via a pre-cooled centrifuge at 5000xg until protein concentration reached 7.5 µM. The 5000X dye stock was diluted with PBS to obtain a 100X solution. The reference solution was obtained by dissolving 4 µL of DMSO into 30 µL of PBS. 16 µL of Rpn-6 protein solution was added to a well of the TSA plate. 2 µL of ligand solution and 2 µL of 100X dye solution was added to the same well later. The ligand

layout on the TSA plate was the same comparing to the ligand plate. In well B7, D10, E3 and G6, 2  $\mu\text{L}$  of reference solution was added instead of the ligand solution. Everything was mixed by tapping the side of the plate gently. The TSA plate was brought to the qPCR instrument for screening and the data was further collected and analyzed. The borderline set for detecting a hit was a change in melting temperature compared to the reference wells greater than or equal to  $2^{\circ}\text{C}$ .

## 2.9 Fluorescent polarization assay (FP) on Rpn-6.

### 2.9.1 FP tag synthesis.

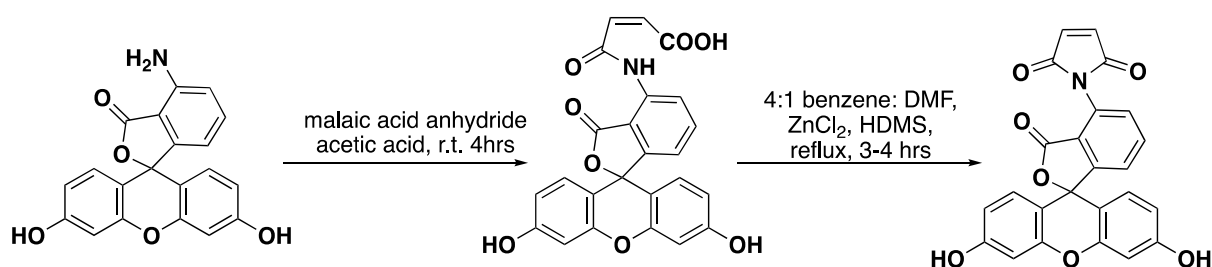


**Figure 2.22.** Fluorescein synthesis.

170 mg of fluorescein isomer and 50 mg of malaic acid anhydride were added to 50 mL of acetic acid. The mixture was stirred at room temperature. for 4 hours. Orange Precipitate was separated from the mixture by filtration and the solid was washed with EtOAc 5 times. The dark orange solid was further dried under vacuum pump covered with aluminum foil. 195 mg of the intermediate was dissolved in 20 mL of 4:1 benzene: DMF solution and 121 mg of  $\text{ZnCl}_2$  and 200  $\mu\text{L}$  of HDMS were added to the solution. The mixture was refluxed for 3-4 hours. Benzene was removed under reduced pressure when the reaction was finished. The reaction was quenched by pouring the mixture into 50 mL of ice water and acidified to pH 3-4. The red orange precipitate was separated from the mixture by filtration and the solid was washed with cold water at least 5 times. The yellow-orange solid was collected and further dried under vacuum pump. The isolated compound was stored at  $-20^{\circ}\text{C}$  in the dark and the purity was checked by LC-MS. The reaction yield is 41%. (**Figure 2.22**)

### 2.9.2 FP peptoid linker synthesis.

500 mg of Rink amide resin (0.708 mmol/g, 0.354 mmol) was suspended in DCM in the syringe for 10 mins to allow the beads to expand. The DCM was drained and the Fmoc was removed by 20% piperidine twice with 15 mins each at room temperature. to give a positive Kaiser test. Fmoc-Cys(Mmt)-OH (4 eq, 1.416 mmol, 871.9 mg), Oxyma pure (4 eq, 1.416 mmol, 201.2 mg) and DIC (4 eq, 1.416 mmol, 222  $\mu$ L) were dissolved in 3 mL DMF each. They were mixed to yield a yellow solution before being added to the resin. The syringe was agitated for 1 hour to give a negative Kaiser test. The Fmoc was removed by 20% piperidine twice for 15 mins each at room temperature. to give a positive Kaiser test. Fmoc-miniPEG-OH (4 eq, 1.416 mmol, 545.7 mg), Oxyma pure (4 eq, 1.416 mmol, 201.2 mg) and DIC (4 eq, 1.416 mmol, 222  $\mu$ L) were dissolved in 2.35 mL DMF each. They were mixed to yield a yellow solution before being added to the resin. The syringe was agitated for 1 hour to give a negative Kaiser test. The resin was separated into 20 syringes with 25 mg of resin each. The resin was stored at 4°C for further peptoid synthesis.

### 2.9.3 FP peptoid synthesis.

Resin with the FP-PEG linker conjugated was suspended in DCM in the syringe for 10 mins to allow the beads to expand. The DCM was drained and the Fmoc was removed by 20% piperidine twice for 15 mins each at room temperature. 1 mL of 2M BAA solution and 1M DIC solution were mixed until a white precipitate formed. The mixture was added to the syringe and agitated at 37°C for 20 mins. The resin was rinsed with anhydrous DMF 3 times and 1 mL of the 1M amine solution was added to the syringe and agitated at 37°C for one hour. The resin was later rinsed with anhydrous DMF for 3 times and the above step was repeated for two more rounds to obtain a 3-mer-FP peptoid. The resin was washed with DCM three times when the last coupling was finished. The Mmt group on Cys was removed by agitating the resin with 1 mL of 96% DCM, 3% TFA and 1% TIPS for 30 seconds, repeated 5 times. The resin was further rinsed with DMF, 10 mL of 10% TEA in DMF, then DMF. 3 mg of fluorescein was measured and dissolved in 1.5 mL of DMSO then the solution was added to the syringe with 2.5 mL of anhydrous DMF. The syringe was agitated at room temperature. for 3 hours in dark. The resin was washed with DCM 3 times. The bead was further cleaved with a mixed solution of 95% TFA, 2.5% DCM, 2.5% TIPS

at room temperature. for one hour in dark. The cleaved solution was collected and dried under a stream of argon to yield yellow oil-like liquid. The liquid was dissolved in 1:1 H<sub>2</sub>O: AcCN (HPLC grade, 0.1% TFA) and separated by RP-HPLC. The purity of the fraction was checked by LC-MS and fractions containing pure substance were combined, froze, lyophilized and stored at -20°C.

#### **2.9.4 Fluorescence polarization (FP) assay.**

The Rpn-6 protein solution in PBS was added to a centrifugal filter unit and was concentrated via a pre-cooled centrifuge at 5000xg until protein concentration reached at least 40 µM checked by Nanodrop<sup>TM</sup>. The protein was serially diluted 11 times. The protein fractions were put on ice to maintain the structural integrity of Rpn-6. The dried FP peptoid was dissolved in 100 µL of DMSO and was transferred into a black Eppendorf tube. 10 µL of the DMSO stock was dissolved into 990 µL of PBS solution and the concentration was measured by Nanodrop<sup>TM</sup>. The 1 mL FP peptoid stock was further diluted by PBS to obtain 1 mL of a 120 nM FP peptoid solution. 11 µL of PBS was added separately into three wells on the plate. 11 µL of diluted Rpn-6 solution was added after blank from higher concentration to lower concentration, respectively. 1 µL of peptoid stock was added to each well simultaneously. The plate was agitated by tapping the side of the plate for 30 seconds. The milli-polarization was then measured by a Synergy 4 plate reader. The above steps were repeated until data for all peptoids was recorded. The data was collected and graphed by Prism version number 7. FP experiments were repeated in experimental and technical triplicate and all data was averaged to generated binding curves.

#### **2.9.5 Fluorescent polarization (FP) assay with other proteins.**

Protein preparation: bovine serum albumin, β-Amylase from sweet potato, carbonic Anhydrase from bovine erythrocytes and cytochrome C from bovine heart protein powders were obtained from Sigma-Aldrich. The above protein powders were measured and dissolved in 1 mL of PBS to acquire a 70 µM solution. Rpn-13 was obtained from Christine Muli from our lab. The protein solution was rocked in a cold room for 10 mins and seated on ice for 30 mins.

The above protein solution was serially diluted to 0.54 µM. The TXS-8-FP peptoid was dissolved in 100 µL of DMSO and was transferred into a black Eppendorf tube. 10 µL of the DMSO stock was dissolved into 990 µL of PBS solution and the concentration was measured by

Nanodrop™. The 1 mL peptoid stock was further diluted by PBS to obtain 1mL of 100 nM FP peptoid solution.

9  $\mu$ L of PBS was added separately into three wells on the plate. 9  $\mu$ L of diluted protein solution was added after blank from higher concentration to lower concentration, 1  $\mu$ L of TXS-8-FP 100 nM solution was added to each well simultaneously. The plate was agitated by tapping the side of the plate for 30 seconds. The polarization was then measured by Synergy 4. The above steps were repeated until all proteins were measured. The data was collected and graphed by Graphpad.

### **2.10 Pull-down assay with diazirine biotin dual labeled TXS-8 on purified Rpn-6 in blocking buffer.**

The diazirine biotin dual-labeled peptoid will be abbreviated in to BDzn-peptoid in the future chapters. Mono-MMt-ethylenediamine was inserted in front of the sequence of TXS-8/TXS-14 after mini-PEG for later diazirine coupling with peptoid synthesis protocol described above. The MMt protecting groups on both cysteine and ethylenediamine were removed by 3% of TFA in DCM (1% TIPS). The removal of the MMt on ethylenediamine was examined with Kaiser test to result in a positive result. 0.95 eq of NHS-EZ-link-diazirine was dissolved in 1.2 mL anhydrous DMF with 1.1 eq of DIPEA mixed in a 1.5 ep tube and the above mixture was agitated for about 5 mins in dark. The mixture was later added to the resin and the resin was agitated for 30-40 mins in the dark to allow coupling of diazirine to ethylenediamine. The completion of the experiment was monitored by Kaiser. Later, 1.1 eq of BMCC-biotin was added to a 1.5 mL ep tube and dissolved with about 300  $\mu$ L of anhydrous DMSO. 900  $\mu$ L of anhydrous DMF was added later and the solution was added to resin. The resin was agitated for 1.5 to 2 hours in dark. The resin was further washed with DCM three times and cleaved with a mixture of 95% TFA, 2.5% DCM and 2.5% TIPS for 40 mins in dark. The cleaved solution was collected and dried under argon to yield colorless oil-like liquid. The liquid was dissolved in 2:1 H<sub>2</sub>O: AcCN (HPLC grade, 0.1% TFA) and separated by HPLC. The purity of the fraction was checked by LC-MS and fractions containing pure substance were combined, froze, lyophilized and stored at -20°C.

Rpn-6 was prepared as previously described. The protein was concentrated to 7.5  $\mu$ M. To avoid overwhelming the streptavidin beads during the assay, the protein was diluted with PBS to 0.014 mg/mL for experiment. DMSO was used as a negative control to examine if Rpn-6 aggregates on the bead. Approximately 0.16 mg of BDzn-TXS-8 was dissolved in 16  $\mu$ L of DMSO

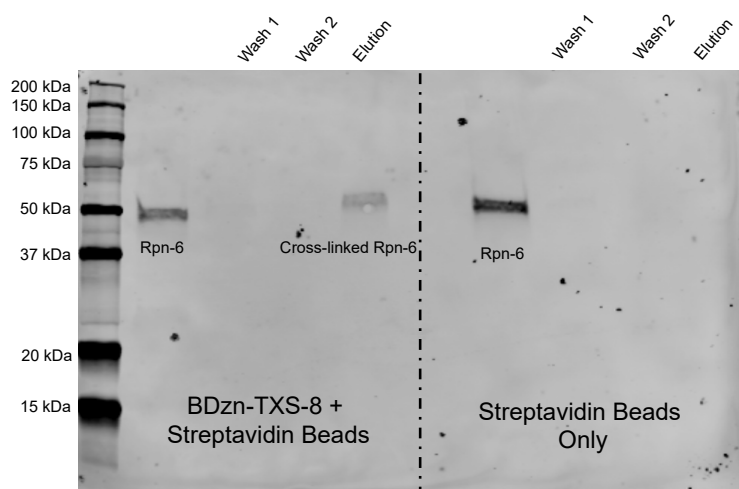


Figure 2.23. Pull-down assay of purified Rpn-6 diluted in blocking buffer using BMCC-BDzn-TXS-8.

and the stock was further diluted with 700  $\mu$ L of 50 mM Tris binding buffer (pH 7.35, 1% Tween). The Rpn-6 stock was added to the above peptoid solution and the mixture was incubated with mixing at room temperature. for one hour in the dark. The ligand protein mixture was transferred into transparent ep tubes and 365 nm UV light was applied to the tube at 4°C for

30 mins to allow diazirine crosslinking to proteins. The mixture was added to Tris binding buffer pre-washed streptavidin magnetic beads and the mixture was incubated at room temperature. with mixing for one hour. The washing procedure was the same as the ThermoFisher procedure and flow-through, W1, W2 and elution fractions were all subjected to SDS-PAGE for either Coomassie staining or western blot (**Figure 2.23**).

### 2.11 Pull-down assay with diazirine biotin dual labeled TXS-8/TXS-14 on cell lysates.

Ramos B-cells were incubated in a 10 cm<sup>2</sup> dish till confluency. The cells were collected and separated evenly into two parts. The cells were lysed with 700  $\mu$ L of M-PER (100:1 M-PER/HALT protease inhibitor) at room temperature. for 35 mins. The cell lysate was further centrifuged at 12,000xg for 12 mins and the cell debris was left in the tube. The whole cell protein concentration was measured with Nanodrop<sup>TM</sup>. Based on measured protein concentration, the mass for whole cell protein was calculated and BDzn-TXS-8/14 were measured accordingly as 10% of the whole cell protein mass. The above peptoids were dissolved in 25  $\mu$ L of DMSO then further diluted with 700  $\mu$ L of 50 mM Tris binding buffer (pH 7.35, 1% Tween). The cell lysate was added to the above peptoid solution and the mixture was incubated with mixing at room temperature. for one hour in dark. The ligand protein mixture was transferred into transparent ep tubes and 365 nm UV light was applied to the tube at 4°C for 30 mins to allow diazirine crosslinking to proteins. The mixture was added to Tris binding buffer pre-washed streptavidin magnetic beads and the mixture

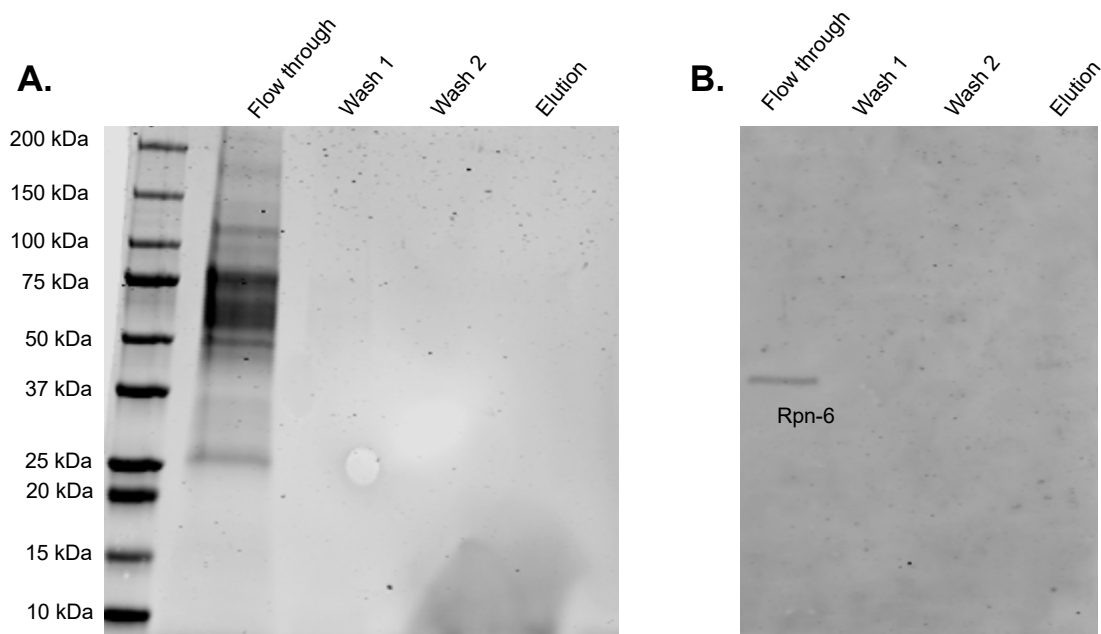


**Figure 2.24. TXS-14 pull-down experiment (A) SDS-PAGE Coomassie stain and. (B) Western blot using BMCC-BDzn-TXS-14 for pull-down with Ramos B-cell lysate.**

was incubated at room temperature. with mixing for one hour. The washing procedure was the same compared to ThermoFisher procedure and W1, W2, W3 and elution fractions were all subjected to SDS-PAGE for either Coomassie staining or western blot (**Figure 2.24**).

## 2.12 Proteomic analysis on BMCC-BDzn-TXS-8 target.

The band elution band from cell lysate pull-down was cut off and submitted to Purdue Proteomic Facility for protein analysis. (**Figure 2.25, Table 2.2**)

10 20 30 40 50  
 MAAAVVEFQ RAQSLLSTDR EASIDILHSI VKRDIQENDE EAVQVKEQSI  
 60 70 80 90 100  
 LELGSLLAKT GQAAELGGLL KYVRPFLNSI SKAKAARLVR SLLDLFLDME  
 110 120 130 140 150  
 AATGQEVELC LECIEWAKSE KRTFLRQALE ARLVSLYFDT KRYQEALHLG  
 160 170 180 190 200  
 SQLLRELKKM DDKALLVEVQ LLESKYHAL SNLPKARAAL TSARTTANAI  
 210 220 230 240 250  
 YCPPKLQATL DMQSGIIHAA EEKDWKTAYS YFYEA FEGYD SIDSPKAITS  
 260 270 280 290 300  
 LKYMILLCKIM LNTPEDVQAL VSGKLALRYA GRQTEALKCV AQASKNRS LA  
 310 320 330 340 350  
 DFEKALTDYR AELRDDPIIS THLAKLYDNL LEQNLIRVIE PFSRVQIEHI  
 360 370 380 390 400  
 SSLIKLSKAD VERKLSQMIL DKKFHGILDQ GEGVLIIFDE PPVDKTYEAA  
 410 420  
 LETIQNMSKV VDSLYNKAKK LT

**Figure 2.25.** Peptide fragments (highlighted in yellow) observed during gel band analysis by proteomics.

**Table 2.2.** List of the peptides observed during proteomics, their location within the Rpn-6 sequence, and the corresponding LFQ intensity observed for each peptide.

Peptide sequence	Residues	LFQ Intensity
AQSLLSTDR	12-20	86285000
RDIQENDEEAVQVK	33-46	24948000
EQSILELGSLLAK	47-59	148790000
YVRPFLNSISK	72-82	51305000
LVSLYFDTK	133-141	90810000
RYQEALHLGSQLLR	142-155	89747000
ALLVEVQLLESK	164-175	71509000
TAYSIFYEAFEGYDSIDSPK	227-246	91069000
LYDNLLEQNLIR	326-337	302270000
VIEPFSR	338-344	48285000
VQIEHISSLIK	345-355	45673000
TYEAALETIQNMSK	396-409	66757000

## 2.13 Reference.

- (1) Santamaría, P. G.; Finley, D.; Ballesta, J. P. G.; Remacha, M. Rpn6p, a Proteasome Subunit from *Saccharomyces Cerevisiae*, Is Essential for the Assembly and Activity of the 26 S Proteasome. *Journal of Biological Chemistry* **2003**, 278 (9), 6687–6695. <https://doi.org/10.1074/jbc.M209420200>.
- (2) Isono, E.; Saito, N.; Kamata, N.; Saeki, Y.; Toh-e, A. Functional Analysis of Rpn6p, a Lid Component of the 26 S Proteasome, Using Temperature-Sensitive *Rpn6* Mutants of the Yeast *Saccharomyces Cerevisiae*. *Journal of Biological Chemistry* **2005**, 280 (8), 6537–6547. <https://doi.org/10.1074/jbc.M409364200>.
- (3) Pathare, G. R.; Nagy, I.; Bohn, S.; Unverdorben, P.; Hubert, A.; Korner, R.; Nickell, S.; Lasker, K.; Sali, A.; Tamura, T.; Nishioka, T.; Forster, F.; Baumeister, W.; Bracher, A. The Proteasomal Subunit Rpn6 Is a Molecular Clamp Holding the Core and Regulatory Subcomplexes Together. *Proceedings of the National Academy of Sciences* **2012**, 109 (1), 149–154. <https://doi.org/10.1073/pnas.1117648108>.
- (4) Das, A. K. The Structure of the Tetratricopeptide Repeats of Protein Phosphatase 5: Implications for TPR-Mediated Protein-Protein Interactions. *The EMBO Journal* **1998**, 17 (5), 1192–1199. <https://doi.org/10.1093/emboj/17.5.1192>.
- (5) Zeytuni, N.; Zarivach, R. Structural and Functional Discussion of the Tetra-Trico-Peptide Repeat, a Protein Interaction Module. *Structure* **2012**, 20 (3), 397–405. <https://doi.org/10.1016/j.str.2012.01.006>.
- (6) Luan, B.; Huang, X.; Wu, J.; Mei, Z.; Wang, Y.; Xue, X.; Yan, C.; Wang, J.; Finley, D. J.; Shi, Y.; Wang, F. Structure of an Endogenous Yeast 26S Proteasome Reveals Two Major Conformational States. *Proc Natl Acad Sci USA* **2016**, 113 (10), 2642–2647. <https://doi.org/10.1073/pnas.1601561113>.
- (7) Ellisdon, A. M.; Stewart, M. Structural Biology of the PCI-Protein Fold. *BioArchitecture* **2012**, 2 (4), 118–123. <https://doi.org/10.4161/bioa.21131>.
- (8) Hofmann, K.; Bucher, P. The PCI Domain: A Common Theme in Three Multiprotein Complexes. *Trends in Biochemical Sciences* **1998**, 23 (6), 204–205. [https://doi.org/10.1016/S0968-0004\(98\)01217-1](https://doi.org/10.1016/S0968-0004(98)01217-1).
- (9) Zhang, W.; Zhao, C.; Hu, Y.; Jin, C. NMR 1H, 13C, 15N Backbone and Side Chain Resonance Assignment of the N-Terminal Domain of Yeast Proteasome Lid Subunit Rpn5. *Biomol NMR Assign* **2019**, 13 (1), 1–4. <https://doi.org/10.1007/s12104-018-9840-5>.
- (10) Pick, E.; Hofmann, K.; Glickman, M. H. PCI Complexes: Beyond the Proteasome, CSN, and EIF3 Troika. *Molecular Cell* **2009**, 35 (3), 260–264. <https://doi.org/10.1016/j.molcel.2009.07.009>.

- (11) Rousseau, A.; Bertolotti, A. An Evolutionarily Conserved Pathway Controls Proteasome Homeostasis. *Nature* **2016**, *536* (7615), 184–189. <https://doi.org/10.1038/nature18943>.
- (12) Valas, R. E.; Bourne, P. E. Rethinking Proteasome Evolution: Two Novel Bacterial Proteasomes. *J Mol Evol* **2008**, *66* (5), 494–504. <https://doi.org/10.1007/s00239-008-9075-7>.
- (13) Fort, P.; Kajava, A. V.; Delsuc, F.; Coux, O. Evolution of Proteasome Regulators in Eukaryotes. *Genome Biology and Evolution* **2015**, *7* (5), 1363–1379. <https://doi.org/10.1093/gbe/evv068>.
- (14) Bar-Nun, S.; Glickman, M. H. Proteasomal AAA-ATPases: Structure and Function. *Biochimica et Biophysica Acta (BBA) - Molecular Cell Research* **2012**, *1823* (1), 67–82. <https://doi.org/10.1016/j.bbamcr.2011.07.009>.
- (15) Adams, J. The Proteasome in Cell-Cycle Regulation. In *Proteasome Inhibitors in Cancer Therapy*; Adams, J., Ed.; Humana Press: Totowa, NJ, 2004; pp 77–84. [https://doi.org/10.1007/978-1-59259-794-9\\_6](https://doi.org/10.1007/978-1-59259-794-9_6).
- (16) Bassermann, F.; Eichner, R.; Pagano, M. The Ubiquitin Proteasome System — Implications for Cell Cycle Control and the Targeted Treatment of Cancer. *Biochimica et Biophysica Acta (BBA) - Molecular Cell Research* **2014**, *1843* (1), 150–162. <https://doi.org/10.1016/j.bbamcr.2013.02.028>.
- (17) Karpov, D. S.; Spasskaya, D. S.; Tutyaeva, V. V.; Mironov, A. S.; Karpov, V. L. Proteasome Inhibition Enhances Resistance to DNA Damage via Upregulation of Rpn4-Dependent DNA Repair Genes. *FEBS Letters* **2013**, *587* (18), 3108–3114. <https://doi.org/10.1016/j.febslet.2013.08.007>.
- (18) Moiseeva, T. N.; Bottrill, A.; Melino, G.; Barlev, N. A. DNA Damage-Induced Ubiquitylation of Proteasome Controls Its Proteolytic Activity. *Oncotarget* **2013**, *4* (9), 1338–1348. <https://doi.org/10.18632/oncotarget.1060>.
- (19) Salceda, S.; Caro, J. Hypoxia-Inducible Factor 1 $\alpha$  (HIF-1 $\alpha$ ) Protein Is Rapidly Degraded by the Ubiquitin-Proteasome System under Normoxic Conditions. *Journal of Biological Chemistry* **1997**, *272* (36), 22642–22647. <https://doi.org/10.1074/jbc.272.36.22642>.
- (20) Dong, Y.; Zhang, S.; Wu, Z.; Li, X.; Wang, W. L.; Zhu, Y.; Stoilova-McPhie, S.; Lu, Y.; Finley, D.; Mao, Y. Cryo-EM Structures and Dynamics of Substrate-Engaged Human 26S Proteasome. *Nature* **2018**. <https://doi.org/10.1038/s41586-018-0736-4>.
- (21) Huang, X.; Luan, B.; Wu, J.; Shi, Y. An Atomic Structure of the Human 26S Proteasome. *Nature Structural & Molecular Biology* **2016**, *23* (9), 778–785. <https://doi.org/10.1038/nsmb.3273>.
- (22) Dambacher, C. M.; Worden, E. J.; Herzik, M. A.; Martin, A.; Lander, G. C. Atomic Structure of the 26S Proteasome Lid Reveals the Mechanism of Deubiquitinase Inhibition. *eLife* **2016**, *5*, e13027. <https://doi.org/10.7554/eLife.13027>.

- (23) Guan, H.; Wang, Y.; Yu, T.; Huang, Y.; Li, M.; Saeed, A. F. U. H.; Perčulija, V.; Li, D.; Xiao, J.; Wang, D.; Zhu, P.; Ouyang, S. Cryo-EM Structures of the Human PA200 and PA200-20S Complex Reveal Regulation of Proteasome Gate Opening and Two PA200 Apertures. *PLoS Biol* **2020**, *18* (3), e3000654. <https://doi.org/10.1371/journal.pbio.3000654>.
- (24) Lier, S.; Paululat, A. The Proteasome Regulatory Particle Subunit Rpn6 Is Required for *Drosophila* Development and Interacts Physically with Signalosome Subunit Alien/CSN2. *Gene* **2002**, *298* (2), 109–119. [https://doi.org/10.1016/S0378-1119\(02\)00930-7](https://doi.org/10.1016/S0378-1119(02)00930-7).
- (25) Bai, M.; Zhao, X.; Sahara, K.; Ohte, Y.; Hirano, Y.; Kaneko, T.; Yashiroda, H.; Murata, S. In-Depth Analysis of the Lid Subunits Assembly Mechanism in Mammals. *Biomolecules* **2019**, *9* (6), 213. <https://doi.org/10.3390/biom9060213>.
- (26) Greene, E. R.; Goodall, E. A.; de la Peña, A. H.; Matyskiela, M. E.; Lander, G. C.; Martin, A. *Specific Lid-Base Contacts in the 26S Proteasome Control the Conformational Switching Required for Substrate Engagement and Degradation*; preprint; Biochemistry, 2019. <https://doi.org/10.1101/687921>.
- (27) Eisele, M. R.; Reed, R. G.; Rudack, T.; Schweitzer, A.; Beck, F.; Nagy, I.; Pfeifer, G.; Plitzko, J. M.; Baumeister, W.; Tomko, R. J.; Sakata, E. Expanded Coverage of the 26S Proteasome Conformational Landscape Reveals Mechanisms of Peptidase Gating. *Cell Reports* **2018**, *24* (5), 1301–1315.e5. <https://doi.org/10.1016/j.celrep.2018.07.004>.
- (28) Li, F.; Tian, G.; Langager, D.; Sokolova, V.; Finley, D.; Park, S. Nucleotide-Dependent Switch in Proteasome Assembly Mediated by the Nas6 Chaperone. *Proc Natl Acad Sci USA* **2017**, *114* (7), 1548–1553. <https://doi.org/10.1073/pnas.1612922114>.
- (29) Park, S.; Li, X.; Kim, H. M.; Singh, C. R.; Tian, G.; Hoyt, M. A.; Lovell, S.; Battaile, K. P.; Zolkiewski, M.; Coffino, P.; Roelofs, J.; Cheng, Y.; Finley, D. Reconfiguration of the Proteasome during Chaperone-Mediated Assembly. *Nature* **2013**, *497* (7450), 512–516. <https://doi.org/10.1038/nature12123>.
- (30) Finley, D.; Chen, X.; Walters, K. J. Gates, Channels, and Switches: Elements of the Proteasome Machine. *Trends in Biochemical Sciences* **2016**, *41* (1), 77–93. <https://doi.org/10.1016/j.tibs.2015.10.009>.
- (31) Park, S.; Tian, G.; Roelofs, J.; Finley, D. Assembly Manual for the Proteasome Regulatory Particle: The First Draft. *Biochemical Society Transactions* **2010**, *38* (1), 6–13. <https://doi.org/10.1042/BST0380006>.
- (32) Ding, Z.; Fu, Z.; Xu, C.; Wang, Y.; Wang, Y.; Li, J.; Kong, L.; Chen, J.; Li, N.; Zhang, R.; Cong, Y. High-Resolution Cryo-EM Structure of the Proteasome in Complex with ADP-AlFx. *Cell Res* **2017**, *27* (3), 373–385. <https://doi.org/10.1038/cr.2017.12>.

- (33) Zhu, Y.; Wang, W. L.; Yu, D.; Ouyang, Q.; Lu, Y.; Mao, Y. Structural Mechanism for Nucleotide-Driven Remodeling of the AAA-ATPase Unfoldase in the Activated Human 26S Proteasome. *Nat Commun* **2018**, *9* (1), 1360. <https://doi.org/10.1038/s41467-018-03785-w>.
- (34) de la Peña, A. H.; Goodall, E. A.; Gates, S. N.; Lander, G. C.; Martin, A. Substrate-Engaged 26 S Proteasome Structures Reveal Mechanisms for ATP-Hydrolysis–Driven Translocation. *Science* **2018**, *362* (6418), eaav0725. <https://doi.org/10.1126/science.aav0725>.
- (35) *Macromolecular Protein Complexes III: Structure and Function*; Harris, J. R., Marles-Wright, J., Eds.; Subcellular Biochemistry; Springer International Publishing: Cham, 2021; Vol. 96. <https://doi.org/10.1007/978-3-030-58971-4>.
- (36) Unverdorben, P.; Beck, F.; led, P.; Schweitzer, A.; Pfeifer, G.; Plitzko, J. M.; Baumeister, W.; Forster, F. Deep Classification of a Large Cryo-EM Dataset Defines the Conformational Landscape of the 26S Proteasome. *Proceedings of the National Academy of Sciences* **2014**, *111* (15), 5544–5549. <https://doi.org/10.1073/pnas.1403409111>.
- (37) Guo, X.; Huang, X.; Chen, M. J. Reversible Phosphorylation of the 26S Proteasome. *Protein Cell* **2017**, *8* (4), 255–272. <https://doi.org/10.1007/s13238-017-0382-x>.
- (38) Lokireddy, S.; Kukushkin, N. V.; Goldberg, A. L. CAMP-Induced Phosphorylation of 26S Proteasomes on Rpn6/PSMD11 Enhances Their Activity and the Degradation of Misfolded Proteins. *Proceedings of the National Academy of Sciences* **2015**, *112* (52), E7176–E7185. <https://doi.org/10.1073/pnas.1522332112>.
- (39) Vilchez, D.; Morantte, I.; Liu, Z.; Douglas, P. M.; Merkwirth, C.; Rodrigues, A. P. C.; Manning, G.; Dillin, A. RPN-6 Determines C. Elegans Longevity under Proteotoxic Stress Conditions. *Nature* **2012**, *489* (7415), 263–268. <https://doi.org/10.1038/nature11315>.
- (40) Suh, K. S.; Tanaka, T.; Sarojini, S.; Nightingale, G.; Gharbaran, R.; Pecora, A.; Goy, A. The Role of the Ubiquitin Proteasome System in Lymphoma. *Critical Reviews in Oncology/Hematology* **2013**, *87* (3), 306–322. <https://doi.org/10.1016/j.critrevonc.2013.02.005>.
- (41) Csizmar, C. M.; Kim, D.-H.; Sachs, Z. The Role of the Proteasome in AML. *Blood Cancer Journal* **2016**, *6* (12), e503–e503. <https://doi.org/10.1038/bcj.2016.112>.
- (42) Siegel, R. L.; Miller, K. D.; Jemal, A. Cancer Statistics, 2017. *CA: A Cancer Journal for Clinicians* **2017**, *67* (1), 7–30. <https://doi.org/10.3322/caac.21387>.
- (43) Lam, K. S.; Lebl, M.; Krchňák, V. The “One-Bead-One-Compound” Combinatorial Library Method. *Chemical Reviews* **1997**, *97* (2), 411–448. <https://doi.org/10.1021/cr9600114>.

- (44) Lam, K. S.; Liu, R.; Miyamoto, S.; Lehman, A. L.; Tuscano, J. M. Applications of One-Bead One-Compound Combinatorial Libraries and Chemical Microarrays in Signal Transduction Research. *Acc. Chem. Res.* **2003**, *36* (6), 370–377. <https://doi.org/10.1021/ar0201299>.
- (45) Liu, T.; Qian, Z.; Xiao, Q.; Pei, D. High-Throughput Screening of One-Bead-One-Compound Libraries: Identification of Cyclic Peptidyl Inhibitors against Calcineurin/NFAT Interaction. *ACS Comb. Sci.* **2011**, *13* (5), 537–546. <https://doi.org/10.1021/co200101w>.
- (46) Maclean, D.; Schullek, J. R.; Murphy, M. M.; Ni, Z.-J.; Gordon, E. M.; Gallop, M. A. Encoded Combinatorial Chemistry: Synthesis and Screening of a Library of Highly Functionalized Pyrrolidines. *Proceedings of the National Academy of Sciences* **1997**, *94* (7), 2805–2810. <https://doi.org/10.1073/pnas.94.7.2805>.
- (47) Palomo, J. M. Solid-Phase Peptide Synthesis: An Overview Focused on the Preparation of Biologically Relevant Peptides. *RSC Adv.* **2014**, *4* (62), 32658–32672. <https://doi.org/10.1039/C4RA02458C>.
- (48) Grøftehaug, M. K.; Hajizadeh, N. R.; Swann, M. J.; Pohl, E. Protein–Ligand Interactions Investigated by Thermal Shift Assays (TSA) and Dual Polarization Interferometry (DPI). *Acta Crystallogr D Biol Crystallogr* **2015**, *71* (1), 36–44. <https://doi.org/10.1107/S1399004714016617>.
- (49) Jafari, R.; Almqvist, H.; Axelsson, H.; Ignatushchenko, M.; Lundbäck, T.; Nordlund, P.; Molina, D. M. The Cellular Thermal Shift Assay for Evaluating Drug Target Interactions in Cells. *Nature Protocols* **2014**, *9* (9), 2100–2122. <https://doi.org/10.1038/nprot.2014.138>.
- (50) Huynh, K.; Partch, C. L. Analysis of Protein Stability and Ligand Interactions by Thermal Shift Assay. *Current Protocols in Protein Science* **2015**, *79* (1). <https://doi.org/10.1002/0471140864.ps2809s79>.
- (51) Martinez, N. J.; Asawa, R. R.; Cyr, M. G.; Zakharov, A.; Urban, D. J.; Roth, J. S.; Wallgren, E.; Klumpp-Thomas, C.; Coussens, N. P.; Rai, G.; Yang, S.-M.; Hall, M. D.; Marugan, J. J.; Simeonov, A.; Henderson, M. J. A Widely-Applicable High-Throughput Cellular Thermal Shift Assay (CETSA) Using Split Nano Luciferase. *Scientific Reports* **2018**, *8* (1). <https://doi.org/10.1038/s41598-018-27834-y>.
- (52) Tanaka, M.; Roberts, J. M.; Seo, H.-S.; Souza, A.; Paulk, J.; Scott, T. G.; DeAngelo, S. L.; Dhe-Paganon, S.; Bradner, J. E. Design and Characterization of Bivalent BET Inhibitors. *Nat Chem Biol* **2016**, *12* (12), 1089–1096. <https://doi.org/10.1038/nchembio.2209>.
- (53) Divakaran, A.; Talluri, S. K.; Ayoub, A. M.; Mishra, N. K.; Cui, H.; Widen, J. C.; Berndt, N.; Zhu, J.-Y.; Carlson, A. S.; Topczewski, J. J.; Schonbrunn, E. K.; Harki, D. A.; Pomerantz, W. C. K. Molecular Basis for the N-Terminal Bromodomain-and-Extra-Terminal-Family Selectivity of a Dual Kinase–Bromodomain Inhibitor. *J. Med. Chem.* **2018**, *61* (20), 9316–9334. <https://doi.org/10.1021/acs.jmedchem.8b01248>.

- (54) Scott, D. E.; Ehebauer, M. T.; Pukala, T.; Marsh, M.; Blundell, T. L.; Venkitaraman, A. R.; Abell, C.; Hyvönen, M. Using a Fragment-Based Approach To Target Protein-Protein Interactions. *ChemBioChem* **2013**, *14* (3), 332–342. <https://doi.org/10.1002/cbic.201200521>.
- (55) Kranz, J. K.; Schalk-Hihi, C. Protein Thermal Shifts to Identify Low Molecular Weight Fragments. In *Methods in Enzymology*; Elsevier, 2011; Vol. 493, pp 277–298. <https://doi.org/10.1016/B978-0-12-381274-2.00011-X>.
- (56) Martinez, N. J.; Asawa, R. R.; Cyr, M. G.; Zakharov, A.; Urban, D. J.; Roth, J. S.; Wallgren, E.; Klumpp-Thomas, C.; Coussens, N. P.; Rai, G.; Yang, S.-M.; Hall, M. D.; Marugan, J. J.; Simeonov, A.; Henderson, M. J. A Widely-Applicable High-Throughput Cellular Thermal Shift Assay (CETSA) Using Split Nano Luciferase. *Sci Rep* **2018**, *8* (1), 9472. <https://doi.org/10.1038/s41598-018-27834-y>.
- (57) McNulty, D. E.; Bonnette, W. G.; Qi, H.; Wang, L.; Ho, T. F.; Waszkiewicz, A.; Kallal, L. A.; Nagarajan, R. P.; Stern, M.; Quinn, A. M.; Creasy, C. L.; Su, D.-S.; Graves, A. P.; Annan, R. S.; Sweitzer, S. M.; Holbert, M. A. A High-Throughput Dose-Response Cellular Thermal Shift Assay for Rapid Screening of Drug Target Engagement in Living Cells, Exemplified Using SMYD3 and IDO1. *SLAS DISCOVERY: Advancing the Science of Drug Discovery* **2018**, *23* (1), 34–46. <https://doi.org/10.1177/2472555217732014>.
- (58) Singhal, N.; Kumar, M.; Kanaujia, P. K.; Viridi, J. S. MALDI-TOF Mass Spectrometry: An Emerging Technology for Microbial Identification and Diagnosis. *Front. Microbiol.* **2015**, *6*. <https://doi.org/10.3389/fmicb.2015.00791>.
- (59) Culf, A. S.; Ouellette, R. J. Solid-Phase Synthesis of N-Substituted Glycine Oligomers (A-Peptoids) and Derivatives. *Molecules* **2010**, *15* (8), 5282–5335. <https://doi.org/10.3390/molecules15085282>.
- (60) Hall, M. D.; Yasgar, A.; Peryea, T.; Braisted, J. C.; Jadhav, A.; Simeonov, A.; Coussens, N. P. Fluorescence Polarization Assays in High-Throughput Screening and Drug Discovery: A Review. *Methods Appl. Fluoresc.* **2016**, *4* (2), 022001. <https://doi.org/10.1088/2050-6120/4/2/022001>.
- (61) Jameson, D. M.; Ross, J. A. Fluorescence Polarization/Anisotropy in Diagnostics and Imaging. *Chem. Rev.* **2010**, *110* (5), 2685–2708. <https://doi.org/10.1021/cr900267p>.
- (62) Moerke, N. J. Fluorescence Polarization (FP) Assays for Monitoring Peptide-Protein or Nucleic Acid-Protein Binding. *Current Protocols in Chemical Biology* **2009**, *1* (1), 1–15. <https://doi.org/10.1002/9780470559277.ch090102>.
- (63) Lea, W. A.; Simeonov, A. Fluorescence Polarization Assays in Small Molecule Screening. *Expert Opinion on Drug Discovery* **2011**, *6* (1), 17–32. <https://doi.org/10.1517/17460441.2011.537322>.

- (64) Weiss, G. A.; Watanabe, C. K.; Zhong, A.; Goddard, A.; Sidhu, S. S. Rapid Mapping of Protein Functional Epitopes by Combinatorial Alanine Scanning. *Proceedings of the National Academy of Sciences* **2000**, 97 (16), 8950–8954. <https://doi.org/10.1073/pnas.160252097>.
- (65) Trader, D. J.; Simanski, S.; Kodadek, T. A Reversible and Highly Selective Inhibitor of the Proteasomal Ubiquitin Receptor Rpn13 Is Toxic to Multiple Myeloma Cells. *Journal of the American Chemical Society* **2015**, 137 (19), 6312–6319. <https://doi.org/10.1021/jacs.5b02069>.
- (66) Das, J. Aliphatic Diazirines as Photoaffinity Probes for Proteins: Recent Developments. *Chem. Rev.* **2011**, 111 (8), 4405–4417. <https://doi.org/10.1021/cr1002722>.
- (67) Preston, G. W.; Wilson, A. J. Photo-Induced Covalent Cross-Linking for the Analysis of Biomolecular Interactions. *Chem. Soc. Rev.* **2013**, 42 (8), 3289. <https://doi.org/10.1039/c3cs35459h>.
- (68) MacKinnon, A. L.; Taunton, J. Target Identification by Diazirine Photo-Cross-Linking and Click Chemistry. *Current Protocols in Chemical Biology* **2009**, 1 (1), 55–73. <https://doi.org/10.1002/9780470559277.ch090167>.
- (69) Murale, D. P.; Hong, S. C.; Haque, Md. M.; Lee, J.-S. Photo-Affinity Labeling (PAL) in Chemical Proteomics: A Handy Tool to Investigate Protein-Protein Interactions (PPIs). *Proteome Sci* **2016**, 15 (1), 14. <https://doi.org/10.1186/s12953-017-0123-3>.
- (70) Dundas, C. M.; Demonte, D.; Park, S. Streptavidin–Biotin Technology: Improvements and Innovations in Chemical and Biological Applications. *Appl Microbiol Biotechnol* **2013**, 97 (21), 9343–9353. <https://doi.org/10.1007/s00253-013-5232-z>.
- (71) Jain, A.; Cheng, K. The Principles and Applications of Avidin-Based Nanoparticles in Drug Delivery and Diagnosis. *Journal of Controlled Release* **2017**, 245, 27–40. <https://doi.org/10.1016/j.jconrel.2016.11.016>.
- (72) Almond, J.; Cohen, G. The Proteasome: A Novel Target for Cancer Chemotherapy. *Leukemia* **2002**, 16 (4), 433–443. <https://doi.org/10.1038/sj.leu.2402417>.
- (73) Dantuma, N. P.; Bott, L. C. The Ubiquitin-Proteasome System in Neurodegenerative Diseases: Precipitating Factor, yet Part of the Solution. *Frontiers in Molecular Neuroscience* **2014**, 7. <https://doi.org/10.3389/fnmol.2014.00070>.
- (74) Gong, B.; Radulovic, M.; Figueiredo-Pereira, M. E.; Cardozo, C. The Ubiquitin-Proteasome System: Potential Therapeutic Targets for Alzheimer’s Disease and Spinal Cord Injury. *Front. Mol. Neurosci.* **2016**, 9. <https://doi.org/10.3389/fnmol.2016.00004>.
- (75) Deng, L.; Meng, T.; Chen, L.; Wei, W.; Wang, P. The Role of Ubiquitination in Tumorigenesis and Targeted Drug Discovery. *Sig Transduct Target Ther* **2020**, 5 (1), 11. <https://doi.org/10.1038/s41392-020-0107-0>.

- (76) Dang, F.; Nie, L.; Wei, W. Ubiquitin Signaling in Cell Cycle Control and Tumorigenesis. *Cell Death Differ* **2021**, *28* (2), 427–438. <https://doi.org/10.1038/s41418-020-00648-0>.
- (77) Dou, Q.; Zonder, J. Overview of Proteasome Inhibitor-Based Anti-Cancer Therapies: Perspective on Bortezomib and Second Generation Proteasome Inhibitors versus Future Generation Inhibitors of Ubiquitin-Proteasome System. *Current Cancer Drug Targets* **2014**, *14* (6), 517–536. <https://doi.org/10.2174/1568009614666140804154511>.
- (78) Selimovic, D.; Porzig, B. B. O. W.; El-Khattouti, A.; Badura, H. E.; Ahmad, M.; Ghanjati, F.; Santourlidis, S.; Haikel, Y.; Hassan, M. Bortezomib/Proteasome Inhibitor Triggers Both Apoptosis and Autophagy-Dependent Pathways in Melanoma Cells. *Cellular Signalling* **2013**, *25* (1), 308–318. <https://doi.org/10.1016/j.cellsig.2012.10.004>.
- (79) Chen, D.; Frezza, M.; Schmitt, S.; Kanwar, J.; P. Dou, Q. Bortezomib as the First Proteasome Inhibitor Anticancer Drug: Current Status and Future Perspectives. *Current Cancer Drug Targets* **2011**, *11* (3), 239–253. <https://doi.org/10.2174/156800911794519752>.
- (80) Lü, S.; Wang, J. The Resistance Mechanisms of Proteasome Inhibitor Bortezomib. *Biomarker Research* **2013**, *1* (1). <https://doi.org/10.1186/2050-7771-1-13>.
- (81) Oerlemans, R.; Franke, N. E.; Assaraf, Y. G.; Cloos, J.; van Zantwijk, I.; Berkers, C. R.; Scheffer, G. L.; Debipersad, K.; Vojtekova, K.; Lemos, C.; van der Heijden, J. W.; Ylstra, B.; Peters, G. J.; Kaspers, G. L.; Dijkmans, B. A. C.; Scheper, R. J.; Jansen, G. Molecular Basis of Bortezomib Resistance: Proteasome Subunit B5 (PSMB5) Gene Mutation and Overexpression of PSMB5 Protein. *Blood* **2008**, *112* (6), 2489–2499. <https://doi.org/10.1182/blood-2007-08-104950>.
- (82) Yang, W.-C.; Lin, S.-F. Mechanisms of Drug Resistance in Relapse and Refractory Multiple Myeloma. *BioMed Research International* **2015**, *2015*, 1–17. <https://doi.org/10.1155/2015/341430>.

## **CHAPTER 3. TXS-8 TOXICITY IN HEMATOLOGICAL CANCER CELLS AND DEVELOPMENT OF A GENERAL WORKFLOW ON INVESTIGATING THE IMPACT OF A SMALL MOLECULE ON PROTEASOME.**

### **3.1 Introduction.**

As described in **Chapter 2**, our screen of a one-bead-one-compound library against purified Rpn-6, resulted in the discovery a small molecule, TXS-8, as a selective binder of proteasomal subunit Rpn-6. We observed a binding affinity  $K_d$  of 14  $\mu$ M to Rpn-6 via a fluorescence polarization assay. We also validated that TXS-8 is selective towards Rpn-6 by a covalent cross-linking pull-down experiment. To further investigate the impacts of TXS-8 on cell viability and determine whether TXS-8 affects proteasome activity, we designed and performed multiple cell-based experiments which will be discussed in this Chapter.<sup>1</sup>

Previously, to monitor the changes in proteasome activities, researchers have been developing small molecule probes that can be selectively cleaved by certain proteasome subunits. Among these probes, a 4-amino-7-methylcoumarin (AMC) moiety was used that the release of the moiety upon hydrolysis of the amide bond will generate fluorescence signal that can be quantified. Ac-GPLD-AMC (Ac stands for acetyl group),<sup>2,3</sup> Boc-LRR-AMC (Boc stands for tert-butyloxycarbonyl group),<sup>4,5</sup> and Suc-LLVY-AMC (Suc stands for succinyl group) were developed as selective probes for the caspase-like  $\beta$ 1 subunit, trypsin-like  $\beta$ 2 subunit and chymotrypsin-like  $\beta$ 5 subunit, respectively.<sup>6-8</sup> These small molecule probes have been very useful on proteasome characterization especially on studying proteasome inhibitors.<sup>9,10</sup>

However, these probes were only suitable for monitoring proteasome activity changes in biochemical assays due to the cell impermeability of the probes.<sup>11</sup> Therefore, researchers have been developing cell permeable fluorescence probes or monitor protein degradation in cells to monitor proteasome activity changes in cells.<sup>8,12,13</sup> By combining using cell permeable fluorescence probe and monitoring protein degradation in cells, we developed a three-step general workflow to investigate the impact of a small molecule on proteasome activity which will be presented in this chapter.

### 3.2 Rpn-6 overexpression in hematological cancer cells.

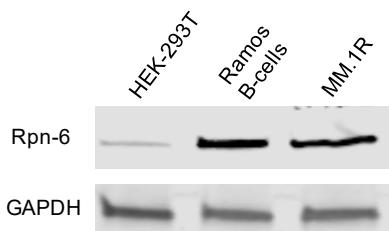


**Figure 3.1 Rpn-6 expression in HEK-293T, Ramos B-cells and MM.1R cells.** Hematological cancer cells overly express Rpn-6.

As described in **Chapter 2.5.5** that we investigated expression levels of Rpn-6 in several cell lines. According to literature, hematological cancer cells, like multiple myeloma and Ramos B-cell lymphoma, are sensitive to proteasome activity inhibition.<sup>14,15</sup> However, proteasome inhibitor resistance had been observed among patients.<sup>16–19</sup> As **Chapter 2.1** indicated, Rpn-6 expression was strongly correlated with proteasome activity. Therefore, we

hypothesized that hematological cancer cells overexpress Rpn-6 to facilitate proteasome activity and inhibition of Rpn-6 function in these cells may lead to significant toxic effects.<sup>20–23</sup> The result of HEK-293T (human embryonic kidney cells), Ramos B-cells, and MM.1R (multiple myeloma resistant to dexamethasone) cells are described here and we confirmed that Ramos B-cells and MM.1R cells express a significant amount of Rpn-6 compared to HEK-293T cells (**Figure 3.1**).

### 3.3 Toxicity Assay with TXS-8 and Several Cell Lines.

The result from Rpn-6 expression in cells in **Chapter 3.2** confirmed our hypothesis that hematological cancer cells with high proteasome activity also overexpress Rpn-6. We next wanted

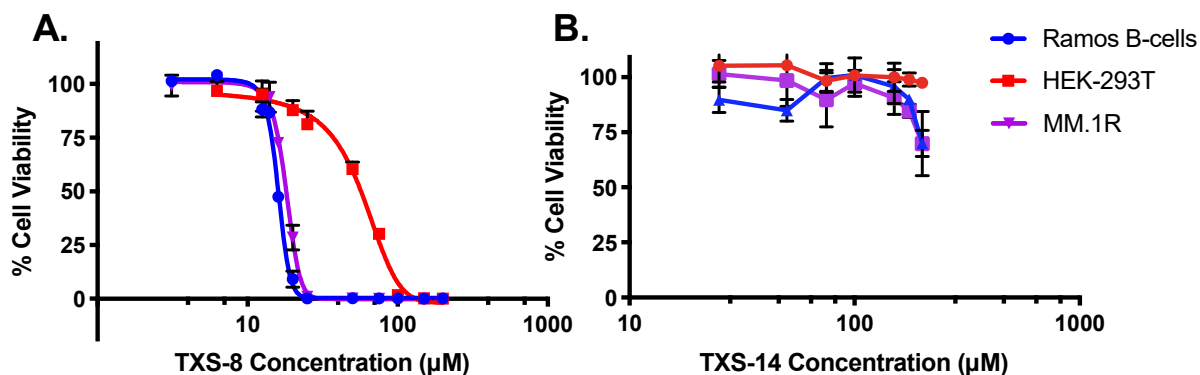


**Figure 3.2 TXS-8/14 toxicity assay (A)** Cell viability assay with HEK-293T cells, Ramos B-cells and MM.1R cells dosed with TXS-8. The  $IC_{50}$  of TXS-8 in Ramos B-cells and MM.1R was 15 µM. **3.2 (B)** TXS-14 showed no significant toxicity in all cell lines tested, even at 200 µM. This result validates our previous conclusion that the all three amines of TXS-8 was essential for its binding towards Rpn-6.

to investigate the impacts of TXS-8 on cell viability. TXS-14 was included as a negative control and we hypothesized that TXS-14 would not be toxic since it could not bind Rpn-6. We dosed the

cells with varying concentrations of TXS-8 and TXS-14 for 18 hours. A luminescent cell viability assay was used to monitor the toxicity of TXS-8 and TXS-14. We observed that hematological cancer cells (MM.1R and Ramos B-cells) were no longer viable at 20  $\mu$ M but our control HEK-293T cells did not show significant cell death until 80  $\mu$ M (**Figure 3.2A, Table 3.1**). This data illustrated that TXS-8 was more toxic to cells that overexpress Rpn-6 than normal cells and this was an exciting discovery as our lead compound TXS-8 showed some selectivity for this toxicity assay.

For our negative control, TXS-14, we had previously demonstrated that it did not bind Rpn-6 via fluorescence polarization and thermal shift assays, and it showed no significant toxicity to any of the cell lines tested (**Figure 3.2B**). This result validates our previous conclusion in **Chapter**

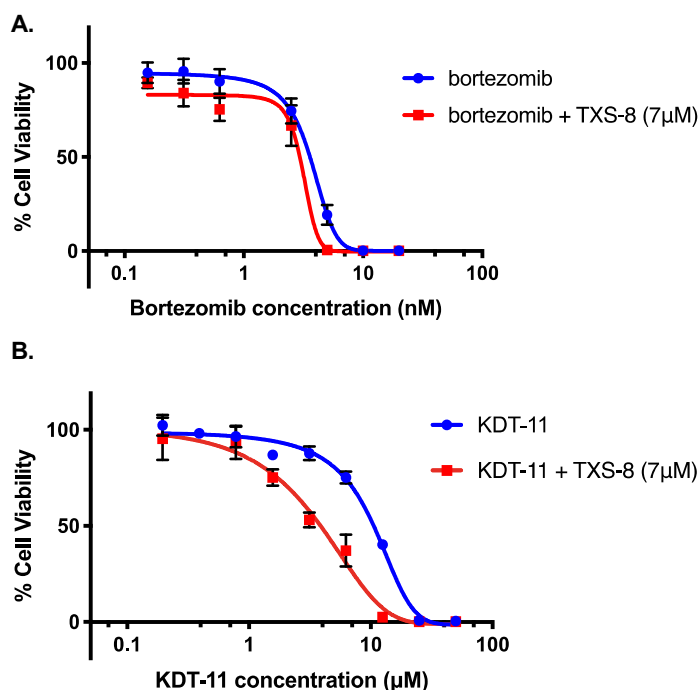


**Figure 3.3 TXS-8/bortezomib dual dosing.** Dual dosing of bortezomib/KDT-11 with TXS-8 on MM.1R cells. The viability of the cells was examined and plotted to obtain a curve.

**2.4.3** that all amine moieties on TXS-8 are essential for binding to Rpn-6. To further investigate the toxicity of TXS-8 in various cell lines, we submitted TXS-8 for a NIH NCI-60 single dose screening panel where TXS-8 showed moderate growth inhibition to leukemia cancer cells (**Table 3.2**). The result from the NCI-60 single dose screening showed that TXS-8 could potentially be developed into a therapeutic for some cancers.

### 3.4 Dual Dosing Using Bortezomib/KDT-11 and TXS-8.

We have demonstrated that TXS-8 showed moderate toxicity toward hematological cancer cells like Ramos B-cells and multiple myeloma cells. However, the  $IC_{50}$  of TXS-8 on both cell lines was around 14  $\mu$ M and could only be considered as a moderately toxic small molecule for these cancer cells. To further investigate if targeting Rpn-6 with TXS-8 could be beneficial, we decided to perform TXS-8 dual dosing experiments using bortezomib and KDT-11. Bortezomib, described in **Chapter 1.3.1** as the first

FDA approved small molecule proteasome inhibitor, was selected for the experiment.<sup>14,24,25</sup> It showed an IC<sub>50</sub> around 2-6 nM towards multiple myeloma cells and we wanted to use bortezomib to investigate if TXS-8 could lead to an additive or synergistic effect.<sup>15,26–28</sup> KDT-11 was discovered in 2015 as a selective binder of Rpn-13, one of the two ubiquitin receptor of the 26S proteasome. The IC<sub>50</sub> of KDT-11 on multiple myeloma cells was around 8 μM.<sup>29</sup> We sought to determine if dosing cancer cells with two 19S RP inhibitors would result in improved toxicity.

To perform the dual dosing experiment, we decided to use 50% of the IC<sub>50</sub> concentration (7 μM) of TXS-8 with varying concentrations of bortezomib or KDT-11. The inhibitors were mixed and then to cells, the viability of the cells was examined after 24 hours and plotted for comparison with only bortezomib or KDT-11 treated cells (**Figure 3.3**). Based on the results with MM.1R with bortezomib/KDT-11 dual dosing, no significant additive or synergistic effect was observed with bortezomib when dual dosed with 7 μM of TXS-8. Although dual dosing of KDT-11 with 7 μM of TXS-8 increased the toxicity of the mixed ligand, the overall toxicity increase of the mixed

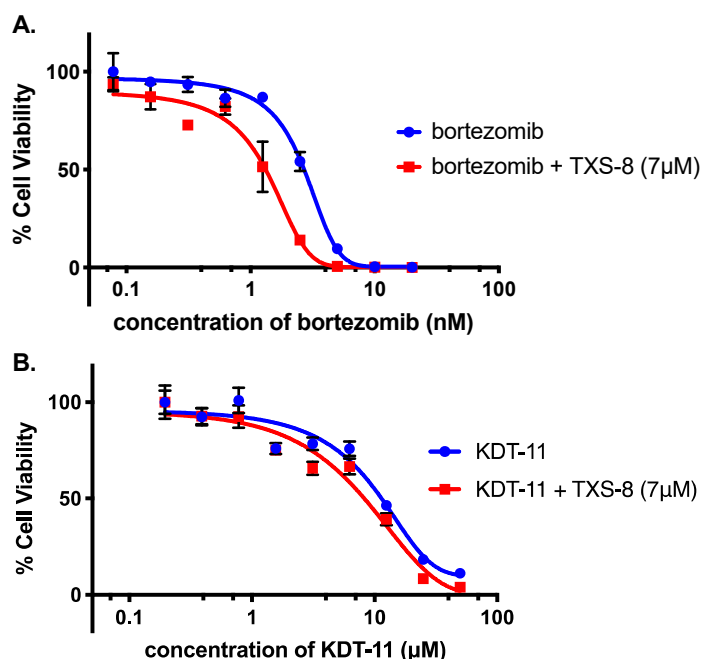


**Figure 3.4 TXS-8/KDT-11 dual dosing.** Dual dosing of bortezomib/KDT-11 with TXS-8 on Ramos B-cells. The viability of the cells was examined and plotted to obtain a curve.

ligand was less than 2-fold compared to KDT-11 treated MM.1R cells. We were unable to conclude whether an additive or synergistic effect was observed when dual dosed by TXS-8. To further investigate the dual dosing effect of TXS-8 with bortezomib/KDT-11, we also included Ramos B-cells for our dual dosing experiment as Ramos B-cells also overexpress Rpn-6. We performed the dual dosing experiment with the same conditions previously described (**Figure 3.4**). Interestingly, with Ramos B-cells, TXS-8 did not change the IC<sub>50</sub> when dual dosed with KDT-11.

However, the mixed ligand of TXS-8 and bortezomib decreased the IC<sub>50</sub> of bortezomib by 2-fold. Although we observed lower IC<sub>50</sub> with TXS-8 dual dosing in certain experimental conditions regarding bortezomib or KDT-11, the change was not significant. Therefore, with these limited

dual dosing results, we were unable to conclude if TXS-8 serves additive or synergistic effect with KDT-11/bortezomib. A more potent Rpn-6 binder is needed to determine if a synergistic or additive effect with these other proteasome inhibitors is possible.

### 3.5 Preliminary Study of the Impact of TXS-8 on Proteasome Activity.

#### 3.5.1 Establishing TXS-8 Induced Cell Stress Condition.

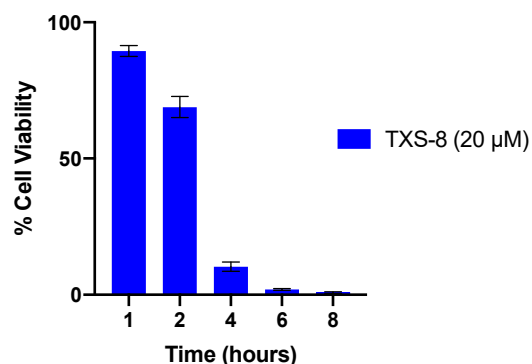


**Figure 3.5 Viability of Ramos B-cell treated with constant concentration of TXS-8.** 20  $\mu$ M of TXS-8 was added to Ramos B-cells at given time period, the viability of the cells was investigated to find out when the cells started dying.

The uncertain result from the dual dosing experiment with TXS-8 and bortezomib/KDT-11 motivated us to look into the impact of TXS-8 on proteasome activity because we were uncertain about the cellular pathway impacted by TXS-8 that resulted in cell death. To establish proper conditions to investigate the impact of TXS-8 on proteasome activity, we wanted to determine the toxic effect of TXS-8 at different dosing time period. Previously we had determined the  $IC_{50}$  of TXS-8 at around 14  $\mu$ M in Ramos B-cells. Based on this, we decided to use a higher concentration of TXS-8 for the experiment to

induce cell stress, but not toxicity. 20  $\mu$ M of TXS-8 was used to investigate the viability of Ramos B-cells in a time-dependent manner where we added TXS-8 to Ramos B-cells at certain time points and monitored viability (**Figure 3.5**). From the result of this experiment, we concluded that 20  $\mu$ M of TXS-8 could induce cell stress in less than two hours. Moving forward, we decided to dose cells with 20  $\mu$ M of TXS-8 for 1.5 hours for future experiments.

### 3.5.2 Investigating the Impact of TXS-8 on Proteasome Activity with a Biochemical Assay.

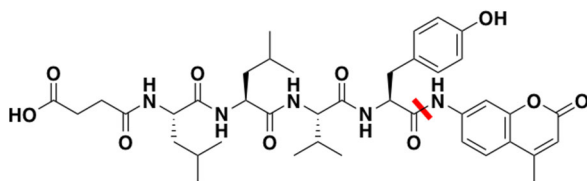


**Figure 3.6 Structure of Suc-LLVY-AMC probe.** the red marker represents the cleavage site of the compound by the chymotrypsin-like site.

In the literature, bortezomib and KDT-11 have been shown to induced ubiquitinated protein accumulation in cells and we wanted to determine if TXS-8, as a proteasomal subunit selective binder like KDT-11, could induce a similar effect.<sup>14,26,29,30</sup> To begin our studies we decided to first monitor changes in proteasome activity with biochemical assays using purified 26S proteasome and commercially available probes. Suc-LLVY-AMC (Suc stands for succinyl group, AMC stands for 7-amino-4-methylcoumarin group) probe was selected for the assay; this probe was developed as a selective substrate for the chymotrypsin-like  $\beta 5$  subunit. The cleavage of the amide bond releases the aminocoumarin group to generate fluorescence signal for quantification (**Figure 3.6**).<sup>31–35</sup> To perform the experiment, we incubated 26S proteasome, TXS-8?, and proteasome probe. The final concentration of 26S

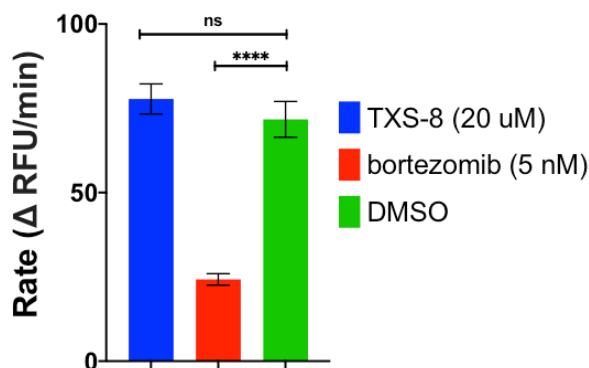


**Figure 3.7 Rate of fluorescence signal comparison with purified 26S proteasome.** Rate ( $\Delta$ RFU/min) of TXS-8, bortezomib and DMSO. No significant inhibition of proteasome activity was observed with dosage of TXS-8. Error bars represent SEM and  $n=3$ , \*\*\*\* $p<0.00005$ , ns= $p>0.05$ .

proteasome was 5 nM and the Suc-LLVY-AMC probe was 10  $\mu$ M. TXS-8 was set to a final concentration of 20  $\mu$ M and as a control, bortezomib was utilized at 5 nM. The Suc-LLVY-AMC probe was added to each well and the plate was gently agitated for five minutes. The plate was then placed on a plate reader and fluorescence signal was monitored. The data was analyzed and the rate of fluorescence signal increase ( $\Delta$ RFU/min) was plotted (**Figure 3.7**). The data demonstrated that 20  $\mu$ M of TXS-8 did not significantly inhibit proteasome activity while our positive control, bortezomib, showed significant inhibition of proteasome activity.

### 3.5.3 Investigating the Impact of TXS-8 on Proteasome Activity in Ramos B-cell Lysate Using Proteasome Probes.

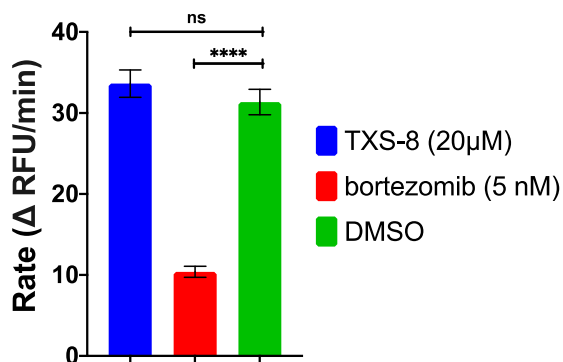


**Figure 3.8 Rate of fluorescence signal comparison in Ramos B-cell lysate.** Rate (ΔRFU/min) of TXS-8, bortezomib and DMSO. No significant inhibition of proteasome activity was observed with dosage of TXS-8. Error bars represent SEM and n=3, \*\*\*\*p<0.00005, ns=p>0.05.

The result from the purified 26S proteasome activity assay illustrated that TXS-8 may not be affecting proteasome activity. However, we decided to move forward to investigate the impact of TXS-8 in cells to determine if TXS-8 was affecting proteasome assembly. We chose to use Ramos B-cells for the experiment as we had previously established proper conditions to induce cell stress in these cells. Since Ramos-B cells are difficult to use for cell-based assay with our probes because the AMC probes were generally cell impermeable, we

decided to perform a proteasome activity assay with Ramos B-cell lysate with the Suc-LLVY-AMC probe.<sup>6</sup> Cells were dosed with TXS-8, bortezomib or DMSO for 1.5 hours. The cells were then collected and lysed with a non-denaturing buffer. The Suc-LLVY-AMC probe was added to the cell lysate along with 20 μM of TXS-8, 5 nM bortezomib, or DMSO so the ligands were still present in the cell lysate. The cell lysate was transferred to a 96-well plate and the fluorescent signal was monitored over time. The data was analyzed and the rate of fluorescence signal increase was graphed (**Figure 3.8**). The result from this assay indicated that 20 μM of TXS-8 did not decrease the cleavage rate of the Suc-LLVY-AMC probe significantly. Meanwhile, our positive control bortezomib-treated Ramos B-cells exhibited a significant decrease of proteasome activity. Although both the purified 26S proteasome and Ramos B-cell lysate assays indicated that TXS-8 did not significantly affect proteasome activity, Suc-LLVY-AMC is a small substrate of the proteasome and is rapidly cleaved. We hypothesized this probe may not be sensitive enough to detect inhibition of the proteasome by TXS-8 as it can be rapidly degraded through a ubiquitin-independent mechanism that does not require Rpn-6 to be functional.<sup>7,36,37</sup> To overcome this issue, our lab had developed a FRET (Fluorescence Resonance Energy Transfer) based probe for proteasome activity measurement (**Figure 3.9**).<sup>7</sup> This probe was longer than the AMC probes therefore it was harder to be degraded rapidly by the proteasome as the long substrate cannot easily fit into the gate of the 20S CP. We decided to use this probe to monitor proteasome activity in

response to dosage with TXS-8. We also sought to monitor K-48 polyubiquitin accumulation with a western blot assay to investigate ubiquitin-dependent proteasome activity changes.

### 3.5.4 Investigating TXS-8 Impact on Proteasome Activity with FRET Probe and K-48 Immunoblot.

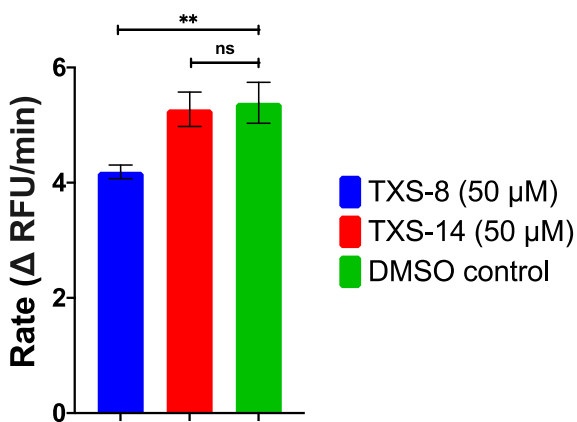


**Figure 3.10 Rate of fluorescence signal comparison with purified 26S proteasome.** Rate ( $\Delta$ RFU/min) of TXS-8, TXS-14 and DMSO. Proteasome activity was significantly decreased with 50  $\mu$ M of TXS-8 but TXS-14 showed no impact on proteasome activity. Error bars represent SEM and  $n=3$ ,  $**p<0.005$ ,  $ns=p>0.05$ .

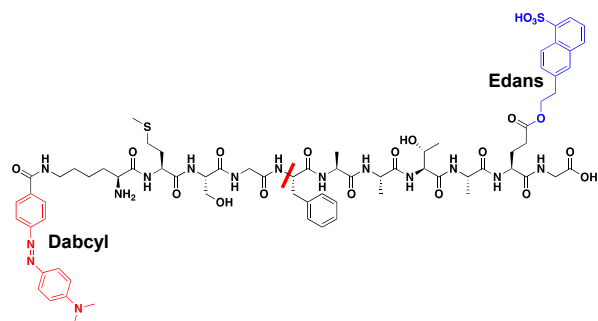


**Figure 3.9 Structure of the FRET probe designed by our lab.** The red marker indicates the cleavage site of the peptide. Edan is colored in blue and dabcyll is colored in red.

To investigate the changes of proteasome activity in response to TXS-8, we decided to perform two experiments; 1) We wanted to use the FRET probe with purified 26S proteasome; 2) We wanted to monitor accumulation of K-48 polyubiquitinated proteins in TXS-8-treated Ramos B-cells. Similar to our previous experiments with Suc-LLVY-AMC probe, the final concentration of the FRET probe was 10  $\mu$ M but we increased the concentration of TXS-8 to 50  $\mu$ M. We included TXS-14 as our negative control (**Figure 3.10, Figure 3.23**). The result of the assay indicated that TXS-8 did inhibit the proteasome but TXS-14 did not.

In addition to monitoring proteasome activity changes with TXS-8 dosing, we also investigated polyubiquitinated protein accumulation in cells when treated with TXS-8. Bortezomib was included as a positive control. Ramos B-cells were dosed with 20  $\mu$ M of TXS- or 5 nM bortezomib for two hours and then lysed with M-PER solution. A K-48 polyubiquitin immunoblot

was performed to monitor the relative amount of polyubiquitinated proteins in cells (**Figure 3.11**). As mentioned previously in **Chapter 1.1.1** ubiquitin can be modified in various positions and K-

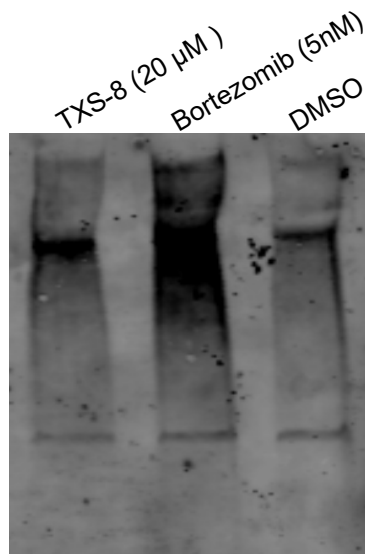


**Figure 3.11** K-48 polyubiquitin immunoblot in Ramos B-cells treated with TXS-8 or bortezomib and DMSO. TXS-8 did not significantly induce ubiquitinated protein accumulation like positive control bortezomib.

48 modification is related to proteasomal degradation. The immunoblot indicated that 20  $\mu\text{M}$  of TXS-8 treatment did not significantly increased K-48 polyubiquitinated protein accumulation like our positive control, bortezomib. Although we observed a proteasome activity decrease in FRET assay, 50  $\mu\text{M}$  of TXS-8 is a high concentration and will induce significant cell death in Ramos B-cells or multiple myeloma cells. The FRET probe is not cell permeable, so we were unable to directly monitor proteasome activity changes in living cells. However, the K-48 ubiquitin immunoblot may suggest that TXS-8 does not affect proteasome activity at non-lethal concentrations.

### 3.6 A Three-Step Workflow of Investigating the Impacts of Small Molecules on Proteasome Activity.

Recently, our lab has developed a series of rhodamine-based

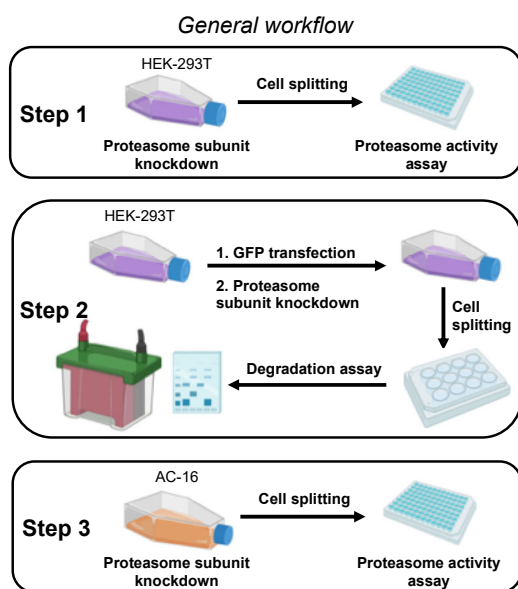


**Figure 3.12** A three-step general workflow of investigating the impact of a small molecule on proteasome activity. Figure made by BioRender.com.

probes that are cell permeable.<sup>6,38</sup> These probes exhibit much slower cleavage compared to the Suc-LLVY-AMC probe. Our probes are also resistant to cellular protease cleavage. But most importantly, these probes are cell permeable and we are able to directly monitor proteasome activity in live cells. In addition to being able to directly monitor proteasome activity changes, we had also acquired experience in knocking down subunits in cells with silencing RNA (siRNA) and transfecting cells to induce specific protein expression.

Therefore, we planned to develop and apply multiple assays to evaluate small molecules, such as TXS-8, which can bind selectively with noncatalytic proteasome subunits to determine if they can affect proteasome activity *in cellulo* (Figure 3.12, Figure 3.28).<sup>39</sup> While we had initially planned to use

Ramos B-cells in our experiments, we found that it was difficult to transfect these cells.<sup>40–44</sup> Therefore, we selected HEK-293T cells for the assay development, starting with monitoring proteasome activity biochemically followed by monitoring degradation of full-length proteins by immunoblot analysis. Finally, TXS-8 was tested in a primary cell line with the proteasome selective probe for validation. Through the above experiments, we were able to develop critical assays to study future Rpn-6 small molecule binders and apply these assays to the evaluation of small molecule binders of other proteasome subunits.

### 3.6.1 Testing Proteasome Activity Changes Using Proteasome Selective Probes in Normal and Rpn-6 Knocked Down Cells.

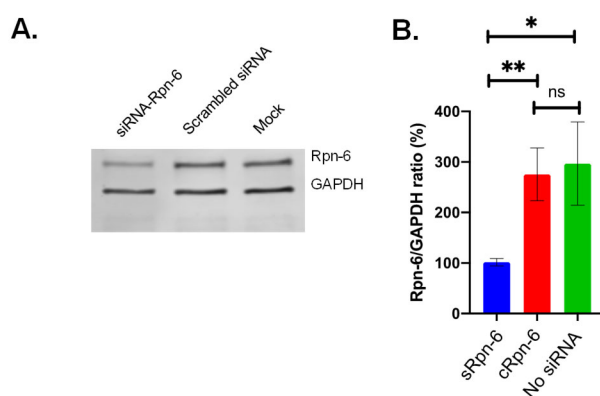


**Figure 3.13 Rpn-6 knockdown in HEK-293T cells with sRpn-6.** (A) Immunoblot of Rpn-6 in knockdown/control and mock treated HEK-293T cells. (B) Relative Rpn-6 expression in knockdown/control and mock treated HEK-293T cells. Error bars represent SEM and n=3, \*p<0.05, \*\*p<0.005, ns=p>0.05

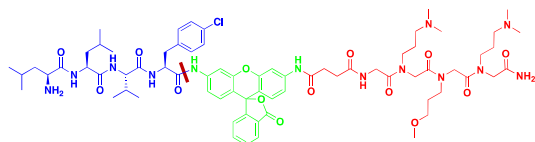


**Figure 3.14 Structure of the TAS-2 probe.** It is recognized by the  $\beta 5$  subunit. The red marker represents the cleavage site. The compound is a hybrid of a peptide (blue) and a peptoid (red). Upon cleavage by the proteasome the release of the rhodamine will generate fluorescence for quantification.

#### 3.6.1.1 Target Protein Knockdown and Proteasome Activity Measurement.

We first sought to determine if proteasome activity in cells was decreased when Rpn-6 expression is reduced. HEK-293T cells were transfected with siRNA for Rpn-6 (sRpn-6) that was previously reported to reduce Rpn-6 expression.<sup>45</sup> A complete knockout of Rpn-6 is not possible, as the 26S proteasome could not form and would result in cell death.<sup>21,46</sup>

HEK-293T cells were transfected with the sRpn-6 or a scrambled version of the siRNA (cRpn-6) as a control using lipofectamine RNAimax. 48 hours after transfection, the cells were lysed and the relative amount of Rpn-6 compared to GAPDH in treated cells was quantitated using immunoblot analysis (Figure 3.13, Figure 3.24). We observed a 60% decrease in the amount of Rpn-6 in sRpn-6 treated cells compared to cRpn-6 or untreated cells.

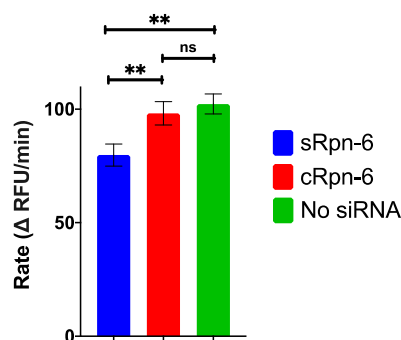


**Figure 3.15 Rate of fluorescence signal comparison in sRpn-6, cRpn-6, or mock transfected HEK-293T cells.** The sRpn-6 treated cells exhibited a 15% decrease. Error bars represent SEM and n=4, \*\*p<0.005, ns=p>0.05.

As mentioned previously, our lab has developed a cell permeable rhodamine-based proteasome selective probe that allow us to monitor proteasome activity in real-time, called TAS-2 (**Figure 3.14**).<sup>6</sup> Cleavage of the probe by proteasomes in cells is monitored over time. The rate of the proteasome cleavage can be calculated via linear regression. After transfecting HEK-293T cells with sRpn-6 or cRpn-6, TAS-2 was added to the cells to monitor proteasome activity. The Rpn-6 knocked down cells exhibited a significant decrease in proteasome activity compared to the two controls (**Figure 3.15**). This observation indicated that decreasing Rpn-6 expression could lead to a decrease in

proteasome activity and validates previous literature reports that Rpn-6 is crucial to maintain the proper function of the 26S proteasome.<sup>20,21,47,48</sup>

### 3.6.1.2 Establishing dosing conditions using viability assay with varying concentration of TXS-8.

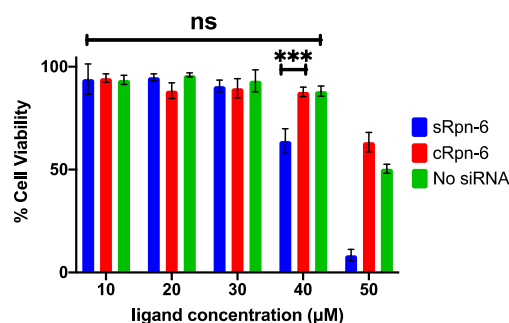


**Figure 3.16 Viability of sRpn-6, cRpn-6, or no siRNA transfected HEK-293T cells.** A significant cell death was observed above 40 μM. Error bars represent SEM and n=3, \*\*\*p<0.0005, ns=p>0.05.

With the success of acquiring Rpn-6 knocked down HEK-293T cells, we wanted to monitor proteasome activity changes in these cells when dosed with TXS-8. First, we had to establish proper experimental conditions for TXS-8 dosing, as decreasing Rpn-6 expression in cells may alter the toxicity of TXS-8 in HEK-293T cells. Based on our previous cell stress experiments with Ramos B-cells in **Chapter 3.5.1**, we dosed HEK-293T cells with various concentration of TXS-8 for 7.5 hours. The dosing time

was determined based on our designed workflow that we will first pre-treat the cells for 3.5 hours and monitor proteasome activity for 3 hours post-treatment. The viability of the HEK-293T cells were examined after 7.5 hours (**Figure 3.16**, **Figure 3.25**). The viability assay indicated that knocking down Rpn-6 in HEK-293T cells did significantly alter the toxicity of TXS-8, as the Rpn-6 knockdown cells were more sensitive to TXS-8 than control cells. We decided to use 30 μM of

TXS-8 for our future experiments as 40  $\mu$ M of TXS-8 resulted in significant cell death in sRpn-6 treated by the end of the experiment.

### 3.6.1.3 Proteasome Activity Measurement in sRpn-6, cRpn-6, or No siRNA Treated Cells.

After determining that we would use 30  $\mu$ M of TXS-8 for dosing, we moved forward to measure proteasome activity changes in HEK-293T cells. As mentioned in **Chapter 3.6.1.2**, we

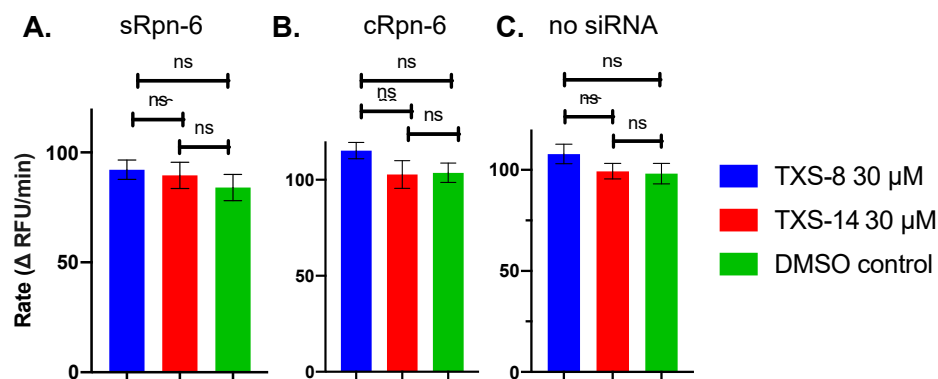


**Figure 3.17. Rate of fluorescence signal comparison in sRpn-6, cRpn-6, or mock transected HEK-293T cells.** (A) TAS-2 cleavage rate in sRpn-6 treated HEK-293T cells, no significant proteasome activity changes were observed. (B) TAS-2 cleavage rate in cRpn-6 treated HEK-293T cells, no significant proteasome activity changes were observed. (C) TAS-2 cleavage rate in no siRNA treated HEK-293T cells, no significant proteasome activity changes were observed. Error bars represent SEM and  $n=4$ ,  $ns=p>0.05$ .

negative control (**Figure 3.17**, **Figure 3.26**). We discovered that 30  $\mu$ M of TXS-8 did not significantly alter proteasome activity of the cells. However, based on our previous results from FRET probe proteasome assay and K-48 polyubiquitin immunoblot, we were not disappointed by the result that TXS-8 did not significantly change proteasome activity at non-lethal concentration.

### 3.6.2 Monitoring Full-Length Protein Degradation in Rpn-6 Knockdown and Normal HEK-293T Cells Dosed with TXS-8.

The proteasome activity assay result from **Chapter 3.6.1** indicated that TXS-8 may not be affecting proteasome activity at a non-lethal concentration. However, it is possible that TXS-8 could be only affecting ubiquitin-dependent degradation of proteins. Since TAS-2 is a small probe compared to a full-length protein, it can be cleaved in a ubiquitin-independent manner, *i.e.*, without the association of the 19S RP with the 20S CP, for which Rpn-6 is critical. Therefore, in the second

decided to dose the HEK-293T cells with our small molecule for 3.5 hours as pre-treatment then added our proteasome probe with more TXS-8 or -TXS-14 and measure proteasome activity changes for 3 hours. TXS-14 was included in this study as a

step of our workflow, we wanted to evaluate if our small molecule could affect the ubiquitin-dependent activity of the proteasome.

### 3.6.2.1 Protein Plasmid Preparation and Transfection and Viability Testing.

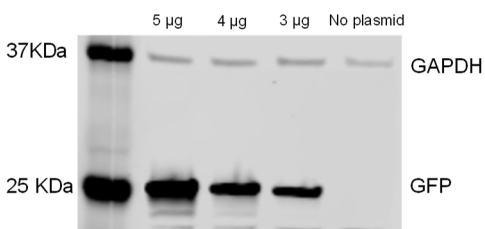


**Figure 3.18.** GFP transfection in HEK-293T cells with various amount of GFP plasmid.

To evaluate full-length protein degradation in HEK-293T cells, we decided to use green fluorescent protein (GFP) for the experiment, as literature demonstrates that GFP is degraded through the ubiquitin-dependent pathway.<sup>49</sup> The GFP plasmid was prepared from DH5-alpha *E.Coli* strain with a starter culture. A mini-prep was then performed to extract the DNA from the

bacteria. Cells were transfected with varying amounts of DNA to determine the optimal amount for future transfections, 3 µg of GFP plasmid was selected for our future experiments (**Figure 3.18**). We also tried to co-transfect the GFP plasmid and sRpn-6 siRNA but the cells were not viable after 48 hours. We hypothesized that the high amount of chemical transfecting reagent may severely damage the cell membrane and resulted in cell death. Therefore, we decided to transfect GFP first overnight then add the siRNA for 48 hours.

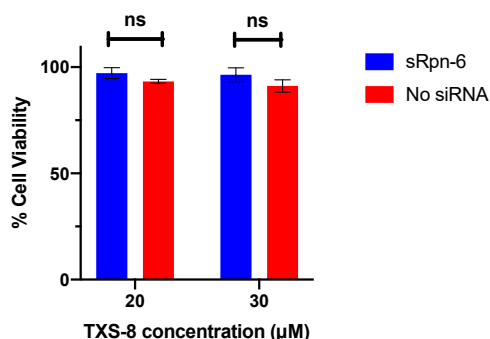


**Figure 3.19.** Viability result in GFP transfected sRpn-6 or no siRNA treated HEK-293T cells. Error bars represent SEM n=6, ns=p>0.05.

Before we performed the GFP degradation assay in HEK-293T cells, we wanted to examine the toxicity TXS-8 in these cells, as we were uncertain if transfecting with GFP would affect the viability of the cells when dosed with TXS-8. Similar to what we had previously observed, 30 µM of TXS-8 was the maximum concentration that Rpn-6 knocked down cells could tolerate without showing significant cell death (**Figure 3.19, Figure 3.27A**). Therefore, we decided to keep

using 30 µM of TXS-8 for our protein degradation assay.

### 3.6.2.2 Full-Length Protein Degradation Assay in Knockdown and Normal Cells Dosed with TXS-8.

After establishing the conditions for transfecting GFP, knocking down Rpn-6, and inducing maximum stress in HEK-293T cells, we next moved forward to monitor GFP degradation in HEK-

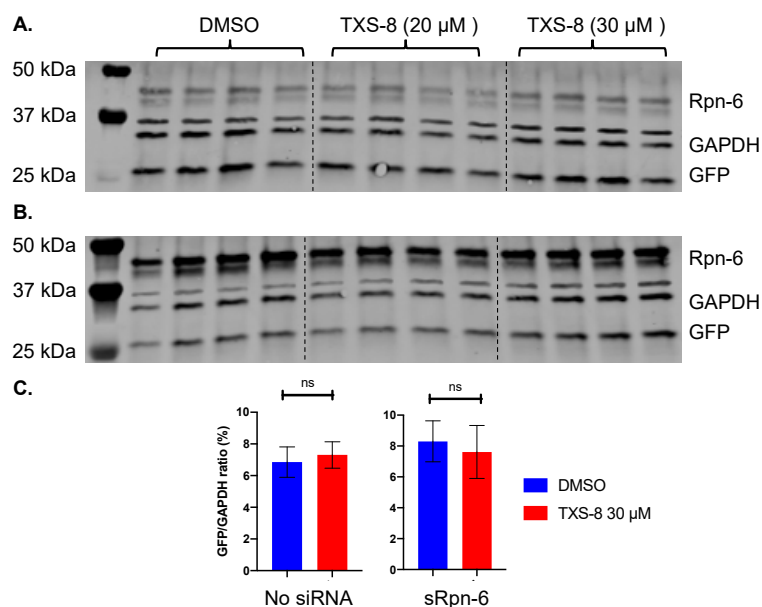


**Figure 3.20. GFP degradation in sRpn-6 and no siRNA treated HEK-293T cells.** (A) Immunoblot of Rpn-6, GAPDH and GFP in Rpn-6 knocked down HEK-293T cells. (B) Immunoblot of Rpn-6, GAPDH and GFP in Rpn-6 normal HEK-293T cells. (C) GFP/GAPDH relative ratio comparison between 30 μM TXS-8 and DMSO treated cells. In both Rpn-6 knocked down and normal HEK-293T cells, no significant GFP degradation difference was observed. Error bars represent SEM n=4, ns=p>0.05.

μM of TXS-8 did not significantly alter degradation of GFP in both normal and Rpn-6 knocked down cells (**Figure 3.20**). The result from the GFP degradation assay validated our previous observation in the proteasome probe activity assay that TXS-8 did not significantly change proteasome activity at non-lethal concentration.

### 3.6.3 Proteasome Activity Changes in a Primary Cell Line.

The results from the first two steps of the workflow indicated that TXS-8 may not be significantly affecting proteasome activity at non-lethal concentrations. In the last step of the workflow, we turned our attention to using a primary cell line, as the impacts of TXS-8 may be more pronounced than immortalized cell lines. We selected the primary cardiomyocyte cell line

293T cells. Cells were first transfected with GFP then treated with sRpn-6/or no siRNA. The cells were then separated into a 12-well plate to allow for cell attachment to the plate overnight. TXS-8, TXS-14, or DMSO was added to the cells, and incubated with HEK-293T cells for 3.5 hours. The cells were lysed and protein concentration was normalized. The lysates were subjected to SDS-PAGE followed by immunoblotting with antibodies to GFP, Rpn-6 and GAPDH (loading control). Similar to what we have observed in **Chapter 3.6.1.3**, 30

AC16 for further study. Recent studies have indicated that prolonged exposure to the proteasome inhibitor bortezomib results in cardiac cell damage and reduced proteasome activity.<sup>50,51</sup> It was hypothesized that TXS-8 could also damage these cells through a proteasome-mediated pathway.

### 3.6.3.1 Rpn-6 expression and viability assay in AC16 cells.

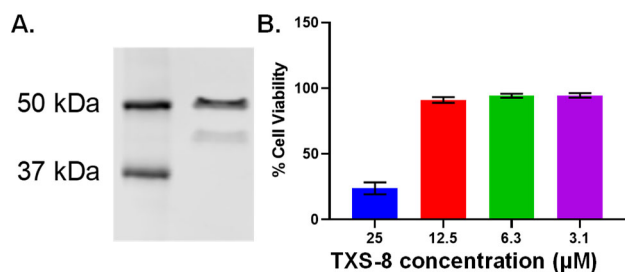


**Figure 3.21.** (A) Immunoblot of AC16 cell lysate, Rpn-6 was detected. (B) Viability of TXS-8 in AC16 cells with various concentration.

Since cardiomyocytes are more sensitive to proteasome inhibition, we sought to determine if TXS-8 could modulate their proteasome activity. First, lysate from AC16 cells was subjected to immunoblot analysis to ensure that the Rpn-6 subunit was detectable in this cell line (Figure 3.21A). A band corresponding to the

molecular weight of Rpn-6 (49 kDa) was observed. We then wanted to establish viability of the cells in response to dosing with various concentrations of TXS-8 (Figure 3.21B). The AC16 cells appeared to be more sensitive to TXS-8 than HEK-293T, as reflected by significant cell death after dosing with 25 μM of the compound while HEK-293T cells were still viable. Therefore, we decided to dose with 12.5 μM of TXS-8 for this experiment as this concentration did not affect viability.

### 3.6.3.2 Proteasome Activity Assay in a Primary Cell Line.

After establishing the proper dosing conditions, we next sought to determine if dosage of TXS-8 resulted in alterations of proteasome activity in AC16 cells. Cells were dosed with a final concentration of TXS-8 at 12.5 μM for 3.5 hours. As a control, AC16 cells were also dosed with DMSO or 5 μM of MG-132, a known proteasome inhibitor.<sup>52</sup> Cells were then washed with PBS, and the corresponding compounds and TAS-2 were added to the wells. Fluorescence signal was monitored over time (Figure 3.22). TXS-8 did not appear to significantly impact proteasome activity, but dosing with MG-132 resulted in reduced proteasome activity, as expected. This result

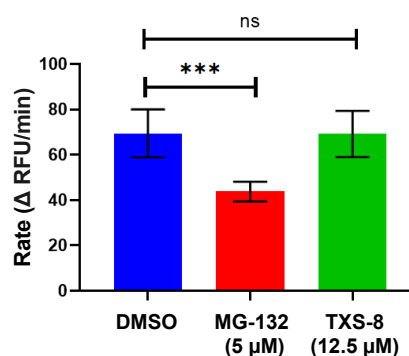


**Figure 3.22. Rate of fluorescence signal comparison in AC16 cells.** TAS-2 cleavage rate in AC16 cells, no significant proteasome activity changes were observed in TXS-8 treated cells. The Proteasome inhibitor MG-132 significantly inhibited proteasome activity. Error bars represent SEM n=4, \*\*\*p<0.0005, ns=p>0.05.

suggests that although AC16 cells were more sensitive to TXS-8 than HEK-293T cells, TXS-8 does not alter proteasome activity in this cell line at non-lethal concentrations.

### 3.6.4 Summary of the Workflow and Potential Application.

Although we did not observe a significant impact of TXS-8 on proteasome activity, we were able to describe a convenient method for investigating the impacts of small molecules on proteasome activity with three assays. The results from all three steps were consistent which suggested that the order of implementation may not affect the final result of the workflow. We would still suggest that using an immortal cell line with proteasome probe for the first step, as this step is the fastest step in the workflow. The workflow we proposed for elucidating the impacts of a small molecule on proteasome activity could also be used to study other small molecule modulators of the proteasome.

## 3.7 Conclusion.

In this chapter, we demonstrated cellular experiments with TXS-8 and a general workflow of investigating if the impacts of small molecule binders to proteasome subunits causes a change in activity, using TXS-8 as an example.<sup>1</sup> We discovered that TXS-8 showed moderate toxicity to hematological cancer cells like Ramos B-cells and multiple myeloma cells. These cancer cells also express a relatively significant amount of Rpn-6 compared to our control HEK-293T cells. A further study with a NIH NCI-60 single dose screening also indicated TXS-8 capable of inhibiting cell growth of leukemia cells. We further explored whether TXS-8 could show additive or synergistic effect with other reported proteasome inhibitors like KDT-11 and bortezomib.<sup>14,24,25</sup> However, we were unable to conclude if TXS-8 exhibited any of the above effect when dual dosed with KDT-11 and bortezomib in either Ramos B-cells or multiple myeloma cells because the shift of IC<sub>50</sub> was not significant.

We also performed preliminary studies on the impact of TXS-8 on proteasome activity. Since TXS-8 was discovered as a selective binder of Rpn-6, we hypothesized that TXS-8 may

interfere with Rpn-6 function and eventually affect proteasome activity. However, our initial experiments with the commercially available proteasome probe, Suc-LLVY-AMC with both purified 26S proteasome and Ramos B-cell lysate indicated that TXS-8 may not be affecting activity of the proteasome. To further explore the impact of TXS-8 on proteasome activity, we monitored proteasome activity changes with a FRET probe and monitored K-48 polyubiquitinated protein accumulation in cells. Results from the Suc-LLVY-AMC probe, FRET probe and K-48 immunoblot experiments exhibited a discrepancy and we were unable to summarize a conclusion based on the results. However, with the newly developed rhodamine-based probes from our lab, we restarted the investigation of the impact of TXS-8 on proteasome activity.<sup>24</sup>

We also noticed that there is a lack of a general workflow of investigating the impacts of small molecules on proteasome activity. Therefore, we designed and described a three-step general workflow to make characterizing small molecule proteasome activity modulators more streamline. Starting with monitoring proteasome activity changes in cells, followed by monitoring full-length protein degradation and monitoring proteasome activity changes in a primary cell line, we were able to develop critical assays to study the impact of a small molecule on proteasome activity. We concluded that although TXS-8 was a selective binder of Rpn-6, it may not be able to significantly affect proteasome activity at non-lethal concentrations. Additionally, these assays could also be amenable for the evaluation of small molecule binders to other proteasome subunits of interest.

The conclusion that TXS-8 may not affect proteasome activity at non-lethal concentration raised multiple questions: How did TXS-8 induce cytotoxicity in Rpn-6 overexpressing cells? Does Rpn-6 serve other cellular roles other than being a subunit of proteasome? All these questions remain to be answered. Meanwhile, the discovery of the binding site of TXS-8 on Rpn-6 will greatly help to answer some of the above questions and provide guidance for future structural optimization of TXS-8 into a more drug-like small molecule.

### **3.8 General methods and materials.**

All chemicals were obtained from Sigma-Aldrich, Acros Organics, Alfa Aesar or Fisher Scientific and used without any further purification. Solid-phase peptoid synthesis reactions for TXS-8 and TXS-14 were performed in fritted syringes (Sass Wolfe) as reported previously. TXS-8/14 were tested by fluorescence polarization assay. Resin was purchased from Chem-Impex Int'l Inc. All peptoids were purified by reverse phase HPLC. (Agilent S9 1260 infinity II), HEK-293T

(CRL-3216<sup>TM</sup>), MM.1R (CRL-2975<sup>TM</sup>), Ramos B-cells (CRL-1596<sup>TM</sup>) frozen cell stocks were obtained from ATCC. Cell growth media was also obtained from ATCC including ATCC-formulated Eagle's minimum essential medium (EMEM, 30-2003<sup>TM</sup>), ATCC-formulated RPMI-1640 Medium (30-2001<sup>TM</sup>) and Dulbeco's modified eagle's medium (DMEM 30-2002<sup>TM</sup>). The Fetal bovine serum (FBS obtained from VWR) was added to the growth media by 10% of the total volume. 1% PEST was added alone to the DMEM media after FBS was added. CellTiter Glo was obtained from Promega. The 96-well plate with lid was obtained from Corning<sup>®</sup> Costar<sup>®</sup>. The 0.25% trypsin cell dissociation buffer was obtained from Corning<sup>®</sup>. The Suc-LLVY-AMC probe was acquired from ThermoFisher. The purified 26S proteasome was acquired from Boston Biochem at a stock concentration of 2  $\mu$ M. The black 96-well plate with lid was obtained from Corning<sup>®</sup> Costar<sup>®</sup>. The square bottom 384-well plates were acquired from Fisher Scientific. The 12-well transparent round bottom plates were obtained from VWR. The FRET peptide was synthesized by Dr. Rachel Coleman from the Trader lab. The K-48 monoclonal antibody was acquired from both Boston Biochem and ThermoFisher. The 0.25% trypsin cell dissociation buffer, 1X PBS buffer, and the collagen type I from rat tail was obtained from Corning<sup>®</sup>. The lipofectamine<sup>®</sup> RNAiMAX and lipofectamine<sup>®</sup> 2000 were acquired from Invitrogen. The sRpn-6 PSMD11 Silencer<sup>®</sup> and cRpn-6 negative control were obtained from Ambion through Thermo-Fisher. The Opti-MEM<sup>®</sup> media and all cell flasks and dishes were also obtained from Thermo-Fisher. M-PER<sup>TM</sup> mammalian protein extraction solution and HALT<sup>TM</sup> protease & phosphatase inhibitor cocktail (100X) was obtained from Thermo-Fisher. The Laemmli SDS-sample buffer (4X) was acquired from Fisher. Nitrocellulose membranes and filter paper were obtained from Bio-Rad. Rpn-6 primary antibody (rabbit), GAPDH primary antibody (mouse) and GFP primary antibody (rabbit) were obtained from Novus Biologicals. The secondary antibody (goat anti-rabbit) was obtained from LI-COR. The GFP plasmid was acquired at 1.54  $\mu$ g/ $\mu$ L concentration. AC16 (Millipore Sigma, Cat. #SCC109) cells were thawed from a liquid nitrogen stock and cultured in sterile filtered 50% DMEM 50% F-12K media supplemented with 12.5% FBS and 1% Penicillin-Streptomycin (PEST).

### **3.9 General Cell Culture and TXS-8 Toxicity Experiments.**

#### **3.9.1 Suspension Cell Culturing and Dosing.**

The purchased cell stock was taken out from the liquid nitrogen storage tank and defrost to room temperature. The stock was then transferred into a 15 mL falcon tube with an additional 1 mL of the RPMI media. The tube was centrifuged for 5 mins at 1000 k rpm. The cell medium was removed, and the cell pellet was re-suspended in 10 mL of growth media. The media was transferred into a T-75 plate (or a 10 cm dish) and the plate was incubated at 37°C until cells were confluent.

##### ***3.9.1.1 Suspension Cell Splitting Protocol.***

The cells were transferred into a 15 mL falcon tube and the tube was centrifuged at 1,000 xg for 5 mins. Media was aspirated and the cell pellet was re-suspended in 5 mL of media. Another 15 mL falcon tube was prepared with 9 mL of cell media. 1 mL of the media containing the suspension cells was added to the falcon tube and in total 10 mL of the cell medium was transferred to a new T-75 plate. The T-75 plate was incubated at 37°C until cells were confluent.

##### ***3.9.1.2 Suspension Cell Dosing Protocol.***

The peptoid was taken out from the -20°C and was warmed up to ROOM TEMPERATURE. 1 mg of the peptoid was measured and dissolved in DMSO to make a 20 mM stock. A dilution of 15 mM, 10 mM, 7.5 mM, 5 mM, 2.5 mM, 2 mM, 1.6 mM, 1.4 mM, 1.25 mM, 0.625 mM and 0.3125 mM in DMSO were prepared. The DMSO solutions were further diluted by adding 4 µL of the stock into 196 µL of media to obtain the final dosing concentration. 4 µL of DMSO was also added to 196 µL of the cell media to prepare the negative control. The 4 mL cell media left over in previous step was kept for dosing. 10 uL from the falcon tube was added to each side of a hemocytometer with a glass cover on top. The amount of the media needed for dilution was further calculated to fulfill the need of 10,000 cells per well on a 96-well plate. The cells in the falcon tube were diluted with cell media to obtain 2 mL of a 200,000 cell/ mL solution. 36 wells were used on a 96-well plate. 50 uL of cell solution was added to wells. Another 50 uL of each ligand was added to the wells in triplicate. DMSO was added as negative control. Another three wells with cells were added with media only to determine if DMSO would have negative effect on the cells. The

plate was placed in the incubator for 24 hours. The plate was taken out and equilibrated to ROOM TEMPERATURE. 50  $\mu$ L of Cell Titer Glo was added to each well. The plate was agitated in dark for 1.5 min and was settled for another 10 mins in the dark. The luminescent in each well was measured with a Synergy 4 plate reader system. The readings were converted and normalized to % viability and were graphed in Prism 8 software.

### **3.9.2 Adherent Cell Culturing and Dosing.**

The purchased cell stock was taken out from the liquid nitrogen storage tank and defrosted to ROOM TEMPERATURE. The stock was then transferred into a 15 mL falcon tube with an additional 1 mL of the media (DMEM). The tube was centrifuged for 5 mins at 1,000 xg. The cell media was removed and the cell pellet was re-suspended in 10 mL of media. The cells were transferred into a T-75 plate (or a 10 cm dish) and the plate was incubated at 37°C until cells were confluent.

#### ***3.9.2.1 Adherent Cell Splitting Protocol.***

The media in the plate was removed and the plate was washed with 10 mL of sterilized 1X PBS gently. The PBS was removed and 1 mL of trypsin buffer was added to the plate. The plate was agitated by hand to allow the buffer to cover the whole plate and the plate was incubated for 5-10 mins to dissociate cells. The dissociation buffer was collected into a 15 mL falcon tube and was centrifuged at 1,000 xg for 5 mins. The buffer was removed, and 5 mL of media was added to the tube. Another 15 mL falcon tube was prepared with 9 mL of cell medium inside. 1 mL of the media containing the cells was added to the falcon tube and in total 10 mL of the cell medium was transferred into another new T-75 plate. The T-75 plate was incubated at 37°C until cells were confluent.

#### ***3.9.2.2 Adherent Cell Dosing Protocol.***

The peptoid was taken out from the freezer and was warmed up to ROOM TEMPERATURE. 1 mg of the peptoid was weighed and dissolved in DMSO to make a 20 mM stock solution. A dilution of 15 mM, 10 mM, 7.5 mM, 5 mM, 2.5 mM, 2 mM, 1.25 mM, 0.625 mM and 0.3125 mM in DMSO were prepared. All above DMSO solutions were further diluted by diluting 4  $\mu$ L of the

stock into 196  $\mu$ L of media to obtain the final dosing concentration. 4  $\mu$ L of DMSO was also diluted in 196  $\mu$ L of the cell media to prepare the negative control. The 4 mL cell media left over was kept for cell dosing. 10  $\mu$ L from the falcon tube was added to each side of a hemocytometer with a glass cover on top. The cells were counted. The amount of the cell suspension needed for dilution was further calculated to fulfill the need of 10,000 cells per well on a 96-well plate. The cells in the falcon tube were taken out and diluted with cell media to obtain 2 mL of a 200,000 cell/ mL solution. 36 wells were used on a 96-well plate. 50  $\mu$ L of cell solution was added to wells on the 96-well plate. Another 50  $\mu$ L of the ligands was added to the wells in triplicate. DMSO was added as negative control. Another three wells with cells were added with media only to determine if DMSO would have negative effect on the cells. The plate was placed in the incubator for 24 hours. The plate was taken out and equilibrated to ROOM TEMPERATURE. 50  $\mu$ L of CellTiter Glo was added to each well. The plate was agitated in the dark for 1.5 min and was settled for another 10 mins in the dark. The luminescent signal from each well was measured with a Synergy 4 plate reader system. The readings were converted and normalized to % viability and were graphed in Prism 8 software.

### **3.10 Dual dosing of TXS-8 with KDT-11/bortezomib.**

TXS-8 was synthesized via solid-phase synthesis. KDT-11 was synthesized from Christine Muli from Trader lab and bortezomib was acquired from Fisher Scientific. TXS-8 and KDT-11 were dissolved in DMSO to make a 20 mM stock and bortezomib was dissolved in DMSO to make a 2 mM stock.

#### **3.10.1 Dual Dosing of TXS-8 with KDT-11 in Ramos B-cells and Multiple Myeloma Cells.**

Cells were split into the wells of a 96-well plate such that there were 10,000 cells per well. The plate incubated overnight.

The next day, the DMSO stock of TXS-8 and KDT-11 were prepared. A dilution of KDT-11 in 10 mM, 5 mM, 2.5 mM, 1.25 mM, 0.62 mM, 0.31 mM, 0.15 mM, 0.078 mM and 0.039 mM were made prepared. A stock of 1.4 mM TXS-8 solution in DMSO was also made. All above DMSO solutions were further diluted by adding 2  $\mu$ L of the KDT-11 stock and 2  $\mu$ L of TXS-8 stock into 196  $\mu$ L of media to obtain the final dosing concentration. 4  $\mu$ L of DMSO was also

diluted in 196  $\mu$ L of the cell media to prepare the negative control. 50  $\mu$ L of the TXS-8/KDT-11 mixed solution was added to the wells in triplicate. DMSO was added as negative control. Another three wells with cells were added with media only to determine if DMSO would have negative effect on the cells. The plate was placed in the incubator for 24 hours. The plate was taken out and equilibrated to ROOM TEMPERATURE. 50  $\mu$ L of CellTiter Glo was added to each well. The plate was agitated in the dark for 1.5 min and was settled for another 10 mins in the dark. The luminescent signal of each well was measured with a Synergy 4 plate reader. The readings were converted and normalized to % viability and were graphed in Prism 8.

### **3.10.2 Dual Dosing of TXS-8 with Bortezomib in Ramos B-cells and Multiple Myeloma Cells.**

Cells were split into the wells of a 96-well plate such that there were 10,000 cells per well. The plate incubated overnight. The next day, the DMSO stock of TXS-8 and bortezomib were prepared. A dilution of KDT-11 in 4  $\mu$ M, 2  $\mu$ M, 1  $\mu$ M, 0.5  $\mu$ M, 0.25  $\mu$ M, 0.12  $\mu$ M, 0.062  $\mu$ M, 0.031  $\mu$ M and 0.015  $\mu$ M were prepared. A stock of 1.4 mM TXS-8 solution in DMSO was also made. All above DMSO solutions were further diluted by adding 2  $\mu$ L of the bortezomib stock and 2  $\mu$ L of TXS-8 stock into 196  $\mu$ L of media to obtain the final dosing concentration. 4  $\mu$ L of DMSO was also diluted in 196  $\mu$ L of the cell media to prepare the negative control. 50  $\mu$ L of the TXS-8/bortezomib mixed solution was added to the wells in triplicate. DMSO was added as negative control. Another three wells with cells were added with media only to determine if DMSO would have negative effect on the cells. The plate was placed in the incubator for 24 hours. The plate was taken out and equilibrated to ROOM TEMPERATURE. 50  $\mu$ L of CellTiter Glo was added to each well. The plate was agitated in the dark for 1.5 min and was settled for another 10 mins in the dark. The luminescent signal from each well was measured by a Synergy 4 plate reader system. The readings were converted and normalized to % viability and were graphed in Prism 8.

**Table 3.1.** Raw chemo-luminescence values for TXS-8 toxicity testing. Values were normalized to DMSO control to generate % viability.

TXS-8 concentration ( $\mu$ M)	Ramos B-cells			HEK-293T cells			MM.1R cells		
200	56	10	98	124	23	259	20	92	55
150	4	4	69	262	251	299	48	18	208
100	36	51	89	5719	4499	4427	54	103	101
75	43	33	57	92378	92527	82931	3	22	167
50	142	106	116	188150	179459	169112	42	37	166
25	117	77	47	254771	246697	220394	492	823	1435
20	5713	7600	3076	254799	274829	249598	33850	25483	23194
16	28964	27765	29321				70788	72513	67468
14	52017	51731	53496				96316	93177	83204
12.5	53348	55362	51071	284171	299050	262100	91642	93124	83881
6.25	62041	63916	62661	291731	296258	271684	101067	99510	97966
3.125	62468	60465	60604				99248	98179	90672
DMSO Control	57365	62020	61658	282418	314466	290565	95308	97644	97242

### 3.11 TXS-8 Induced Cell Stress Conditions.

Ramos B-cells were split into the wells of a 96-well plate such that there were 10,000 cells per well. The plate incubated overnight.

The next day, a stock of 2 mM of TXS-8 in DMSO was made. The DMSO solution was further diluted by adding 4  $\mu$ L of the TXS-8 stock into 196  $\mu$ L of media to obtain the final dosing concentration. 4  $\mu$ L of DMSO was also dissolved in 196  $\mu$ L of the cell media to prepare the negative control. 50  $\mu$ L of TXS-8 solution was added to the wells in triplicate. Two hours after the addition, TXS-8 was added to the plate in a triplicate again. This step was repeated several times. The last addition was conducted one hour after previous TXS-8 addition. DMSO was added as negative control the first time TXS-8 was added. Another three wells with cells were added with media only to determine if DMSO would have negative effect on the cells. The plate was taken out from the incubator and equilibrated to ROOM TEMPERATURE. 50  $\mu$ L of CellTiter Glo was added to each well. The plate was agitated in the dark for 1.5 min and was settled for another 10 mins in the dark. The luminescent signal from each well was measured with a Synergy 4 plate

reader system. The readings were converted and normalized to % viability and were graphed in Prism 8.

### **3.12 TXS-8 Impact on Proteasome Activity Using 26S Purified Proteasome and Ramos B-cell Lysate.**

#### **3.12.1 Monitoring Proteasome Activity Changes with Purified 26S Proteasome.**

Buffer or the assay was made in 50 mM Tris buffer (pH 7.62) with 1 mM ATP and 10 mM of  $\text{MgCl}_2$ . The 26S proteasome was diluted in the Tris buffer to a 50 nM concentration. The Suc-LLVY-AMC probe was dissolved in DMSO to prepare a 20 mM stock. It was further diluted by the Tris buffer to obtain a concentration of 111.11  $\mu\text{M}$ . TXS-8 and bortezomib were separately diluted in the Suc-LLVY-AMC solution to obtain a concentration of 22.22  $\mu\text{M}$  and 5.55 nM solution, respectively. After the solutions were prepared, 5  $\mu\text{L}$  of the 26S proteasome was added to the wells and 45  $\mu\text{L}$  of corresponding TXS-8 or bortezomib solution were also added. The final concentration in each well was 5 nM of 26S proteasome, 100  $\mu\text{M}$  of the Suc-LLVY-AMC probe and 20  $\mu\text{M}$  of TXS-8/5 nM of bortezomib. The solution was slowly pipetted up and down to gently mix the proteasome with the probe and our small molecules. DMSO was used as a negative control. The plate was covered with a lid and the plate was placed on a plate reader for an assay lasting 3 hours. RFU was measured every 2 mins and the reader internal temperature was set to be 37 °C. The collected data was exported and graphed in Prism to calculate the rate of cleavage of the probe.

#### **3.12.2 Monitoring Proteasome Activity Changes with Ramos B-cell Lysate.**

The cell lysis buffer was prepared by dissolving 50 mM of Tris-HCl, 150 mM NaCl, 1% Triton X-100, 5 mM EDTA in 50 mL of ultrapure water (pH: 7.4).

Ramos B-cells were split into the wells of a transparent 96-well plate such that there were 100,000 cells per well. The plate incubated overnight.

The next day, a 20 mM TXS-8 DMSO stock was diluted by adding 6  $\mu\text{L}$  of the TXS-8 stock to 1 mL of media to obtain a 120  $\mu\text{M}$  stock. A 2 mM bortezomib stock was diluted to a 5  $\mu\text{M}$  stock with DMSO and 6  $\mu\text{L}$  of the 5  $\mu\text{M}$  bortezomib stock was further diluted with 1 mL of cell media. 6  $\mu\text{L}$  of DMSO was also dissolved in 1 mL of cell media to prepare the negative control. 250  $\mu\text{L}$  of TXS-8 or bortezomib and DMSO solution was added to wells in replicates of four. After

1.5 hours of dosing, the cells were washed and collected. Cells were lysed with the above lysis buffer for 10 mins and the mixture was centrifuged at 12,000 xg for 5 mins. The supernatant was collected, and protein concentration was determined with a NanoDrop One system and normalized. The Suc-LLVY-AMC probe was diluted in the lysis buffer to acquire a 111.11  $\mu\text{M}$  concentration and TXS-8 and bortezomib were diluted in the Suc-LLVY-AMC solution to acquire a concentration of 200  $\mu\text{M}$  and 50 nM, respectively. 5  $\mu\text{L}$  of the ligand was added onto a 96-well plate in triplicate and 45  $\mu\text{L}$  of Ramos B-cell lysate treated with TXS-8, bortezomib, or DMSO was added to each well. The plate was covered with a lid and placed on a plate reader for an assay lasting 1.5 hours, RFU was measured every 1 min and the reader internal temperature was set to be 37  $^{\circ}\text{C}$ . The collected data was exported and graphed in Prism to calculate rate of cleavage of the probe.

### 3.13 Impact of TXS-8 on Proteasome Activity with the FRET Probe and K-48 Immunoblot.

#### 3.13.1 TXS-8 impact on proteasome activity with FRET probe.

50 mM Tris buffer (pH 7.62) with 1 mM ATP and 10 mM of  $\text{MgCl}_2$  was prepared. The FRET peptide DMSO stock was diluted in the above buffer to achieve a final concentration of 20  $\mu\text{M}$ . 26S proteasome was added to the FRET peptide solution to acquire a final concentration of 9 nM. 23  $\mu\text{L}$  of the above mixture was added to 384-well plate. A negative control was prepared by adding the FRET peptide solution alone to 3 wells. TXS-8, TXS-14 or DMSO solution was added

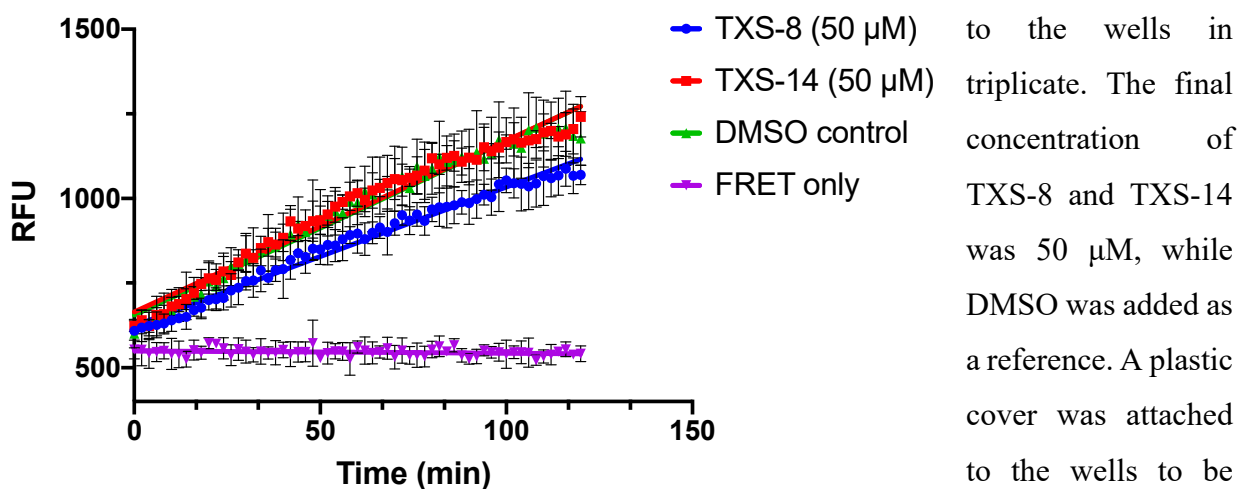


**Figure 3.23.** FRET probe assay with 26S proteasome dosed with TXS-8/TXS-14/DMSO. tested to prevent sample evaporation.

The plate was placed on a plate reader for an assay lasting 3 hours. RFU was measured every 2 mins and the reader internal temperature was set to be 37 °C. The collected data was exported and graphed in Prism 8 to calculate the rate of cleavage of the probe (**Figure 3.23**).

### **3.13.2 TXS-8 Impact on Proteasome Activity Using K-48 Polyubiquitin Immunoblot.**

Ramos B-cells were split into the wells of a 6-well plate such that there were 200,000 cells per well. The final volume in each well was 2.5 mL. The plate incubated overnight.

The next day, a 20 mM TXS-8 DMSO stock was diluted by adding 3 µL of the TXS-8 stock into 0.5 mL of media to obtain a 120 µM concentration. A 2 mM bortezomib stock was diluted to a 5 µM stock with DMSO and 3 µL of the 5 µM bortezomib stock was further diluted with 0.5 mL of cell media. 3 µL of DMSO was also diluted in 0.5 mL of the cell media to prepare a negative control. 500 uL of TXS-8 or bortezomib and DMSO solution was added to wells in a singlet. After 1.5 hours of dosing, the cells were washed with PBS and collected. The cells were lysed with MPER buffer supplemented with HALT for 10 mins and the mixture was centrifuged at 12,000 xg for 10 mins. The protein concentration was normalized, and 4X lammelli was added to the samples. The tubes were heated up for 3 mins. SDS-PAGE was performed, and proteins were transferred to a nitrocellulose membrane with Trans-blot® Turbo™ system from Bio-Rad. The membrane was blocked with a 5% milk solution in PBS. Then the primary antibody incubated with the blot overnight. The membrane was washed 3 times with PBS, then the secondary antibody was added. The blot was then imaged with a LI-COR CLx imaging system.

## **3.14 HEK-293T Cell Rpn-6 Knockdown Experiment.**

### **3.14.1 Cell culture of HEK-293T cells.**

A HEK-293T cell stock was taken out from the liquid nitrogen storage tank and defrosted to ROOM TEMPERATURE. The stock was then transferred into a 15 mL falcon tube with an additional 1 mL of the DMEM media. The tube was centrifuged for 3 mins at 1,000 x g. The media was removed, and the cell pellet was re-suspended in 10 mL of media. The media was transferred into a T-75 flask (or a 10 cm dish) and the plate was incubated at 37°C until cells were confluent.

### **3.14.2 HEK-293T Cell Rpn-6 Knockdown Protocol.**

Media was aspirated from the plate and the plate was washed with 10 mL of sterilized 1X PBS gently. The PBS was removed, and 2 mL of trypsin buffer was added to the plate. The plate was agitated by hand to allow the buffer to cover the whole plate and the plate was put back in the incubator for 5 mins to dissociate cells. The liquid was transferred into a 15 mL falcon tube and the plate was further washed with twice with 3 mL media and collected. The tube was centrifuged for 5 mins at 1,000 x g. The media was aspirated from the tube and the cell pellet was resuspended in 5-8 mL of cell media. Cells were plated on three T-25 plates at 25% confluency and the total volume was 4.5 mL in each plate. The plates were left in the incubator overnight at 37°C to allow the cells to adhere to the plate. The next day, media was aspirated from the plate. The sRpn-6 and cRpn-6 siRNA were prepared according to protocol from Thermo-Fisher. A final amount of 100 pmol of the RNA was mixed with 21 µL of lipofectamine RNAiMax in 500 µL of Opti-MEM and the solution was allowed to incubate for 5 mins. During this period, 4 mL of fresh DMEM media was added to the cells. Then the sRpn-6 or cRpn-6 mixture was carefully added to the corresponding plate. The third plate was designated as the untreated control and 500 µL of Opti-MEM (with 21 µL of lipofectamine RNAiMax) was added to the plate. All plates were carefully agitated by hand to distribute the Opti-MEM media evenly across the plate. The plates were left in the incubator at 37°C for 2 days.

### **3.14.3 Rpn-6 Expression Measurement in sRpn-6, cRpn-6, or No siRNA Treated HEK-293T Cells.**

Cells were removed from the T-25 plates from previous step in **Chapter 3.14.2**. The cells were centrifuged at 1,000 x g for 5 mins. The cell pellet was washed with PBS to remove the media and centrifuged again. 300 µL of M-PER solution was added to the cell pellet (final concentration of HALT protease inhibitor was 1X). The lysate was agitated at ROOM TEMPERATURE for 10 mins and was centrifuged at 12,000 x g for 15 mins at 4 °C. The cell lysate was carefully removed from the eppitube leaving the pellet debris at the bottom of the tube. The protein concentration was measured with a Nanodrop One system. The protein concentration was normalized to the lowest concentration by diluting samples with PBS. 10 µL of Laemmli buffer was mixed with 40 µL of normalized lysate and the tube was heated at 95 °C for 5 mins. SDS-PAGE was performed, and protein was transferred to the nitrocellulose membrane by a Trans-blot® Turbo™ system from

Bio-Rad. The membrane was blocked with 5% milk in PBS for 1hr. Rpn-6 antibody was diluted 1:1,000 in LI-COR intercept blocking buffer and added to the blots. This was allowed to incubate overnight at 4C. The membrane was washed with PBS three times, then an anti-rabbit antibody was diluted 1:10,000 in LI-COR intercept blocking buffer and allowed to incubate at ROOM TEMPERATURE. for 1.5 hours, the membrane was then washed with PBS for three times. The membrane was scanned on an Odyssey CLx imaging system from LI-COR and the expression level of Rpn-6 and GAPDH among the sRpn-6, cRpn-6 and no siRNA treated cells were analyzed and plotted. (Figure 3.24 & Figure 3.13B)

### 3.15 Cellular TAS-2 Assay in HEK-293T Cells.

#### 3.15.1 Viability Assay.

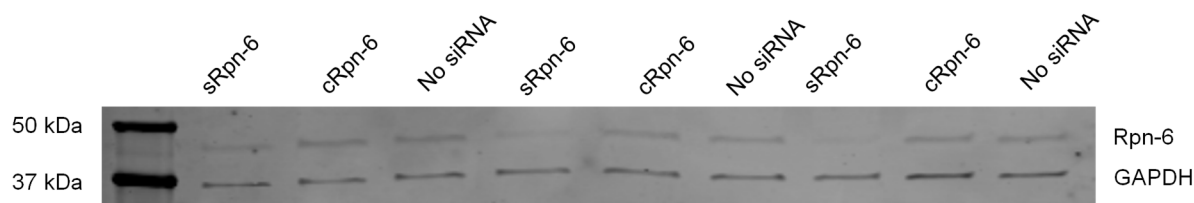


**Figure 3.24. Western blot analysis of sRpn-6, cRpn-6 and no siRNA treated HEK-293T cells.** The blot showed the expression level of Rpn-6 in different time period. The analyzed data was plotted by the ratio of Rpn-6/GAPDH among the cells in **Figure 3.13B**.

##### 3.15.1.1. 96-well Plate Preparation.

One day prior to the start of the experiment, a black 96-well round bottom plate was treated with collagen by adding 50  $\mu$ L of 25  $\mu$ g/mL collagen solution in 0.02M acetic acid solution (12  $\mu$ L of acetic acid added into 10 mL of ultrapure water). The plate was left in the incubator overnight. The next day, the plate was taken out from the incubator and the collagen solution was removed from the plate. The wells were washed with 100  $\mu$ L of PBS three times and the plate was then put back to the incubator for at least 30 mins to dry.

### 3.15.1.2 HEK-293T Cell Preparation for Viability Assay.

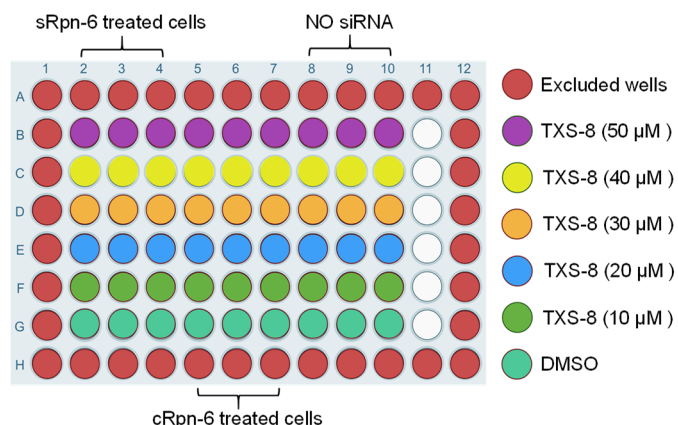


**Figure 3.25. Plate layout for the viability assay.** The white wells were intentionally left for an additional 2 wells of sRpn-6/cRpn-6/no siRNA treated cells as a backup.

The sRpn-6, cRpn-6, or no siRNA treated cells were taken out from the incubator. The media was carefully removed from each plate to prevent disturbing the cells. 1 mL of trypsin buffer was added to each plate and the plate was agitated by hand to allow the buffer to cover the whole plate. The plate was put back into the incubator for 5 mins to dissociate cells. The liquid was transferred into a 15 mL falcon tube and the plate was

further washed twice with 1 mL cell media to collect all cells. The tube was centrifuged for 5 mins at 1,000 x g. The trypsin media was carefully removed from the tube and the cell pellet was resuspended in 5-8 mL of cell media. 10  $\mu$ L of solution from the falcon tube was added to each side of a hemocytometer with a glass cover on top. Cell numbers on each side of the hemocytometer were counted under a microscope and an average cell number was taken from the number obtained. The total number of cells in the falcon tube was calculated later through the average cell number. The cells were further diluted to  $1 \times 10^5$  cell/mL with media. A white 96-well round bottom plate was prepared by adding 5,000 cells to each well according to **Figure 3.25**. The plate was prepared for a viability assay to determine the TXS-8 concentration for the experiment.

### 3.15.1.3 Cell Dosing and Viability Assay.

TXS-8 was dissolved in DMSO to make a 20 mM stock solution. A dilution stock of 5 mM, 4 mM, 3 mM, 2 mM, and 1 mM of TXS-8 in DMSO were prepared. All above DMSO solutions were further diluted by diluting 10  $\mu$ L of the dilution stock into 490  $\mu$ L of media to obtain the final dosing concentration. 10  $\mu$ L of DMSO was also diluted in 490  $\mu$ L of cell media. The plate from the previous step 3.1.2 was taken out from the incubator and 50  $\mu$ L of each test compound was added to corresponding wells according to **Figure 3.25**. The plate was placed in the incubator for

7.5 hours then was taken out and equilibrated to ROOM TEMPERATURE. 50  $\mu$ L of Cell-Titer-Glo solution was added to each well with pipetting to mix. The plate was agitated for 2 min and incubated for another 10 mins in the dark. The luminescence in each well was measured by a Synergy NEO plate reader system. The readings were recorded and normalized to the DMSO control to obtain percent viability and were graphed in Prism 8.

### 3.15.2 TAS-2 Assay with HEK-293T Cells.

#### 3.15.2.1 HEK-293T Cell Preparation for TAS-2 Assay.

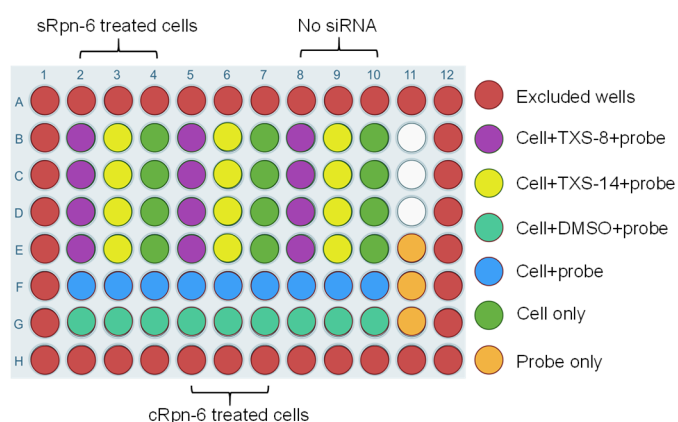


**Figure 3.26. Plate layout for the TAS-2 assay.** The white wells were intentionally left for an additional 1 well of sRpn-6/cRpn-6/no siRNA treated cells as a backup.

One day prior to transferring the cells for the TAS-2 assay, a black 96-well round bottom plate was prepared according to 3.1.1. The next day, the sRpn-6/cRpn-6/no siRNA treated cells were taken out from the incubator. The cell media was carefully removed to prevent disturbing the cells. 1 mL of trypsin buffer was added to each plate and was agitated by hand to allow the buffer to cover the whole plate.

The plate was put back to the incubator for 5 mins to dissociate cells. The liquid was transferred into a 15 mL falcon tube and the plate was further washed twice with 1 mL cell media to collect all cells. The tube was centrifuged for 5 mins at 1,000 x g. The trypsin media was carefully removed from the tube and the cell pellet was resuspended in 5-8 mL of cell media. 10  $\mu$ L of solution from the falcon tube was added to each side of a hemocytometer with a glass cover on top. Cell numbers on each side of the hemocytometer was counted under a microscope and an average cell number was taken from the number obtained. The total number of cells in the falcon tube was calculated later through the average cell number. The cells were further diluted to  $1 \times 10^5$  cell/mL with media. A black 96-well round bottom plate was prepared by adding 5,000 cells to each well according to **Figure 3.26**.

### **3.15.2.2 Cell Dosing and TAS-2 Assay.**

A stock of 3 mM TXS-8 or 14 were prepared. The above DMSO stocks were further diluted by diluting 5  $\mu$ L of the test compound into 245  $\mu$ L of media to obtain the final dosing concentration. The above TXS-8 solution was prepared in triplicate so sRpn-6/cRpn-6/no siRNA treated cell would have their own TXS-8 solution for dosing. 5  $\mu$ L of DMSO was also diluted in 245  $\mu$ L of the cell media and prepared accordingly to TXS-8 solution. The plate from the previous step 3.2.1 was taken out from the incubator and 50  $\mu$ L test compounds were added to corresponding wells according to Figure\_\_\_ and plate was placed incubator for 3.5 hours. 30 mins before the end of 3.5 hours dosing, a 20 mM TAS-2 DMSO stock was prepared. The TAS-2 stock was further diluted into a 2 mM stock and a 6 mM stock of TXS-8 or 14 were also prepared. 1.25  $\mu$ L of the 2 mM TAS-2 stock was mixed with 1.25  $\mu$ L of TXS-8 or 14 stocks. The tubes were kept in the dark and used right before the start of the TAS-2 assay. A Tecan Infinite M200 Pro plate reader system was pre-heated to 37°C and the gain was set to 80. After 3.5 hours, the plate was taken out from the incubator and the cell media was carefully removed from the wells with a pipette. Cells were washed three times with 100  $\mu$ L of PBS. The mixed probe/ligand DMSO stocks were then diluted with 247.5  $\mu$ L of KRBH buffer to acquire the final dosing concentration. 2.5  $\mu$ L of DMSO was also diluted in 247.5  $\mu$ L of KRBH buffer as well. The purpose of using a total amount of 2.5  $\mu$ L of DMSO is to ensure that each well has only 1% amount of DMSO compared to the previous TXS-8 or 14 dosing. 50  $\mu$ L of TAS-2, TXS-8 or 14 mixed solution was then added to the corresponding wells according to **Figure 3.26**. Cell only wells were added with only KRBH buffer and probe only wells were also prepared at the same time. The plate was then put back to the incubator for 10 mins and the plate was transferred to the plate reader. The lid was kept on during the assay and the plate reader was set to read for 3 hours at a 1 min interval. The data was collected, and the slope of each well was measured and plotted for analysis.

## **3.16 Green Fluorescent protein (GFP) Degradation Assay.**

### **3.16.1 HEK-293T Cell GFP Transfection and Rpn-6 Knockdown.**

A T-75 (or 10 cm dish) plate was taken out from the incubator and cells were examined under a microscope to determine confluency. The cell media in the plate was removed and the plate was washed with 10 mL of sterilized PBS gently to prevent washing off the cells. The PBS was

removed, and 2 mL of trypsin buffer was added to the plate. The plate was agitated by hand to allow the buffer to cover the whole plate and the plate was put back to the incubator for 5 mins to dissociate cells. The liquid was transferred into a 15 mL falcon tube and the plate was further washed twice with 3 mL cell media to collect all cells. The tube was centrifuged for 5 mins at 1,000 x g. The trypsin media was carefully removed from the tube and the cell pellet was resuspended in 5-8 mL of cell media. 10  $\mu$ L of solution from the falcon tube was added to each side of a hemocytometer with a glass cover on top. Cell numbers on each side of the hemocytometer was counted under a microscope and an average cell number was taken from the number obtained. The total number of cells in the falcon tube was calculated later through the average cell number.

Cells were plated on one T-25 plate at 80% confluency and the total cell media volume was 4 mL in the plate. The plate was left in the incubator overnight at 37°C to allow the cells to adhere to the plate. The next day, the GFP plasmid and lipofectamine 2000 were prepared according to protocol from Thermo-Fisher. A final amount of 3  $\mu$ g of GFP plasmid and 5  $\mu$ L of lipofectamine 2000 were mixed in 500  $\mu$ L of Opti-MEM media and incubated for 5 mins. The mixture was then carefully added to the T-25 plate and the plate was left in the incubator at 37°C overnight. The next day, the plate was taken out from the incubator and the cell media was removed from the plate. 1 mL of the trypsin buffer was added to the plate and the plate was agitated with hand to allow the buffer to cover the whole plate. The plate was put back to the incubator for 5 mins to dissociate cells. The liquid was transferred into a 15 mL falcon tube and the plate was further washed twice with 1 mL cell media to collect all cells. The tube was centrifuged for 5 mins at 1,000 x g, the cell pellet was collected, and the trypsin media was carefully removed from the tube and the cell pellet was resuspended in 5-8 mL of cell media. 10  $\mu$ L of solution from the falcon tube was added to each side of a hemocytometer with a glass cover on top. Cell numbers on each side of the hemocytometer was counted under a microscope and an average cell number was taken from the number obtained. The total number of cells in the falcon tube was calculated later through the average cell number. Two T-25 plates were plated at 25% confluency with the GFP transfected HEK-293T cells. The plates were left in the incubator at 37°C overnight to allow the cells to adhere to the plate. The next day, the cell media in the plate was carefully removed to prevent removing cells. The sRpn-6 siRNA was prepared according to protocol from Thermo-Fisher. A final amount of 100 pmol of the RNA was mixed with 21  $\mu$ L of lipofectamine RNAiMax in 500  $\mu$ L of Opti-

MEM media and the mixture solution was incubated for 5 mins. During the period, 4 mL of fresh DMEM media was carefully added to each plate to prevent disturbing the cells. Then the siRNARpn-6 mixture was carefully added to the corresponding plate. The second plate was designated as the untreated control and 500  $\mu$ L of Opti-MEM (with 21  $\mu$ L of lipofectamine RNAimax) media was added to the plate. All plates were carefully agitated by hand to distribute the Opti-MEM media evenly across the plate. The plates were left in the incubator at 37°C for 2 days.

### 3.16.2 12-well Plate and HEK-293T Cell Preparation.

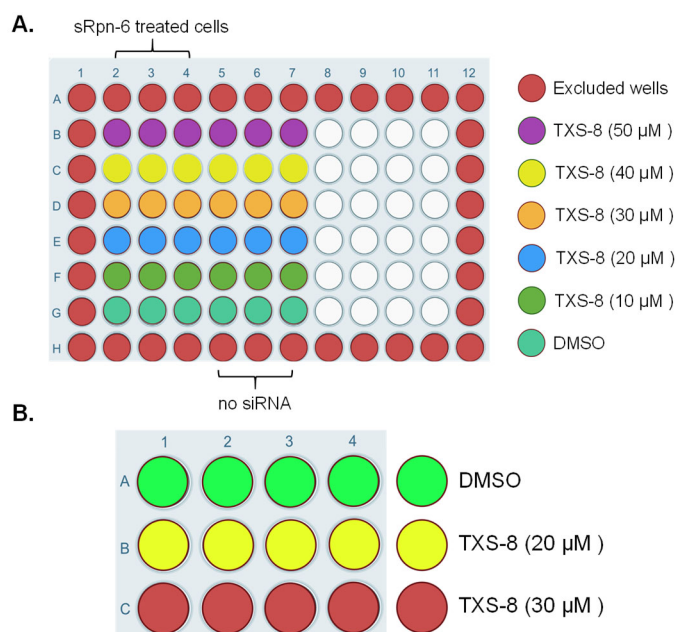


Figure 3.27(A) Layout of the 96-well plate for viability assay. (B) The sRpn-6/no siRNA treated HEK-293T cells have the same 12-well plate layout.

The sRpn-6 or no siRNA treated cells were taken out from the incubator. The cell media was carefully removed from each plate to prevent disturbing the cells. 1 mL of the trypsin buffer was added to each plate and the plate was agitated by hand to allow the buffer to cover the whole plate. The plate was put back to the incubator for 5 mins to dissociate cells. The liquid was transferred into a 15 mL falcon tube and the plate was further washed twice with 1 mL cell media to collect all cells. The tube was centrifuged for 5 mins at 1,000 x g. The trypsin media was carefully removed from the tube and

the cell pellet was resuspended in 5-8 mL of cell media. 10  $\mu$ L of solution from the falcon tube was added to each side of a hemocytometer with a glass cover on top. Cell numbers on each side of the hemocytometer was counted under a microscope and an average cell number was taken from the number obtained. The sRpn-6 and no siRNA treated HEK-293T cells were plated in all wells on two 12-well plates at 80% confluency (Figure 3.27A). The total volume in the wells was 1.25 mL. At the same time, a black 96-well round bottom plate was prepared to have 5,000 cells in 50

μL of cell media in each well according to **Figure 3.27B**. This plate was prepared for viability assay to confirm that the cells were still viable at the end of the degradation assay.

### **3.16.3 HEK-293T Cell Dosing and Western Blot Analysis of GFP Degradation Assay.**

Cells were seeded in a 12-well plate or 96-well plate the day (or however many days) prior to the experiment. A dilution of TXS-8 at 2 mM and 3 mM in 15 μL of DMSO were made. The above TXS-8 stock was further diluted with 235 μL of cell media. All 250 μL of the ligand solution was carefully added to a single well of the 12-well plate to, the process was repeated in quadruplicate. A DMSO control solution was also prepared accordingly. After all ligands were added, the 12-well plate was agitated gently by hand for 30s to allow the ligand evenly distributed across the well. The plates were then put back to the incubator for 3.5 hours. At the same time, a dilution stock of 5 mM, 4 mM, 3 mM, 2 mM and 1 mM of TXS-8 in DMSO were made. All above DMSO solutions were further diluted by adding 8 μL of the dilution stock into 392 μL of media to obtain the final dosing concentration. 8 μL of DMSO was also diluted in 392 μL of cell media. 50 μL of the test compounds were added to corresponding wells of the 96-well plate according to **Figure 3.27A**. The plate was placed in the incubator for 3.5 hours then was taken out and equilibrated to ROOM TEMPERATURE. 50 μL of CellTiter Glo solution was added to each well with pipetting to mix. The plate was agitated for 2 min and incubated for another 10 mins in the dark. The luminescent signal of each well was measured with a Synergy NEO plate reader system. The readings were recorded and normalized to the DMSO control to obtain percent viability and were graphed in Prism 8.

After 3.5 hours, the 12-well plate was then taken out from the incubator and the cell media was carefully removed from each well. Each well was then washed with 1 mL of PBS with vigorous pipetting. The mixture was then transferred to a 1.5 mL eppitube. The tube was centrifuged at 1,000 x g for 3 min. The PBS was then carefully removed from the tube and 300 μL M-PER solution (final concentration of HALT protease inhibitor was 1X) was added to each eppitube. The lysate was agitated at R. T. for 10 mins and was centrifuged at 12,000 x g for 15 mins at 4 °C. The cell lysate was carefully removed from the eppitube leaving the pellet debris at the bottom of the tube. The protein concentration was measured by Nanodrop One system. The protein concentration was normalized to the lowest concentrated sample by diluting samples in PBS. 10 μL of Laemmli buffer was mixed with 40 μL of normalized lysate and the tube was heated

at 95 °C for 5 mins. SDS-PAGE was performed, and protein was transferred to the nitrocellulose membrane with a Trans-blot® Turbo™ from Bio-Rad. The membrane was blocked with a 5% milk solution in PBS. All antibodies were diluted 1:1,000 in LI-COR intercept blocking buffer and allowed to incubate with the membranes overnight at 4 °C. The membrane was washed with PBS three times before secondary antibody binding. Secondary antibodies were diluted 1:10,000 in LI-COR intercept blocking buffer and allowed to gently agitate for 1 hour at ROOM TEMPERATURE. The membrane was scanned on an Odyssey CLx imaging system and the expression level of Rpn-6, GAPDH and GFP among the sRpn-6/cRpn-6/no siRNA treated cells were analyzed and plotted.

### **3.17 Dosing Cardiomyocytes with TXS-8.**

#### **3.17.1 Determining Rpn-6 Levels in AC16 Cells by Western Blot.**

To ensure expression of Rpn-6 could be detected in AC16 cells, we conducted western blots in which we blotted for Rpn-6. AC16 cell were removed from a well of a six well plate by treating with a 0.25% trypsin-EDTA solution. 500 µL of media was then added to the well and cells were transferred to a 1.5 mL eppitube. Cells were centrifuged at 1,000 x g for 5 min at 4 °C. Cells were lysed by adding 300 µL of an MPER solution supplemented with HALT to a final concentration of 1X. Cells were gently rotated for 10 min at ROOM TEMPERATURE. and the lysate was then centrifuged at 14,000 x g for 15 min at 4 °C. The supernatant was transferred to a new eppitube and the protein concentration was determined with a Nanodrop One system. 11 µL of the lysate was mixed with 4 µL of Laemmli buffer and the sample was heated for five minutes. After running on SDS-PAGE, protein was transferred to a nitrocellulose membrane using a Trans-blot® Turbo™ from Bio-Rad. The membrane was washed three times with deionized water and blocked for 40 min at ROOM TEMPERATURE. with a 5% milk solution in PBS. A primary Rpn-6 antibody (Novus Biologicals) was then diluted 1:1,000 in intercept blocking buffer (LI-COR) and added to the blot. The blot was allowed to incubate overnight with the antibody. The following morning, the antibody was collected, and the blot was washed three times with PBS. Then, a rabbit 800 CW secondary antibody (LI-COR) was diluted 1:10,000 in intercept blocking buffer (LI-COR). The secondary antibody was incubated with the membrane for 40 min at ROOM TEMPERATURE. with gentle agitation and was protected from light. The antibody was then collected, the blot was

washed three times with PBS and the membrane was scanned on an Odyssey CLx imaging system from LI-COR.

### **3.17.2 Establishing Cell Viability with AC16 Cells in Response to Dosing with TXS-8.**

The day prior the experiment, 800,000 cells were resuspended in 4 mL growth media. 100  $\mu$ L of the above mixture was added to the wells of a white 96-well plate, excluding the edge wells to have 20,000 cells per well. Cells were allowed to adhere overnight. The following day, a 11 mM stock of TXS-8 was prepared by diluting a 20 mM stock in DMSO. This was serial diluted a total of twelve times. 3.5  $\mu$ L of each TXS-8 dilution stock was further diluted in 31.5  $\mu$ L of cell media and 10  $\mu$ L was added to the wells in triplicate. As a control, 3.5  $\mu$ L of DMSO was diluted in 31.5  $\mu$ L of cell media and added to three wells. Cells were incubated for 3.5 hours at 37 °C. The plate was then taken out from the incubator and equilibrated to ROOM TEMPERATURE. Then, 50  $\mu$ L of CellTiter Glo was added to each well with pipetting. The plate was agitated for 2 min and incubated for another 10 mins in the dark. Luminescence from each well was read with a Synergy Neo plate reader system.

The luminescent signal from each well was measured by a Synergy NEO plate reader system. The readings were recorded and normalized to the DMSO control to obtain percent viability and were graphed in Prism 8.

### **3.17.3 Monitoring Proteasome Activity in Response to TXS-8 with TAS-2.**

The day prior to the experiment, media was removed from the T-75 flask containing AC16 cells and the cells were rinsed with 5 mL of PBS. 2 mL of a 0.25% Trypsin-EDTA solution was added to the plate and the plate was incubated at 37 °C for five minutes. 3 mL of media was then added to the flask and the cells were transferred to a 15 mL falcon tube. Cells were counted with a hemocytometer as described above, then 100,000 cells were resuspended in 2 mL of media. 100  $\mu$ L of cells was added to the wells of a black 96-well plate excluding edge wells, producing a final cell amount of 5,000 cells per well. Cells were allowed to adhere to the plate overnight.

The following day, a 1,375  $\mu$ M stock of TXS-8 was prepared by diluting a 20mM stock in DMSO. As a negative control, cells were also dosed with MG-132, a known proteasome inhibitor. A 550  $\mu$ M stock of MG-132 was prepared. 5.5  $\mu$ L of TXS-8, MG-132, or DMSO were diluted in

49.5  $\mu$ L of media and thoroughly vortexed to mix. 10  $\mu$ L of each stock was added to wells in replicates of five. The final concentration of TXS-8 in each well was 12.5  $\mu$ M, while the final MG-132 concentration was 5  $\mu$ M. Cells were incubated with the compounds for 3.5 hours at 37 °C. Media was then carefully removed from the wells and the cells were washed 3 times with 50  $\mu$ L of PBS. A 2.5 mM stock of TXS-8 was prepared by diluting a 20mM stock in DMSO and a 1 mM stock of MG-132 was prepared as well. A 2 mM stock of TAS-2 was prepared by diluting a 20 mM stock in DMSO. 1.4  $\mu$ L TXS-8 or DMSO was diluted in 272.2  $\mu$ L of KRBH buffer followed by 1.4  $\mu$ L of the 2 mM TAS-2 stock. As a control, 1.4  $\mu$ L of TAS-2 was diluted in 248.6  $\mu$ L of KRBH buffer. 50  $\mu$ L of each solution was added to the cells in replicates of five. The plate was then incubated for 10 mins at 37 °C before transferring to the plate reader. Fluorescence intensity from each well was measured with a Tecan F200Infinite Pro plate reader system that had been pre-heated to 37 °C with the gain set to 80. Fluorescence was read every two minutes for two hours. The results were compiled and graphed. This experiment was performed in technical quintuplicate and experimental duplicate. Similar results were obtained between both experimental trials.

Acknowledgement:

### Workflow of investigating small molecule impact on proteasome activity

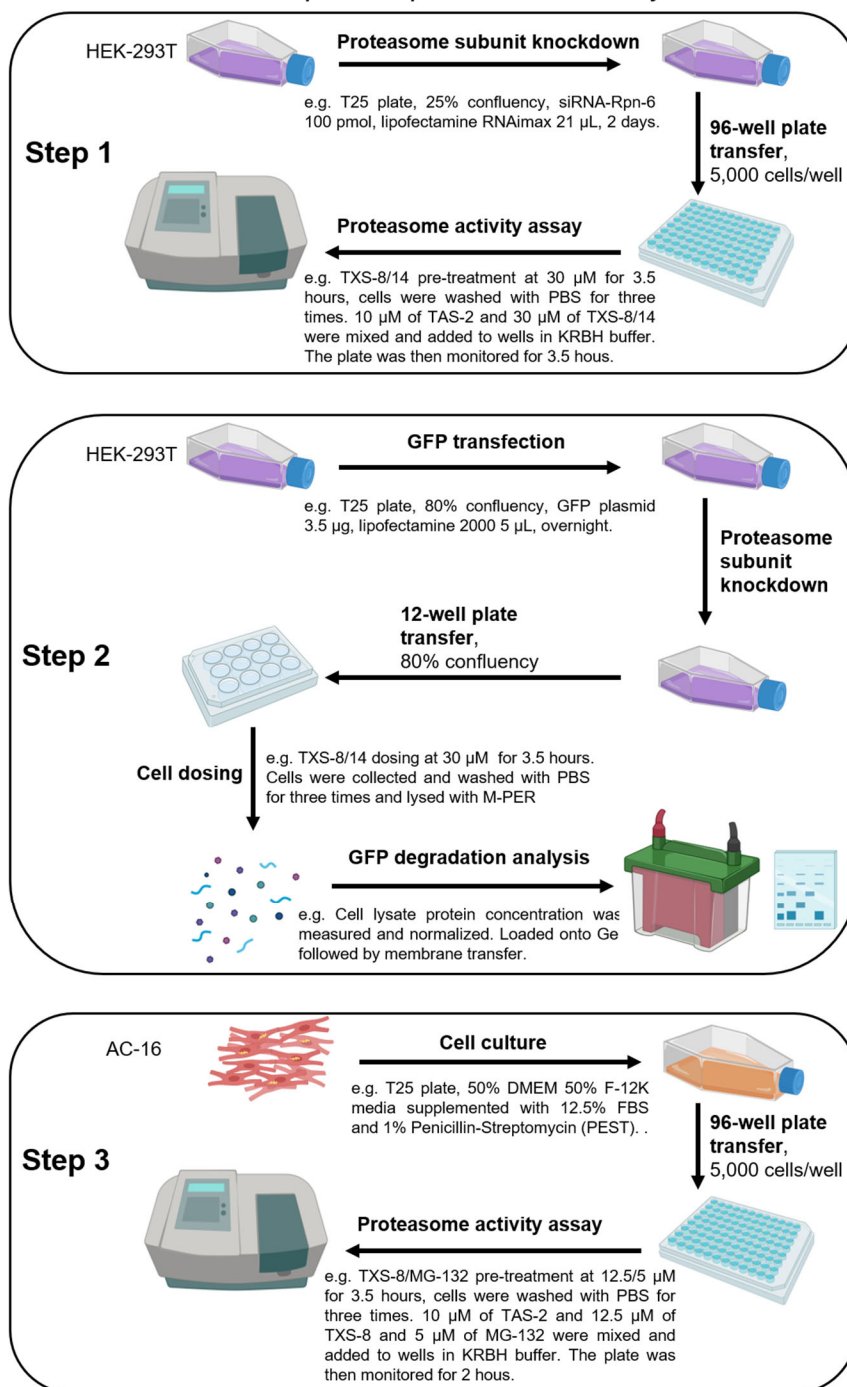
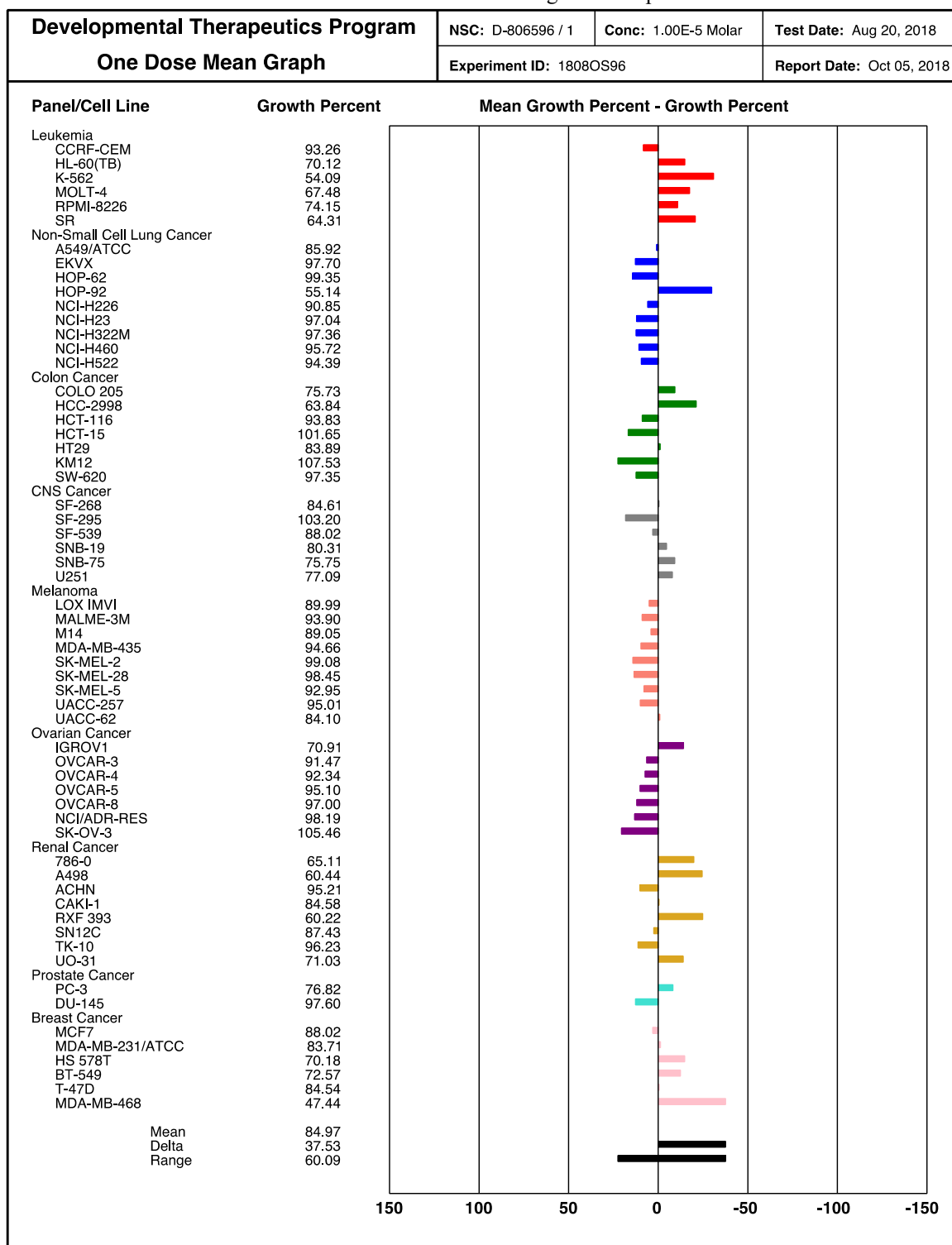


**Figure 3.28.** Detailed workflow of investigating the impact of a small molecule on proteasome activity.

The figures were created with BioRender.com

Table 3.2. NIH NCI-60 single dose experiment.



### 3.18 Reference.

- (1) Tian, W.; Trader, D. J. Discovery of a Small Molecule Probe of Rpn-6, an Essential Subunit of the 26S Proteasome. *ACS Chemical Biology* **2020**, *15* (2), 554–561. <https://doi.org/10.1021/acscchembio.9b01019>.
- (2) Lee, N. K.; Park, S. E.; Kwon, S. J.; Shim, S.; Byeon, Y.; Kim, J.-H.; Na, D. L.; Chang, J. W. Agouti Related Peptide Secreted Via Human Mesenchymal Stem Cells Upregulates Proteasome Activity in an Alzheimer's Disease Model. *Sci Rep* **2017**, *7* (1), 39340. <https://doi.org/10.1038/srep39340>.
- (3) Götze, S.; Saborowski, R.; Martínez-Cruz, O.; Muhlia-Almazán, A.; Sánchez-Paz, A. Proteasome Properties of Hemocytes Differ between the Whiteleg Shrimp *Penaeus Vannamei* and the Brown Shrimp *Crangon Crangon* (Crustacea, Decapoda). *Cell Stress and Chaperones* **2017**, *22* (6), 879–891. <https://doi.org/10.1007/s12192-017-0819-4>.
- (4) Ye, M.; Qiu, H.; Cao, Y.; Zhang, M.; Mi, Y.; Yu, J.; Wang, C. Curcumin Improves Palmitate-Induced Insulin Resistance in Human Umbilical Vein Endothelial Cells by Maintaining Proteostasis in Endoplasmic Reticulum. *Front. Pharmacol.* **2017**, *08*. <https://doi.org/10.3389/fphar.2017.00148>.
- (5) Lan, X.; Zhao, C.; Chen, X.; Zhang, P.; Zang, D.; Wu, J.; Chen, J.; Long, H.; Yang, L.; Huang, H.; Wang, X.; Shi, X.; Liu, J. Platinum Pyrithione Induces Apoptosis in Chronic Myeloid Leukemia Cells Resistant to Imatinib via DUB Inhibition-Dependent Caspase Activation and Bcr-Abl Downregulation. *Cell Death Dis* **2017**, *8* (7), e2913–e2913. <https://doi.org/10.1038/cddis.2017.284>.
- (6) Zerfas, B. L.; Coleman, R. A.; Salazar-Chaparro, A. F.; Macatangay, N. J.; Trader, D. J. Fluorescent Probes with Unnatural Amino Acids to Monitor Proteasome Activity in Real-Time. *ACS Chemical Biology* **2020**, *15* (9), 2588–2596. <https://doi.org/10.1021/acscchembio.0c00634>.
- (7) Coleman, R. A.; Trader, D. J. Development and Application of a Sensitive Peptide Reporter to Discover 20S Proteasome Stimulators. *ACS Combinatorial Science* **2018**, *20* (5), 269–276. <https://doi.org/10.1021/acscombsci.7b00193>.
- (8) Coleman, R. A.; Trader, D. J. Methods to Discover and Evaluate Proteasome Small Molecule Stimulators. *Molecules* **2019**, *24* (12), 2341. <https://doi.org/10.3390/molecules24122341>.
- (9) Li, Y.; Tomko, R. J.; Hochstrasser, M. Proteasomes: Isolation and Activity Assays. *Current Protocols in Cell Biology* **2015**, *67* (1). <https://doi.org/10.1002/0471143030.cb0343s67>.
- (10) Blackburn, C.; Gigstad, K. M.; Hales, P.; Garcia, K.; Jones, M.; Bruzzese, F. J.; Barrett, C.; Liu, J. X.; Soucy, T. A.; Sappal, D. S.; Bump, N.; Olhava, E. J.; Fleming, P.; Dick, L. R.; Tsu, C.; Sintchak, M. D.; Blank, J. L. Characterization of a New Series of Non-Covalent Proteasome Inhibitors with Exquisite Potency and Selectivity for the 20S B5-Subunit. *Biochemical Journal* **2010**, *430* (3), 461–476. <https://doi.org/10.1042/BJ20100383>.

- (11) Rodgers, K. J.; Dean, R. T. Assessment of Proteasome Activity in Cell Lysates and Tissue Homogenates Using Peptide Substrates. *The International Journal of Biochemistry & Cell Biology* **2003**, 35 (5), 716–727. [https://doi.org/10.1016/S1357-2725\(02\)00391-6](https://doi.org/10.1016/S1357-2725(02)00391-6).
- (12) Gan, J.; Leestemaker, Y.; Sapmaz, A.; Ovaa, H. Highlighting the Proteasome: Using Fluorescence to Visualize Proteasome Activity and Distribution. *Front. Mol. Biosci.* **2019**, 6, 14. <https://doi.org/10.3389/fmolb.2019.00014>.
- (13) Zhang, L.; Gurskaya, N. G.; Merzlyak, E. M.; Staroverov, D. B.; Mudrik, N. N.; Samarkina, O. N.; Vinokurov, L. M.; Lukyanov, S.; Lukyanov, K. A. Method for Real-Time Monitoring of Protein Degradation at the Single Cell Level. *BioTechniques* **2007**, 42 (4), 446–450. <https://doi.org/10.2144/000112453>.
- (14) Chen, D.; Frezza, M.; Schmitt, S.; Kanwar, J.; P. Dou, Q. Bortezomib as the First Proteasome Inhibitor Anticancer Drug: Current Status and Future Perspectives. *Current Cancer Drug Targets* **2011**, 11 (3), 239–253. <https://doi.org/10.2174/156800911794519752>.
- (15) Chauhan, D.; Catley, L.; Li, G.; Podar, K.; Hideshima, T.; Velankar, M.; Mitsiades, C.; Mitsiades, N.; Yasui, H.; Letai, A.; Ovaa, H.; Berkers, C.; Nicholson, B.; Chao, T.-H.; Neuteboom, S. T. C.; Richardson, P.; Palladino, M. A.; Anderson, K. C. A Novel Orally Active Proteasome Inhibitor Induces Apoptosis in Multiple Myeloma Cells with Mechanisms Distinct from Bortezomib. *Cancer Cell* **2005**, 8 (5), 407–419. <https://doi.org/10.1016/j.ccr.2005.10.013>.
- (16) Suh, K. S.; Tanaka, T.; Sarojini, S.; Nightingale, G.; Gharbaran, R.; Pecora, A.; Goy, A. The Role of the Ubiquitin Proteasome System in Lymphoma. *Critical Reviews in Oncology/Hematology* **2013**, 87 (3), 306–322. <https://doi.org/10.1016/j.critrevonc.2013.02.005>.
- (17) Schenkein, D. Proteasome Inhibitors in the Treatment of B-Cell Malignancies. *Clinical Lymphoma* **2002**, 3 (1), 49–55. <https://doi.org/10.3816/CLM.2002.n.011>.
- (18) Weigert, O.; Pastore, A.; Rieken, M.; Lang, N.; Hiddemann, W.; Dreyling, M. Sequence-Dependent Synergy of the Proteasome Inhibitor Bortezomib and Cytarabine in Mantle Cell Lymphoma. *Leukemia* **2007**, 21 (3), 524–528. <https://doi.org/10.1038/sj.leu.2404511>.
- (19) Lü, S.; Chen, Z.; Yang, J.; Chen, L.; Gong, S.; Zhou, H.; Guo, L.; Wang, J. Overexpression of the PSMB5 Gene Contributes to Bortezomib Resistance in T-Lymphoblastic Lymphoma/Leukemia Cells Derived from Jurkat Line. *Experimental Hematology* **2008**, 36 (10), 1278–1284. <https://doi.org/10.1016/j.exphem.2008.04.013>.
- (20) Isono, E.; Saito, N.; Kamata, N.; Saeki, Y.; Toh-e, A. Functional Analysis of Rpn6p, a Lid Component of the 26 S Proteasome, Using Temperature-Sensitive *Rpn6* Mutants of the Yeast *Saccharomyces Cerevisiae*. *Journal of Biological Chemistry* **2005**, 280 (8), 6537–6547. <https://doi.org/10.1074/jbc.M409364200>.

- (21) Pathare, G. R.; Nagy, I.; Bohn, S.; Unverdorben, P.; Hubert, A.; Korner, R.; Nickell, S.; Lasker, K.; Sali, A.; Tamura, T.; Nishioka, T.; Forster, F.; Baumeister, W.; Bracher, A. The Proteasomal Subunit Rpn6 Is a Molecular Clamp Holding the Core and Regulatory Subcomplexes Together. *Proceedings of the National Academy of Sciences* **2012**, *109* (1), 149–154. <https://doi.org/10.1073/pnas.1117648108>.
- (22) Lokireddy, S.; Kukushkin, N. V.; Goldberg, A. L. CAMP-Induced Phosphorylation of 26S Proteasomes on Rpn6/PSMD11 Enhances Their Activity and the Degradation of Misfolded Proteins. *Proc Natl Acad Sci USA* **2015**, *112* (52), E7176–E7185. <https://doi.org/10.1073/pnas.1522332112>.
- (23) Guo, X.; Huang, X.; Chen, M. J. Reversible Phosphorylation of the 26S Proteasome. *Protein Cell* **2017**, *8* (4), 255–272. <https://doi.org/10.1007/s13238-017-0382-x>.
- (24) Dou, Q.; Zonder, J. Overview of Proteasome Inhibitor-Based Anti-Cancer Therapies: Perspective on Bortezomib and Second Generation Proteasome Inhibitors versus Future Generation Inhibitors of Ubiquitin-Proteasome System. *Current Cancer Drug Targets* **2014**, *14* (6), 517–536. <https://doi.org/10.2174/1568009614666140804154511>.
- (25) Selimovic, D.; Porzig, B. B. O. W.; El-Khattouti, A.; Badura, H. E.; Ahmad, M.; Ghanjati, F.; Santourlidis, S.; Haikel, Y.; Hassan, M. Bortezomib/Proteasome Inhibitor Triggers Both Apoptosis and Autophagy-Dependent Pathways in Melanoma Cells. *Cellular Signalling* **2013**, *25* (1), 308–318. <https://doi.org/10.1016/j.cellsig.2012.10.004>.
- (26) Heider, U.; Rademacher, J.; Lamottke, B.; Mieth, M.; Moebs, M.; von Metzler, I.; Assaf, C.; Sezer, O. Synergistic Interaction of the Histone Deacetylase Inhibitor SAHA with the Proteasome Inhibitor Bortezomib in Cutaneous T Cell Lymphoma. *European Journal of Haematology* **2009**, *82* (6), 440–449. <https://doi.org/10.1111/j.1600-0609.2009.01239.x>.
- (27) Ri, M.; Iida, S.; Nakashima, T.; Miyazaki, H.; Mori, F.; Ito, A.; Inagaki, A.; Kusumoto, S.; Ishida, T.; Komatsu, H.; Shiotsu, Y.; Ueda, R. Bortezomib-Resistant Myeloma Cell Lines: A Role for Mutated PSMB5 in Preventing the Accumulation of Unfolded Proteins and Fatal ER Stress. *Leukemia* **2010**, *24* (8), 1506–1512. <https://doi.org/10.1038/leu.2010.137>.
- (28) Horton, T. M.; Gannavarapu, A.; Blaney, S. M.; D'Argenio, D. Z.; Plon, S. E.; Berg, S. L. Bortezomib Interactions with Chemotherapy Agents in Acute Leukemia in Vitro. *Cancer Chemother Pharmacol* **2006**, *58* (1), 13–23. <https://doi.org/10.1007/s00280-005-0135-z>.
- (29) Trader, D. J.; Simanski, S.; Kodadek, T. A Reversible and Highly Selective Inhibitor of the Proteasomal Ubiquitin Receptor Rpn13 Is Toxic to Multiple Myeloma Cells. *Journal of the American Chemical Society* **2015**, *137* (19), 6312–6319. <https://doi.org/10.1021/jacs.5b02069>.
- (30) Muli, C.; Tian, W.; Trader, D. J. Small Molecule Inhibitors of the Proteasome's Regulatory Particle. *ChemBioChem* **2019**. <https://doi.org/10.1002/cbic.201900017>.

- (31) Leestemaker, Y.; Ovaa, H. Tools to Investigate the Ubiquitin Proteasome System. *Drug Discovery Today: Technologies* **2017**, *26*, 25–31. <https://doi.org/10.1016/j.ddtec.2017.11.006>.
- (32) Choi, W. H.; de Poot, S. A. H.; Lee, J. H.; Kim, J. H.; Han, D. H.; Kim, Y. K.; Finley, D.; Lee, M. J. Open-Gate Mutants of the Mammalian Proteasome Show Enhanced Ubiquitin-Conjugate Degradation. *Nat Commun* **2016**, *7* (1), 10963. <https://doi.org/10.1038/ncomms10963>.
- (33) Leestemaker, Y.; de Jong, A.; Witting, K. F.; Penning, R.; Schuurman, K.; Rodenko, B.; Zaal, E. A.; van de Kooij, B.; Laufer, S.; Heck, A. J. R.; Borst, J.; Scheper, W.; Berkers, C. R.; Ovaa, H. Proteasome Activation by Small Molecules. *Cell Chemical Biology* **2017**, *24* (6), 725–736.e7. <https://doi.org/10.1016/j.chembiol.2017.05.010>.
- (34) Thibaudeau, T. A.; Smith, D. M. A Practical Review of Proteasome Pharmacology. *Pharmacol Rev* **2019**, *71* (2), 170–197. <https://doi.org/10.1124/pr.117.015370>.
- (35) Meng, L.; Mohan, R.; Kwok, B. H. B.; Elofsson, M.; Sin, N.; Crews, C. M. Epoxomicin, a Potent and Selective Proteasome Inhibitor, Exhibits in Vivo Antiinflammatory Activity. *Proceedings of the National Academy of Sciences* **1999**, *96* (18), 10403–10408. <https://doi.org/10.1073/pnas.96.18.10403>.
- (36) Chandu, D.; Kumar, A.; Nandi, D. PepN, the Major Suc-LLVY-AMC-Hydrolyzing Enzyme In *Escherichia Coli*, Displays Functional Similarity with Downstream Processing Enzymes in Archaea and Eukarya. *Journal of Biological Chemistry* **2003**, *278* (8), 5548–5556. <https://doi.org/10.1074/jbc.M207926200>.
- (37) Kisselev, A. F.; Akopian, T. N.; Castillo, V.; Goldberg, A. L. Proteasome Active Sites Allosterically Regulate Each Other, Suggesting a Cyclical Bite-Chew Mechanism for Protein Breakdown. *Molecular Cell* **1999**, *4* (3), 395–402. [https://doi.org/10.1016/S1097-2765\(00\)80341-X](https://doi.org/10.1016/S1097-2765(00)80341-X).
- (38) Zerfas, B. L.; Trader, D. J. Monitoring the Immunoproteasome in Live Cells Using an Activity-Based Peptide–Peptoid Hybrid Probe. *J. Am. Chem. Soc.* **2019**, *9*.
- (39) Tian, W.; Maresh, M.; Trader, D. J. Approaches to Evaluate the Impact of a Small Molecule Binder to a Non-catalytic Site of the Proteasome. *ChemBioChem* **2021**, cbic.202100023. <https://doi.org/10.1002/cbic.202100023>.
- (40) Ottis, P.; Toure, M.; Cromm, P. M.; Ko, E.; Gustafson, J. L.; Crews, C. M. Assessing Different E3 Ligases for Small Molecule Induced Protein Ubiquitination and Degradation. *ACS Chemical Biology* **2017**, *12* (10), 2570–2578. <https://doi.org/10.1021/acscchembio.7b00485>.
- (41) Ling Yong, C. L.; Siak-Wei Ow, D.; Tandiono, T.; Mei Heng, L. L.; Kwok-Keung Chan, K.; Ohl, C.-D.; Klaseboer, E.; Ohl, S.-W.; Boon-Hwa Choo, A. Microbubble-Mediated Sonoporation for Highly Efficient Transfection of Recalcitrant Human B- Cell Lines. *Biotechnology Journal* **2014**, *9* (8), 1081–1087. <https://doi.org/10.1002/biot.201300507>.

- (42) Kimura, H.; Caturegli, P.; Takahashi, M.; Suzuki, K. New Insights into the Function of the Immunoproteasome in Immune and Nonimmune Cells. *Journal of Immunology Research* **2015**, *2015*, 1–8. <https://doi.org/10.1155/2015/541984>.
- (43) Salimzadeh, L.; Jaberipour, M.; Hosseini, A.; Ghaderi, A. Non-Viral Transfection Methods Optimized for Gene Delivery to a Lung Cancer Cell Line. **2013**, *5* (2), 10.
- (44) Fajrial, A. K.; He, Q. Q.; Wirusanti, N. I.; Slansky, J. E.; Ding, X. A Review of Emerging Physical Transfection Methods for CRISPR/Cas9-Mediated Gene Editing. *Theranostics* **2020**, *10* (12), 5532–5549. <https://doi.org/10.7150/thno.43465>.
- (45) Welk, V. Inhibition of Proteasome Activity Induces Formation of Alternative Proteasome Complexes\*. **2016**, *291* (25), 13.
- (46) Semren, N.; Welk, V.; Korfei, M.; Keller, I. E.; Fernandez, I. E.; Adler, H.; Günther, A.; Eickelberg, O.; Meiners, S. Regulation of 26S Proteasome Activity in Pulmonary Fibrosis. *Am J Respir Crit Care Med* **2015**, *192* (9), 1089–1101. <https://doi.org/10.1164/rccm.201412-2270OC>.
- (47) Vilchez, D.; Morante, I.; Liu, Z.; Douglas, P. M.; Merkwirth, C.; Rodrigues, A. P. C.; Manning, G.; Dillin, A. RPN-6 Determines C. Elegans Longevity under Proteotoxic Stress Conditions. *Nature* **2012**, *489* (7415), 263–268. <https://doi.org/10.1038/nature11315>.
- (48) Vilchez, D.; Boyer, L.; Morante, I.; Lutz, M.; Merkwirth, C.; Joyce, D.; Spencer, B.; Page, L.; Masliah, E.; Berggren, W. T.; Gage, F. H.; Dillin, A. Increased Proteasome Activity in Human Embryonic Stem Cells Is Regulated by PSMD11. *Nature* **2012**, *489* (7415), 304–308. <https://doi.org/10.1038/nature11468>.
- (49) Mahieu, E.; Covès, J.; Krüger, G.; Martel, A.; Moulin, M.; Carl, N.; Härtlein, M.; Carlomagno, T.; Franzetti, B.; Gabel, F. Observing Protein Degradation by the PAN-20S Proteasome by Time-Resolved Neutron Scattering. *Biophysical Journal* **2020**, *119* (2), 375–388. <https://doi.org/10.1016/j.bpj.2020.06.015>.
- (50) Hasinoff, B. B.; Patel, D.; Wu, X. Molecular Mechanisms of the Cardiotoxicity of the Proteasomal-Targeted Drugs Bortezomib and Carfilzomib. *Cardiovascular Toxicology* **2017**, *17* (3), 237–250. <https://doi.org/10.1007/s12012-016-9378-7>.
- (51) Orciuolo, E.; Buda, G.; Cecconi, N.; Galimberti, S.; Versari, D.; Cervetti, G.; Salvetti, A.; Petrini, M. Unexpected Cardiotoxicity in Haematological Bortezomib Treated Patients. *British Journal of Haematology* **2007**, *138* (3), 396–397. <https://doi.org/10.1111/j.1365-2141.2007.06659.x>.
- (52) Crawford, L. J. A.; Walker, B.; Ovaa, H.; Chauhan, D.; Anderson, K. C.; Morris, T. C. M.; Irvine, A. E. Comparative Selectivity and Specificity of the Proteasome Inhibitors BzLLCCHO, PS-341, and MG-132. *Cancer Res.* **2006**, *66* (12), 6379–6386. <https://doi.org/10.1158/0008-5472.CAN-06-0605>.

## CHAPTER 4. TXS-8 PROTAC DEVELOPMENT/BINDING SITE STUDY AND PROTEASOME PROBE DEVELOPMENT.

### 4.1 Introduction.

Based on our previous studies with TXS-8 in **Chapter 2** and **Chapter 3**. We concluded that TXS-8 was a selective binder of proteasomal subunit Rpn-6 and showed moderate toxicity towards Rpn-6 overexpressing hematological cancers like multiple myeloma and B-cell lymphoma.<sup>1</sup> However, the toxicity effect of TXS-8 on these cancer cells remained unclear. Although we investigated the impact of TXS-8 on proteasome activity, it was difficult to conclude that TXS-8 could affect proteasome activity at non-lethal concentrations.<sup>2</sup>

To further investigate the impact of TXS-8 onto Rpn-6, we decided to develop TXS-8 based proteolysis targeting chimera (PROTAC). We will investigate the toxicity of TXS-8-based PROTACs and study if they could efficiently degrade Rpn-6. Meanwhile, we also believe revealing the binding site of TXS-8 on Rpn-6 will also greatly benefit our future research on TXS-8 like structural optimization for potency improvement or even rational drug design in the future. Therefore, by adopting what we previously did in **Chapter 2** with TXS-8 covalent pull-down, we came up with two approaches to study the general binding site of TXS-8 on Rpn-6.

During our research on the impact of TXS-8 on proteasome activity in **Chapter 3**, the TAS-1 (LLVY-Rh) probe we used for proteasome activity monitoring was a sensitive probe only for the chymotrypsin-like  $\beta 5$  subunit. Due to limitation of cell permeable probes, we were unable to investigate the impact of TXS-8 on the caspase-like  $\beta 1$  and trypsin-like  $\beta 2$  subunit of the proteasome in our previous studies. Although TXS-8 did not alter the chymotrypsin-like activity at non-lethal concentration, examining the effect of TXS-8 on the caspase-like and trypsin-like activity could still benefit our research. Besides, we also desire to expand our proteasome activity toolbox by developing more sensitive proteasome probes. Therefore, by analyzing and combining the commercially available proteasome probes and LLVY-Rh probes, we decided to develop selective proteasome probes for the  $\beta 1$  and  $\beta 2$  subunit to provide useful tools for future potential small molecule proteasome regulator characterization.

## 4.2 TXS-8 PROTAC development.

### 4.2.1 Using PROTAC to selectively degrade target protein and induce toxicity.

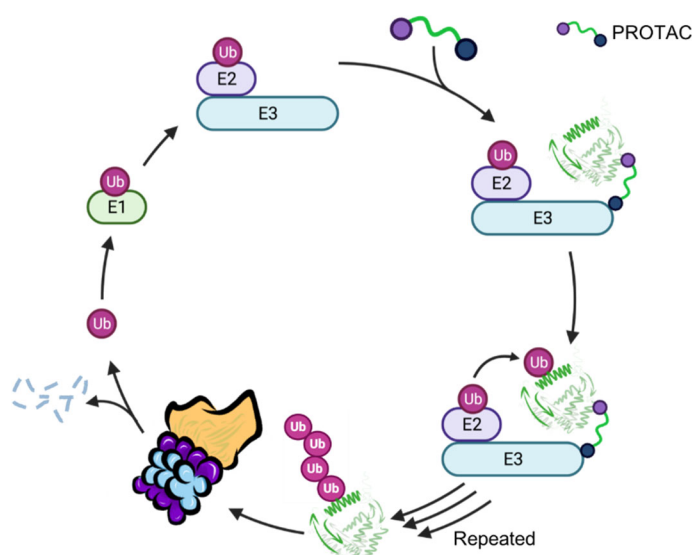


**Figure 4.1 Cellular process of how PROTAC works.** The addition of PROTAC will induce the co-recruitment of the target protein and E3 ligase. The target protein could be poly-ubiquitinated and eventually be degraded by the 26S proteasome.

Proteolysis targeting chimera (PROTAC) is defined as a bifunctional small molecule that can utilize the ubiquitin proteasome system (UPS) to selectively induce specific protein degradation and impact cellular processes.<sup>3-6</sup> As the name chimera indicates, the molecule is a hybrid of two major components. One part of the small molecule is a selective binder or inhibitor of the target protein, and the other part of the small molecule binds selectively to an E3 ligase. Between them, a linker is used to connect both moieties.<sup>6-8</sup> When a

PROTAC is presented in cells, the PROTAC will both bind its target protein and a E3 ligase and bring these two proteins in close contact. The E3 ligase will then transfer a ubiquitin to the target protein. By repeating the above steps, the target protein will eventually be polyubiquitinated and undergo proteasome degradation (**Figure 4.1**). The idea of hijacking the UPS to selectively degrade proteins provide a new approach to target “undruggable” proteins.<sup>3,9-11</sup> “Undruggable” proteins refer to proteins perceived to be difficult to target pharmacologically. Normally, these proteins own either large flat protein-protein interaction surfaces or lack deep protein pockets.<sup>12</sup> Developing small molecule inhibitors for these proteins are extremely difficult as some of the target proteins do not provide a known pocket for binding. Small molecule binders are also difficult to inhibit protein-protein interactions when facing a large interaction surface area. However, modifying low affinity small molecules into PROTACs may solve the issue. Research has shown that forming stable ternary complexes between the E3 ligase and the target protein significantly affect ubiquitination of the target protein.<sup>11,13-15</sup> This means that small molecules with low affinity toward a target protein could still induce significant protein degradation if a stable ternary complex between E3 ligase and the target protein could be achieved. However, no exact correlation has

been established between the affinity of the PROTAC towards target protein and the extent of protein degradation largely due to the variations of linkers presented in PROTACs. Although linker presents no binding function, it can significantly affect the protein degradation capacity of PROTACs.<sup>14,16</sup> This remains one of the biggest puzzles in PROTAC development as trial and error tend to be the best way to discover the optimal linker length while no general trend has been established.<sup>7,17</sup> Computational methods have also been used to facilitate the development of PROTACs recently.<sup>18,19</sup> Currently, the most studied E3 ligases are cereblon (CRBN) and von Hippel-Lindau E3 ligase (VHL).<sup>9,14,20–23</sup> Other E3 ligases like Cullin-Ring ligase family,<sup>24,25</sup> parkin and  $\beta$ -TRCP,<sup>26–28</sup> MDM2 etc.<sup>28–30</sup> have also been reported to be used for PROTAC development targeting different proteins. In addition, there is around 600-700 E3 ligases presented in human cells and a lot of them remained undeveloped for PROTAC design.<sup>31</sup> With the development of PROTAC techniques and better understanding of E3 ligases, more choices will be provided when PROTACs are designed.

## 4.2.2 TXS-8 PROTAC development.

### 4.2.2.1 Thalidomide TXS-8 PROTAC development.

#### 4.2.2.1.1 Thalidomide synthesis and TXS-8 PROTAC development.

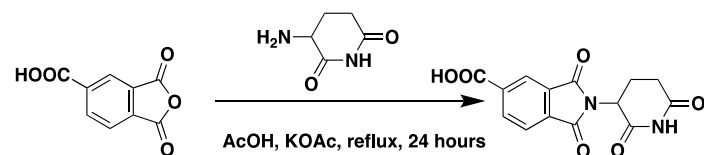


**Figure 4.2. Synthesis route of thalidomide derivative.** This is a one-step synthesis.

As previously mentioned in **Chapter 4.2.1** that thalidomide was one of the most widely used ligands to recruit E3

ligase CRBN, we wanted to also use thalidomide to construct our TXS-8 PROTAC.<sup>9,14,20–23</sup> However, modification on thalidomide was required as the small molecule does not present “handles” to allow attachment of other molecules. Therefore, we designed and synthesized a derivative of thalidomide with a carboxylic acid group for further addition reactions (**Figure 4.2**).<sup>32</sup> After acquiring the thalidomide derivative, we started building TXS-8 PROTAC. As literature pointed out, maintaining a proper ternary structure between the E3 ligase and the target protein is crucial to induce significant ubiquitination, which is largely affected by linker, so we decided to incorporate different linkers to our PROTAC. Polyethylene glycol (PEG) was one of the most commonly used linker on constructing PROTACs. Since our lab possessed only PEG-

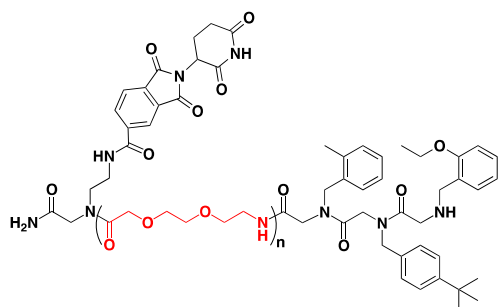


**Figure 4.3 General structure of the PROTAC.** The linker is consisted of one or two PEG-2 moieties ( $n=1$ ; TWT-1,  $n=2$ ; TWT-2).

2 linker by the start of the experiment, we initially constructed our TXS-8 PROTAC with either 1 or 2 PEG-2 linkers connecting thalidomide and TXS-8 (**Figure 4.3**).<sup>22,33</sup>

#### 4.2.2.1.2 Thalidomide TXS-8 PROTAC toxicity assay.

After acquiring the thalidomide-based TXS-8 PROTACs, we wanted to investigate the impact of these PROTACs on Ramos B-cells, which overexpress Rpn-6. The cells were dosed with varying concentrations of TWT-1 and TWT-2, with TXS-8 was as a positive control. The

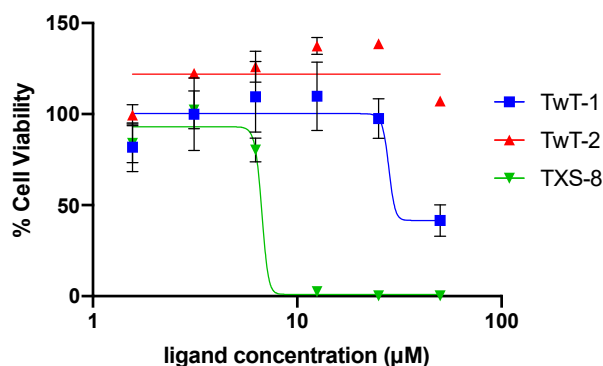


**Figure 4.5 Viability test of the PROTACs.** No significant cell death was observed with either thalidomide-based TXS-8 PROTACs.

cells were dosed with the small molecule for 24 hours and the viability of the cells were examined (**Figure 4.4**). Although significant cell death was observed with TWT-1 after 24 hours of treatment, the PROTAC was no better than TXS-8 regarding the toxicity effect on Ramos B-cells. The fluctuated data in TWT-2 indicated that longer linker on the PROTAC may attenuate the toxicity of these molecules.

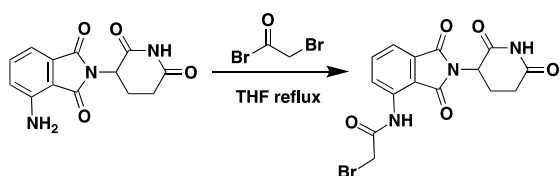


**Figure 4.4 Synthesis route of pomalidomide derivative.** This is a one-step synthesis.

#### 4.2.2.2 Pomalidomide TXS-8 PROTAC development.

##### 4.2.2.2.1 Pomalidomide synthesis, PROTAC development and toxicity test.

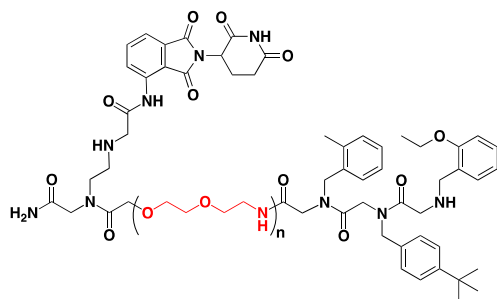


**Figure 4.6. General structure of the PROTAC.** The linker is consisted with various PEG moieties (n=0 named as TwT-3, 2 named as TwT-4, 3 named as TwT-5, 4 named as TwT-6).

The result from the thalidomide-based TXS-8 PROTACs shown in **Chapter 4.2.2.1.2** led us to use another CRBN ligand to construct our PROTAC to investigate if we could use CRBN for TXS-8 PROTAC development. Pomalidomide was an analog of thalidomide that has also been used to construct PROTACs.<sup>34–36</sup> However, the free amine on pomalidomide was on the benzene ring, which made solid phase synthesis conditions too mild for coupling reactions.<sup>37</sup> Therefore, we decided to modify pomalidomide using bromoacetic bromide to allow easy coupling with solid phase synthesis(**Figure 4.5**). The addition of the acetyl group on pomalidomide made the pomalidomide-based PROTAC longer than the thalidomide-based PROTACs. Therefore, when constructing the PROTACs, we decided to include a PROTAC TwT-3 that exhibited no linker at all. We also included PEG-3 and PEG-4 linker in our design of the pomalidomide-based PROTACs. In total, we acquired 4 pomalidomide-based PROTACs (**Figure 4.6**). We investigated the toxicity of these

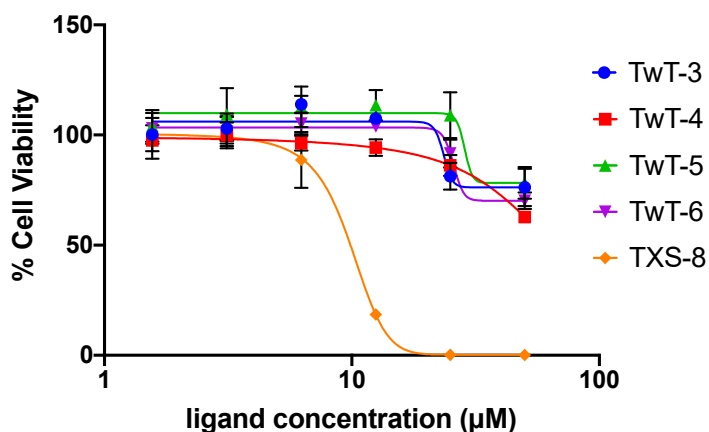


**Figure 4.7. Viability test of the PROTACs.** No significant cell death was observed with all pomalidomide-based TXS-8 PROTACs.

pomalidomide-based PROTACs in Ramos B-cells in the same conditions compared to the thalidomide-based PROTACs. However, no significant cell death was observed with any of the testing PROTACs (**Figure 4.7**).

#### 4.2.2.2 Rpn-6 degradation assay with TXS-8 PROTACs.

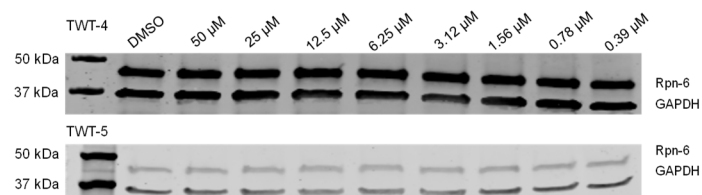


**Figure 4.8. Rpn-6 degradation with PROTACs.** No significant Rpn-6 degradation was observed in either TWT-4 or TWT-5 treated Ramos B-cells. Band intensity difference was caused by different amounts of primary antibody used for immunoblot.

Although none of the thalidomide or pomalidomide-based PROTACs showed significant toxicity to Ramos B-cells, we still wanted to investigate if these PROTACs could potentially induce the degradation of Rpn-6. Therefore, we decided to monitor the Rpn-6 level in

cells treated with PROTACs, TWT-4 and TWT-5 were selected for the experiment. The cells were treated with varying concentration of the PROTACs for 24 hours, and cells were collected and lysed with M-PER solution. The whole cell protein concentration was normalized and analyzed by immunoblot. Generally, a PROTAC should reduce the relative amount of target protein in cells within 24 hours period.<sup>14</sup> We compared the relative amount of Rpn-6 to the amount of GAPDH in cells. Unfortunately, no significant changes of Rpn-6 amount were observed with any concentration of TXS-8 PROTACs (**Figure 4.8**).

#### 4.2.3 Summary of TXS-8 PROTAC development.

The lack of significant Rpn-6 degradation and cell death with the above TXS-8 PROTACs showed that our attempt of using CRBN ligand to develop TXS-8 PROTACs was a failure. We concluded that either the PROTACs were cell impermeable that could not reach its target, the PROTACs were unable to induce a stable ternary complex between Rpn-6 and CRBN, or Rpn-6 in cells was mostly integrated on the 26S proteasome while ubiquitination of Rpn-6 on 26S proteasome could not trigger protein degradation. Unfortunately, answering any of above questions required a lot of effort, and we decide to suspend the research on TXS-8 PROTAC development until we understood the general binding site of TXS-8 on Rpn-6. Based on recent development with computational modeling, performing computational stimulation to calculate the optimal linker length could greatly benefit future research.<sup>18</sup> Using fluorescence resonance energy transfer (FRET) pairs to construct labeled E3 ligase and target protein will also allow *in vitro* experiments to investigate if the PROTAC can bring the E3 ligase and target protein in proximity and form a stable ternary complex.<sup>38–40</sup>

### 4.3 TXS-8 binding site study.

#### 4.3.1 Introduction to binding site study.

As previously mentioned in **Chapter 4.2.3**, discovering the general binding site of TXS-8 onto Rpn-6 could greatly benefit TXS-8 PROTAC development. It would also benefit future optimization of the structure of TXS-8 to improve potency. Currently, the most widely used techniques involving binding site study are x-ray crystallography (co-crystallography),<sup>41,42</sup> cryogenic electron microscopy (cryo-EM),<sup>43,44</sup> nuclear magnetic resonance (NMR)<sup>45–47</sup> and cross-linking.<sup>48,49</sup> However, some of the above techniques were unsuitable for TXS-8 binding site study in a limited time period. X-ray was the gold standard for small molecule binding site study as it will precisely reveal the binding pocket and orientation of the small molecule on the protein. However, obtaining a qualified co-crystal structure of TXS-8 and Rpn-6 may take years. Besides, our lab is unfamiliar with the technique. As previously mentioned in **Chapter 2.1**, the development of cryo-EM in recent years had allowed researchers to reach atomic levels of resolution.<sup>50–53</sup> It can also provide dynamic analysis regarding the target protein. However, the lower limit of molecular weight accessible of cryo-EM only reaches the upper weight range for NMR at 50 kDa. Rpn-6 is a protein around 47 kDa, acquiring the binding site of TXS-8 on Rpn-6 may be difficult since Rpn-6 is below the detecting limit.<sup>54</sup> Similarly, using NMR for TXS-8 binding site could also be difficult as the weight of Rpn-6 has reached the upper detection limit of NMR. Besides, another pitfall of using NMR for Rpn-6 study is the lack of solved NMR structure of Rpn-6. We would have to solve the NMR structure of unbound Rpn-6 before analyzing the binding of TXS-8 with Rpn-6, which could potentially take multiple years. Since the above three approaches were challenging for us, we came up with two alternative solutions using cross-linking techniques.

#### 4.3.2 Approach one: Cross-linking, trypsin digestion and HPLC separation.

When we started designing approaches to investigate the binding site of TXS-8 on Rpn-6, we set our goal to only discover the general binding site instead of the precise binding site. Combining cross-linking and trypsin-digestion and HPLC, we designed a workflow of investigating the general binding site of TXS-8 on Rpn-6 (**Figure 4.9**).<sup>48,49,55,56</sup> There were four reasons on this; first, precise binding site study required the above techniques which our lab did not readily have access to. Second, TXS-8 was not a potent binder of Rpn-6, further optimization of TXS-8 was

required to improve the potency of TXS-8. Third, discovering the general binding site could allow us to get access to computational methods with a narrowed region for calculation, therefore providing us a predicted binding site of TXS-8 on Rpn-6. We could then perform an alanine scan on Rpn-6 to validate the key peptide sequence or amino acid(s) for TXS-8 binding. Most importantly, this work could be done by only one person with accessible equipment as this is a new attempt on TXS-8 investigation and I am the only person in charge of the research.

The first approach we designed involved cross-linking, trypsin-digestion and HPLC separation. In detailed, Rpn-6 was first bound to Dzn-TXS-8-FP followed by UV cross-linking. Then the protein will be digested by trypsin yielding a mixture of peptides where one or several

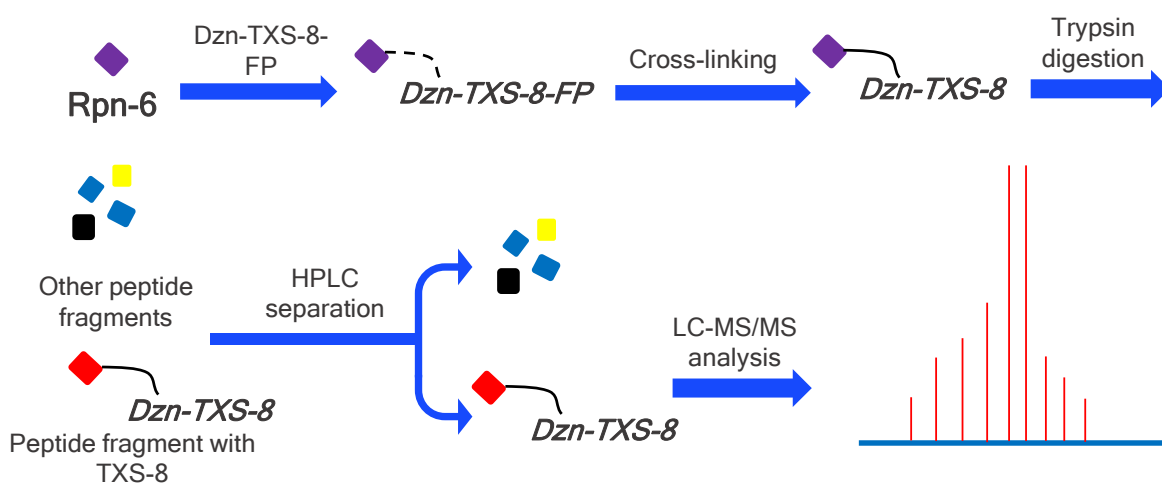


**Figure 4.9. Workflow of approach one.** The protein was first cross-linked with Dzn-TXS-8-FP, a trypsin digestion was performed on the protein to acquire a pool of peptides, and the mixture was subjected to HPLC. Peptide(s) carrying Dzn-TXS-8-FP would show unique fluorescence signal that could be collected. The fractions will then be analyzed by LC-MS/MS or MALDI-TOF MS/MS.

peptide fragments will be covalently linked with Dzn-TXS-8-FP. The mixture will then be subjected to HPLC and fluorescence signal from the peptides carrying Dzn-TXS-8-FP will be detected due to the fluorescein tag. The fractions will be collected and subjected to LC-MS/MS or MALDI-TOF MS/MS.

#### 4.3.2.1 Competitive binding on Rpn-6.

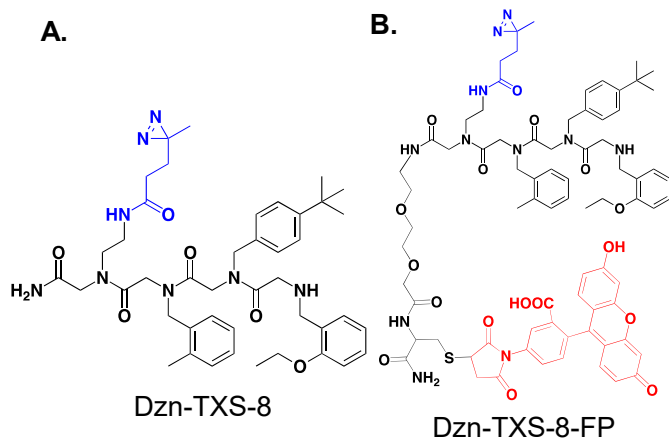


**Figure 4.10.** Structure of Dzn-TXS-8 and Dzn-TXS-8-FP.

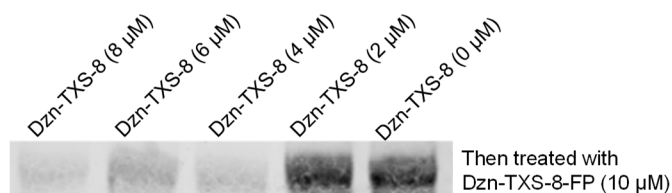


**Figure 4.11. Rpn-6 competitive binding study.** Rpn-6 was pre-treated with Dzn-TXS-8 followed by cross-linking. It was then treated with Dzn-TXS-8-FP, followed by cross-linking again. The gel was directly scanned without staining. Distinct bands were observed on the gel indicating Dzn-TXS-8-FP being added to Rpn-6.

concentration of Dzn-TXS-8. However, no significant fluorescence signal difference between 0 and 2  $\mu$ M Dzn-TXS-8 pre-treated was observed. The above experiment validated that Dzn-TXS-8 and Dzn-TXS-8-FP were binding to the same region on Rpn-6. We were also able to observe the labeled Rpn-6 band on the gel with naked eye therefore we could trim the gel without staining.

#### 4.3.2.2 Cross-linking, trypsin digestion, HPLC separation, MALDI-TOF MS/MS.



**Figure 4.12. Rpn-6 cross-linking with Dzn-TXS-8-FP.** Rpn-6 was treated with Dzn-TXS-8-FP followed by cross-linking. Multiple bands were cut from the gel for trypsin digestion.

To ensure that Dzn-TXS-8-FP bound to the same binding site as Dzn-TXS-8, we first performed a competitive binding study on Rpn-6 (**Figure 4.10**). 4  $\mu$ M of purified Rpn-6 was pre-treated with varying concentrations of Dzn-TXS-8, and the small molecule was then cross-linked to Rpn-6. Then Rpn-6 was treated with a constant concentration of Dzn-TXS-8-FP, followed by cross-linking again. The mixture was then subjected to sodium dodecyl sulfate - polyacrylamide gel electrophoresis (SDS-PAGE), the gels were scanned without staining for in-gel fluorescence (scanning wavelength 488nm) (**Figure 4.11**). From the experiment, we observed a decrease of fluorescence signal with higher

With the success in competitive binding experiment, we moved forward to use Dzn-TXS-8-FP to label Rpn-6. Based on previous competitive binding assay result, we decided to use a 2:1 ligand to protein ratio for the experiment as our previous experience during the

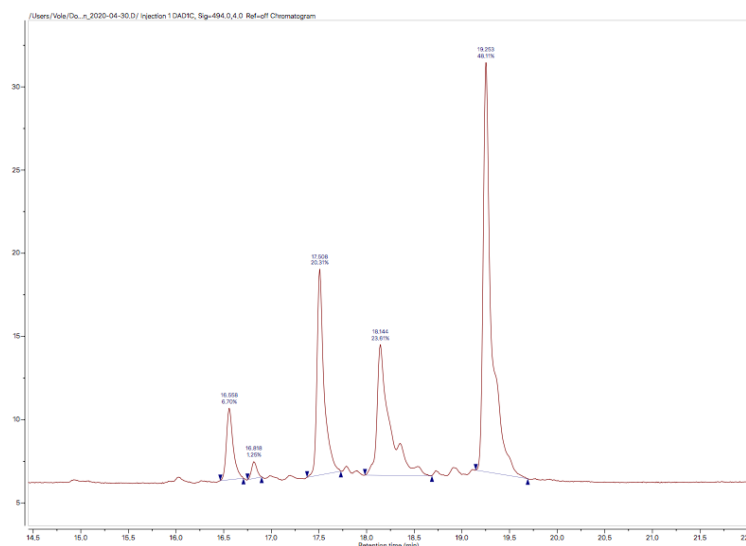


**Figure 4.13. HPLC chromatograph.** Distinct peaks were observed at 494 nm channel corresponding to fluorescein on Dzn-TXS-8-FP.

covalent pull-down experiment described in **Chapter 2.5.3** indicated the cross-linking efficiency of diazirine was only around 1.5%. To maximize the amount of cross-linked Rpn-6 we could acquire, multiple bands were cut off from the SDS-PAGE gel (**Figure 4.12**). We did not perform in-solution trypsin digestion right after cross-linking as SDS-PAGE served as a purification step to remove unbound Dzn-TXS-8-FP

from the protein mixture. The collected bands from SDS-PAGE gel were digested with trypsin and dried under vacuum. The mixture was then suspended in HPLC buffer and subjected to HPLC separation. We observed some peaks at the 494 nm channel (fluorescein excitation: 494 nm, emission: 521 nm), and the fractions were collected (**Figure 4.13**). The samples were submitted to the Purdue Proteomics Facility for LC-MS/MS and MALDI-TOF MS/MS analysis. MALDI-TOF MS/MS was selected mainly due to the availability of LC-MS/MS in Purdue Proteomics Facility as the instrument was tightly scheduled. However, we only observed MS peaks for unlabeled peptide fragments from trypsin digestion, none of the masses we observed in LC-MS/MS and MALDI-TOF MS/MS could be converted to the sum of Dzn-TXS-8-FP mass and Rpn-6 peptide fragment mass. Currently we were working on improving cross-linking efficiency to obtain a higher labeled peptide ratio in HPLC fractions to allow us to observe signals from LC-MS/MS or MALDI-TOF MS/MS.

### 4.3.3 Approach two: Cross-linking, trypsin digestion, click chemistry and enrichment.

In addition to the first approach of using HPLC for separation, our second approach utilized biotin for enrichment. The core concept of this approach was similar to previous approach where we cross-linked TXS-8 to Rpn-6 and then separated the labeled peptide fragment from unlabeled ones.

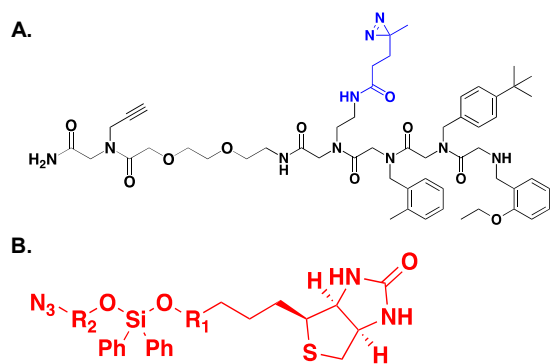


**Figure 4.14. alkyne-Dzn-TXS-8 and DADPS probes.** (A) TXS-8 was synthesized with an alkyne handle for click chemistry. (B) General structure of dialkoxy-diphenylsilane (DADPS) probes, the azide group on the probe can be attached to alkyne with click chemistry. The silyl group was acid sensitive and could be hydrolyzed with 10% formic acid rapidly.

However, the BMCC-BDzn-TXS-8 probe we previously used for covalent pull-down experiment in **Chapter 2.5.3** was over 1.5 kDa. When it was cross-linked to a potential peptide fragment from Rpn-6, the expected average mass for the ligand-peptide molecule would be over 2 kDa. To maintain the relatively small molecular weight of the target peptide fragment and due to our previous observation that biotinylated probes would drag on column leaving contaminations difficult to clear, we decided to incorporate a clickable cleavable biotin to

TXS-8. Click chemistry had been widely used to cross link small molecule to proteins with alkyne handles.<sup>57,58</sup> With recent development of cleavable biotin probes, we decided to modify TXS-8 to carry moieties for click chemistry and allow the attachment of cleavable biotin (**Figure 4.14**).<sup>8659-61</sup>

The workflow was also similar to what just described in **Chapter 4.3.2** but instead of subjecting the peptide mixture to HPLC, DADPS probe was added to the mixture for click chemistry, which adds a biotin moiety to TXS-8. Similar to previous covalent pull-down experiments, we perform a pull-down experiment in the trypsin digested peptide mixture to enrich

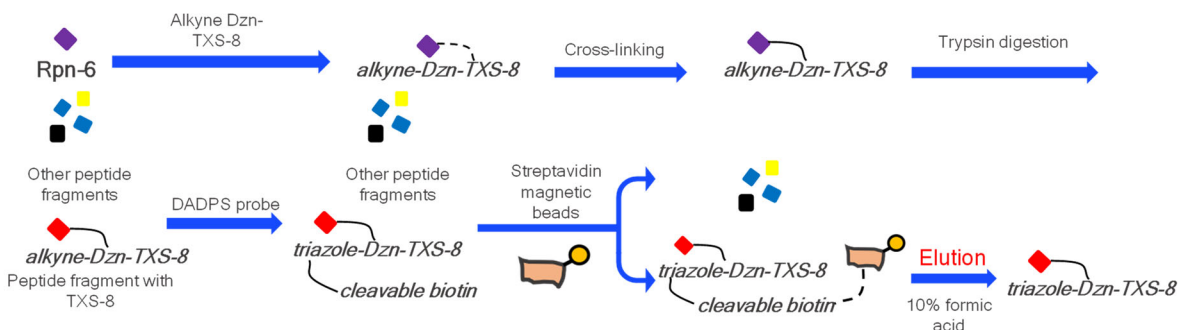


**Figure 4.15. Workflow of peptide enrichment with DADPS probes.** Rpn-6 was first treated with alkyne-Dzn-TXS-8 followed by cross-linking. The protein was trypsin digested, and click chemistry was performed to append the DADPS probe to TXS-8. The peptide fragment carrying TXS-8 was enriched via a pull-down experiment and analyzed.

fragments carrying the biotin moiety. These fragments will then be combined, treated with 10% formic acid to hydrolyze the DADPS probe, and allow us to reduce the molecular weight of the target peptide fragment. The enriched peptide will then be subjected to either LC-MS/MS or

MALDI-TOF MS/MS to allow us to identify the peptide sequence (**Figure 4.15**). Currently, we were working on optimizing the conditions for in-solution trypsin digestion to minimize the amount of trypsin used in the experiment.

#### **4.3.4 Summary of TXS-8 binding site study on Rpn-6.**

Although we have proposed two approaches to investigate the binding site of TXS-8 on Rpn-6, we were still unable to acquire significant results regardless of the methods we use. Approach one was cost-efficient and time-saving due to less experiment steps. However, Dzn-TXS-8-FP unlabeled Rpn-6 peptide fragments could also co-elute with the Dzn-TXS-8-FP labeled peptide fragment at the same time during HPLC separation. Since it was difficult to determine the ratio of labeled and unlabeled peptide fragment in the same fraction, we were experiencing difficulty on acquiring meaningful data from mass spectrometry. The second approach eliminated the contaminations of unlabeled peptide fragments during mass spectrometry. But it involved more steps than the first approach and could result in a low overall yield.

Despite the difficulties in both approaches, we were still working on discovering the general binding site of TXS-8 on Rpn-6. The success of any of the above approach will greatly benefit our understanding of TXS-8 on Rpn-6 and facilitate our future structural optimization of TXS-8 to a more drug-like molecule.

### **4.4 New rhodamine-based proteasome probe development.**

#### **4.4.1 Limitations of current commercially available proteasome probes and development of rhodamine-based probes to monitor proteasome's chymotrypsin-like activity.**

As mentioned in **Chapter 1.1** that proteasome is the major component of the UPS and multiple steps are involved for target protein degradation.<sup>62–66</sup> These steps are accomplished with different subunits where the polypeptide hydrolysis is accomplished by the 20S CP (**Figure 4.16**).<sup>67</sup> The  $\beta$  ring of the 20S CP resides the protease-like catalytic  $\beta 1$ ,  $\beta 2$  and  $\beta 5$  subunits. They present caspase-like, trypsin-like and chymotrypsin-like activities, respectively.

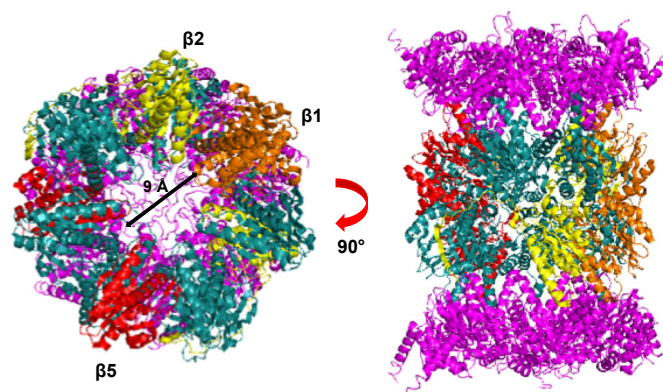


**Figure 4.16.** Bottom view on the  $\beta$  ring ( $\alpha$  ring removed) and side view of 20S CP. The  $\beta 1$ ,  $\beta 2$  and  $\beta 5$  subunits were colored orange, yellow and red, respectively. The gate of the  $\alpha$  ring is around 9 Å diameter in closed gate form.

To monitor the changes in proteasome activities, researchers have been developing small molecule probes that can be selectively cleaved by certain proteasome subunits. Among these probes, a 4-amino-7-methylcoumarin (AMC) moiety was used that the release of the moiety upon hydrolysis of the amide bond will generate fluorescence signal that can be quantified.

Ac-GPLD-AMC (Ac stands for acetyl group),<sup>68,69</sup> Boc-LRR-AMC (boc stands for tert-butyloxycarbonyl group),<sup>70,71</sup> and Suc-LLVY-AMC (suc stands for succinyl group) were developed as selective probes for the caspase-like  $\beta 1$  subunit, trypsin-like  $\beta 2$  subunit and chymotrypsin-like  $\beta 5$  subunit, respectively (**Figure 4.17**).<sup>72–</sup>

<sup>74</sup> These three small molecule probes utilized a These AMC based proteasome probes have been very useful on proteasome characterization especially on studying proteasome inhibitors.<sup>75,76</sup>

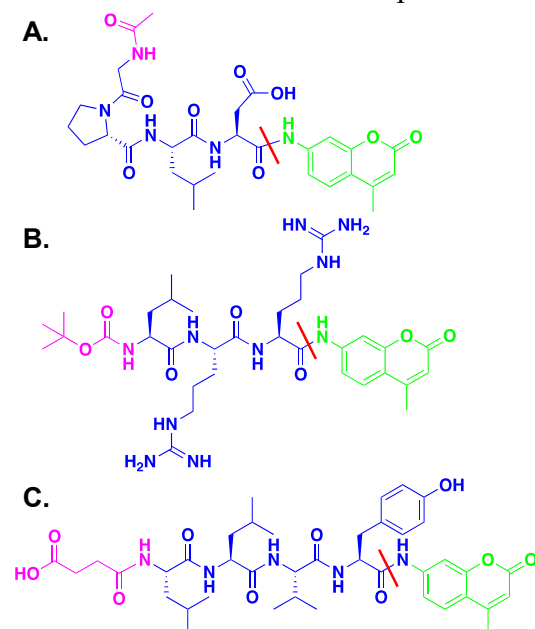


**Figure 4.17.** Commercially available proteasome probes. AMC in green, peptide in blue, protecting group in purple, cleavage site marked in red line. (A) Ac-GPLD-AMC, selective probe for the caspase-like  $\beta 1$  subunit. (B) Boc-LRR-AMC, selective probe for the trypsin-like  $\beta 2$  subunit. (C) Suc-LLVY-AMC, selective probe for the chymotrypsin-like  $\beta 5$  subunit.

Despite their availability, the AMC probes still suffer from several limitations. These probes are generally cell impermeable, which limits their application to live cells. Assays can be performed using cell lysate without protease inhibitors but this makes the evaluation of small molecule modulators of proteasome activity confusing as cellular protease may contribute to probe cleavage.<sup>77</sup> Furthermore, the poor fluorescence properties of AMC probes requires a high concentration of probe. This increases the possibility that the probe will be hydrolyzed non-selectively by other cellular proteases.<sup>72</sup>

To overcome the limitations of the AMC probes, our lab has developed a series of rhodamine 110 (Rh 110)

based peptide-peptoid hybrid probes selective for the chymotrypsin-like  $\beta 5$  subunit (**Figure 4.18**).<sup>72,78</sup> Comparing to the AMC probes, the rhodamine-based probes were cell permeable and required less concentration to acquire significant fluorescence signals from probe hydrolysis.

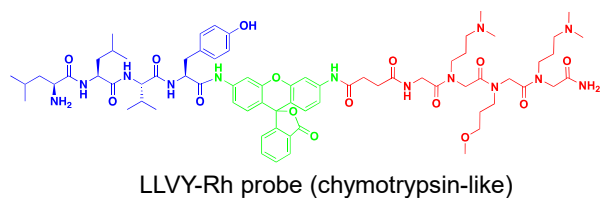


**Figure 4.18. LLVY-Rh probe.** Peptoid region in red, rhodamine 110 showed in green, peptide region showed in blue. Cleavage site is marked in red line.

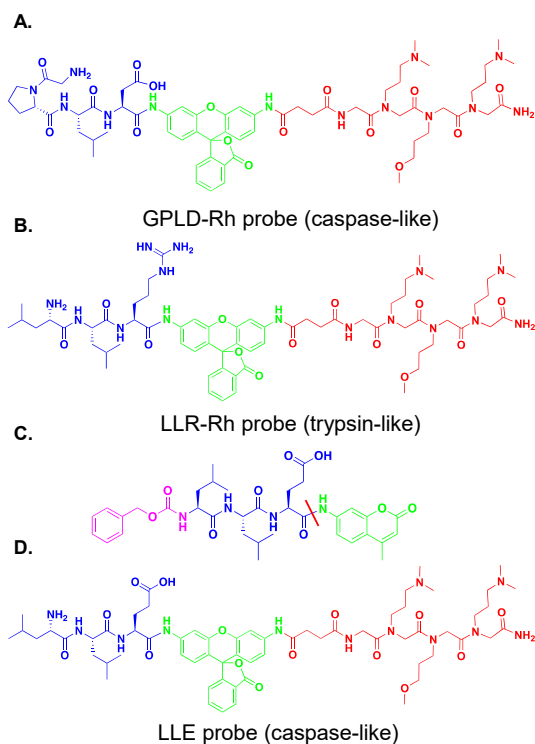


**Figure 4.19 (A)** GPLD-Rh probe (peptoid in red, rhodamine in green, peptide in blue). **(B)** LLR-Rh probe (peptoid in red, rhodamine in green, peptide in blue). **(C)** Z-LLE-AMC, selective probe for the caspase-like  $\beta 1$  subunit. **(D)** LLE-Rh probe (peptoid in red, rhodamine in green, peptide in blue).

#### 4.4.2 Synthesis of LLE-Rh, LLR-Rh probes and testing with 20S CP.

Our previous build of the rhodamine probe for the chymotrypsin-like  $\beta 5$  subunit was based on the Suc-LLVY-AMC probe. Therefore, our new probes for trypsin-like and caspase-like followed

the same design concept where we adopted the Boc-LRR-AMC probe and Ac-GPLD-AMC probe. We designed GPLD-Rh and LRR-Rh probes and attempted synthesizing them accordingly using solid-phase synthesis (**Figure 4.19A**). However, the LRR-Rh probe synthesis was problematic as the arginine we used for synthesis was Pbf (2,2,4,6,7-pentamethyl-2,3-dihydrobenzofuran-5-sulfonyl) protected, the bulky hydrobenzofuran ring on the pbf group resulted in a low coupling efficiency on the second arginine leading to a low overall reaction yield. We hypothesized that the LRR-Rh probe was recognized by the trypsin-like  $\beta 2$  subunit and the cleavage site would be the amide bond between rhodamine and arginine. We modified the LRR-Rh probe to LLR-Rh probe for a higher synthesis yield (**Figure 4.19B**). These proteasome probes were synthesized and purified via HPLC. To test the new probes, we

performed a proteasome hydrolysis assay monitoring the cleavage of the probe by measuring the increase of fluorescence signal. 10  $\mu$ M probes were mixed with purified 20S CP at 5 nM, similar to standard concentrations of our lab's previously characterized LLVY-Rh probe. The probes with

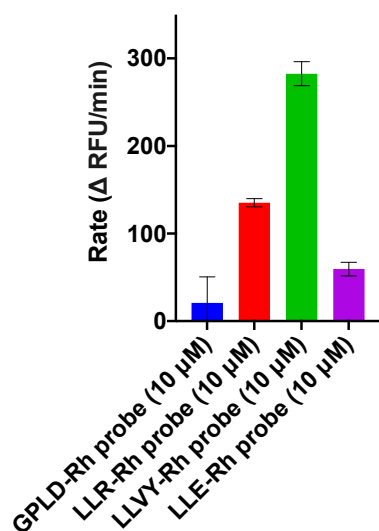


**Figure 4.20. Rate of Rh probes with 20S CP.** The GPLD-Rh probe showed inconsistent hydrolysis profile during the assay and we decided to use LLE-Rh probe to replace the GPLD-Rh probe for monitoring caspase-like activity on the 20S CP. LLE-Rh, LLR-Rh and LLVY-Rh probes were all cleaved by the 20S CP.

for the proteasome activity assay and significant probe cleavage was observed (**Figure 4.20**). The success of the experiment indicated the feasibility of using rhodamine to construct probes to monitor proteasome activity changes. The testing conditions were later optimized so we were able

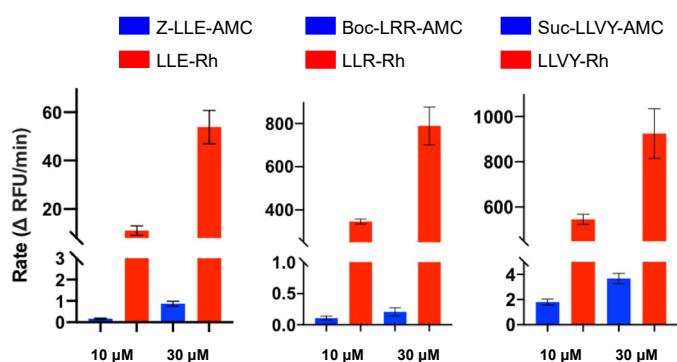


**Figure 4.21. Rate (Δ RFU/min) comparison between AMC probes and Rh probes.** AMC probes required a high concentration (30 μM) to be observed with significant signal, but Rh probes showed better sensitivity comparing to the AMC probes even at low concentration (10 μM). The result from indicated that Rh probes were useful tools to monitor proteasome activity changes.

20S CP were monitored on a plate reader for one hour. The acquired fluorescence signal was plotted, and the increase of the fluorescence signal was calculated (ΔRFU/min). Surprisingly, we discovered that the GPLD-Rh probe showed no cleavage activity during the assay (**Figure 4.20, Figure 4.29**). We repeated the experiment two more times, but no significant probe cleavage was observed with the GPLD-Rh probe. We concluded that GPLD-Rh was a longer probe than GPLD-AMC probe and the fitting of GPLD-Rh probe to the β1 subunit was hindered by a combined effect of length and the proline in the sequence. We went back for literature search and found another commercially available caspase probe, Z-LLE-AMC (Z stands for benzyl carbamate group).<sup>79,80</sup> We decided to redesign the caspase probe using the LLE peptide sequence and synthesized LLE-Rh probe for the β1 subunit (**Figure 4.19C, D**). We tested the LLE-Rh probe with the 20S CP

to observe significant signal changes with lower gain setting on the plate reader because high gain setting maximized out in the middle of the assay.

#### 4.4.3 Comparison between the commercially available AMC probes and rhodamine-based probes.

Excited about the discovery of the new proteasome probes, we further

conducted experiments on comparing the Rh based proteasome probes with the commercially available AMC probes. Similar to what we have previously did with the LLVY-Rh probes, we compared the cleavage rate of the rhodamine-based probes with the AMC probes at both 10 and 30  $\mu\text{M}$ .<sup>72</sup> Like what we have observed previously with the LLVY-Rh probes, the new LLE-Rh and LLR-Rh probes showed significant signal increase compared to the AMC probes (**Figure 4.21**, **Figure 4.31**). This experiment validated our previous conclusion that the LLVY-Rh probes were more sensitive than the AMC probes and required less amount to be observed with a significant signal change.

#### 4.4.4 Using proteasome inhibitors can significantly reduce the probe cleavage *in vitro* and *in cellulo*.

To further validated that the probes were hydrolyzed by the proteasome, we included proteasome inhibitor MG-132 in our biochemical assay. MG-132 is a known proteasome inhibitor specific for the chymotrypsin-like activity on the  $\beta 5$  subunit. However, it could also inhibit the  $\beta 1$  and  $\beta 2$  subunit at high dosage concentration.<sup>81–83</sup> 15  $\mu\text{M}$  of MG-132 was included in our biochemical assay with the rhodamine-based proteasome probes. With MG-132, we observed a significant probe hydrolysis decrease where the chymotrypsin-like activity suffered the greatest decrease but the impact of MG-132 on  $\beta 1$  and  $\beta 2$  subunit activities were moderate (**Figure 4.22A**, **Figure 4.32**). To further validate the probes were degraded by the proteasome, we investigated the probe cleavage in living cells. A549 cells were selected for the assay, the cells were first pre-

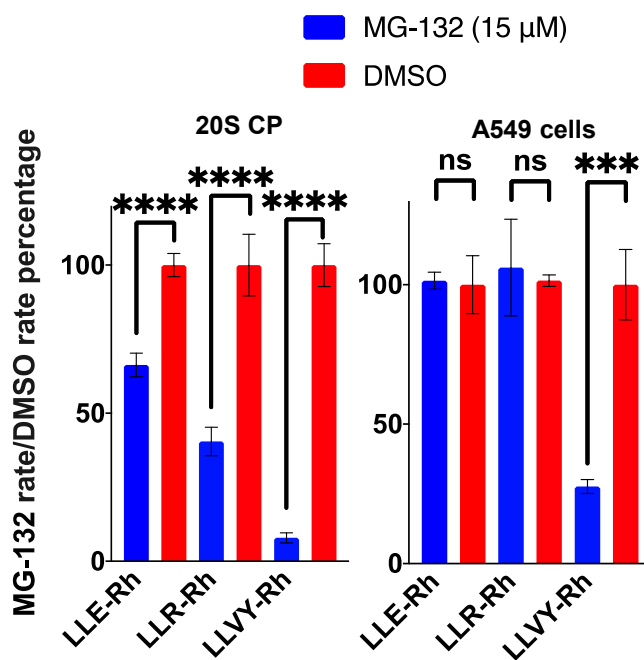


**Figure 4.22. (A) Purified 20S CP:** Cleavage rate comparison with different proteasome probes when treated with MG-132 in 20S CP. A significant probe hydrolysis rate decrease was observed with all subunits. **(B) A549 cells:** Cleavage rate comparison with different proteasome probes when treated with bortezomib in A549 cells. A significant probe hydrolysis rate decrease was observed the chymotrypsin-like subunit. Error bars represent SEM and  $n=4$ , \*\*\*\* $p<0.00005$ , \*\*\* $p<0.0005$ , \*\* $p<0.005$ .

treated with MG-132 at 15  $\mu$ M or DMSO for one hour. The small molecule and the cell media were then removed and the cells were washed with PBS. MG-132 and DMSO dissolved in the corresponding proteasome probe solution were added back to individual wells and the cleavage of the proteasome probes were monitored on a plate reader. However, we did not observe a significant proteasome activity decrease with the  $\beta$ 1 and  $\beta$ 2 subunit (**Figure 4.22B**, **Figure 4.33**). Despite MG-132 being a good proteasome inhibitor in biochemical assays, it may not be potent to significantly inhibit cellular proteasome activities in a short amount of dosing time. Therefore, we decided to switch to use bortezomib for the experiment. Bortezomib was the first FDA approved proteasome inhibitor to treat multiple myeloma.<sup>45–47</sup> Similar to MG-132, bortezomib could also inhibit the  $\beta$ 1 and  $\beta$ 2 subunit at high dosage concentration.<sup>87–89</sup> We examined the cleavage rate of rhodamine-based probes in A549 cells again and pre-treated the cells with 15  $\mu$ M bortezomib for one hour. Later, we were able to observe a significant decrease of the hydrolysis of the probes in A549 cells (**Figure 4.34**, **Figure 4.35**). The result of the experiment indicated that our proteasome probe was cell permeable and proteasome inhibitors like bortezomib could inhibit the hydrolysis of these probes. Overall, the above experiments demonstrated that we have developed a new series of rhodamine-based proteasome probes for the caspase-like  $\beta$ 1 subunit and the trypsin-like  $\beta$ 2 subunit of the 20S CP. These new probes could be used in other research investigating the impact of a small molecule on proteasome activity.

#### 4.4.5 Summary of the development of the selective proteasome probes.

Above, we demonstrated our development of a new series of rhodamine-based proteasome probes. Comparing to commercially available AMC probes, the rhodamine-based probes we developed were more sensitive upon proteasome hydrolysis, so it required less amount of probes for experiments. Our cellular experiments with A549 also indicated that our probes were cell permeable which was a significant advantage comparing to cell impermeable AMC probes. These experiments validated the LLE-Rh and LLR-Rh probes as useful tools to monitor proteasome activities both in biochemical and cellular assays. With the developed rhodamine probes for all three catalytic subunits on the 20S CP, they will significantly benefit our future experiments to identify potential small molecule proteasome regulators. Currently, our lab has discovered a new series of small molecule proteasome stimulators with these probes.

#### **4.5 Conclusion in TXS-8 PROTAC development, binding site study and proteasome probe development.**

Although TXS-8 was discovered as a selective binder for proteasomal subunit Rpn-6, modification of TXS-8 into a PROTAC to selectively degrade Rpn-6 was problematic. We were unable to observe significant cell death with the thalidomide and pomalidomide-based PROTACs. The Rpn-6 degradation assay result also indicated that the PROTAC we developed were not working as expected. We summarized three possible reasons regarding the TXS-8 PROTAC failure: the PROTACs were cell impermeable that couldn't reach its target; the PROTACs were unable to induce a stable ternary complex between Rpn-6 and CRBN; Rpn-6 in cells was mostly integrated on the 26S proteasome while ubiquitination of Rpn-6 on 26S proteasome could not trigger protein degradation. The failure of TXS-8 PROTAC development again highlighted the necessity of a convenient general biochemical assay development to allow potential PROTACs to be tested in easier way before cellular experiments.

The failure of the TXS-8 PROTAC development made us to decide to investigate the general binding site of TXS-8 on Rpn-6 as this could provide us guidance on future PROTAC design. Due to the lack of solved Rpn-6 structure and availability of experimental equipment, we decided to investigate the general binding site of TXS-8 on Rpn-6 with two approaches. The first approach is cost-effective and timesaving but we had discovered that the unlabeled Rpn-6 peptide fragments would co-elute with the labeled ones and contaminated the sample. The second approach theoretically eliminated the contamination by performing a pull-down enrichment. However, the multiple-step process could potentially lead to a low overall yield. We are still actively investigating both approaches currently, and we are still working to discover the general binding site of TXS-8 on Rpn-6.

The lack of testing the impact of TXS-8 on proteasome caspase-like and trypsin-like activities in cells and the demand of developing more sensitive proteasome probes comparing to the commercially available AMC probes pushed us to design rhodamine-based proteasome probes that were cell permeable and sensitive to proteasome cleavage. Combining commercially available probes and rhodamine-based probes our lab previously developed, we designed and synthesized LLE-Rh and LLR-Rh probes aimed to be selective for the caspase-like and trypsin-like subunits on the 20S CP, respectively. We also showed that these rhodamine-based probes were more sensitive comparing to AMC probes and required less amount to be observed with significant

hydrolysis rate. Using proteasome inhibitors, we also observed significant probe cleavage inhibition both biochemically and cellularly. The development of new proteasome probes could greatly benefit the discovery of other potential small molecule proteasome regulators.

#### **4.6 General methods and materials.**

All chemicals were obtained from Sigma-Aldrich, Acros Organics, Alfa Aesar or Fisher Scientific and used without any further purification. Solid-phase peptoid synthesis reactions for all TXS-8 and proteasome probes were performed in fritted syringes (Sass Wolfe) as reported previously. Resin was purchased from Chem-Impex Int'l Inc. All TXS-8 and proteasome probes were purified by reverse phase HPLC. (Agilent S9 1260 infinity II). Ramos B-cells (CRL-1596<sup>TM</sup>), A549 (CCL-185<sup>TM</sup>) frozen cell stocks were obtained from ATCC. Cell growth media was also obtained from ATCC including ATCC-formulated RPMI-1640 Medium (30-2001<sup>TM</sup>) and Kaighn's modification of Ham's F-12 medium (30-2004<sup>TM</sup>). The Fetal bovine serum (FBS obtained from VWR) was added to the growth media by 10% of the total volume. CellTiter Glo was obtained from Promega. The 96-well plate with lid was obtained from Corning<sup>®</sup> Costar<sup>®</sup>. The 0.25% trypsin cell dissociation buffer was obtained from Corning<sup>®</sup>. All cell flasks and dishes were obtained from Thermo-Fisher. The Z-LLE-AMC, Boc-LRR-AMC and Suc-LLVY-AMC probe were acquired from ThermoFisher. The purified 26S proteasome was acquired from Boston Biochem at a stock concentration of 2  $\mu$ M. M-PER<sup>TM</sup> mammalian protein extraction solution and HALT<sup>TM</sup> protease & phosphatase inhibitor cocktail (100X) was obtained from Thermo-Fisher. The Laemmli SDS-sample buffer (4X) was acquired from Fisher. Nitrocellulose membranes and filter paper were obtained from Bio-Rad. Rpn-6 primary antibody (rabbit) and GAPDH primary antibody (mouse) was obtained from Novus Biologicals. The secondary antibody (goat anti-rabbit) was obtained from LI-COR.

## 4.7 Thalidomide and thalidomide-based PROTAC TXS-8 synthesis.

### 4.7.1 Thalidomide synthesis.

The 1,3-dioxo-1,3-dihydroisobenzofuran-5-carboxylic acid (1 mmol, 1 eq) was added to a flask containing 3 mL of acetic acid. Potassium acetate was then added to the flask (3 mmol, 3 eq). 3-aminopiperidine-2,6-dione hydrochloride was also added to the flask (1 mmol, 1 eq). The reaction

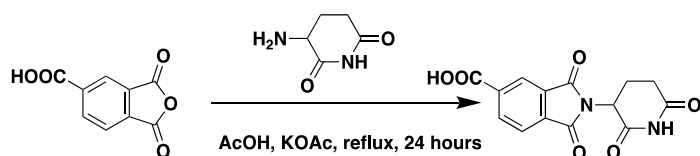


Figure 4.23. Synthesis route of thalidomide derivative.

mixture was stirred and reflux for 24 hours. The reaction mixture was then cooled to room temperature and the solvent was removed on a rotovap. The solid was washed with water for multiple

times until the filtrate maintained colorless. The solid was then carefully gently washed with 10% acetic acid. The solid was then washed with 2 mL of ethyl acetate for 2 times. The solid was dried under vacuum and used without further purification.

### 2-(2,6-dioxopiperidin-3-yl)-1,3-dioxoisindoline-5-carboxylic acid, Chemical Formula:

$C_{14}H_{10}N_2O_6$ : MS:  $M+H^+$ : 303.1 (expected 302.24),  $^1H$  NMR (500 MHz, DMSO)  $\delta$  13.83 (s, 1H), 11.16 (d,  $J = 2.6$  Hz, 1H), 8.40 (dt,  $J = 8.1, 2.1$  Hz, 1H), 8.27 (d,  $J = 2.5$  Hz, 1H), 8.05 (dd,  $J = 7.8, 2.7$  Hz, 1H), 5.20 (ddd,  $J = 12.9, 5.6, 2.6$  Hz, 1H), 2.95 – 2.84 (m, 1H), 2.66 – 2.58 (m, 1H), 2.58 – 2.51 (m, 1H), 2.08 (m, 1H).  $^{13}C$  NMR (126 MHz,  $CDCl_3$ )  $\delta$  173.07, 170.03, 166.72, 166.06, 137.25, 136.02, 134.72, 131.98, 124.18, 123.74, 49.52, 31.24, 22.24.

### 4.7.2 Thalidomide-based TXS-8 PROTAC synthesis

500 mg of Rink amide resin (0.708 mmol/g, 0.354 mmol) was suspended in DCM in the syringe for 10 mins to allow the beads to expand. The DCM was drained and the Fmoc was removed by 20% piperidine twice with 15 mins each at room temperature to give a positive Kaiser test. 1 mL of 2M BAA solution and 1M DIC solution were mixed until a white precipitate formed. The mixture was added to the syringe and agitated at 37°C for 20 mins. The resin was rinsed with anhydrous DMF 3 times and 1 mL of the 1M MMt-ethylenediamine solution was added to the syringe and agitated at 37°C for one hour. The Fmoc was removed by 20% piperidine twice for 15 mins each at room temperature to give a positive Kaiser test. Fmoc-miniPEG-OH (4 eq, 1.416

mmol, 545.7 mg), Oxyma pure (4 eq, 1.416 mmol, 201.2 mg) and DIC (4 eq, 1.416 mmol, 222  $\mu$ L) were dissolved in 2.35 mL DMF each. They were mixed to yield a yellow solution before being added to the resin. The syringe was agitated for 1 hour to give a negative Kaiser test. The resin was separated into two portions with 250 mg each. One portion of the resin with one mini-PEG linker was coupled again with another mini-PEG linker on these resins. The resins were treated with BAA and corresponding amine to couple TXS-8 onto the resin. The Mmt group on ethylenediamine was removed by agitating the resin with 1 mL of 96% DCM, 3% TFA and 1% TIPS for 30 seconds, repeated 5 times. The resin was further rinsed with DMF, 10 mL of 10% TEA in DMF, then DMF. Thalidomide was coupled onto the resin using a 10 eq amount with 9.5 eq of HBTU and 30 eq of triethylamine. The resin was washed with DCM 3 times. The bead was further cleaved with a mixed solution of 95% TFA, 2.5% DCM, 2.5% TIPS at room temperature for one hour in dark. The cleaved solution was collected and dried under a stream of argon to yield yellow oil-like liquid. The liquid was dissolved in 1:1 H<sub>2</sub>O: AcCN (HPLC grade, 0.1% TFA) and separated by RP-HPLC. The purity of the fraction was checked by LC-MS and fractions containing pure substance were combined, froze, lyophilized and stored at -20°C.

#### **4.7.3 Viability test of the thalidomide-based TXS-8 PROTACs**

The purchased cell stock was taken out from the liquid nitrogen storage tank and defrosted to ROOM TEMPERATURE. The stock was then transferred into a 15 mL falcon tube with an additional 1 mL of the media (RPMI-1640). The tube was centrifuged for 5 mins at 1,000 xg. The cell media was removed and the cell pellet was re-suspended in 10 mL of media. The cells were transferred into a T-75 plate (or a 10 cm dish) and the plate was incubated at 37°C until cells were confluent. The PROTACs was taken out from the -20°C and was warmed up to ROOM TEMPERATURE. 1 mg of the peptoid was measured and dissolved in DMSO to make a 20 mM stock. A dilution of 5 mM, 2.5 mM, 2 mM, 1.6 mM, 1.4 mM, 1.25 mM, 0.625 mM and 0.3125 mM in DMSO were prepared. The DMSO solutions were further diluted by adding 4  $\mu$ L of the stock into 196  $\mu$ L of media to obtain the final dosing concentration. 4  $\mu$ L of DMSO was also added to 196  $\mu$ L of the cell media to prepare the negative control. The 4 mL cell media left over in previous step was kept for dosing. 10  $\mu$ L from the falcon tube was added to each side of a hemocytometer with a glass cover on top. The amount of the media needed for dilution was further calculated to fulfill the need of 10,000 cells per well on a 96-well plate. The cells in the falcon tube

were diluted with cell media to obtain 2 mL of a 200,000 cell/ mL solution. 36 wells were used on a 96-well plate. 50 uL of cell solution was added to wells. Another 50 uL of each ligand was added to the wells in triplicate. DMSO was added as negative control. Another three wells with cells were added with media only to determine if DMSO would have negative effect on the cells. The plate was placed in the incubator for 24 hours. The plate was taken out and equilibrated to ROOM TEMPERATURE 50  $\mu$ L of Cell Titer Glo was added to each well. The plate was agitated in dark for 1.5 min and was settled for another 10 mins in the dark. The luminescent in each well was measured with a Synergy NEO plate reader system. The readings were converted and normalized to % viability and were graphed in Prism 8 software.

## 4.8 Pomalidomide and pomalidomide-based TXS-8 PROTAC synthesis.

### 4.8.1 Pomalidomide synthesis.

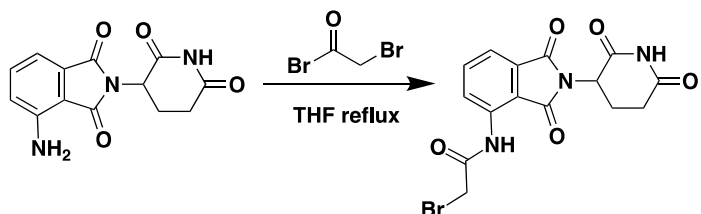


Figure 4.24. Synthesis route of pomalidomide derivative.

Pomalidomide was dissolved in 4 mL of anhydrous THF in a flame dried flask (1 mmol, 1 eq). Bromo-acetic bromide was added to the flask (5 mmol, 5 eq). The reaction mixture was heated and reflux for 24 hours. After

the reaction was finished, the reaction mixture was cooled to room temperature. The solvent and excess bromo acetic bromide were removed by a rotovap. The solid was dried under vacuum and used without further purification.

### 2-bromo-N-(2-(2,6-dioxopiperidin-3-yl)-1,3-dioxoisindolin-4-yl) acetamide

**Chemical Formula:**  $C_{15}H_{12}BrN_3O_5$ ; MS:  $M+H^+$ : **395.4** (expected 394.18),  $^1H$  NMR (500 MHz, DMSO)  $\delta$  11.17 (s, 1H), 10.26 (s, 1H), 8.46 (d,  $J$  = 8.4 Hz, 1H), 7.90 – 7.85 (m, 1H), 7.68 (d,  $J$  = 7.3 Hz, 1H), 5.16 (dd,  $J$  = 12.9, 5.4 Hz, 1H), 4.33 (s, 2H), 2.89 (ddd,  $J$  = 17.1, 14.1, 5.4 Hz, 1H), 2.61 – 2.51 (m, 2H), 2.08 (dtd,  $J$  = 12.8, 5.3, 2.2 Hz, 1H).  $^{13}C$  NMR (126 MHz,  $CDCl_3$ )  $\delta$  173.10, 170.11, 167.83, 166.92, 166.06, 136.62, 135.97, 131.91, 126.43, 119.44, 117.93, 65.25, 49.29, 31.26, 30.26, 22.29, 15.51.

#### 4.8.2 Thalidomide-based TXS-8 PROTAC synthesis

500 mg of Rink amide resin (0.708 mmol/g, 0.354 mmol) was suspended in DCM in the syringe for 10 mins to allow the beads to expand. The DCM was drained and the Fmoc was removed by 20% piperidine twice with 15 mins each at room temperature to give a positive Kaiser test. 1 mL of 2M BAA solution and 1M DIC solution were mixed until a white precipitate formed. The mixture was added to the syringe and agitated at 37°C for 20 mins. The resin was rinsed with anhydrous DMF 3 times and 1 mL of the 1M Mmt-ethylenediamine solution was added to the syringe and agitated at 37°C for one hour. Fmoc-miniPEG-OH (4 eq, 1.416 mmol, 545.7 mg), Oxyma pure (4 eq, 1.416 mmol, 201.2 mg) and DIC (4 eq, 1.416 mmol, 222 uL) were dissolved in 2.35 mL DMF each. They were mixed to yield a yellow solution before being added to the resin. The syringe was agitated for 1 hour to give a negative Kaiser test. The resin was separated into two portions with 250 mg each. One portion of the resin was treated with 20% piperidine twice with 15 mins each at room temperature to give a positive Kaiser test to remove the Fmoc group. The mini-PEG linker coupling was repeated again on these resins. The resins were treated with BAA and corresponding amine to couple TXS-8 onto the resin. The Mmt group on ethylenediamine was removed by agitating the resin with 1 mL of 96% DCM, 3% TFA and 1% TIPS for 30 seconds, repeated 5 times. The resin was further rinsed with DMF, 10 mL of 10% TEA in DMF, then DMF. Thalidomide was coupled onto the resin using a 10 eq amount with 9.5 eq of HBTU and 30 eq of triethylamine. The resin was washed with DCM 3 times. The bead was further cleaved with a mixed solution of 95% TFA, 2.5% DCM, 2.5% TIPS at room temperature for one hour in dark. The cleaved solution was collected and dried under a stream of argon to yield yellow oil-like liquid. The liquid was dissolved in 1:1 H<sub>2</sub>O: AcCN (HPLC grade, 0.1% TFA) and separated by RP-HPLC. The purity of the fraction was checked by LC-MS and fractions containing pure substance were combined, froze, lyophilized and stored at -20°C.

#### 4.8.3 Viability test of the pomalidomide-based TXS-8 PROTACs

The purchased cell stock was taken out from the liquid nitrogen storage tank and defrosted to ROOM TEMPERATURE. The stock was then transferred into a 15 mL falcon tube with an additional 1 mL of the media (RPMI-1640). The tube was centrifuged for 5 mins at 1,000 xg. The cell media was removed and the cell pellet was re-suspended in 10 mL of media. The cells were

transferred into a T-75 plate (or a 10 cm dish) and the plate was incubated at 37°C until cells were confluent. The PROTACs was taken out from the -20°C and was warmed up to ROOM TEMPERATURE 1 mg of the peptoid was measured and dissolved in DMSO to make a 20 mM stock. A dilution of 5 mM, 2.5 mM, 2 mM, 1.6 mM, 1.4 mM, 1.25 mM, 0.625 mM and 0.3125 mM in DMSO were prepared. The DMSO solutions were further diluted by adding 4 µL of the stock into 196 µL of media to obtain the final dosing concentration. 4 µL of DMSO was also added to 196 µL of the cell media to prepare the negative control. The 4 mL cell media left over in previous step was kept for dosing. 10 uL from the falcon tube was added to each side of a hemocytometer with a glass cover on top. The amount of the media needed for dilution was further calculated to fulfill the need of 10,000 cells per well on a 96-well plate. The cells in the falcon tube were diluted with cell media to obtain 2 mL of a 200,000 cell/ mL solution. 36 wells were used on a 96-well plate. 50 uL of cell solution was added to wells. Another 50 uL of each ligand was added to the wells in triplicate. DMSO was added as negative control. Another three wells with cells were added with media only to determine if DMSO would have negative effect on the cells. The plate was placed in the incubator for 24 hours. The plate was taken out and equilibrated to ROOM TEMPERATURE 50 µL of Cell Titer Glo was added to each well. The plate was agitated in dark for 1.5 min and was settled for another 10 mins in the dark. The luminescent in each well was measured with a Synergy NEO plate reader system. The readings were converted and normalized to % viability and were graphed in Prism 8 software.

#### **4.8.4 Rpn-6 degradation in Ramos B-cells treated with PROTACs.**

Ramos B-cells were prepared in a 12-well plate with 20,000 cells per well. The cells were dosed with TWT-4 or TWT-5 at a final concentration of 50, 25, 12.5, 6.25, 3.12, 1.56, 0.78 and 0.39 µM for 24 hours. The cells were then washed with PBS to remove the cell media. The cells were pelleted and were lysed with M-PER solution. The protein concentration was normalized, and 4X lamaelli was added to the samples. The tubes were heated up for 3 mins. SDS-PAGE was performed, and proteins were transferred to a nitrocellulose membrane with Trans-blot® Turbo™ system from Bio-Rad. The membrane was blocked with a 5% milk solution in PBS. Then the primary antibody incubated with the blot overnight. The membrane was washed 3 times with PBS, then the secondary antibody was added. The blot was then imaged with a LI-COR CLx imaging system.

## 4.9 Cross-linking, trypsin digestion and HPLC separation

### 4.9.1 Dzn-TXS-8-FP synthesis

200 mg of Rink amide resin (0.708 mmol/g, 0.354 mmol) was suspended in DCM in the syringe for 10 mins to allow the beads to expand. The DCM was drained and the Fmoc was removed by 20% piperidine twice with 15 mins each at room temperature to give a positive Kaiser test. 1 mL of 2M BAA solution and 1M DIC solution were mixed until a white precipitate formed. The mixture was added to the syringe and agitated at 37°C for 20 mins. The resin was rinsed with anhydrous DMF 3 times and 1 mL of the 1M MMT-ethylenediamine solution was added to the syringe and agitated at 37°C for one hour. Fmoc-miniPEG-OH (4 eq), Oxyma pure (4 eq) and DIC (4 eq) were dissolved in 2.35 mL DMF each. They were mixed to yield a yellow solution before being added to the resin. The syringe was agitated for 1 hour to give a negative Kaiser test. The resin was treated with 20% piperidine twice with 15 mins each at room temperature to give a positive Kaiser test to remove the Fmoc group. The resins were treated with BAA and corresponding amine to couple TXS-8 onto the resin. Before removing the MMT protecting group, the resin was treated with boc anhydride (10 eq) in DCM overnight to protect the secondary amine on TXS-8. The Mmt group on ethylenediamine was then removed by agitating the resin with 1 mL of 96% DCM, 3% TFA and 1% TIPS for 30 seconds, repeated 5 times. The resin was further rinsed with DMF, 10 mL of 10% TEA in DMF, then DMF. 0.95 eq of NHS-EZ-link-diazirine was dissolved in 1.2 mL anhydrous DMF with 1.1 eq of DIPEA mixed in a 1.5 mL tube and the above mixture was agitated for about 5 mins in dark. The mixture was later added to the resin and the resin was agitated for 30-40 mins in the dark to allow coupling of diazirine to ethylenediamine. The completion of the experiment was monitored by Kaiser. The resin was washed with DCM 3 times. The bead was further cleaved with a mixed solution of 95% TFA, 2.5% DCM, 2.5% TIPS at room temperature for one hour in dark. The cleaved solution was collected and dried under a stream of argon to yield yellow oil-like liquid. The liquid was dissolved in 1:1 H<sub>2</sub>O: AcCN (HPLC grade, 0.1% TFA) and separated by RP-HPLC. The purity of the fraction was checked by LC-MS and fractions containing pure substance were combined, freeze, lyophilized and stored at -20°C.

#### 4.9.2 Rpn-6 expression and purification

The frozen *E. coli* stock was removed from the -80°C and was defrosted at RT. 8 mL of sterilized LB broth solution with Amp was added to a bacteria culture tube and 20 µL of the *E. coli* stock was suspended in the culture medium. The tube was incubated at 37°C for a minimum of 6 hours. 25 g of LB broth solid was added to a 2.8 L flask and was dissolved with 1L of Mili-Q water. The LB broth solution was sterilized and it was cooled to r.t. 100 mg of Amp was added to the flask before transferring the 8 mL pre-cultured *E. coli*. The flask was further incubated at 37°C until an OD of 0.6-0.8 was reached as measured by Nanodrop<sup>TM</sup> (Thermo Fisher). 119 mg of IPTG (final concentration 1mM) was added to the flask and the flask was further incubated at r.t. overnight. The cell media was transferred into a 1L flask and was spun down at 4700 rpm for 10 mins in a centrifuge (Thermo Scientific Legend<sup>TM</sup> XTR Centrifuge). The cell media was removed and the bacteria pellet was re-suspended in 20 mL of pre-cooled *E. coli* lysis buffer. The lysis buffer was collected and cells were further lysed by an ultrasonic disruptor with a pulse on for two seconds followed by pulse off for 5 seconds. The total time for pulse on was one minute and the process was repeated three times. The lysate was centrifuged at 13000 x g for 30 mins followed by Ni<sup>2+</sup> affinity chromatography in a 4°C fridge. 1 mg of imidazole (5mM) was added to the column before chromatography to limit non-specific binding. 5 mL of 20mM, 40 mM, 80 mM, 160 mM and 320 mM imidazole in PBS were prepared in duplicate and the solution was cooled to 4°C. The cell lysate was drained from the column and the resin was washed with cold PBS 3 times. The imidazole solution was added to elute the protein from the resin from low to high concentration. Gel loading buffer was added to a small amount of the each elution fraction to reach a 1:4 ratio. The mixture was heated up for 3 mins to allow protein to fully denature. SDS-PAGE was applied to the above mixture and the gel was stained with Coomassie. The gel was checked by Li-Cor. Fractions with pure Rpn-6 were collected in a dialysis tube and the tube was stirred in 3 L of cold PBS overnight to remove the imidazole. The protein solution was transferred into a 50 mL falcon tube and was spun down at 13000xg for 10 mins to sediment any suspension in the solution. The protein solution was then transferred into another 50 mL falcon tube and was stored at 4°C fridge.

### **4.9.3 Competitive binding on Rpn-6**

Rpn-6 was prepared as previously described, the protein was concentrated to 6  $\mu$ M. Dzn-TXS-8-FP and Dzn-TXS-8 were dissolved in DMSO to acquire a 5 mM stock. A small portion of the Dzn-TXS-8 stock was further diluted in 50 mM Tris binding buffer (pH 7.35) and added to Rpn-6 to reach a final concentration of 0, 2, 4, 6 and 8  $\mu$ M (Rpn-6 final concentration 4  $\mu$ M). The mixture was incubated with mixing at r.t. for one hour in the dark. The ligand protein mixture was transferred into transparent ep tubes and 365 nm UV light was applied to the tube at 4°C for 30 mins to allow diazirine crosslinking to proteins. A small portion of Dzn-TXS-8-FP DMSO stock was added directly to the Rpn-6 mixture to minimize the change of total volume (Dzn-TXS-8-FP final concentration was 10  $\mu$ M). The mixture was incubated with mixing at r.t. for one hour in the dark. The ligand protein mixture was transferred into transparent ep tubes and 365 nm UV light was applied to the tube at 4°C for 30 mins to allow diazirine crosslinking to proteins. The mixture was subjected to SDS-PAGE and the gels were scanned without staining.

### **4.9.4 Cross-linking**

Rpn-6 was prepared as previously described. The protein was concentrated to 7.5  $\mu$ M. Dzn-TXS-8-FP was dissolved in DMSO to acquire a 5 mM stock. A small portion of the Dzn-TXS-8-FP stock was further diluted 50 mM Tris binding buffer (pH 7.35) and added to Rpn-6 to reach a final concentration of 10  $\mu$ M (Rpn-6 final concentration 5  $\mu$ M, 2:1 ligand/protein ratio). The mixture was incubated with mixing at r.t. for one hour in the dark. The ligand protein mixture was transferred into transparent ep tubes and 365 nm UV light was applied to the tube at 4°C for 30 mins to allow diazirine crosslinking to proteins. The mixture was subjected to SDS-PAGE and the gel was scanned without staining. The gel was then trimmed into small pieces for trypsin digestion.

### **4.9.5 Trypsin digestion and HPLC separation**

The trypsin digestion protocol was modified from the one provided by ThermoFisher. In total, 10 bands from gel were collected for the digestion. The bands were cut into small pieces less than 1 cubic mm. A digestion buffer was prepared with 10 mg of ammonium bicarbonate dissolved in 10 mL of ultrapure water. A destaining buffer was prepared of mixing 80 mg of ammonium bicarbonate with 20 mL of acetonitrile and 20 mL of ultrapure water. The protein was reduced

with 33  $\mu\text{L}$  of TCEP in 300  $\mu\text{L}$  of digestion buffer (final concentration at 50 mM) at 60°C for 10 mins. The sample was cooled to room temperature and the reducing solution was discarded. An alkylation buffer was prepared right before the alkylation step. 7 mg of iodoacetamide was dissolved in 70  $\mu\text{L}$  of ultrapure water, the solution was further diluted with 280  $\mu\text{L}$  of digestion buffer. The solution was added directly to the gel pieces and the mixture was incubated in dark at 37°C for an hour. After the alkylation step was finished, the gel pieces were gently washed with 2 mL of destaining buffer. The gel pieces were then treated with 500 acetonitrile to shrink. The gel pieces were further dried under vacuum to remove acetonitrile. The dried gel pieces were treated with 200  $\mu\text{L}$  trypsin solution (5  $\mu\text{g}$  in total) and 200  $\mu\text{L}$  of digestion buffer was also added to the mixture. The gel pieces were incubated at 50°C for 4 hours. The solution was carefully removed from the tube and the gels were gently washed with the digestion buffer for 2 times with 200  $\mu\text{L}$  each time. The combined solution was lyophilized to remove solvent from the mixture.

#### **4.9.6 HPLC separation and MS analysis**

The dried solid from previous step was dissolved in 100  $\mu\text{L}$  of 65:35 water/acetonitrile (0.1% TFA) solution. The tube was ultrasonicated for 5 mins to have the solid completely dissolved in the HPLC buffer. The mixture was subjected to HPLC ((Agilent S9 1260 infinity II)) and the fractions were collected and lyophilized. Before lyophilizing, a small portion of the solution was transferred onto a MALDI plate for MALDI-TOF MS/MS.

### **4.10 Rhodamine probe synthesis and testing**

#### **4.10.1 Rhodamine LLE-Rh and LLR-Rh probes synthesis**

LS rink amide resin (0.3 mmol/g) was swelled for 60 min in DMF. The Fmoc was removed using 20% piperidine in DMF for 15 min at room temperature. After deprotection, the resin was washed with anhydrous DMF. For bromoacetic acid coupling, 1 M DIC and 2 M bromoacetic acid in anhydrous DMF were mixed in 1:1 ratio and agitated until a precipitate was observed. This was then added to the resin and allowed to agitate for 20 min at 37°C. The solution was removed, and the resin was washed with anhydrous DMF before a 1 M solution of the corresponding amine was added. This was agitated for 1 hour at 37 °C then washed with anhydrous DMF. Completion of coupling was monitored using the chloranil test for secondary amines. After completion of the

peptoid sequences, Fmoc-Gly-OH (4 eq) was coupled with HBTU (3.75 eq) and DIPEA (8 eq) in anhydrous DMF for 3.5 hours at 37 °C. Completion of the coupling was confirmed by a negative chloranil test, and the Fmoc was subsequently deprotected using 20% piperidine in DMF for 30 min at 37 °C. To couple the succinamide group, succinic anhydride (10 eq) and pyridine (12 eq) were dissolved in anhydrous DCM with 10% anhydrous DMF. This was added to the resin and allowed to agitate at room temperature overnight. For rhodamine coupling, the resin was first washed with a solution of 1,8- bis(dimethylamino)naphthalene (20 eq) and DIPEA (20 eq) in DMF. COMU (1 eq) was dissolved in DMF with 1,8-bis(dimethylamino)naphthalene (20 eq) and DIPEA (20 eq) and added to the resin. This was allowed to agitate for 5 min at room temperature to activate the carboxylic acid on the resin. To this resin solution was then added rhodamine 110 chloride (10 eq) dissolved in anhydrous DMF. This was agitated for 3 hours at 60°C. The first amino acid was coupled using similar conditions of time and temperature, but the amino acid (10 eq) was activated with COMU (10 eq) then added to the resin. The first amino acid coupling was repeated once to allow better yield as some amino acids were difficult to couple to the free amine on the rhodamine. Fmoc deprotection was performed using 20% piperidine for 30 min at 37 °C. Subsequent residues were coupled using 10 eq amino acid, 10 eq COMU and 20 eq DIPEA in DMF for 1 hour at 37 °C (60 °C could also be used). It was critical to perform a test cleavage of a small portion of resins after every coupling when rhodamine was added. LC-MS would help to identify the ratio between coupled and uncoupled resins. If less than 60% of the resin was uncoupled after test cleavage, the corresponding amino acid residue should be coupled one more time. After the final Fmoc was removed, the resin was washed with DCM and dried. For resin cleavage and side chain group deprotection, the resin was suspended in 95% TFA, 2.5% DCM, 2.5% TIPS and agitated for 2 hours at room temperature. The crude mixture was directly dissolved in 50/50 water/acetonitrile (with 1% TFA) for HPLC purification (Agilent S9 1260 Infinity system, Eclipse Plus C18 5 µm, 4.6 x 150 mm column). Purity of each probe was confirmed by LC/MS (Agilent 1260 Infinity II with a Zorbax Eclipse Plus C18 column, 2.1x50mm, 1.8-micron attached to an Agilent 6129 quadrupole mass spectrometer). The probes were dissolved in DMSO to acquire a 5 mM stock for later use.

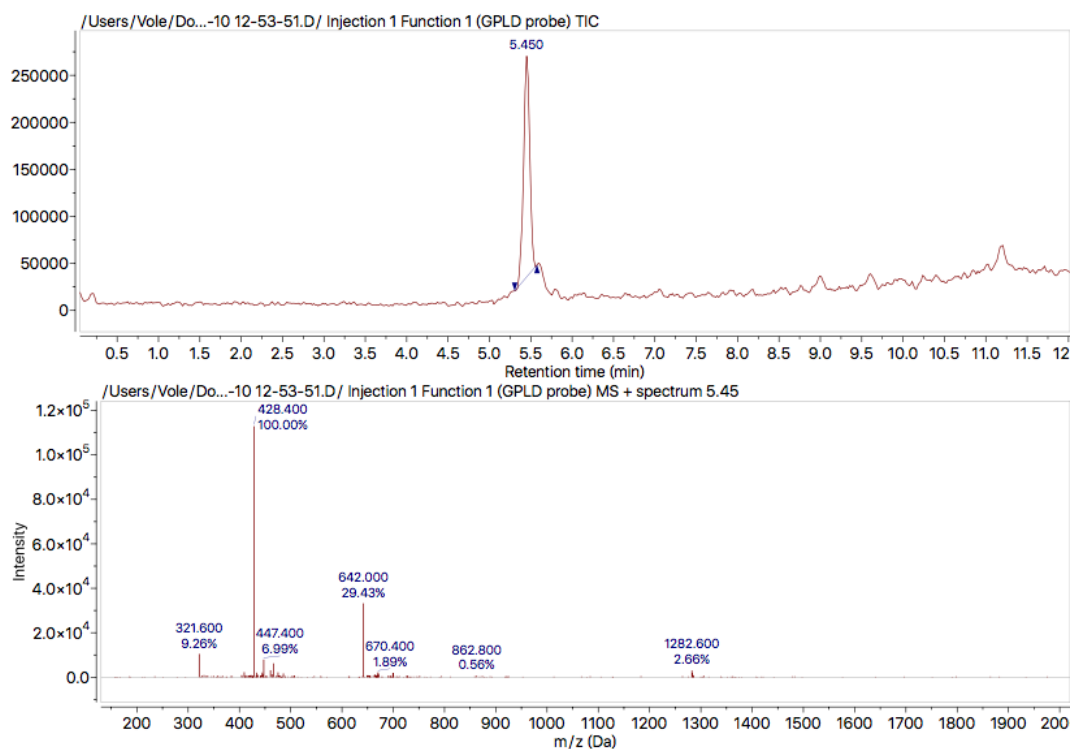


**Figure 4.25.** LC-MS of GPLD-Rh probe.

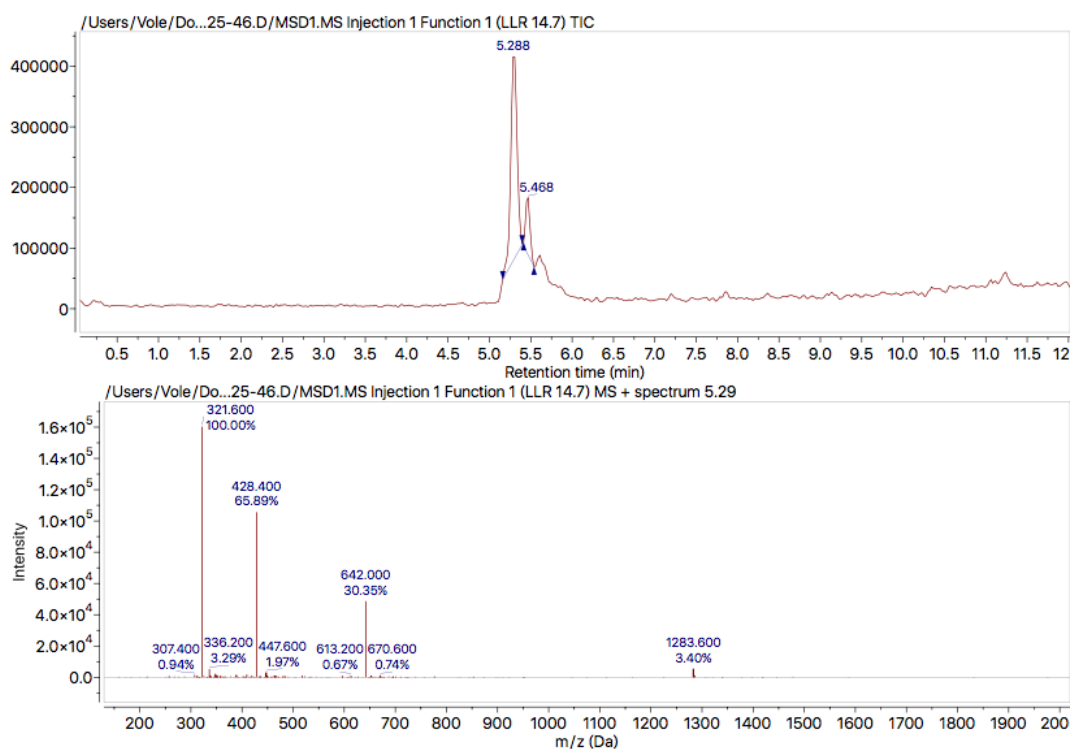


**Figure 4.26.** LC-MS of LLR-Rh probe. Due to the low coupling efficiency of arg-pbf to rhodamine, some rhodamine may not be coupled after two trials and leu could be added to rhodamine. The extra peak was determined as LL-Rh.

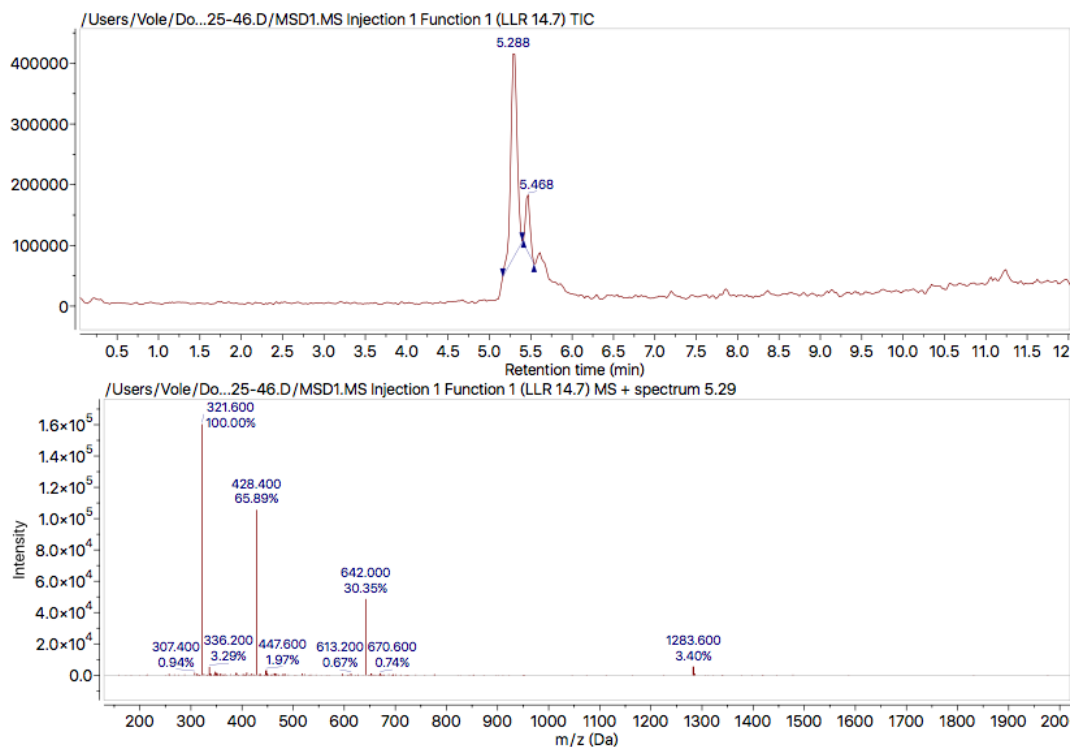


**Figure 4.27.** LC-MS of LLR-Rh probe. Due to the low coupling efficiency of arg-pbf to rhodamine, some rhodamine may not be coupled after two trials and leu could be added to rhodamine. The extra peak was determined as LL-Rh.

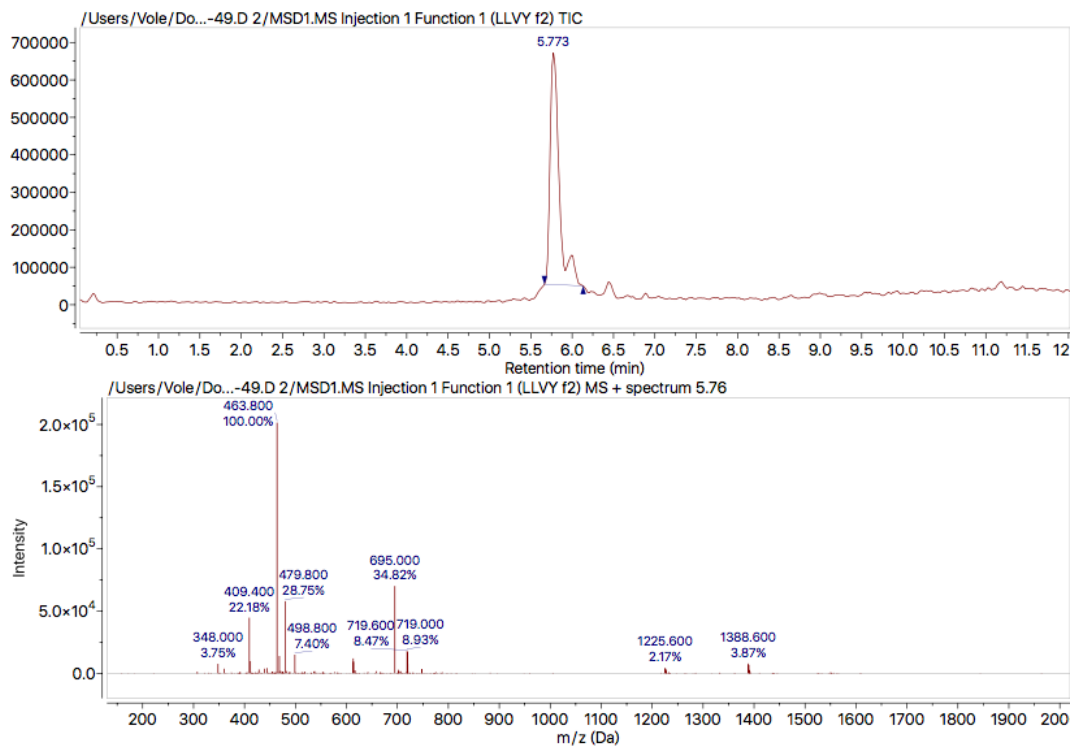


**Figure 4.28.** LC-MS of LLVY-Rh probe. The extra peak was determined as LLV-Rh.

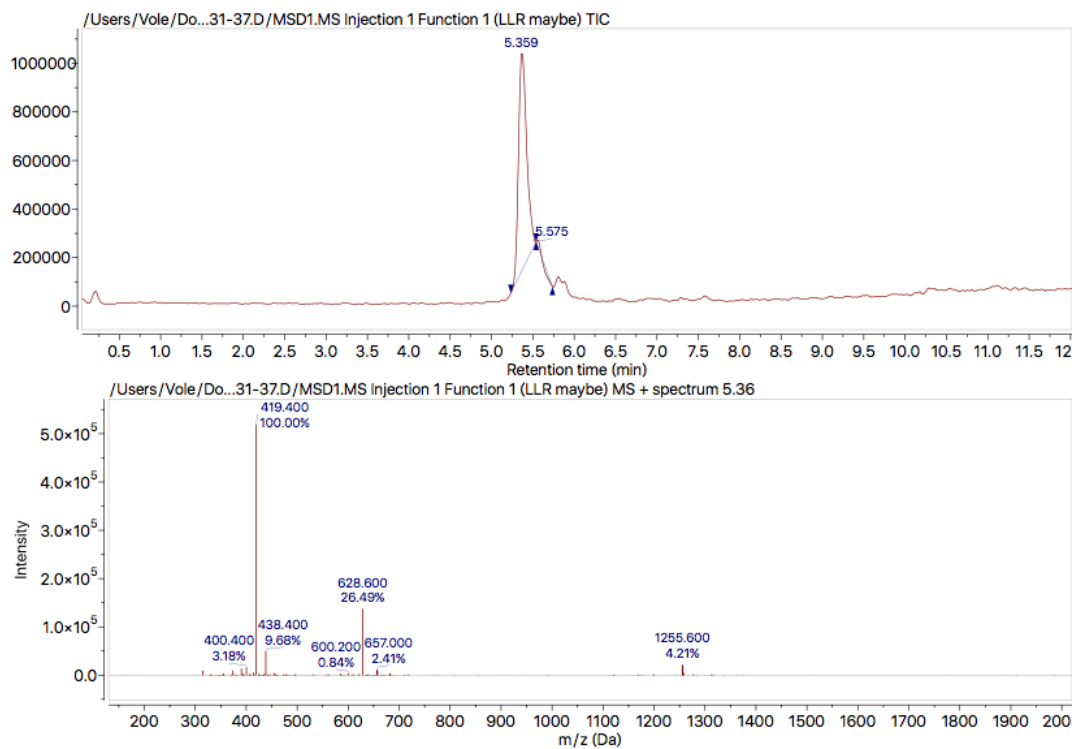


Figure 4.29. LC-MS of LLE-Rh probe.

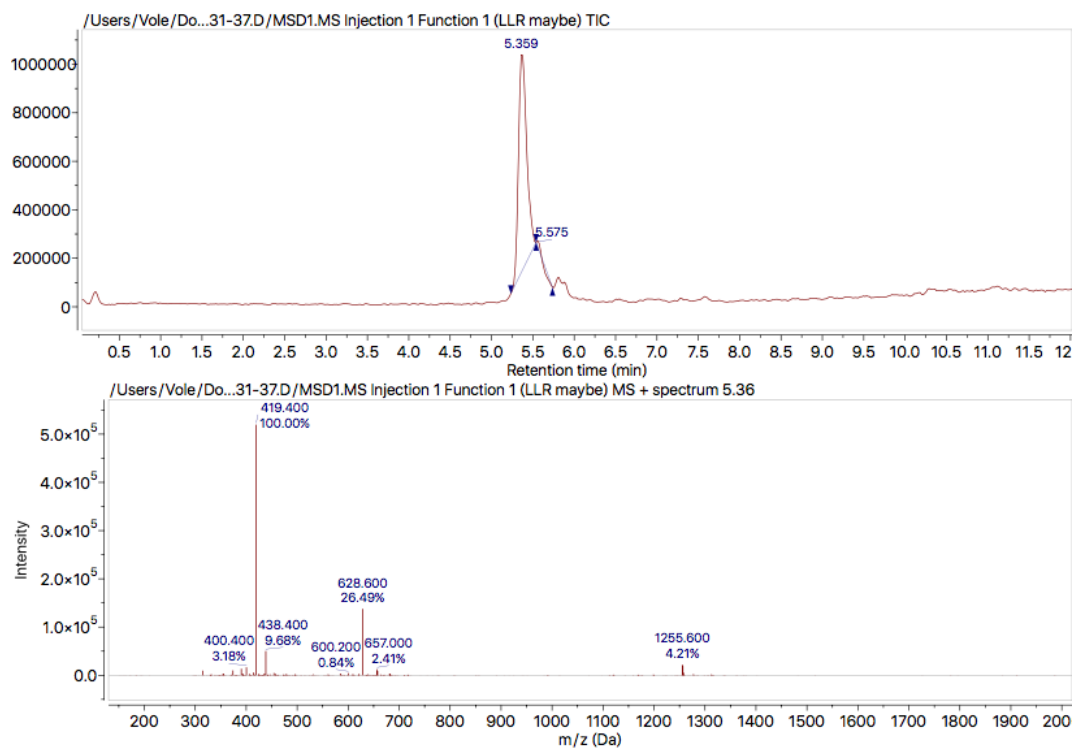
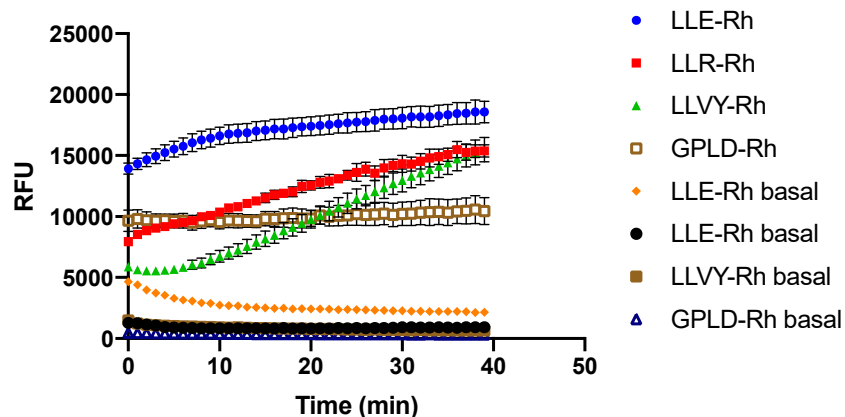


Figure 4.30. LC-MS of LLE-Rh probe.

#### 4.10.2 Biochemical assay with rhodamine probes in 20S CP:



**Figure 4.31. Raw data of probes incubated with 20S CP.** The probes were incubated with the 20S CP at a final concentration of 10  $\mu$ M. The result showed that GPLD-Rh probe was not hydrolyzed significantly by the 20S CP.

The 20S CP was diluted in 50 mM tris buffer, pH (7.6) to acquire a 50 nM stock solution. The probes were also diluted in tris buffer to acquire a concentration of 11.11  $\mu$ M (1.11% DMSO). on a black 96-well plate, 5  $\mu$ L of the 20S CP solution was added to individual wells. 45  $\mu$ L of the probe solution was then added to the wells containing the 20S CP in

a quadruplet. The final 20S CP concentration in wells was 5 nM and final concentration of probes in wells were 10  $\mu$ M (1% DMSO). The probe and the 20S CP were gently mixed by tapping the plate. A Tecan Infinite M200 Pro plate reader system was pre-heated to 37°C and the gain was set to 80. The filter was set to Ex – 485 (20) nm and Em – 535 (20) nm. The 96-well plate was monitored in the plate reader for 40 mins. The result was plotted as the average of the quadruplet samples using GraphPad Prism 8 (**Figure 4.29**).

#### 4.10.3 A549 cell culture and Rh probe testing:

One day prior to the start of the experiment, a black 96-well round bottom plate was treated with collagen by adding 50  $\mu$ L of 25  $\mu$ g/mL collagen solution in 0.02M acetic acid solution (12  $\mu$ L of acetic acid added into 10 mL of ultrapure water). The plate was left in the incubator overnight. The next day, the plate was taken out from the incubator and the collagen solution was removed from the plate. The wells were washed with 100  $\mu$ L of PBS three times and the plate was then put back to the incubator for at least 30 mins to dry.

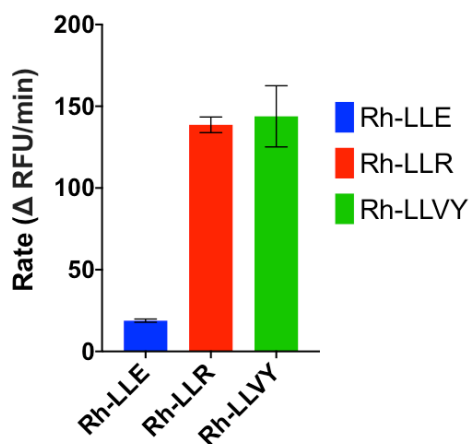


**Figure 4.32:** Rate ( $\Delta$  RFU/min) comparison among three probes in A549 cells at  $10 \mu\text{M}$  of final concentration. Error bars represent SEM and  $n=3$ .

An A549 cell stock was taken out from the liquid nitrogen storage tank and defrosted to R.T. The stock was then transferred into a 15 mL falcon tube with an additional 1 mL of the DMEM media. The tube was centrifuged for 3 mins at  $1,000 \times g$ . The media was removed, and the cell pellet was re-suspended in 10 mL of media. The media was transferred into a T-75 flask (or a 10 cm dish) and the plate was incubated at  $37^\circ\text{C}$  until cells were confluent. The media in the plate was removed and the plate was washed with 10 mL of sterilized 1X PBS gently. The PBS was removed and 2 mL of trypsin buffer was added to the plate. The plate was agitated by hand to allow the buffer to cover the whole plate and the plate was incubated for 5-10 mins to dissociate

cells. The dissociation buffer was collected into a 15 mL falcon tube and was centrifuged at  $1,000 \times g$  for 5 mins. The buffer was removed, and 5 mL of media was added to the tube. Another 15 mL falcon tube was prepared with 9 mL of cell medium inside. 1 mL of the media containing the cells was added to the falcon tube and in total 10 mL of the cell medium was transferred into another new T-75 plate. The T-75 plate was incubated at  $37^\circ\text{C}$  until cells were confluent. The 4 mL cell media left over was kept for cell dosing.  $10 \mu\text{L}$  from the falcon tube was added to each side of a hemocytometer with a glass cover on top. The cells were counted. The amount of the cell suspension needed for dilution was further calculated to fulfill the need of 5,000 cells per well on a 96-well plate. The cells in the falcon tube were taken out and diluted with cell media to obtain 2 mL of a 100,000 cell/ mL solution. The cells were transferred onto a 96 well plate and the plate was incubated overnight. On next day, the plate was taken out from the incubator and the cells were washed with PBS for three times to remove the cell media. The corresponding rhodamine probes were dissolved in KRBH buffer to acquire a final concentration of  $10 \mu\text{M}$  (1% DMSO in total).  $50 \mu\text{L}$  of the probe solution was added to individual wells in triplicate. The plate was gently agitated by hand and the plate was left in the incubator for 10 mins. A Tecan Infinite M200 Pro plate reader system was pre-heated to  $37^\circ\text{C}$  and the gain was set to 80. The filter was set to Ex – 485 (20) nm and Em – 535 (20) nm. The 96-well plate was monitored in the plate reader for 40 mins. The result was plotted as the average of the rate ( $\Delta$  RFU/min) of the triplicate samples using GraphPad Prism 8 (**Figure 4.30**).

#### 4.10.4 Biochemical assay with rhodamine probes and AMC probes in 20S CP:

The 20S CP was diluted in 50 mM tris buffer, pH (7.6) to acquire a 50 nM stock solution. The probes were also diluted in tris buffer to acquire a concentration of 33.33 and 11.11  $\mu\text{M}$  (1.11% DMSO). on a black 96-well plate, 5  $\mu\text{L}$  of the 20S CP solution was added to individual wells. 45  $\mu\text{L}$  of the probe solution was then added to the wells containing the 20S CP in a quadruplet. The final 20S CP concentration in wells was 5 nM and final concentration of probes in wells were 10 or 30  $\mu\text{M}$  (1% DMSO). The probe and the

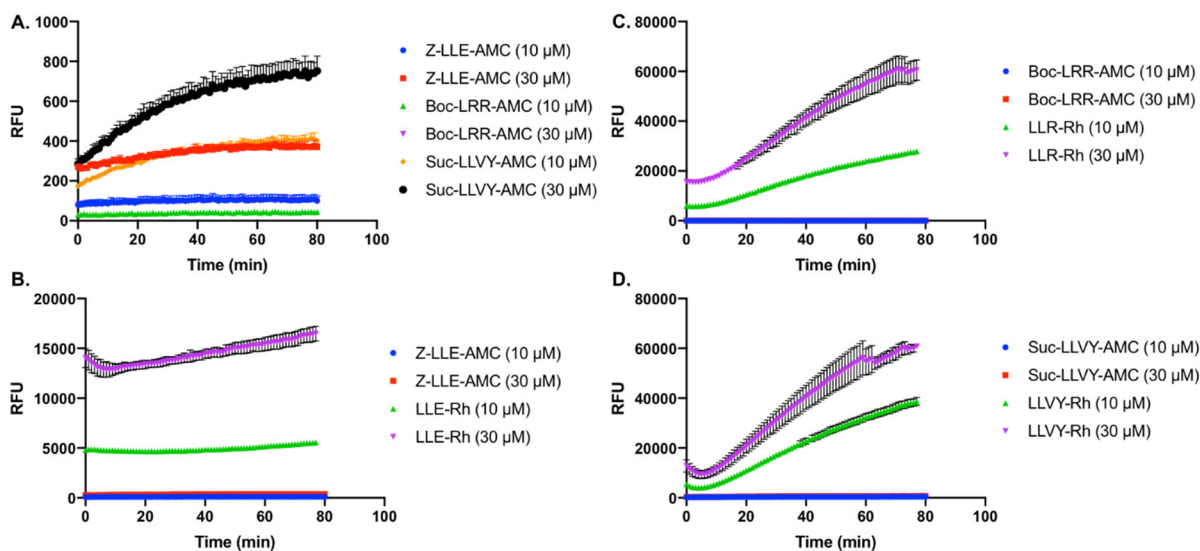


**Figure 4.33. Raw data of rhodamine and AMC probes incubated with 20S CP.** (A) AMC probe raw data comparison. (B) Rh and AMC probe comparison with 10 and 30  $\mu\text{M}$  concentration on the caspase subunit. (C) Rh and AMC probe comparison with 10 and 30  $\mu\text{M}$  concentration on the trypsin subunit. (30  $\mu\text{M}$  LLE-Rh error bar decreased by the end of the experiment because the readings were above detecting limit) (D) Rh and AMC probe comparison with 10 and 30  $\mu\text{M}$  concentration on the chymotrypsin subunit. (30  $\mu\text{M}$  LLVY-Rh error bar decreased by the end of the experiment because the readings were above detecting limit, the data presented in **Figure 5** had last 20 mins removed)

20S CP were gently mixed by tapping the plate. A Tecan Infinite M200 Pro plate reader system was pre-heated to 37°C and the gain was set to 75. The filter was set to Ex – 485 (20) nm and Em – 535 (20) nm for the rhodamine probes and Ex – 340 (20) nm and Em – 460 (20) nm for the AMC probes. The 96-well plate was monitored in the plate reader for 40 mins. The result was plotted as the average RFU of the quadruplet samples using GraphPad Prism 8 (**Figure 4.31**).

#### 4.10.5 Biochemical assay with rhodamine probes in 20S CP and proteasome inhibitor MG-132:

The 20S CP was diluted in 50 mM tris buffer, pH (7.6) to acquire a 50 nM stock solution. The probes were also diluted in tris buffer to acquire a concentration of 12.5  $\mu\text{M}$  (0.625% DMSO). MG-132 was diluted in tris buffer to acquire a concentration of 150  $\mu\text{M}$  (0.625% DMSO). On a black 96-well plate,

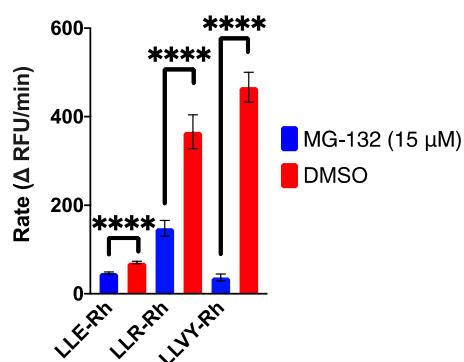


**Figure 4.34.** Rate ( $\Delta$  RFU/min) comparison among three probes treated with MG-132. Significant proteasome activity inhibition was observed with all three catalytic activities. Error bars represent SEM and  $n=4$ . \*\*\*\* $p<0.00005$ .

5  $\mu$ L of the 20S CP solution was added to individual wells, then 5  $\mu$ L of MG-132 solution was added to the same well. Later, 40  $\mu$ L of the probe solution was then added to the wells containing the 20S CP and MG-132 in a quadruplet. The final 20S CP concentration in wells was 5 nM, final concentration of probes in wells were 10  $\mu$ M and final concentration of MG-132 in wells were 15  $\mu$ M (1% DMSO in total). MG-132, Rh probe and the 20S CP were gently mixed by tapping the plate. A Tecan Infinite M200 Pro plate reader system was pre-heated to 37°C and the gain was set to 75. The filter was set to Ex – 485 (20) nm and Em – 535 (20) nm. The 96-well plate was monitored in the plate reader for 40 mins. The result was plotted as the average of the rate ( $\Delta$  RFU/min) of the quadruplet samples using GraphPad

Prism 8 (Figure 4.22A, 32).

#### 4.10.6 Cellular experiments with rhodamine probes in A549 cells and proteasome inhibitor MG-132:

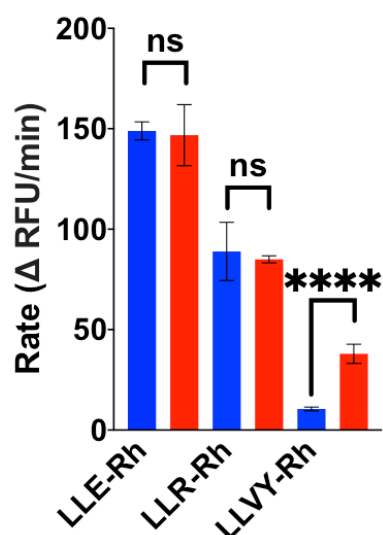


**Figure 4.35.** Rate ( $\Delta$  RFU/min) comparison among three probes in A549 cells at 10  $\mu$ M of final concentration with 15  $\mu$ M of MG-132. Error bars represent SEM and  $n=4$ . \*\*\*\* $p<0.00005$ , ns= $p>0.05$ .

One day prior to the start of the experiment, a black 96-well round bottom plate was treated with collagen by adding 50  $\mu$ L of 25  $\mu$ g/mL collagen solution in 0.02M acetic acid solution (12  $\mu$ L of acetic acid added into 10 mL of ultrapure water). The plate was left in the incubator overnight. The next day, the plate was taken out from the incubator and the collagen solution was removed from the plate. The wells were washed with 100  $\mu$ L of PBS three times and the plate was then put back to the incubator for at least 30 mins to dry.

The next day, A549 cells were transferred into a 96 well plate with 5,000 cells per well. The cells were left in the incubator overnight to adhere. The next day, MG-132 was prepared in a 30  $\mu$ M stock solution (2% DMSO). 50  $\mu$ L of the MG-132 was added to A549 cells in quadruplets. The final concentration of MG-132 in each well was 15  $\mu$ M (1% DMSO in total). The cells were incubated

with the proteasome inhibitor for 1 hour. After 1 hour, the cell media in testing wells were removed and the cells were washed with 1X PBS for three times to remove remaining cell media. The Rh probes were dissolved in KRBH buffer to acquire a 10  $\mu$ M concentration (0.5% DMSO). MG-132 was dissolved in corresponding Rh probe solution to acquire a concentration of 15  $\mu$ M (0.5% DMSO). 50  $\mu$ L of the solution was added to testing wells in quadruplets with a final concentration of MG-132 at 15  $\mu$ M and probe at 10  $\mu$ M (1% DMSO in total). The plate was put back to the incubator for 10 mins. The plate was gently agitated by hand and the plate was left in the incubator for 10 mins. A Tecan Infinite M200 Pro plate reader system was pre-heated to 37°C and the gain was set to 80. The filter was set to Ex – 485 (20) nm and Em – 535 (20) nm. The 96-well plate was monitored in the plate reader for 1 hour. The result was plotted as the average of the rate ( $\Delta$  RFU/min) of quadruplet samples using GraphPad Prism 8 (**Figure 4.33**).

#### 4.10.7 Cellular experiments with rhodamine probes in A549 cells and proteasome inhibitor bortezomib:

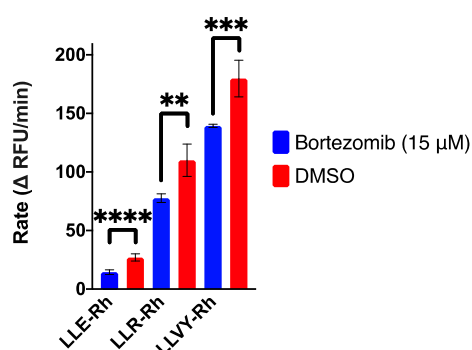


**Figure 4.36.** Rate ( $\Delta$  RFU/min) comparison among three probes in A549 cells at 10  $\mu$ M of final concentration with 15  $\mu$ M of bortezomib. Error bars represent SEM and n=4. \*\*\*\*p<0.0005, \*\*p<0.005, \*\*\*p<0.0005.

One day prior to the start of the experiment, a black 96-well round bottom plate was treated with collagen by adding 50  $\mu$ L of 25  $\mu$ g/mL collagen solution in 0.02M acetic acid solution (12  $\mu$ L of acetic acid added into 10 mL of ultrapure water). The plate was left in the incubator overnight. The next day, the plate was taken out from the incubator and the collagen solution was removed from the plate. The wells were washed with 100  $\mu$ L of PBS three times and the plate was then put back to the incubator for at least 30 mins to dry.

The next day, A549 cells were transferred into a 96 well plate with 5,000 cells per well. The cells were left in the incubator overnight to adhere. The next day, bortezomib was prepared in a 30  $\mu$ M stock solution (2% DMSO). 50  $\mu$ L of the bortezomib was added to A549 cells in quadruplets. The final concentration of bortezomib in each well is 15  $\mu$ M (1% DMSO in total). The cells were incubated with the proteasome inhibitor for 1 hour. After 1 hour, the cell media in testing wells were removed and the cells were washed with 1X PBS for three times to remove remaining cell media. The Rh probes were dissolved in KRBH buffer to acquire a 10  $\mu$ M concentration (0.5% DMSO). MG-132 was dissolved in corresponding Rh probe solution to acquire a concentration of 15  $\mu$ M (0.5% DMSO). 50  $\mu$ L of the solution was added to testing wells in quadruplets

with a final concentration of bortezomib at 15  $\mu$ M and probe at 10  $\mu$ M (1% DMSO in total). The plate was gently agitated by hand and the plate was left in the incubator for 10 mins. A Tecan Infinite M200 Pro plate reader system was pre-heated to 37°C and the gain was set to 80. The filter was set to Ex – 485 (20) nm and Em – 535 (20) nm. The 96-well plate was monitored in the plate reader for 1 hour. The result was plotted as the average of rate ( $\Delta$ RFU/min) of the quadruplet samples using GraphPad Prism 8 (**Figure 4.34**).

#### 4.10.8 Viability assay in A549 cells treated with proteasome inhibitor MG-132 and bortezomib:

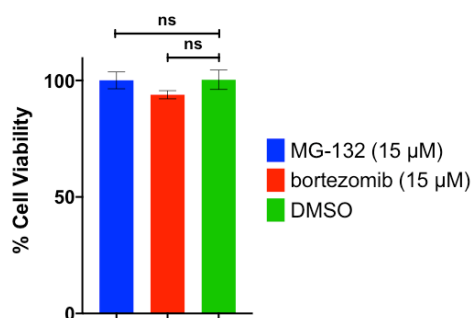


**Figure 4.37.** Viability assay in A549 cells treated with MG-132 or bortezomib. No significant cell death was observed after 2 hours of treatment. Error bars represent SEM and n=5. ns=p>0.05.

A549 cells were transferred into a 96 well plate with 5,000 cells per well. The cells were left in the incubator overnight to adhere. The next day, MG-132 and bortezomib were prepared in a 30  $\mu$ M stock solution (2% DMSO). 50  $\mu$ L of the MG-132 or bortezomib was added to A549 cells in quintuple. The final concentration of MG-132 or bortezomib in each well is 15  $\mu$ M (1% DMSO in total). The cells were incubated with the proteasome inhibitor for 2 hours. The cells were then treated with Cell-Titer Glo for a luminescent viability assay. The result was plotted as the average percentage of cells viable of the quadruplet samples using GraphPad Prism 8. No significant cell death was observed with MG-132 or bortezomib treated cells (**Figure 4.35**).

#### 4.11 Reference.

- (1) Tian, W.; Trader, D. J. Discovery of a Small Molecule Probe of Rpn-6, an Essential Subunit of the 26S Proteasome. *ACS Chemical Biology* **2020**, *15* (2), 554–561. <https://doi.org/10.1021/acscchembio.9b01019>.
- (2) Tian, W.; Maresh, M.; Trader, D. J. Approaches to Evaluate the Impact of a Small Molecule Binder to a Non - catalytic Site of the Proteasome. *ChemBioChem* **2021**, cbic.202100023. <https://doi.org/10.1002/cbic.202100023>.
- (3) An, S.; Fu, L. Small-Molecule PROTACs: An Emerging and Promising Approach for the Development of Targeted Therapy Drugs. *EBioMedicine* **2018**, *36*, 553–562. <https://doi.org/10.1016/j.ebiom.2018.09.005>.

- (4) Sun, X.; Gao, H.; Yang, Y.; He, M.; Wu, Y.; Song, Y.; Tong, Y.; Rao, Y. PROTACs: Great Opportunities for Academia and Industry. *Signal Transduction and Targeted Therapy* **2019**, *4* (1). <https://doi.org/10.1038/s41392-019-0101-6>.
- (5) Cromm, P. M.; Crews, C. M. Targeted Protein Degradation: From Chemical Biology to Drug Discovery. *Cell Chemical Biology* **2017**, *24* (9), 1181–1190. <https://doi.org/10.1016/j.chembiol.2017.05.024>.
- (6) Paiva, S.-L.; Crews, C. M. Targeted Protein Degradation: Elements of PROTAC Design. *Current Opinion in Chemical Biology* **2019**, *50*, 111–119. <https://doi.org/10.1016/j.cbpa.2019.02.022>.
- (7) Cyrus, K.; Wehenkel, M.; Choi, E.-Y.; Han, H.-J.; Lee, H.; Swanson, H.; Kim, K.-B. Impact of Linker Length on the Activity of PROTACs. *Mol. Biosyst.* **2011**, *7* (2), 359–364. <https://doi.org/10.1039/C0MB00074D>.
- (8) Smith, B. E.; Wang, S. L.; Jaime-Figueroa, S.; Harbin, A.; Wang, J.; Hamman, B. D.; Crews, C. M. Differential PROTAC Substrate Specificity Dictated by Orientation of Recruited E3 Ligase. *Nature Communications* **2019**, *10* (1). <https://doi.org/10.1038/s41467-018-08027-7>.
- (9) Gao, H.; Sun, X.; Rao, Y. PROTAC Technology: Opportunities and Challenges. *ACS Med. Chem. Lett.* **2020**, *11* (3), 237–240. <https://doi.org/10.1021/acsmchemlett.9b00597>.
- (10) Crews, C. M. Targeting the Undruggable Proteome: The Small Molecules of My Dreams. *Chemistry & Biology* **2010**, *17* (6), 551–555. <https://doi.org/10.1016/j.chembiol.2010.05.011>.
- (11) Lai, A. C.; Crews, C. M. Induced Protein Degradation: An Emerging Drug Discovery Paradigm. *Nat Rev Drug Discov* **2017**, *16* (2), 101–114. <https://doi.org/10.1038/nrd.2016.211>.
- (12) Dang, C. V.; Reddy, E. P.; Shokat, K. M.; Soucek, L. Drugging the “undruggable” Cancer Targets. *Nat Rev Cancer* **2017**, *17* (8), 502–508. <https://doi.org/10.1038/nrc.2017.36>.
- (13) Roy, M. J.; Winkler, S.; Hughes, S. J.; Whitworth, C.; Galant, M.; Farnaby, W.; Rumpel, K.; Ciulli, A. SPR-Measured Dissociation Kinetics of PROTAC Ternary Complexes Influence Target Degradation Rate. *ACS Chemical Biology* **2019**, *14* (3), 361–368. <https://doi.org/10.1021/acschembio.9b00092>.
- (14) Bondeson, D. P.; Smith, B. E.; Burslem, G. M.; Buhimschi, A. D.; Hines, J.; Jaime-Figueroa, S.; Wang, J.; Hamman, B. D.; Ishchenko, A.; Crews, C. M. Lessons in PROTAC Design from Selective Degradation with a Promiscuous Warhead. *Cell Chemical Biology* **2018**, *25* (1), 78–87.e5. <https://doi.org/10.1016/j.chembiol.2017.09.010>.

- (15) Guo, W.-H.; Qi, X.; Yu, X.; Liu, Y.; Chung, C.-I.; Bai, F.; Lin, X.; Lu, D.; Wang, L.; Chen, J.; Su, L. H.; Nomie, K. J.; Li, F.; Wang, M. C.; Shu, X.; Onuchic, J. N.; Woyach, J. A.; Wang, M. L.; Wang, J. Enhancing Intracellular Accumulation and Target Engagement of PROTACs with Reversible Covalent Chemistry. *Nat Commun* **2020**, *11* (1), 4268. <https://doi.org/10.1038/s41467-020-17997-6>.
- (16) Scheepstra, M.; Hekking, K. F. W.; van Hijfte, L.; Folmer, R. H. A. Bivalent Ligands for Protein Degradation in Drug Discovery. *Computational and Structural Biotechnology Journal* **2019**, *17*, 160–176. <https://doi.org/10.1016/j.csbj.2019.01.006>.
- (17) Troup, R. I.; Fallan, C.; Baud, M. G. J. Current Strategies for the Design of PROTAC Linkers: A Critical Review. *Exploration of Targeted Anti-tumor Therapy* **2020**, *1* (5). <https://doi.org/10.37349/etat.2020.00018>.
- (18) Zaidman, D.; Prilusky, J.; London, N. PROsettaC: Rosetta Based Modeling of PROTAC Mediated Ternary Complexes. *J. Chem. Inf. Model.* **2020**, *60* (10), 4894–4903. <https://doi.org/10.1021/acs.jcim.0c00589>.
- (19) Drummond, M. L.; Williams, C. I. *In Silico* Modeling of PROTAC-Mediated Ternary Complexes: Validation and Application. *Journal of Chemical Information and Modeling* **2019**, *59* (4), 1634–1644. <https://doi.org/10.1021/acs.jcim.8b00872>.
- (20) Anderson, D. J.; Le Moigne, R.; Djakovic, S.; Kumar, B.; Rice, J.; Wong, S.; Wang, J.; Yao, B.; Valle, E.; Kiss von Soly, S.; Madriaga, A.; Soriano, F.; Menon, M.-K.; Wu, Z. Y.; Kampmann, M.; Chen, Y.; Weissman, J. S.; Aftab, B. T.; Yakes, F. M.; Shawver, L.; Zhou, H.-J.; Wustrow, D.; Rolfe, M. Targeting the AAA ATPase P97 as an Approach to Treat Cancer through Disruption of Protein Homeostasis. *Cancer Cell* **2015**, *28* (5), 653–665. <https://doi.org/10.1016/j.ccell.2015.10.002>.
- (21) Del Prete, D.; Rice, R. C.; Rajadhyaksha, A. M.; D'Adamio, L. Amyloid Precursor Protein (APP) May Act as a Substrate and a Recognition Unit for CRL4<sup>CRBN</sup> and Stub1 E3 Ligases Facilitating Ubiquitination of Proteins Involved in Presynaptic Functions and Neurodegeneration. *Journal of Biological Chemistry* **2016**, *291* (33), 17209–17227. <https://doi.org/10.1074/jbc.M116.733626>.
- (22) Wang, Y.; Jiang, X.; Feng, F.; Liu, W.; Sun, H. Degradation of Proteins by PROTACs and Other Strategies. *Acta Pharmaceutica Sinica B* **2020**, *10* (2), 207–238. <https://doi.org/10.1016/j.apsb.2019.08.001>.
- (23) Steinebach, C.; Kehm, H.; Lindner, S.; Vu, L. P.; Köpff, S.; López Mármol, Á.; Weiler, C.; Wagner, K. G.; Reichenzeller, M.; Krönke, J.; Gütschow, M. PROTAC-Mediated Crosstalk between E3 Ligases. *Chemical Communications* **2019**, *55* (12), 1821–1824. <https://doi.org/10.1039/C8CC09541H>.
- (24) Cheng, J.; Guo, J.; North, B. J.; Tao, K.; Zhou, P.; Wei, W. The Emerging Role for Cullin 4 Family of E3 Ligases in Tumorigenesis. *Biochimica et Biophysica Acta (BBA) - Reviews on Cancer* **2019**, *1871* (1), 138–159. <https://doi.org/10.1016/j.bbcan.2018.11.007>.

- (25) Sakamoto, K. M.; Kim, K. B.; Kumagai, A.; Mercurio, F.; Crews, C. M.; Deshaies, R. J. Protacs: Chimeric Molecules That Target Proteins to the Skp1-Cullin-F Box Complex for Ubiquitination and Degradation. *Proceedings of the National Academy of Sciences* **2001**, *98* (15), 8554–8559. <https://doi.org/10.1073/pnas.141230798>.
- (26) Ottis, P.; Toure, M.; Cromm, P. M.; Ko, E.; Gustafson, J. L.; Crews, C. M. Assessing Different E3 Ligases for Small Molecule Induced Protein Ubiquitination and Degradation. *ACS Chemical Biology* **2017**, *12* (10), 2570–2578. <https://doi.org/10.1021/acscchembio.7b00485>.
- (27) Pettersson, M.; Crews, C. M. PROteolysis Targeting Chimeras (PROTACs) — Past, Present and Future. *Drug Discovery Today: Technologies* **2019**, *31*, 15–27. <https://doi.org/10.1016/j.ddtec.2019.01.002>.
- (28) Huang, X.; Dixit, V. M. Drugging the Undruggables: Exploring the Ubiquitin System for Drug Development. *Cell Res* **2016**, *26* (4), 484–498. <https://doi.org/10.1038/cr.2016.31>.
- (29) Hines, J.; Lartigue, S.; Dong, H.; Qian, Y.; Crews, C. M. MDM2-Recruiting PROTAC Offers Superior, Synergistic Antiproliferative Activity via Simultaneous Degradation of BRD4 and Stabilization of P53. *Cancer Research* **2019**, *79* (1), 251–262. <https://doi.org/10.1158/0008-5472.CAN-18-2918>.
- (30) Ishida, T.; Ciulli, A. E3 Ligase Ligands for PROTACs: How They Were Found and How to Discover New Ones. *SLAS DISCOVERY: Advancing the Science of Drug Discovery* **2021**, *26* (4), 484–502. <https://doi.org/10.1177/2472555220965528>.
- (31) George, A. J.; Hoffiz, Y. C.; Charles, A. J.; Zhu, Y.; Mabb, A. M. A Comprehensive Atlas of E3 Ubiquitin Ligase Mutations in Neurological Disorders. *Front. Genet.* **2018**, *9*, 29. <https://doi.org/10.3389/fgene.2018.00029>.
- (32) Périno, S.; Contino-Pépin, C.; Satchi-Fainaro, R.; Butterfield, C.; Pucci, B. Inhibition of Angiogenesis by THAM-Derived Cotelomers Endowed with Thalidomide Moieties. *Bioorganic & Medicinal Chemistry Letters* **2004**, *14* (2), 421–425. <https://doi.org/10.1016/j.bmcl.2003.10.045>.
- (33) Chan, K.-H.; Zengerle, M.; Testa, A.; Ciulli, A. Impact of Target Warhead and Linkage Vector on Inducing Protein Degradation: Comparison of Bromodomain and Extra-Terminal (BET) Degraders Derived from Triazolodiazepine (JQ1) and Tetrahydroquinoline (I-BET726) BET Inhibitor Scaffolds. *J. Med. Chem.* **2018**, *61* (2), 504–513. <https://doi.org/10.1021/acs.jmedchem.6b01912>.
- (34) Lindner, S.; Steinebach, C.; Kehm, H.; Mangold, M.; Gütschow, M.; Krönke, J. Chemical Inactivation of the E3 Ubiquitin Ligase Cereblon by Pomalidomide-Based Homo-PROTACs. *JoVE* **2019**, No. 147, 59472. <https://doi.org/10.3791/59472>.
- (35) Chen, H.; Chen, F.; Pei, S.; Gou, S. Pomalidomide Hybrids Act as Proteolysis Targeting Chimeras: Synthesis, Anticancer Activity and B-Raf Degradation. *Bioorganic Chemistry* **2019**, *87*, 191–199. <https://doi.org/10.1016/j.bioorg.2019.03.035>.

- (36) Liu, J.; Chen, H.; Ma, L.; He, Z.; Wang, D.; Liu, Y.; Lin, Q.; Zhang, T.; Gray, N.; Kaniskan, H. Ü.; Jin, J.; Wei, W. Light-Induced Control of Protein Destruction by Opto-PROTAC. *Sci. Adv.* **2020**, *6* (8), eaay5154. <https://doi.org/10.1126/sciadv.aay5154>.
- (37) Chanan-Khan, A. A.; Swaika, A.; Paulus, A.; Kumar, S. K.; Mikhael, J. R.; Rajkumar, S. V.; Dispenzieri, A.; Lacy, M. Q. Pomalidomide: The New Immunomodulatory Agent for the Treatment of Multiple Myeloma. *Blood Cancer Journal* **2013**, *3* (9), e143–e143. <https://doi.org/10.1038/bcj.2013.38>.
- (38) Liu, X.; Zhang, X.; Lv, D.; Yuan, Y.; Zheng, G.; Zhou, D. Assays and Technologies for Developing Proteolysis Targeting Chimera Degraders. *Future Medicinal Chemistry* **2020**, fmc-2020-0073. <https://doi.org/10.4155/fmc-2020-0073>.
- (39) Arthur, R.; Beatriz Valle-Argos, B.; Steele, A. J.; Packham, G. Development of PROTACs to Address Clinical Limitations Associated with BTK-Targeted Kinase Inhibitors. *Exploration of Targeted Anti-tumor Therapy* **2020**, *1* (3), 131–152. <https://doi.org/10.37349/etat.2020.00009>.
- (40) Zorba, A.; Nguyen, C.; Xu, Y.; Starr, J.; Borzilleri, K.; Smith, J.; Zhu, H.; Farley, K. A.; Ding, W.; Schiemer, J.; Feng, X.; Chang, J. S.; Uccello, D. P.; Young, J. A.; Garcia-Irrizary, C. N.; Czabaniuk, L.; Schuff, B.; Oliver, R.; Montgomery, J.; Hayward, M. M.; Coe, J.; Chen, J.; Niosi, M.; Luthra, S.; Shah, J. C.; El-Kattan, A.; Qiu, X.; West, G. M.; Noe, M. C.; Shanmugasundaram, V.; Gilbert, A. M.; Brown, M. F.; Calabrese, M. F. Delineating the Role of Cooperativity in the Design of Potent PROTACs for BTK. *Proceedings of the National Academy of Sciences* **2018**, *115* (31), E7285–E7292. <https://doi.org/10.1073/pnas.1803662115>.
- (41) Ameh, E. S. A Review of Basic Crystallography and X-Ray Diffraction Applications. *Int J Adv Manuf Technol* **2019**, *105* (7–8), 3289–3302. <https://doi.org/10.1007/s00170-019-04508-1>.
- (42) Shi, Y. A Glimpse of Structural Biology through X-Ray Crystallography. *Cell* **2014**, *159* (5), 995–1014. <https://doi.org/10.1016/j.cell.2014.10.051>.
- (43) Guo, T. W.; Bartesaghi, A.; Yang, H.; Falconieri, V.; Rao, P.; Merk, A.; Eng, E. T.; Raczkowski, A. M.; Fox, T.; Earl, L. A.; Patel, D. J.; Subramaniam, S. Cryo-EM Structures Reveal Mechanism and Inhibition of DNA Targeting by a CRISPR-Cas Surveillance Complex. *Cell* **2017**, *171* (2), 414–426.e12. <https://doi.org/10.1016/j.cell.2017.09.006>.
- (44) Borgnia, M. J.; Banerjee, S.; Merk, A.; Matthies, D.; Bartesaghi, A.; Rao, P.; Pierson, J.; Earl, L. A.; Falconieri, V.; Subramaniam, S.; Milne, J. L. S. Using Cryo-EM to Map Small Ligands on Dynamic Metabolic Enzymes: Studies with Glutamate Dehydrogenase. *Mol Pharmacol* **2016**, *89* (6), 645–651. <https://doi.org/10.1124/mol.116.103382>.
- (45) Rubin, S. M.; Lee, S.-Y.; Ruiz, E. J.; Pines, A.; Wemmer, D. E. Detection and Characterization of Xenon-Binding Sites in Proteins by <sup>129</sup>Xe NMR Spectroscopy. *Journal of Molecular Biology* **2002**, *322* (2), 425–440. [https://doi.org/10.1016/S0022-2836\(02\)00739-8](https://doi.org/10.1016/S0022-2836(02)00739-8).

- (46) Grace, C. R. R.; Perrin, M. H.; DiGruccio, M. R.; Miller, C. L.; Rivier, J. E.; Vale, W. W.; Riek, R. NMR Structure and Peptide Hormone Binding Site of the First Extracellular Domain of a Type B1 G Protein-Coupled Receptor. *Proceedings of the National Academy of Sciences* **2004**, *101* (35), 12836–12841. <https://doi.org/10.1073/pnas.0404702101>.
- (47) Ziarek, J. J.; Peterson, F. C.; Lytle, B. L.; Volkman, B. F. Binding Site Identification and Structure Determination of Protein–Ligand Complexes by NMR. In *Methods in Enzymology*; Elsevier, 2011; Vol. 493, pp 241–275. <https://doi.org/10.1016/B978-0-12-381274-2.00010-8>.
- (48) Hauser, M.; Qian, C.; King, S. T.; Kauffman, S.; Naider, F.; Hettich, R. L.; Becker, J. M. Identification of Peptide-Binding Sites within BSA Using Rapid, Laser-Induced Covalent Cross-Linking Combined with High-Performance Mass Spectrometry. *J Mol Recognit* **2018**, *31* (2), e2680. <https://doi.org/10.1002/jmr.2680>.
- (49) Becker, J. M.; Naider, F. Cross-Linking Strategies to Study Peptide Ligand–Receptor Interactions. In *Methods in Enzymology*; Elsevier, 2015; Vol. 556, pp 527–547. <https://doi.org/10.1016/bs.mie.2014.12.001>.
- (50) Dong, Y.; Zhang, S.; Wu, Z.; Li, X.; Wang, W. L.; Zhu, Y.; Stoilova-McPhie, S.; Lu, Y.; Finley, D.; Mao, Y. Cryo-EM Structures and Dynamics of Substrate-Engaged Human 26S Proteasome. *Nature* **2018**. <https://doi.org/10.1038/s41586-018-0736-4>.
- (51) Huang, X.; Luan, B.; Wu, J.; Shi, Y. An Atomic Structure of the Human 26S Proteasome. *Nature Structural & Molecular Biology* **2016**, *23* (9), 778–785. <https://doi.org/10.1038/nsmb.3273>.
- (52) Dambacher, C. M.; Worden, E. J.; Herzik, M. A.; Martin, A.; Lander, G. C. Atomic Structure of the 26S Proteasome Lid Reveals the Mechanism of Deubiquitinase Inhibition. *eLife* **2016**, *5*, e13027. <https://doi.org/10.7554/eLife.13027>.
- (53) Guan, H.; Wang, Y.; Yu, T.; Huang, Y.; Li, M.; Saeed, A. F. U. H.; Perčulija, V.; Li, D.; Xiao, J.; Wang, D.; Zhu, P.; Ouyang, S. Cryo-EM Structures of the Human PA200 and PA200-20S Complex Reveal Regulation of Proteasome Gate Opening and Two PA200 Apertures. *PLoS Biol* **2020**, *18* (3), e3000654. <https://doi.org/10.1371/journal.pbio.3000654>.
- (54) Murata, K.; Wolf, M. Cryo-Electron Microscopy for Structural Analysis of Dynamic Biological Macromolecules. *Biochimica et Biophysica Acta (BBA) - General Subjects* **2018**, *1862* (2), 324–334. <https://doi.org/10.1016/j.bbagen.2017.07.020>.
- (55) Kolsrud, H.; Malerod, H.; Ray, S.; Reubsæet, L.; Lundanes, E.; Greibrokk, T. A Critical Review of Trypsin Digestion for LC-MS Based Proteomics. In *Integrative Proteomics*; Leung, H.-C., Ed.; InTech, 2012. <https://doi.org/10.5772/29326>.

- (56) Walmsley, S. J.; Rudnick, P. A.; Liang, Y.; Dong, Q.; Stein, S. E.; Nesvizhskii, A. I. Comprehensive Analysis of Protein Digestion Using Six Trypsins Reveals the Origin of Trypsin As a Significant Source of Variability in Proteomics. *J. Proteome Res.* **2013**, *12* (12), 5666–5680. <https://doi.org/10.1021/pr400611h>.
- (57) Nikić, I.; Kang, J. H.; Girona, G. E.; Aramburu, I. V.; Lemke, E. A. Labeling Proteins on Live Mammalian Cells Using Click Chemistry. *Nat Protoc* **2015**, *10* (5), 780–791. <https://doi.org/10.1038/nprot.2015.045>.
- (58) Parker, C. G.; Pratt, M. R. Click Chemistry in Proteomic Investigations. *Cell* **2020**, *180* (4), 605–632. <https://doi.org/10.1016/j.cell.2020.01.025>.
- (59) Wurz, R. P.; Dellamaggiore, K.; Dou, H.; Javier, N.; Lo, M.-C.; McCarter, J. D.; Mohl, D.; Sastri, C.; Lipford, J. R.; Cee, V. J. A “Click Chemistry Platform” for the Rapid Synthesis of Bispecific Molecules for Inducing Protein Degradation. *Journal of Medicinal Chemistry* **2018**, *61* (2), 453–461. <https://doi.org/10.1021/acs.jmedchem.6b01781>.
- (60) Szychowski, J.; Mahdavi, A.; Hodas, J. J. L.; Bagert, J. D.; Ngo, J. T.; Landgraf, P.; Dieterich, D. C.; Schuman, E. M.; Tirrell, D. A. Cleavable Biotin Probes for Labeling of Biomolecules via Azide–Alkyne Cycloaddition. *Journal of the American Chemical Society* **2010**, *132* (51), 18351–18360. <https://doi.org/10.1021/ja1083909>.
- (61) Dundas, C. M.; Demonte, D.; Park, S. Streptavidin–Biotin Technology: Improvements and Innovations in Chemical and Biological Applications. *Appl Microbiol Biotechnol* **2013**, *97* (21), 9343–9353. <https://doi.org/10.1007/s00253-013-5232-z>.
- (62) Anchoori, R. K.; Karanam, B.; Peng, S.; Wang, J. W.; Jiang, R.; Tanno, T.; Orłowski, R. Z.; Matsui, W.; Zhao, M.; Rudek, M. A.; Hung, C.; Chen, X.; Walters, K. J.; Roden, R. B. S. A Bis-Benzylidene Piperidone Targeting Proteasome Ubiquitin Receptor RPN13/ADRM1 as a Therapy for Cancer. *Cancer Cell* **2013**, *24* (6), 791–805. <https://doi.org/10.1016/j.ccr.2013.11.001>.
- (63) Husnjak, K.; Elsasser, S.; Zhang, N.; Chen, X.; Randles, L.; Shi, Y.; Hofmann, K.; Walters, K. J.; Finley, D.; Dikic, I. Proteasome Subunit Rpn13 Is a Novel Ubiquitin Receptor. *Nature* **2008**, *453* (7194), 481–488. <https://doi.org/10.1038/nature06926>.
- (64) Smalle, J.; Kurepa, J.; Yang, P.; Emborg, T. J.; Babychuk, E.; Kushnir, S.; Vierstra, R. D. The Pleiotropic Role of the 26S Proteasome Subunit RPN10 in Arabidopsis Growth and Development Supports a Substrate-Specific Function in Abscissic Acid Signaling. *The Plant Cell* **2003**, *15* (4), 965–980. <https://doi.org/10.1105/tpc.009217>.
- (65) Isasa, M.; Katz, E. J.; Kim, W.; Yugo, V.; González, S.; Kirkpatrick, D. S.; Thomson, T. M.; Finley, D.; Gygi, S. P.; Crosas, B. Monoubiquitination of RPN10 Regulates Substrate Recruitment to the Proteasome. *Molecular Cell* **2010**, *38* (5), 733–745. <https://doi.org/10.1016/j.molcel.2010.05.001>.

- (66) Perez, C.; Li, J.; Parlati, F.; Rouffet, M.; Ma, Y.; Mackinnon, A. L.; Chou, T.-F.; Deshaies, R. J.; Cohen, S. M. Discovery of an Inhibitor of the Proteasome Subunit Rpn11. *Journal of Medicinal Chemistry* **2017**, *60* (4), 1343–1361. <https://doi.org/10.1021/acs.jmedchem.6b01379>.
- (67) Latham, M. P.; Sekhar, A.; Kay, L. E. Understanding the Mechanism of Proteasome 20S Core Particle Gating. *Proceedings of the National Academy of Sciences* **2014**, *111* (15), 5532–5537. <https://doi.org/10.1073/pnas.1322079111>.
- (68) Lee, N. K.; Park, S. E.; Kwon, S. J.; Shim, S.; Byeon, Y.; Kim, J.-H.; Na, D. L.; Chang, J. W. Agouti Related Peptide Secreted Via Human Mesenchymal Stem Cells Upregulates Proteasome Activity in an Alzheimer's Disease Model. *Sci Rep* **2017**, *7* (1), 39340. <https://doi.org/10.1038/srep39340>.
- (69) Götze, S.; Saborowski, R.; Martínez-Cruz, O.; Muhlia-Almazán, A.; Sánchez-Paz, A. Proteasome Properties of Hemocytes Differ between the Whiteleg Shrimp *Penaeus Vannamei* and the Brown Shrimp *Crangon Crangon* (Crustacea, Decapoda). *Cell Stress and Chaperones* **2017**, *22* (6), 879–891. <https://doi.org/10.1007/s12192-017-0819-4>.
- (70) Ye, M.; Qiu, H.; Cao, Y.; Zhang, M.; Mi, Y.; Yu, J.; Wang, C. Curcumin Improves Palmitate-Induced Insulin Resistance in Human Umbilical Vein Endothelial Cells by Maintaining Proteostasis in Endoplasmic Reticulum. *Front. Pharmacol.* **2017**, *08*. <https://doi.org/10.3389/fphar.2017.00148>.
- (71) Lan, X.; Zhao, C.; Chen, X.; Zhang, P.; Zang, D.; Wu, J.; Chen, J.; Long, H.; Yang, L.; Huang, H.; Wang, X.; Shi, X.; Liu, J. Platinum Pyrithione Induces Apoptosis in Chronic Myeloid Leukemia Cells Resistant to Imatinib via DUB Inhibition-Dependent Caspase Activation and Bcr-Abl Downregulation. *Cell Death Dis* **2017**, *8* (7), e2913–e2913. <https://doi.org/10.1038/cddis.2017.284>.
- (72) Zerfas, B. L.; Coleman, R. A.; Salazar-Chaparro, A. F.; Macatangay, N. J.; Trader, D. J. Fluorescent Probes with Unnatural Amino Acids to Monitor Proteasome Activity in Real-Time. *ACS Chemical Biology* **2020**, *15* (9), 2588–2596. <https://doi.org/10.1021/acscchembio.0c00634>.
- (73) Coleman, R. A.; Trader, D. J. Development and Application of a Sensitive Peptide Reporter to Discover 20S Proteasome Stimulators. *ACS Combinatorial Science* **2018**, *20* (5), 269–276. <https://doi.org/10.1021/acscombsci.7b00193>.
- (74) Coleman, R. A.; Trader, D. J. Methods to Discover and Evaluate Proteasome Small Molecule Stimulators. *Molecules* **2019**, *24* (12), 2341. <https://doi.org/10.3390/molecules24122341>.
- (75) Li, Y.; Tomko, R. J.; Hochstrasser, M. Proteasomes: Isolation and Activity Assays. *Current Protocols in Cell Biology* **2015**, *67* (1). <https://doi.org/10.1002/0471143030.cb0343s67>.

- (76) Blackburn, C.; Gigstad, K. M.; Hales, P.; Garcia, K.; Jones, M.; Bruzzese, F. J.; Barrett, C.; Liu, J. X.; Soucy, T. A.; Sappal, D. S.; Bump, N.; Olhava, E. J.; Fleming, P.; Dick, L. R.; Tsu, C.; Sintchak, M. D.; Blank, J. L. Characterization of a New Series of Non-Covalent Proteasome Inhibitors with Exquisite Potency and Selectivity for the 20S B5-Subunit. *Biochemical Journal* **2010**, *430* (3), 461–476. <https://doi.org/10.1042/BJ20100383>.
- (77) Rodgers, K. J.; Dean, R. T. Assessment of Proteasome Activity in Cell Lysates and Tissue Homogenates Using Peptide Substrates. *The International Journal of Biochemistry & Cell Biology* **2003**, *35* (5), 716–727. [https://doi.org/10.1016/S1357-2725\(02\)00391-6](https://doi.org/10.1016/S1357-2725(02)00391-6).
- (78) Zerfas, B. L.; Trader, D. J. Monitoring the Immunoproteasome in Live Cells Using an Activity-Based Peptide–Peptoid Hybrid Probe. *J. Am. Chem. Soc.* **2019**, *9*.
- (79) Hamouda, M.-A.; Belhacene, N.; Puissant, A.; Colosetti, P.; Robert, G.; Jacquiel, A.; Mari, B.; Auberger, P.; Luciano, F. The Small Heat Shock Protein B8 (HSPB8) Confers Resistance to Bortezomib by Promoting Autophagic Removal of Misfolded Proteins in Multiple Myeloma Cells. *Oncotarget* **2014**, *5* (15), 6252–6266. <https://doi.org/10.18632/oncotarget.2193>.
- (80) Orłowski, M.; Cardozo, C.; Hidalgo, M. C.; Michaud, C. Regulation of the Peptidylglutamyl-Peptide Hydrolyzing Activity of the Pituitary Multicatalytic Proteinase Complex. *Biochemistry* **1991**, *30* (24), 5999–6005. <https://doi.org/10.1021/bi00238a025>.
- (81) Kisselev, A. F.; van der Linden, W. A.; Overkleeft, H. S. Proteasome Inhibitors: An Expanding Army Attacking a Unique Target. *Chemistry & Biology* **2012**, *19* (1), 99–115. <https://doi.org/10.1016/j.chembiol.2012.01.003>.
- (82) Nakajima, S.; Kato, H.; Takahashi, S.; Johno, H.; Kitamura, M. Inhibition of NF- $\kappa$ B by MG132 through ER Stress-Mediated Induction of LAP and LIP. *FEBS Letters* **2011**, *585* (14), 2249–2254. <https://doi.org/10.1016/j.febslet.2011.05.047>.
- (83) Crawford, L. J. A.; Walker, B.; Ovaa, H.; Chauhan, D.; Anderson, K. C.; Morris, T. C. M.; Irvine, A. E. Comparative Selectivity and Specificity of the Proteasome Inhibitors BzLLLCOCHO, PS-341, and MG-132. *Cancer Research* **2006**, *66* (12), 6379–6386. <https://doi.org/10.1158/0008-5472.CAN-06-0605>.
- (84) Dou, Q.; Zonder, J. Overview of Proteasome Inhibitor-Based Anti-Cancer Therapies: Perspective on Bortezomib and Second Generation Proteasome Inhibitors versus Future Generation Inhibitors of Ubiquitin-Proteasome System. *Current Cancer Drug Targets* **2014**, *14* (6), 517–536. <https://doi.org/10.2174/1568009614666140804154511>.
- (85) Selimovic, D.; Porzig, B. B. O. W.; El-Khattouti, A.; Badura, H. E.; Ahmad, M.; Ghanjati, F.; Santourlidis, S.; Haikel, Y.; Hassan, M. Bortezomib/Proteasome Inhibitor Triggers Both Apoptosis and Autophagy-Dependent Pathways in Melanoma Cells. *Cellular Signalling* **2013**, *25* (1), 308–318. <https://doi.org/10.1016/j.cellsig.2012.10.004>.

- (86) Chen, D.; Frezza, M.; Schmitt, S.; Kanwar, J.; P. Dou, Q. Bortezomib as the First Proteasome Inhibitor Anticancer Drug: Current Status and Future Perspectives. *Current Cancer Drug Targets* **2011**, *11* (3), 239–253. <https://doi.org/10.2174/156800911794519752>.
- (87) Hasinoff, B. B.; Patel, D.; Wu, X. Molecular Mechanisms of the Cardiotoxicity of the Proteasomal-Targeted Drugs Bortezomib and Carfilzomib. *Cardiovascular Toxicology* **2017**, *17* (3), 237–250. <https://doi.org/10.1007/s12012-016-9378-7>.
- (88) Jerkins, J. Bortezomib-Induced Severe Congestive Heart Failure. *Cardiol* **2010**. <https://doi.org/10.4021/cr105e>.
- (89) Orciuolo, E.; Buda, G.; Cecconi, N.; Galimberti, S.; Versari, D.; Cervetti, G.; Salvetti, A.; Petrini, M. Unexpected Cardiotoxicity in Haematological Bortezomib Treated Patients. *British Journal of Haematology* **2007**, *138* (3), 396–397. <https://doi.org/10.1111/j.1365-2141.2007.06659.x>.

## CHAPTER 5. CONCLUSION AND FUTURE DIRECTIONS.

### 5.1 General conclusion.

The ubiquitin-proteasome system is responsible for protein recycling and maintaining proper protein balance in cells.<sup>1,2</sup> According to research, this system is responsible for more than 80% of cellular protein recycling.<sup>3,4</sup> Besides regulating protein balance in cells, the UPS is also tightly related to immune response as some partially degraded protein fragments will be presented on MHC-I complexes for immune cell examination.<sup>5-7</sup>

Since the UPS is responsible for most protein recycling in cells, abnormal protein regulation in cells could trigger severe consequences such as tumorigenesis.<sup>8-10</sup> In response to elevated expression of transcriptional proteins in tumor cells, rapid degradation of these proteins by UPS is required to avoid cell apoptosis. Therefore, researchers have begun to investigate the use of small molecules to inhibit proteasome activities to treat cancer. Bortezomib,<sup>11-13</sup> carfilzomib<sup>14,15</sup> and ixazomib<sup>16,17</sup> were approved by FDA for multiple myeloma treatment. All these small molecules interact with the same enzymatic subunit of the 20S CP and inhibit proteasome from hydrolyzing its substrates. However, drug resistance has been observed among patients administering these proteasome inhibitors.<sup>18-20</sup> To develop new proteasome inhibitors and avoid current drug resistance, researchers have also been looking into other subunits of the proteasome.

The subunits on the 19S regulatory particle (RP) also significantly contribute to the activity of the 26S proteasome.<sup>21-24</sup> Small molecule inhibitors have been developed to inhibit the activities of some subunits of the 19S RP. Rpn-10 and Rpn-13 are ubiquitin receptors of the 26S proteasome but Rpn-13 is a nonessential subunit of the 19S RP in normal cells.<sup>25-27</sup> However, it is crucial for hematological cancer cells like multiple myeloma.<sup>28,29</sup> Inhibiting Rpn-13 function with a small molecule could prevent it from recognizing poly-ubiquitinated protein and eventually affect proteasome activity.<sup>28</sup> Rpt-4 is a subunit of the ATPase ring of the 19S RP.<sup>30,31</sup> Inhibiting this subunit could prevent the translocation of the target peptide and gate opening of the 20S CP and affect proteasome activity.<sup>32</sup> There are other subunits on the 19S RP that are crucial for proteasome function like the de-ubiquitinase subunit Rpn-11,<sup>25,33-36</sup> molecular clamp subunit Rpn-6,<sup>37,38</sup> protein-protein interaction platform subunits Rpn-1 and Rpn-2.<sup>39,40</sup> While these subunits are

attractive for small molecule binder development, little or none molecule binders were reported. The lack of detailed understanding and enzymatic pocket of these subunits make small molecule binder development on these subunits difficult. Even though, more and more research are directed to better understand the subunits in 19S RP and small molecules are developed to inhibit the subunits on the 19S RP because 19S RP is considered as a vital component of the proteasome for its assistant function on the 20S CP.

Among the 19S RP subunits, we noticed that Rpn-6 is a crucial proteasome subunit for structural integrity of the 26S proteasome and presents multiple protein-protein interactions with other proteasome subunits including Rpn-5, Rpn-7 and  $\alpha 2$  subunits.<sup>37,38,41,42</sup> Phosphorylation of Ser14 on Rpn-6 boosts proteasome activity by enhancing the formation of the 30S proteasome to clear short-lived proteins.<sup>43</sup> Rpn-6 is also upregulated in some cancer cells, making Rpn-6 a potential target for drug development.<sup>43,44</sup> Since Rpn-6 makes multiple protein-protein interactions with other proteasomal subunits, we hypothesized that using a small molecule binder of Rpn-6 to interact with Rpn-6 will disrupt the protein-protein interaction of Rpn-6 with other subunits and eventually decrease proteasome activity in cells.

Based on the hypothesis, we started our research on developing a one-bead-one-compound (OBOC) peptoid library for screening.<sup>45-47</sup> By combing OBOC library with thermal shift assay, we discovered potential small molecules that can bind with Rpn-6 *in vitro*.<sup>48-51</sup> We reconstructed some small molecules based on the result from the screening and tested their binding affinity toward Rpn-6 *in vitro* using fluorescence polarization assay.<sup>52-55</sup> TXS-8 was discovered from the screening as the best small molecule binder of Rpn-6. *N*-methylamine scan on TXS-8 generated TXS-13/14/15 and these three derivatives revealed all amines presented on TXS-8 were essential for its binding towards Rpn-6. Further structural study on TXS-8 indicated that adding linear side chain amines on the C-terminal of TXS-8 like ethylenediamine was tolerated, although no significant binding affinity improvement was observed. By modifying TXS-8, we later converted the small molecule into a covalent cross-linking binder upon UV treatment. Our covalent pull-down experiment in purified Rpn-6 and Ramos B-cell lysate all indicated that TXS-8 was selective towards Rpn-6. Proteomic analysis on the covalent pull-down experiment validated Rpn-6 as the major target of TXS-8.<sup>56</sup>

The discovery of selective binder of Rpn-6, TXS-8, provided us a tool to study the subunit. Since Rpn-6 was overexpressed in some hematological cancer cells like multiple myeloma and

Ramos B-cell, we wanted to investigate the toxicity of TXS-8 in these cell lines. As we expected, TXS-8 showed moderate toxicity in both multiple myeloma and Ramos B-cells with an  $IC_{50}$  of 14  $\mu$ M. We also investigated dual dosing TXS-8 in multiple myeloma and Ramos B-cells with proteasome inhibitor bortezomib and Rpn-13 inhibitor KDT-11. However, no significant improved toxicity was observed regarding either bortezomib or KDT-11. We were unable to determine if TXS-8 could serve additive or synergistic effect with the above inhibitors.

To study the cause of cell death when dosed with TXS-8, we started some preliminary research on the effect of TXS-8 on proteasome activity. Using commercially available probe Suc-LLVY-AMC, we tested the impact of TXS-8 with purified 26S proteasome and Ramos B-cell lysate.<sup>57-61</sup> However, TXS-8 showed no significantly effect on proteasome activity in either experiments. We also investigated the K-48 polyubiquitinated protein accumulations in Ramos B-cells when treated with non-lethal concentration of TXS-8.<sup>62-67</sup> No significant difference was observed with TXS-8 treated and DMSO treated cells regarding the relative amount of K-48 polyubiquitinated protein. However, we observed a significant proteasome activity decrease in proteasome activity biochemical assay where we replaced Suc-LLVY-AMC probe with a FRET probe developed by our lab.<sup>68</sup> The inconsistency of experimental results required us to develop sensitive cell permeable probes to directly monitor proteasome activity in cells.

Our lab later developed a series of rhodamine-based proteasome probes that were selective for the chymotrypsin-like activity on the 20S CP. These probes were more sensitive comparing to the commercially available AMC probes and were cell-permeable that allowed us to monitor proteasome activity in living cells.<sup>69,70</sup> By combining previous reported methods of using proteasome activity changes using fluorescence probes and examining protein degradation in cells to monitor proteasome activity changes, we developed a three-step general workflow to investigate if a small molecule could affect proteasome activity using TXS-8 as example.<sup>71-74</sup> We first knocked down Rpn-6 expression in HEK-293T cells using a small silencing RNA and observed a 65% Rpn-6 expression decrease. When we compared the hydrolysis rate of the rhodamine-based proteasome probe between Rpn-6 knocked down HEK-293T cells and normal HEK-293T cells, a 15% decrease was observed with the Rpn-6 knocked down cells. However, when we treated the HEK-293T cells with non-lethal concentration of TXS-8, no significant proteasome activity changes were observed in either Rpn-6 knocked down or normal cells using the rhodamine-based probe. In the second step of workflow, we investigated the degradation of a full-length protein in

cells and GFP was selected. GFP was reported to be degraded by the UPS.<sup>75</sup> We transfected HEK-293T cells with GFP and knocked down Rpn-6 in these cells. We examined the relative GFP amount in these HEK-293T cells treated with DMSO and non-lethal concentration of TXS-8. Similar to what we observed previously, TXS-8 did not significantly change the degradation of GFP in either Rpn-6 knocked down or normal HEK-293T cell lines. The last step in the workflow involved investigating proteasome activity changes using rhodamine-based probe in primary cells lines as some were more sensitive towards proteasome activity inhibition like heart cells.<sup>76,77</sup> Like what we have observed in the first two steps, when we treated the AC16 cardiomyocyte cells with non-lethal concentration of TXS-8, no significant proteasome activity changes were observed. All three steps in the workflow demonstrated the same conclusion that TXS-8 did not alter proteasome activity at non-lethal concentrations. Meanwhile, the consistent result from these assays validated the reliability of the workflow and the processes are also amenable for the evaluation of small molecule binders to other proteasome subunits of interest in the future.

The conclusion that TXS-8 may not affect proteasome activity at non-lethal concentration raised multiple questions: Can we improve the toxicity of TXS-8 in Rpn-6 overexpressed cancer cells? Can we find the binding site of TXS-8 on Rpn-6? To address these questions, we designed and performed multiple researches to further investigate TXS-8.

To improve the toxicity of TXS-8 in Rpn-6 overexpressed cells and provide guidance for structural optimization in the future to increase potency, we wanted to investigate the general binding pocket of TXS-8 on Rpn-6 and developing TXS-8-based PROTACs.<sup>78-80</sup> Besides studying TXS-8, we also wanted to explore the development of new sensitive cell permeable proteasome probes to monitor the caspase-like and trypsin-like activities on the 20S CP because we did not investigate the impact of TXS-8 on these two subunits due to the availability of only chymotrypsin-like probes by the time the three-step workflow was designed.

To develop TXS-8-based PROTACs, we decided to use thalidomide and pomalidomide as E3 ligand to recruit CRBN. A derivative of thalidomide and pomalidomide were synthesized for coupling and we incorporated them to TXS-8. Since the linker of PROTAC mattered on target protein degradation, we chose to use varying length linker for our PROTAC development.<sup>81,82</sup> After we acquired all PROTACs, we performed a viability assay in Ramos B-cells with TXS-8-based PROTACs. However, after 24 hours of dosing, none of the PROTACs induced significant cell death in Ramos B-cells. We also investigated if the PROTAC can sufficiently induce Rpn-6

degradation in cells and we treated Ramos B-cell with varying concentrations of TWT-4 and TWT-5. We monitored the relative Rpn-6 amount in these cells and compared them accordingly with DMSO treated cells. No significant Rpn-6 degradation was observed in either PROTAC treated Ramos B-cells. The above experiments indicated a failure on TXS-8-based PROTAC development. We concluded that the PROTACs were either cell impermeable that could not reach its target, the PROTACs were unable to induce a stable ternary complex between Rpn-6 and CRBN, or Rpn-6 in cells was mostly integrated on the 19S RP while ubiquitination of Rpn-6 on the 19S RP could not trigger protein degradation.

When we were developing PROTACs for TXS-8, we were also investigating the general binding site of TXS-8 on Rpn-6. Discovering the general binding site of TXS-8 on Rpn-6 could greatly benefit our future structural optimization of TXS-8 to increase potency. It can also benefit our future TXS-8-based PROTAC development as computational methods have been used to facilitate the development of PROTACs to optimize the linker length and predict the orientation between the E3 ligase and the target protein.<sup>83,84</sup> However, due the availability of instrument access, we decided to use cross-linking technique to investigate the general binding site of TXS-8 on Rpn-6.<sup>85,86</sup> We came up with two approaches to investigate the binding site of TXS-8. In our first approach, Dzn-TXS-8-FP was covalently cross-linked to Rpn-6 first and the excess ligand was removed by SDS-PAGE. The protein was trypsin digested and HPLC was used to separate peptide fragments. We collected the fractions showing fluorescence signal during HPLC and submitted these samples to Purdue Proteomic Facility for LC-MS/MS and MALDI-TOF MS/MS analysis. However, we only observed MS peaks for unlabeled peptide fragments from trypsin digestion.

In our second approach of TXS-8 binding site investigation, we decided to perform a pull-down assay on digested Rpn-6 peptide. The protein was first cross-linked with alkyne-Dzn-TXS-8 and the protein was then trypsin digested. A cleavable biotin probe was added onto the peptide fragment carrying TXS-8 via click chemistry. A pull-down experiment was performed to enrich the biotinylated peptide fragment and these fragments were later submitted for LC-MS/MS or MALDI-TOF MS/MS analysis.

As mentioned previously, we were also developing sensitive proteasome probes to monitor the caspase-like and trypsin-like activities on the 20S CP. Combining commercially available AMC probes and rhodamine-based probes our lab previously developed, we designed LLE-Rh and LLR-Rh probes for the 20S CP caspase-like and trypsin-like activities. We compared these probes with

their corresponding AMC probes and the result showed the rhodamine-based probes were more sensitive on proteasome hydrolysis and required less amount to be observed with significant fluorescence signal. Further proteasome inhibitor MG-132 and bortezomib experiment validated that inhibiting proteasome activity also significantly decreased the hydrolysis rate of these probes. We concluded that the development of new proteasome probes could greatly benefit the discovery of other potential small molecule proteasome regulators.

## **5.2 Future directions.**

### **5.2.1 Future directions regarding TXS-8 toxicity evaluation.**

We mentioned that we were unable to determine if TXS-8 served as additive or synergistic effect with combined with other small molecules like bortezomib or KDT-11. However, we used a constant concentration of TXS-8 during our dual dosing experiment. To fully investigate the dual dosing effect of TXS-8 with other small molecules, various concentrations of TXS-8 showed be included in the experiment. To better understand how TXS-8 induced toxicity in Rpn-6 overexpressing cells, investigating the cell permeability of TXS-8 is also important. The calculated cLogP of TXS-8 is greater than 7 which is above the upper limit of Lipinski rule.<sup>87</sup> A potential poor permeability of TXS-8 may result the small molecule accumulation on the membrane surface. Therefore, optimization of the small molecule is necessary to improve the permeability and potency.<sup>88</sup> To investigate the cause of cell death, we can use flow cytometry to investigate if TXS-8 can induce apoptosis in Rpn-6 overexpressed cancer cells like Ramos B-cells or multiple myeloma cells.<sup>89,90</sup>

### **5.2.2 Future directions regarding TXS-8 PROTAC development.**

Although we early conclude that the thalidomide and pomalidomide based TXS-8 PROTACs are not working as expected, developing bifunctional molecules to disrupt target protein is still a trend of future molecule development.<sup>91-93</sup> There are small molecules that can recruit protein kinase to phosphorylate target protein to regulate their function.<sup>93,94</sup> To better develop TXS-8-based PROTACs, understanding the localization of Rpn-6 is crucial. Previously, a RA190 based PROTAC for Rpn-13 was described to sufficiently degrade Rpn-13 in cells and reduced tumor size *in vivo*.<sup>95</sup> The Rpn-13 PROTAC indicated proteasome subunit as potential

subunits for PROTAC development. However, Rpn-13 was a ubiquitin receptor subunit located on the top surface of 19S RP. Cryo-EM study also revealed that Rpn-13 might be the most extended subunit from the 19S RP lid.<sup>39,96</sup> Unlike Rpn-6 buried deep in the 19S RP, Rpn-13 was released after the substrate was delivered to the 20S CP to avoid unspecific degradation of free ubiquitin and other ubiquitinated proteins.<sup>23</sup> Therefore, free Rpn-13 in cell can be captured by the PROTAC and be degraded by the proteasome. Currently, no literature has reported the localization of Rpn-6. If Rpn-6 mainly exists in the 19S RP, ubiquitination of Rpn-6 may not be able to induce protein degradation as Rpn-6 is tightly bound to the 19S RP. Besides, the giant size of 19S RP may also block the approach of E3 ligase for sufficient ubiquitination which could also potentially explained our previous observation that the PROTACs we developed failed to induce Rpn-6 degradation in Ramos B-cells.

To investigate the localization of Rpn-6, a pull-down experiment could be applied. Cell lysate will be treated first with BMCC-BDzn-TXS-8 for covalent cross-linking. The biotinylated protein will then be pulled down using streptavidin magnetic beads. Both SDS-PAGE and native gel will be performed on the eluent from pull-down experiment. Immunoblot will be performed to blot Rpn-6 and Rpn-5/7/2 (or other subunits on 19S RP). In denatured immunoblot, we will be comparing the protein amounts among Rpn-6 and other 19S RP subunits to estimate if Rpn-6 is overly expressed than other subunits because one 19S RP contains only one of each subunit. In native immunoblot, we will be comparing the protein amounts between Rpn-6 in 19S RP and free Rpn-6 to estimate the bound and unbound Rpn-6 ratio. With the above two experiments, we will be able to estimate the relative amount of Rpn-6 bound to 19S RP and free Rpn-6. If Rpn-6 mainly exists only in 19S RP, development of Rpn-6 PROTAC should be suspended. However, if Rpn-6 exists mainly in unbound form, we should continue our research on Rpn-6 PROTAC development. We could either using other E3 ligase like VHL,<sup>81,97–101</sup> extending the dosing time from 24 hours to 6 days with continuous viability and Rpn-6 degradation monitoring or use FRET pairs to construct labeled E3 ligase and target protein to investigate the proximity of the target protein and E3 ligase.<sup>102–104</sup>

### **5.2.3 Future directions regarding TXS-8 binding site study.**

Currently we have not acquired meaningful data from the binding site study. The first approach is cost-effective but co-elution of unlabeled peptide fragment consistently contaminate

our sample making later analysis difficult. The second approach is more promising as the pull-down step serves as both separation and enrichment step. However, we have not reached the final step yet. We are currently optimizing the cross-linking conditions with better UV instrument and reducing the salt presented in samples by using less buffer in the whole experiment. The extra salt brought by buffer in the cross-linking step changed the buffer composition during trypsin digestion step and makes the result uncertain. We are also uncertain if streptavidin will be hydrolyzed during the pull-down step due to the leftover trypsin after protein digestion. Despite the potential difficulties on the second approach, we still want to implement the workflow for once. Currently our lab has brought a new UV instrument for cross-linking and we have worked out click-chemistry conditions with high yield. To reduce the amount of salt in the process, we plan to perform SDS-PAGE to remove the salt and excess unbound alkyne-Dzn-TXS-8 from Rpn-6 after the cross-linking step and perform in-gel trypsin digestion to maximize digestion efficiency.

### **5.3 Final conclusion.**

Proteasome is a crucial component in cells to maintain the protein balance and it is made up with a 20S CP and a 19S RP. Dysregulation of proteasome could lead to various diseases such as tumorigenesis. Developing novel small molecules to inhibit the enzymatic subunit on the proteasome has been proven to be efficient on treating cancers with high proteasome activities. However, drug resistance observed among patients administrating current proteasome inhibitors indicates that new molecules are required to facilitate current known proteasome inhibitors. 19S RP serves to facilitate the function of the 20S CP and it is critical to initialize ubiquitin-dependent proteasome degradation. Various subunits exist on 19S RP with different functions. Inhibiting the function of these proteasome subunits with a small molecule is a promising field of research as no inhibitors have been approved by FDA. However, since most of the subunits on 19S RP does not present enzymatic function, it is very difficult to target these subunits. In this work, we demonstrated the workflow of using a OBOC library combining with other techniques like thermal shift and fluorescence polarization assay to discover a selective binder of proteasomal subunit Rpn-6. We demonstrated how we validated the target of TXS-8 and its impact on proteasome activity. We believe that demonstrating our work could provide ideas to investigate other proteasome subunits that currently have not been studied yet. Developing new molecules of proteasome can not only help us to understand the proteasome, but also provides us different tools

to study proteasome related diseases. We believe with the effort of ours and other researchers', we will make rapid progress in proteasome small molecule binder discovery that can regulate proteasome activity to treat diseases.

#### 5.4 Reference.

- (1) Fuertes, G.; Villarroya, A.; Knecht, E. Role of Proteasomes in the Degradation of Short-Lived Proteins in Human Fibroblasts under Various Growth Conditions. *The International Journal of Biochemistry & Cell Biology* **2003**, 35 (5), 651–664. [https://doi.org/10.1016/S1357-2725\(02\)00382-5](https://doi.org/10.1016/S1357-2725(02)00382-5).
- (2) Ciechanover, A.; Schwartz, A. L. The Ubiquitin-Proteasome Pathway: The Complexity and Myriad Functions of Proteins Death. *Proceedings of the National Academy of Sciences* **1998**, 95 (6), 2727–2730. <https://doi.org/10.1073/pnas.95.6.2727>.
- (3) Ciechanover, A. The Ubiquitin-Proteasome Proteolytic Pathway. *Cell* **1994**, 79 (1), 13–21. [https://doi.org/10.1016/0092-8674\(94\)90396-4](https://doi.org/10.1016/0092-8674(94)90396-4).
- (4) Bedford, L.; Paine, S.; Sheppard, P. W.; Mayer, R. J.; Roelofs, J. Assembly, Structure, and Function of the 26S Proteasome. *Trends in Cell Biology* **2010**, 20 (7), 391–401. <https://doi.org/10.1016/j.tcb.2010.03.007>.
- (5) Kloetzel, P.-M. The Proteasome and MHC Class I Antigen Processing. *Biochimica et Biophysica Acta (BBA) - Molecular Cell Research* **2004**, 1695 (1–3), 225–233. <https://doi.org/10.1016/j.bbamcr.2004.10.004>.
- (6) Leone, P.; Shin, E.-C.; Perosa, F.; Vacca, A.; Dammacco, F.; Racanelli, V. MHC Class I Antigen Processing and Presenting Machinery: Organization, Function, and Defects in Tumor Cells. *JNCI Journal of the National Cancer Institute* **2013**, 105 (16), 1172–1187. <https://doi.org/10.1093/jnci/djt184>.
- (7) Sijts, E. J. A. M.; Kloetzel, P.-M. The Role of the Proteasome in the Generation of MHC Class I Ligands and Immune Responses. *Cell. Mol. Life Sci.* **2011**, 68 (9), 1491–1502. <https://doi.org/10.1007/s00018-011-0657-y>.
- (8) Klaunig, J. E.; Wang, Z. Oxidative Stress in Carcinogenesis. *Current Opinion in Toxicology* **2018**, 7, 116–121. <https://doi.org/10.1016/j.cotox.2017.11.014>.
- (9) Haase, V. H. The VHL/HIF Oxygen-Sensing Pathway and Its Relevance to Kidney Disease. *Kidney International* **2006**, 69 (8), 1302–1307. <https://doi.org/10.1038/sj.ki.5000221>.
- (10) Reuter, S.; Gupta, S. C.; Chaturvedi, M. M.; Aggarwal, B. B. Oxidative Stress, Inflammation, and Cancer: How Are They Linked? *Free Radical Biology and Medicine* **2010**, 49 (11), 1603–1616. <https://doi.org/10.1016/j.freeradbiomed.2010.09.006>.

- (11) Dou, Q.; Zonder, J. Overview of Proteasome Inhibitor-Based Anti-Cancer Therapies: Perspective on Bortezomib and Second Generation Proteasome Inhibitors versus Future Generation Inhibitors of Ubiquitin-Proteasome System. *Current Cancer Drug Targets* **2014**, *14* (6), 517–536. <https://doi.org/10.2174/1568009614666140804154511>.
- (12) Selimovic, D.; Porzig, B. B. O. W.; El-Khattouti, A.; Badura, H. E.; Ahmad, M.; Ghanjati, F.; Santourlidis, S.; Haikel, Y.; Hassan, M. Bortezomib/Proteasome Inhibitor Triggers Both Apoptosis and Autophagy-Dependent Pathways in Melanoma Cells. *Cellular Signalling* **2013**, *25* (1), 308–318. <https://doi.org/10.1016/j.cellsig.2012.10.004>.
- (13) Chen, D.; Frezza, M.; Schmitt, S.; Kanwar, J.; P. Dou, Q. Bortezomib as the First Proteasome Inhibitor Anticancer Drug: Current Status and Future Perspectives. *Current Cancer Drug Targets* **2011**, *11* (3), 239–253. <https://doi.org/10.2174/156800911794519752>.
- (14) Arastu-Kapur, S.; Anderl, J. L.; Kraus, M.; Parlatti, F.; Shenk, K. D.; Lee, S. J.; Muchamuel, T.; Bennett, M. K.; Driessen, C.; Ball, A. J.; Kirk, C. J. Nonproteasomal Targets of the Proteasome Inhibitors Bortezomib and Carfilzomib: A Link to Clinical Adverse Events. *Clin Cancer Res* **2011**, *17* (9), 2734–2743. <https://doi.org/10.1158/1078-0432.CCR-10-1950>.
- (15) Berenson, J. R.; Hilger, J. D.; Yellin, O.; Dichmann, R.; Patel-Donnelly, D.; Boccia, R. V.; Bessudo, A.; Stampleman, L.; Gravenor, D.; Eshaghian, S.; Nassir, Y.; Swift, R. A.; Vescio, R. A. Replacement of Bortezomib with Carfilzomib for Multiple Myeloma Patients Progressing from Bortezomib Combination Therapy. *Leukemia* **2014**, *28* (7), 1529–1536. <https://doi.org/10.1038/leu.2014.27>.
- (16) Moreau, P.; Masszi, T.; Grzasko, N.; Bahlis, N. J.; Hansson, M.; Pour, L.; Sandhu, I.; Ganly, P.; Baker, B. W.; Jackson, S. R.; Stoppa, A.-M.; Simpson, D. R.; Gimsing, P.; Palumbo, A.; Garderet, L.; Cavo, M.; Kumar, S.; Touzeau, C.; Buadi, F. K.; Laubach, J. P.; Berg, D. T.; Lin, J.; Di Bacco, A.; Hui, A.-M.; van de Velde, H.; Richardson, P. G. Oral Ixazomib, Lenalidomide, and Dexamethasone for Multiple Myeloma. *New England Journal of Medicine* **2016**, *374* (17), 1621–1634. <https://doi.org/10.1056/NEJMoa1516282>.
- (17) Al-Salama, Z. T.; Garnock-Jones, K. P.; Scott, L. J. Ixazomib: A Review in Relapsed and/or Refractory Multiple Myeloma. *Targ Oncol* **2017**, *12* (4), 535–542. <https://doi.org/10.1007/s11523-017-0504-7>.
- (18) Lü, S.; Wang, J. The Resistance Mechanisms of Proteasome Inhibitor Bortezomib. *Biomarker Research* **2013**, *1* (1). <https://doi.org/10.1186/2050-7771-1-13>.
- (19) Oerlemans, R.; Franke, N. E.; Assaraf, Y. G.; Cloos, J.; van Zantwijk, I.; Berkers, C. R.; Scheffer, G. L.; Debipersad, K.; Vojtekova, K.; Lemos, C.; van der Heijden, J. W.; Ylstra, B.; Peters, G. J.; Kaspers, G. L.; Dijkmans, B. A. C.; Scheper, R. J.; Jansen, G. Molecular Basis of Bortezomib Resistance: Proteasome Subunit B5 (PSMB5) Gene Mutation and Overexpression of PSMB5 Protein. *Blood* **2008**, *112* (6), 2489–2499. <https://doi.org/10.1182/blood-2007-08-104950>.

- (20) Yang, W.-C.; Lin, S.-F. Mechanisms of Drug Resistance in Relapse and Refractory Multiple Myeloma. *BioMed Research International* **2015**, 2015, 1–17. <https://doi.org/10.1155/2015/341430>.
- (21) Lander, G. C.; Martin, A.; Nogales, E. The Proteasome under the Microscope: The Regulatory Particle in Focus. *Current Opinion in Structural Biology* **2013**, 23 (2), 243–251. <https://doi.org/10.1016/j.sbi.2013.02.004>.
- (22) Rosenzweig, R.; Osmulski, P. A.; Gaczynska, M.; Glickman, M. H. The Central Unit within the 19S Regulatory Particle of the Proteasome. *Nat Struct Mol Biol* **2008**, 15 (6), 573–580. <https://doi.org/10.1038/nsmb.1427>.
- (23) Ehlinger, A.; Walters, K. J. Structural Insights into Proteasome Activation by the 19S Regulatory Particle. *Biochemistry* **2013**, 52 (21), 3618–3628. <https://doi.org/10.1021/bi400417a>.
- (24) Tanaka, K. The Proteasome: Overview of Structure and Functions. *Proceedings of the Japan Academy, Series B* **2009**, 85 (1), 12–36. <https://doi.org/10.2183/pjab.85.12>.
- (25) Smalle, J.; Kurepa, J.; Yang, P.; Emborg, T. J.; Babiyshuk, E.; Kushnir, S.; Vierstra, R. D. The Pleiotropic Role of the 26S Proteasome Subunit RPN10 in Arabidopsis Growth and Development Supports a Substrate-Specific Function in Abscissic Acid Signaling. *The Plant Cell* **2003**, 15 (4), 965–980. <https://doi.org/10.1105/tpc.009217>.
- (26) Keren-Kaplan, T.; Zeev Peters, L.; Levin-Kravets, O.; Attali, I.; Kleifeld, O.; Shohat, N.; Artzi, S.; Zucker, O.; Pilzer, I.; Reis, N.; Glickman, M. H.; Ben-Aroya, S.; Prag, G. Structure of Ubiquitylated-Rpn10 Provides Insight into Its Autoregulation Mechanism. *Nat Commun* **2016**, 7 (1), 12960. <https://doi.org/10.1038/ncomms12960>.
- (27) Hamazaki, J.; Sasaki, K.; Kawahara, H.; Hisanaga, S.; Tanaka, K.; Murata, S. Rpn10-Mediated Degradation of Ubiquitinated Proteins Is Essential for Mouse Development. *MCB* **2007**, 27 (19), 6629–6638. <https://doi.org/10.1128/MCB.00509-07>.
- (28) Trader, D. J.; Simanski, S.; Kodadek, T. A Reversible and Highly Selective Inhibitor of the Proteasomal Ubiquitin Receptor Rpn13 Is Toxic To Multiple Myeloma Cells. *Journal of the American Chemical Society* **2015**, 137 (19), 6312. <https://doi.org/10.1021/jacs.5b02069>.
- (29) Anchoori, R. K.; Jiang, R.; Peng, S.; Soong, R.; Algethami, A.; Rudek, M. A.; Anders, N.; Hung, C.-F.; Chen, X.; Lu, X.; Kayode, O.; Dyba, M.; Walters, K. J.; Roden, R. B. S. Covalent Rpn13-Binding Inhibitors for the Treatment of Ovarian Cancer. *ACS Omega* **2018**, 3 (9), 11917–11929. <https://doi.org/10.1021/acsomega.8b01479>.
- (30) Bar-Nun, S.; Glickman, M. H. Proteasomal AAA-ATPases: Structure and Function. *Biochimica et Biophysica Acta (BBA) - Molecular Cell Research* **2012**, 1823 (1), 67–82. <https://doi.org/10.1016/j.bbamcr.2011.07.009>.

- (31) Beyer, A. Sequence Analysis of the AAA Protein Family. *Protein Science* **2008**, *6* (10), 2043–2058. <https://doi.org/10.1002/pro.5560061001>.
- (32) Lim, H.-S.; Cai, D.; Archer, C. T.; Kodadek, T. Periodate-Triggered Cross-Linking Reveals Sug2/Rpt4 as the Molecular Target of a Peptoid Inhibitor of the 19S Proteasome Regulatory Particle. 2.
- (33) Anchoori, R. K.; Karanam, B.; Peng, S.; Wang, J. W.; Jiang, R.; Tanno, T.; Orłowski, R. Z.; Matsui, W.; Zhao, M.; Rudek, M. A.; Hung, C.; Chen, X.; Walters, K. J.; Roden, R. B. S. A Bis-Benzylidene Piperidone Targeting Proteasome Ubiquitin Receptor RPN13/ADRM1 as a Therapy for Cancer. *Cancer Cell* **2013**, *24* (6), 791–805. <https://doi.org/10.1016/j.ccr.2013.11.001>.
- (34) Husnjak, K.; Elsasser, S.; Zhang, N.; Chen, X.; Randles, L.; Shi, Y.; Hofmann, K.; Walters, K. J.; Finley, D.; Dikic, I. Proteasome Subunit Rpn13 Is a Novel Ubiquitin Receptor. *Nature* **2008**, *453* (7194), 481–488. <https://doi.org/10.1038/nature06926>.
- (35) Isasa, M.; Katz, E. J.; Kim, W.; Yugo, V.; González, S.; Kirkpatrick, D. S.; Thomson, T. M.; Finley, D.; Gygi, S. P.; Crosas, B. Monoubiquitination of RPN10 Regulates Substrate Recruitment to the Proteasome. *Molecular Cell* **2010**, *38* (5), 733–745. <https://doi.org/10.1016/j.molcel.2010.05.001>.
- (36) Perez, C.; Li, J.; Parlati, F.; Rouffet, M.; Ma, Y.; Mackinnon, A. L.; Chou, T.-F.; Deshaies, R. J.; Cohen, S. M. Discovery of an Inhibitor of the Proteasome Subunit Rpn11. *Journal of Medicinal Chemistry* **2017**, *60* (4), 1343–1361. <https://doi.org/10.1021/acs.jmedchem.6b01379>.
- (37) Santamaría, P. G.; Finley, D.; Ballesta, J. P. G.; Remacha, M. Rpn6p, a Proteasome Subunit from *Saccharomyces Cerevisiae*, Is Essential for the Assembly and Activity of the 26 S Proteasome. *Journal of Biological Chemistry* **2003**, *278* (9), 6687–6695. <https://doi.org/10.1074/jbc.M209420200>.
- (38) Pathare, G. R.; Nagy, I.; Bohn, S.; Unverdorben, P.; Hubert, A.; Korner, R.; Nickell, S.; Lasker, K.; Sali, A.; Tamura, T.; Nishioka, T.; Forster, F.; Baumeister, W.; Bracher, A. The Proteasomal Subunit Rpn6 Is a Molecular Clamp Holding the Core and Regulatory Subcomplexes Together. *Proceedings of the National Academy of Sciences* **2012**, *109* (1), 149–154. <https://doi.org/10.1073/pnas.1117648108>.
- (39) Lu, X.; Nowicka, U.; Sridharan, V.; Liu, F.; Randles, L.; Hymel, D.; Dyba, M.; Tarasov, S. G.; Tarasova, N. I.; Zhao, X. Z.; Hamazaki, J.; Murata, S.; Burke, T. R.; Walters, K. J. Structure of the Rpn13-Rpn2 Complex Provides Insights for Rpn13 and Uch37 as Anticancer Targets. *Nat Commun* **2017**, *8* (1), 15540. <https://doi.org/10.1038/ncomms15540>.

- (40) Shi, Y.; Chen, X.; Elsasser, S.; Stocks, B. B.; Tian, G.; Lee, B.-H.; Shi, Y.; Zhang, N.; de Poot, S. A. H.; Tuebing, F.; Sun, S.; Vannoy, J.; Tarasov, S. G.; Engen, J. R.; Finley, D.; Walters, K. J. Rpn1 Provides Adjacent Receptor Sites for Substrate Binding and Deubiquitination by the Proteasome. *Science* **2016**, *351* (6275), aad9421–aad9421. <https://doi.org/10.1126/science.aad9421>.
- (41) Isono, E.; Saito, N.; Kamata, N.; Saeki, Y.; Toh-e, A. Functional Analysis of Rpn6p, a Lid Component of the 26 S Proteasome, Using Temperature-Sensitive *Rpn6* Mutants of the Yeast *Saccharomyces Cerevisiae*. *Journal of Biological Chemistry* **2005**, *280* (8), 6537–6547. <https://doi.org/10.1074/jbc.M409364200>.
- (42) Lier, S.; Paululat, A. The Proteasome Regulatory Particle Subunit Rpn6 Is Required for Drosophila Development and Interacts Physically with Signalosome Subunit Alien/CSN2. *Gene* **2002**, *298* (2), 109–119. [https://doi.org/10.1016/S0378-1119\(02\)00930-7](https://doi.org/10.1016/S0378-1119(02)00930-7).
- (43) Lokireddy, S.; Kukushkin, N. V.; Goldberg, A. L. CAMP-Induced Phosphorylation of 26S Proteasomes on Rpn6/PSMD11 Enhances Their Activity and the Degradation of Misfolded Proteins. *Proceedings of the National Academy of Sciences* **2015**, *112* (52), E7176–E7185. <https://doi.org/10.1073/pnas.1522332112>.
- (44) Guo, X.; Huang, X.; Chen, M. J. Reversible Phosphorylation of the 26S Proteasome. *Protein Cell* **2017**, *8* (4), 255–272. <https://doi.org/10.1007/s13238-017-0382-x>.
- (45) Lam, K. S.; Lebl, M.; Krcňák, V. The “One-Bead-One-Compound” Combinatorial Library Method. *Chemical Reviews* **1997**, *97* (2), 411–448. <https://doi.org/10.1021/cr9600114>.
- (46) Lam, K. S.; Liu, R.; Miyamoto, S.; Lehman, A. L.; Tuscano, J. M. Applications of One-Bead One-Compound Combinatorial Libraries and Chemical Microarrays in Signal Transduction Research. *Acc. Chem. Res.* **2003**, *36* (6), 370–377. <https://doi.org/10.1021/ar0201299>.
- (47) Liu, T.; Qian, Z.; Xiao, Q.; Pei, D. High-Throughput Screening of One-Bead-One-Compound Libraries: Identification of Cyclic Peptidyl Inhibitors against Calcineurin/NFAT Interaction. *ACS Comb. Sci.* **2011**, *13* (5), 537–546. <https://doi.org/10.1021/co200101w>.
- (48) Grøftehaug, M. K.; Hajizadeh, N. R.; Swann, M. J.; Pohl, E. Protein–Ligand Interactions Investigated by Thermal Shift Assays (TSA) and Dual Polarization Interferometry (DPI). *Acta Crystallogr D Biol Crystallogr* **2015**, *71* (1), 36–44. <https://doi.org/10.1107/S1399004714016617>.
- (49) Jafari, R.; Almqvist, H.; Axelsson, H.; Ignatushchenko, M.; Lundbäck, T.; Nordlund, P.; Molina, D. M. The Cellular Thermal Shift Assay for Evaluating Drug Target Interactions in Cells. *Nature Protocols* **2014**, *9* (9), 2100–2122. <https://doi.org/10.1038/nprot.2014.138>.

- (50) Huynh, K.; Partch, C. L. Analysis of Protein Stability and Ligand Interactions by Thermal Shift Assay. *Current Protocols in Protein Science* **2015**, 79 (1). <https://doi.org/10.1002/0471140864.ps2809s79>.
- (51) Martinez, N. J.; Asawa, R. R.; Cyr, M. G.; Zakharov, A.; Urban, D. J.; Roth, J. S.; Wallgren, E.; Klumpp-Thomas, C.; Coussens, N. P.; Rai, G.; Yang, S.-M.; Hall, M. D.; Marugan, J. J.; Simeonov, A.; Henderson, M. J. A Widely-Applicable High-Throughput Cellular Thermal Shift Assay (CETSA) Using Split Nano Luciferase. *Scientific Reports* **2018**, 8 (1). <https://doi.org/10.1038/s41598-018-27834-y>.
- (52) Hall, M. D.; Yasgar, A.; Peryea, T.; Braisted, J. C.; Jadhav, A.; Simeonov, A.; Coussens, N. P. Fluorescence Polarization Assays in High-Throughput Screening and Drug Discovery: A Review. *Methods Appl. Fluoresc.* **2016**, 4 (2), 022001. <https://doi.org/10.1088/2050-6120/4/2/022001>.
- (53) Jameson, D. M.; Ross, J. A. Fluorescence Polarization/Anisotropy in Diagnostics and Imaging. *Chem. Rev.* **2010**, 110 (5), 2685–2708. <https://doi.org/10.1021/cr900267p>.
- (54) Moerke, N. J. Fluorescence Polarization (FP) Assays for Monitoring Peptide-Protein or Nucleic Acid-Protein Binding. *Current Protocols in Chemical Biology* **2009**, 1 (1), 1–15. <https://doi.org/10.1002/9780470559277.ch090102>.
- (55) Lea, W. A.; Simeonov, A. Fluorescence Polarization Assays in Small Molecule Screening. *Expert Opinion on Drug Discovery* **2011**, 6 (1), 17–32. <https://doi.org/10.1517/17460441.2011.537322>.
- (56) Tian, W.; Trader, D. J. Discovery of a Small Molecule Probe of Rpn-6, an Essential Subunit of the 26S Proteasome. *ACS Chemical Biology* **2020**, 15 (2), 554–561. <https://doi.org/10.1021/acscchembio.9b01019>.
- (57) Leestemaker, Y.; Ovaa, H. Tools to Investigate the Ubiquitin Proteasome System. *Drug Discovery Today: Technologies* **2017**, 26, 25–31. <https://doi.org/10.1016/j.ddtec.2017.11.006>.
- (58) Choi, W. H.; de Poot, S. A. H.; Lee, J. H.; Kim, J. H.; Han, D. H.; Kim, Y. K.; Finley, D.; Lee, M. J. Open-Gate Mutants of the Mammalian Proteasome Show Enhanced Ubiquitin-Conjugate Degradation. *Nat Commun* **2016**, 7 (1), 10963. <https://doi.org/10.1038/ncomms10963>.
- (59) Leestemaker, Y.; de Jong, A.; Witting, K. F.; Penning, R.; Schuurman, K.; Rodenko, B.; Zaal, E. A.; van de Kooij, B.; Laufer, S.; Heck, A. J. R.; Borst, J.; Scheper, W.; Berkers, C. R.; Ovaa, H. Proteasome Activation by Small Molecules. *Cell Chemical Biology* **2017**, 24 (6), 725–736.e7. <https://doi.org/10.1016/j.chembiol.2017.05.010>.
- (60) Thibaut, T. A.; Smith, D. M. A Practical Review of Proteasome Pharmacology. *Pharmacol Rev* **2019**, 71 (2), 170–197. <https://doi.org/10.1124/pr.117.015370>.

- (61) Meng, L.; Mohan, R.; Kwok, B. H. B.; Elofsson, M.; Sin, N.; Crews, C. M. Epoxomicin, a Potent and Selective Proteasome Inhibitor, Exhibits in Vivo Antiinflammatory Activity. *Proceedings of the National Academy of Sciences* **1999**, *96* (18), 10403–10408. <https://doi.org/10.1073/pnas.96.18.10403>.
- (62) Scheffner, M.; Nuber, U.; Huibregtse, J. M. Protein Ubiquitination Involving an E1–E2–E3 Enzyme Ubiquitin Thioester Cascade. *Nature* **1995**, *373* (6509), 81–83. <https://doi.org/10.1038/373081a0>.
- (63) Lecker, S. H.; Goldberg, A. L.; Mitch, W. E. Protein Degradation by the Ubiquitin–Proteasome Pathway in Normal and Disease States. *JASN* **2006**, *17* (7), 1807–1819. <https://doi.org/10.1681/ASN.2006010083>.
- (64) Strous, G. J.; Govers, R. The Ubiquitin-Proteasome System and Endocytosis. **7**.
- (65) Churcher, I. Protac-Induced Protein Degradation in Drug Discovery: Breaking the Rules or Just Making New Ones? *Journal of Medicinal Chemistry* **2018**, *61* (2), 444–452. <https://doi.org/10.1021/acs.jmedchem.7b01272>.
- (66) Ottis, P.; Toure, M.; Cromm, P. M.; Ko, E.; Gustafson, J. L.; Crews, C. M. Assessing Different E3 Ligases for Small Molecule Induced Protein Ubiquitination and Degradation. *ACS Chemical Biology* **2017**, *12* (10), 2570–2578. <https://doi.org/10.1021/acscchembio.7b00485>.
- (67) Swatek, K. N.; Komander, D. Ubiquitin Modifications. *Cell Research* **2016**, *26* (4), 399–422. <https://doi.org/10.1038/cr.2016.39>.
- (68) Coleman, R. A.; Trader, D. J. Development and Application of a Sensitive Peptide Reporter to Discover 20S Proteasome Stimulators. *ACS Combinatorial Science* **2018**, *20* (5), 269–276. <https://doi.org/10.1021/acscombsci.7b00193>.
- (69) Zerfas, B. L.; Coleman, R. A.; Salazar-Chaparro, A. F.; Macatangay, N. J.; Trader, D. J. Fluorescent Probes with Unnatural Amino Acids to Monitor Proteasome Activity in Real-Time. *ACS Chemical Biology* **2020**, *15* (9), 2588–2596. <https://doi.org/10.1021/acscchembio.0c00634>.
- (70) Zerfas, B. L.; Trader, D. J. Monitoring the Immunoproteasome in Live Cells Using an Activity-Based Peptide–Peptoid Hybrid Probe. *J. Am. Chem. Soc.* **2019**, *9*.
- (71) Coleman, R. A.; Trader, D. J. Methods to Discover and Evaluate Proteasome Small Molecule Stimulators. *Molecules* **2019**, *24* (12), 2341. <https://doi.org/10.3390/molecules24122341>.
- (72) Gan, J.; Leestemaker, Y.; Sapmaz, A.; Ovaa, H. Highlighting the Proteasome: Using Fluorescence to Visualize Proteasome Activity and Distribution. *Front. Mol. Biosci.* **2019**, *6*, 14. <https://doi.org/10.3389/fmolb.2019.00014>.

- (73) Zhang, L.; Gurskaya, N. G.; Merzlyak, E. M.; Staroverov, D. B.; Mudrik, N. N.; Samarkina, O. N.; Vinokurov, L. M.; Lukyanov, S.; Lukyanov, K. A. Method for Real-Time Monitoring of Protein Degradation at the Single Cell Level. *BioTechniques* **2007**, *42* (4), 446–450. <https://doi.org/10.2144/000112453>.
- (74) Tian, W.; Maresh, M.; Trader, D. J. Approaches to Evaluate the Impact of a Small Molecule Binder to a Non-catalytic Site of the Proteasome. *ChemBioChem* **2021**, cbic.202100023. <https://doi.org/10.1002/cbic.202100023>.
- (75) Mahieu, E.; Covès, J.; Krüger, G.; Martel, A.; Moulin, M.; Carl, N.; Härtlein, M.; Carlomagno, T.; Franzetti, B.; Gabel, F. Observing Protein Degradation by the PAN-20S Proteasome by Time-Resolved Neutron Scattering. *Biophysical Journal* **2020**, *119* (2), 375–388. <https://doi.org/10.1016/j.bpj.2020.06.015>.
- (76) Hasinoff, B. B.; Patel, D.; Wu, X. Molecular Mechanisms of the Cardiotoxicity of the Proteasomal-Targeted Drugs Bortezomib and Carfilzomib. *Cardiovascular Toxicology* **2017**, *17* (3), 237–250. <https://doi.org/10.1007/s12012-016-9378-7>.
- (77) Orciuolo, E.; Buda, G.; Cecconi, N.; Galimberti, S.; Versari, D.; Cervetti, G.; Salvetti, A.; Petrini, M. Unexpected Cardiotoxicity in Haematological Bortezomib Treated Patients. *British Journal of Haematology* **2007**, *138* (3), 396–397. <https://doi.org/10.1111/j.1365-2141.2007.06659.x>.
- (78) Paiva, S.-L.; Crews, C. M. Targeted Protein Degradation: Elements of PROTAC Design. *Current Opinion in Chemical Biology* **2019**, *50*, 111–119. <https://doi.org/10.1016/j.cbpa.2019.02.022>.
- (79) Cyrus, K.; Wehenkel, M.; Choi, E.-Y.; Han, H.-J.; Lee, H.; Swanson, H.; Kim, K.-B. Impact of Linker Length on the Activity of PROTACs. *Mol. BioSyst.* **2011**, *7* (2), 359–364. <https://doi.org/10.1039/C0MB00074D>.
- (80) Smith, B. E.; Wang, S. L.; Jaime-Figueroa, S.; Harbin, A.; Wang, J.; Hamman, B. D.; Crews, C. M. Differential PROTAC Substrate Specificity Dictated by Orientation of Recruited E3 Ligase. *Nature Communications* **2019**, *10* (1). <https://doi.org/10.1038/s41467-018-08027-7>.
- (81) Bondeson, D. P.; Smith, B. E.; Burslem, G. M.; Buhimschi, A. D.; Hines, J.; Jaime-Figueroa, S.; Wang, J.; Hamman, B. D.; Ishchenko, A.; Crews, C. M. Lessons in PROTAC Design from Selective Degradation with a Promiscuous Warhead. *Cell Chemical Biology* **2018**, *25* (1), 78–87.e5. <https://doi.org/10.1016/j.chembiol.2017.09.010>.
- (82) Scheepstra, M.; Hekking, K. F. W.; van Hijfte, L.; Folmer, R. H. A. Bivalent Ligands for Protein Degradation in Drug Discovery. *Computational and Structural Biotechnology Journal* **2019**, *17*, 160–176. <https://doi.org/10.1016/j.csbj.2019.01.006>.
- (83) Zaidman, D.; Prilusky, J.; London, N. PROsettaC: Rosetta Based Modeling of PROTAC Mediated Ternary Complexes. *J. Chem. Inf. Model.* **2020**, *60* (10), 4894–4903. <https://doi.org/10.1021/acs.jcim.0c00589>.

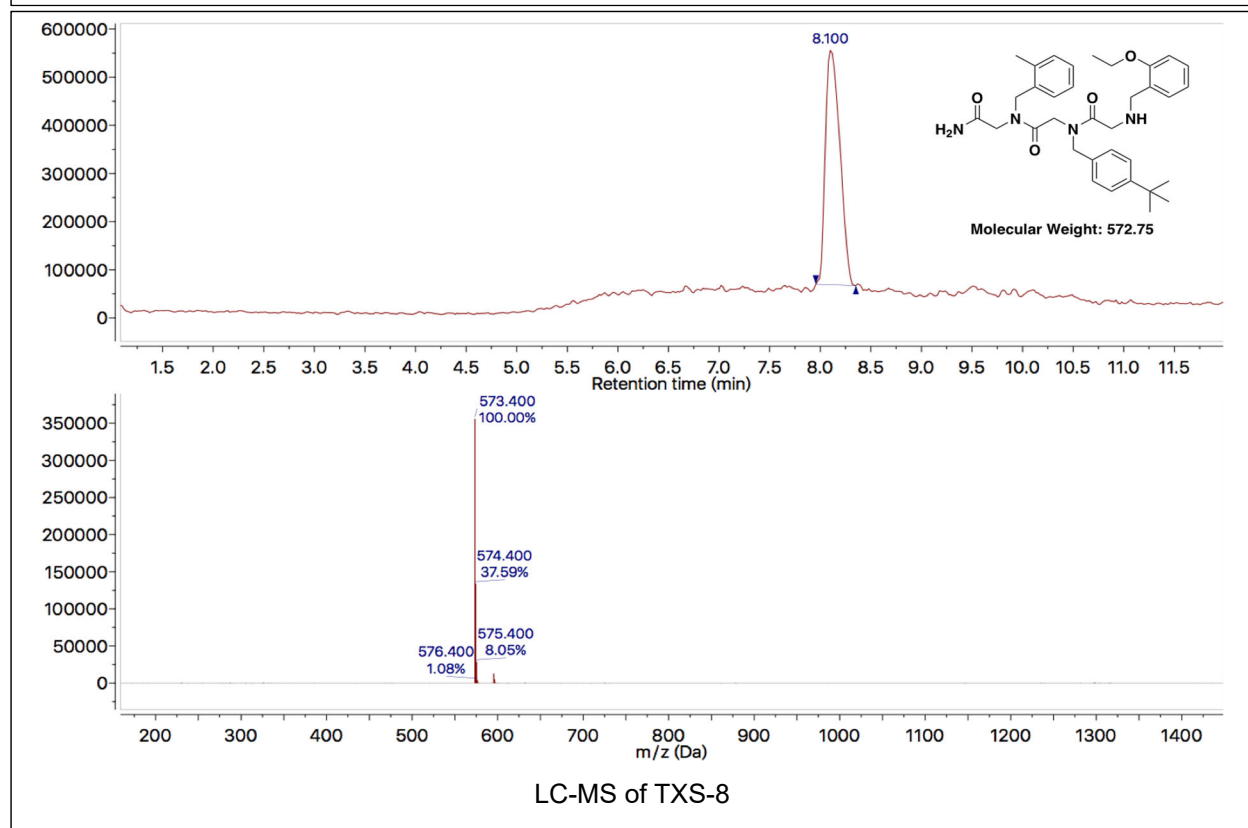
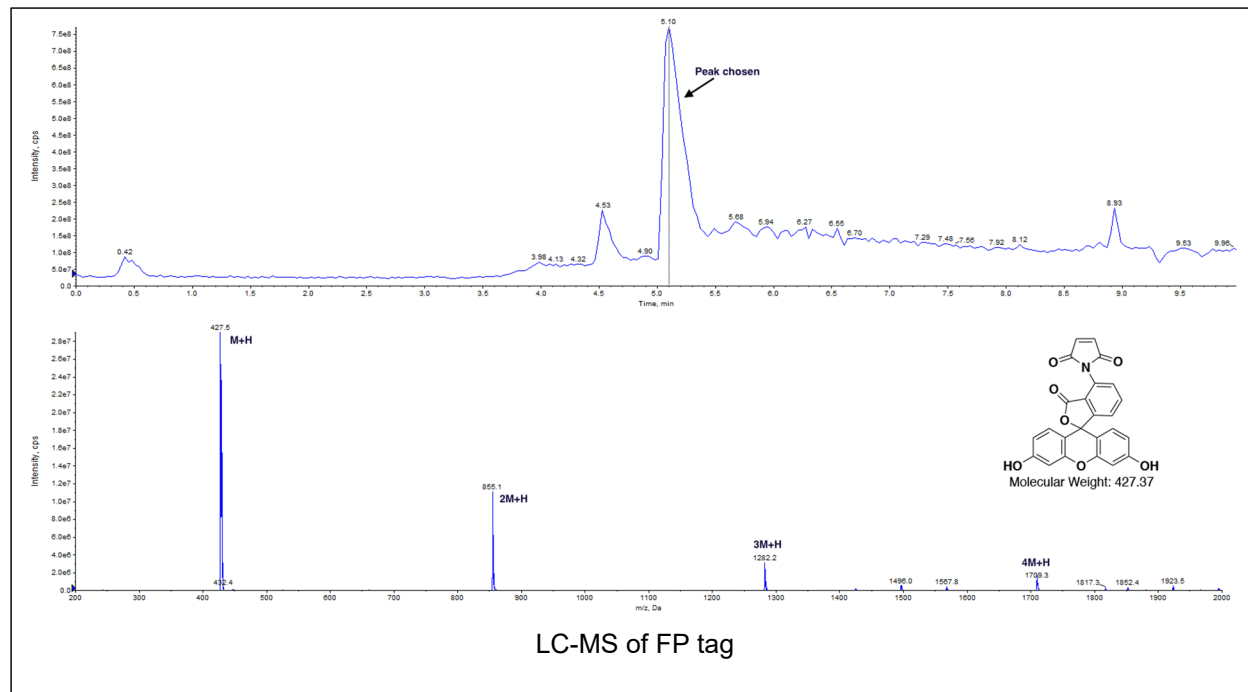
- (84) Drummond, M. L.; Williams, C. I. *In Silico* Modeling of PROTAC-Mediated Ternary Complexes: Validation and Application. *Journal of Chemical Information and Modeling* **2019**, *59* (4), 1634–1644. <https://doi.org/10.1021/acs.jcim.8b00872>.
- (85) Hauser, M.; Qian, C.; King, S. T.; Kauffman, S.; Naider, F.; Hettich, R. L.; Becker, J. M. Identification of Peptide-Binding Sites within BSA Using Rapid, Laser-Induced Covalent Cross-Linking Combined with High-Performance Mass Spectrometry. *J Mol Recognit* **2018**, *31* (2), e2680. <https://doi.org/10.1002/jmr.2680>.
- (86) Becker, J. M.; Naider, F. Cross-Linking Strategies to Study Peptide Ligand–Receptor Interactions. In *Methods in Enzymology*; Elsevier, 2015; Vol. 556, pp 527–547. <https://doi.org/10.1016/bs.mie.2014.12.001>.
- (87) Lipinski, C. A.; Lombardo, F.; Dominy, B. W.; Feeney, P. J. Experimental and Computational Approaches to Estimate Solubility and Permeability in Drug Discovery and Development Settings. *Advanced Drug Delivery Reviews* **2001**, *24*.
- (88) Kokate, A.; Li, X.; Jasti, B. Effect of Drug Lipophilicity and Ionization on Permeability Across the Buccal Mucosa: A Technical Note. *AAPS PharmSciTech* **2008**, *9* (2), 501–504. <https://doi.org/10.1208/s12249-008-9071-7>.
- (89) Wlodkowic, D.; Skommer, J.; Darzynkiewicz, Z. Flow Cytometry-Based Apoptosis Detection. In *Apoptosis*; Erhardt, P., Toth, A., Eds.; Methods in Molecular Biology; Humana Press: Totowa, NJ, 2009; Vol. 559, pp 19–32. [https://doi.org/10.1007/978-1-60327-017-5\\_2](https://doi.org/10.1007/978-1-60327-017-5_2).
- (90) Riccardi, C.; Nicoletti, I. Analysis of Apoptosis by Propidium Iodide Staining and Flow Cytometry. *Nat Protoc* **2006**, *1* (3), 1458–1461. <https://doi.org/10.1038/nprot.2006.238>.
- (91) Gerry, C. J.; Schreiber, S. L. Unifying Principles of Bifunctional, Proximity-Inducing Small Molecules. *Nat Chem Biol* **2020**, *16* (4), 369–378. <https://doi.org/10.1038/s41589-020-0469-1>.
- (92) Corson, T. W.; Aberle, N.; Crews, C. M. Design and Applications of Bifunctional Small Molecules: Why Two Heads Are Better Than One. *ACS Chem. Biol.* **2008**, *3* (11), 677–692. <https://doi.org/10.1021/cb8001792>.
- (93) Conway, S. J. Bifunctional Molecules beyond PROTACs. *J. Med. Chem.* **2020**, *63* (6), 2802–2806. <https://doi.org/10.1021/acs.jmedchem.0c00293>.
- (94) Furumoto, T.; Teramoto, M.; Inada, N.; Ito, M.; Nishida, I.; Watanabe, A. Phosphorylation of a Bifunctional Enzyme, 6-Phosphofructo-2-Kinase/Fructose-2,6-Bisphosphate 2-Phosphatase, Is Regulated Physiologically and Developmentally in Rosette Leaves of *Arabidopsis Thaliana*. *Plant and Cell Physiology* **2001**, *42* (10), 1044–1048. <https://doi.org/10.1093/pcp/pce161>.

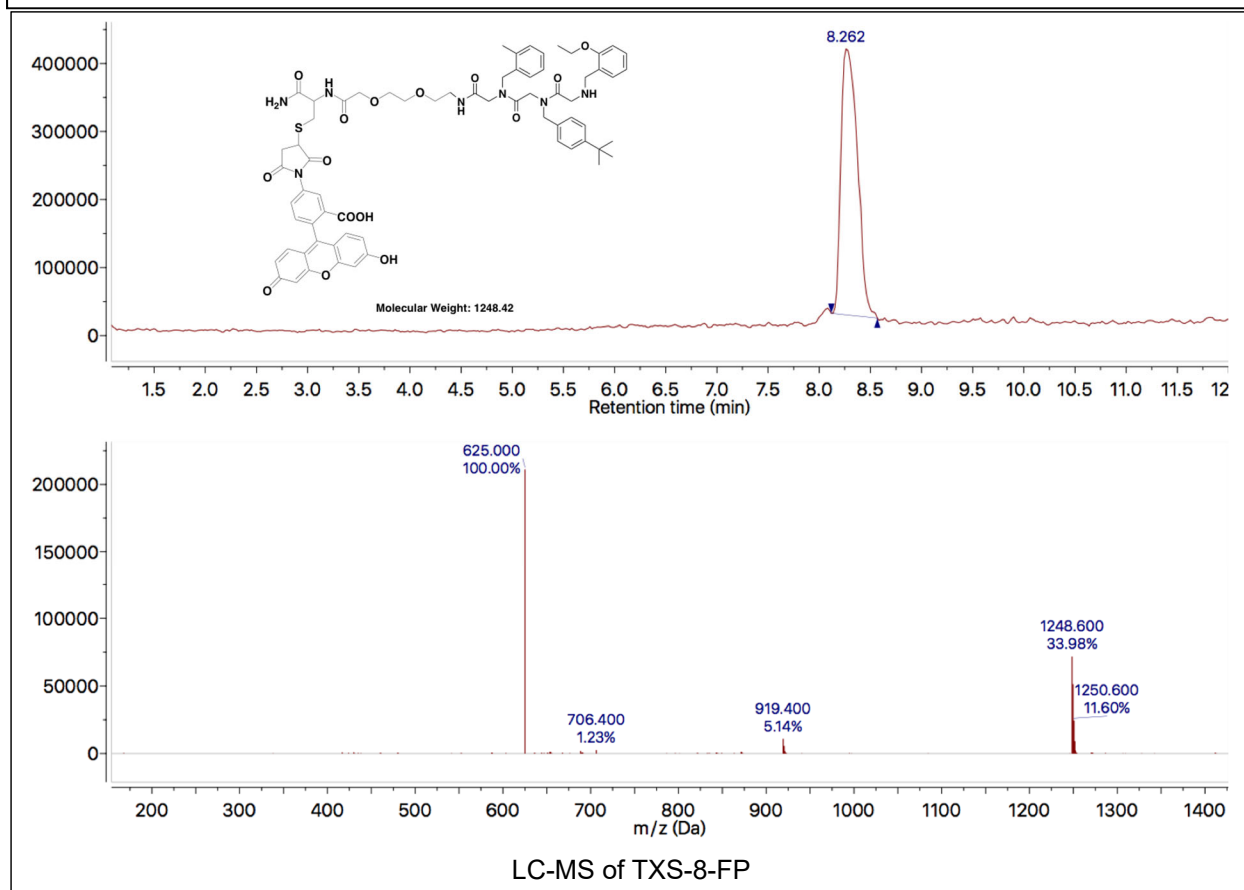
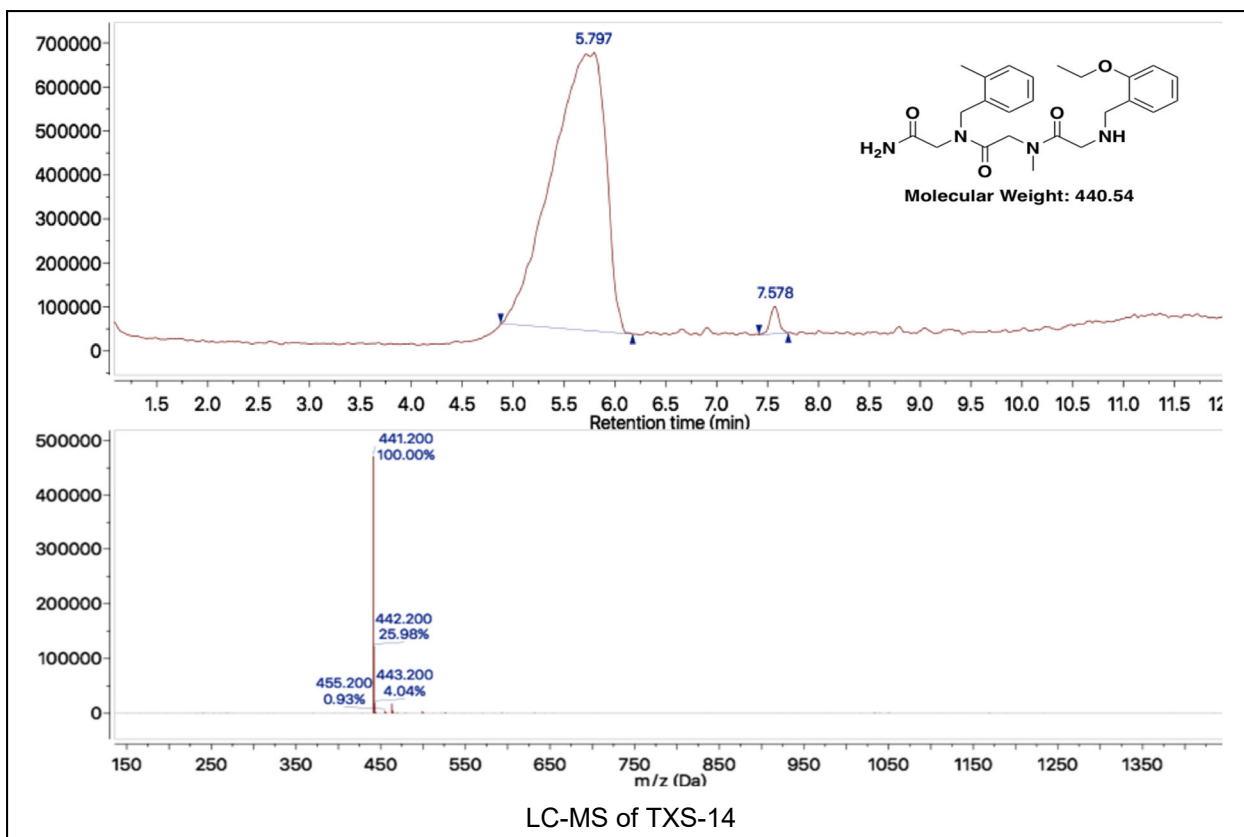
- (95) Song, Y.; Park, P. M. C.; Wu, L.; Ray, A.; Picaud, S.; Li, D.; Wimalasena, V. K.; Du, T.; Filippakopoulos, P.; Anderson, K. C.; Qi, J.; Chauhan, D. Development and Preclinical Validation of a Novel Covalent Ubiquitin Receptor Rpn13 Degradar in Multiple Myeloma. *Leukemia* **2019**, *33* (11), 2685–2694. <https://doi.org/10.1038/s41375-019-0467-z>.
- (96) Sakata, E.; Bohn, S.; Mihalache, O.; Kiss, P.; Beck, F.; Nagy, I.; Nickell, S.; Tanaka, K.; Saeki, Y.; Forster, F.; Baumeister, W. Localization of the Proteasomal Ubiquitin Receptors Rpn10 and Rpn13 by Electron Cryomicroscopy. *Proceedings of the National Academy of Sciences* **2012**, *109* (5), 1479–1484. <https://doi.org/10.1073/pnas.1119394109>.
- (97) Anderson, D. J.; Le Moigne, R.; Djakovic, S.; Kumar, B.; Rice, J.; Wong, S.; Wang, J.; Yao, B.; Valle, E.; Kiss von Soly, S.; Madriaga, A.; Soriano, F.; Menon, M.-K.; Wu, Z. Y.; Kampmann, M.; Chen, Y.; Weissman, J. S.; Aftab, B. T.; Yakes, F. M.; Shawver, L.; Zhou, H.-J.; Wustrow, D.; Rolfe, M. Targeting the AAA ATPase P97 as an Approach to Treat Cancer through Disruption of Protein Homeostasis. *Cancer Cell* **2015**, *28* (5), 653–665. <https://doi.org/10.1016/j.ccell.2015.10.002>.
- (98) Del Prete, D.; Rice, R. C.; Rajadhyaksha, A. M.; D’Adamio, L. Amyloid Precursor Protein (APP) May Act as a Substrate and a Recognition Unit for CRL4<sup>CRBN</sup> and Stub1 E3 Ligases Facilitating Ubiquitination of Proteins Involved in Presynaptic Functions and Neurodegeneration. *Journal of Biological Chemistry* **2016**, *291* (33), 17209–17227. <https://doi.org/10.1074/jbc.M116.733626>.
- (99) Gao, H.; Sun, X.; Rao, Y. PROTAC Technology: Opportunities and Challenges. *ACS Med. Chem. Lett.* **2020**, *11* (3), 237–240. <https://doi.org/10.1021/acsmchemlett.9b00597>.
- (100) Wang, Y.; Jiang, X.; Feng, F.; Liu, W.; Sun, H. Degradation of Proteins by PROTACs and Other Strategies. *Acta Pharmaceutica Sinica B* **2020**, *10* (2), 207–238. <https://doi.org/10.1016/j.apsb.2019.08.001>.
- (101) Steinebach, C.; Kehm, H.; Lindner, S.; Vu, L. P.; Köpf, S.; López Mármol, Á.; Weiler, C.; Wagner, K. G.; Reichenzeller, M.; Krönke, J.; Gütschow, M. PROTAC-Mediated Crosstalk between E3 Ligases. *Chemical Communications* **2019**, *55* (12), 1821–1824. <https://doi.org/10.1039/C8CC09541H>.
- (102) Liu, X.; Zhang, X.; Lv, D.; Yuan, Y.; Zheng, G.; Zhou, D. Assays and Technologies for Developing Proteolysis Targeting Chimera Degraders. *Future Medicinal Chemistry* **2020**, fmc-2020-0073. <https://doi.org/10.4155/fmc-2020-0073>.
- (103) Arthur, R.; Beatriz Valle-Argos, B.; Steele, A. J.; Packham, G. Development of PROTACs to Address Clinical Limitations Associated with BTK-Targeted Kinase Inhibitors. *Exploration of Targeted Anti-tumor Therapy* **2020**, *1* (3), 131–152. <https://doi.org/10.37349/etat.2020.00009>.

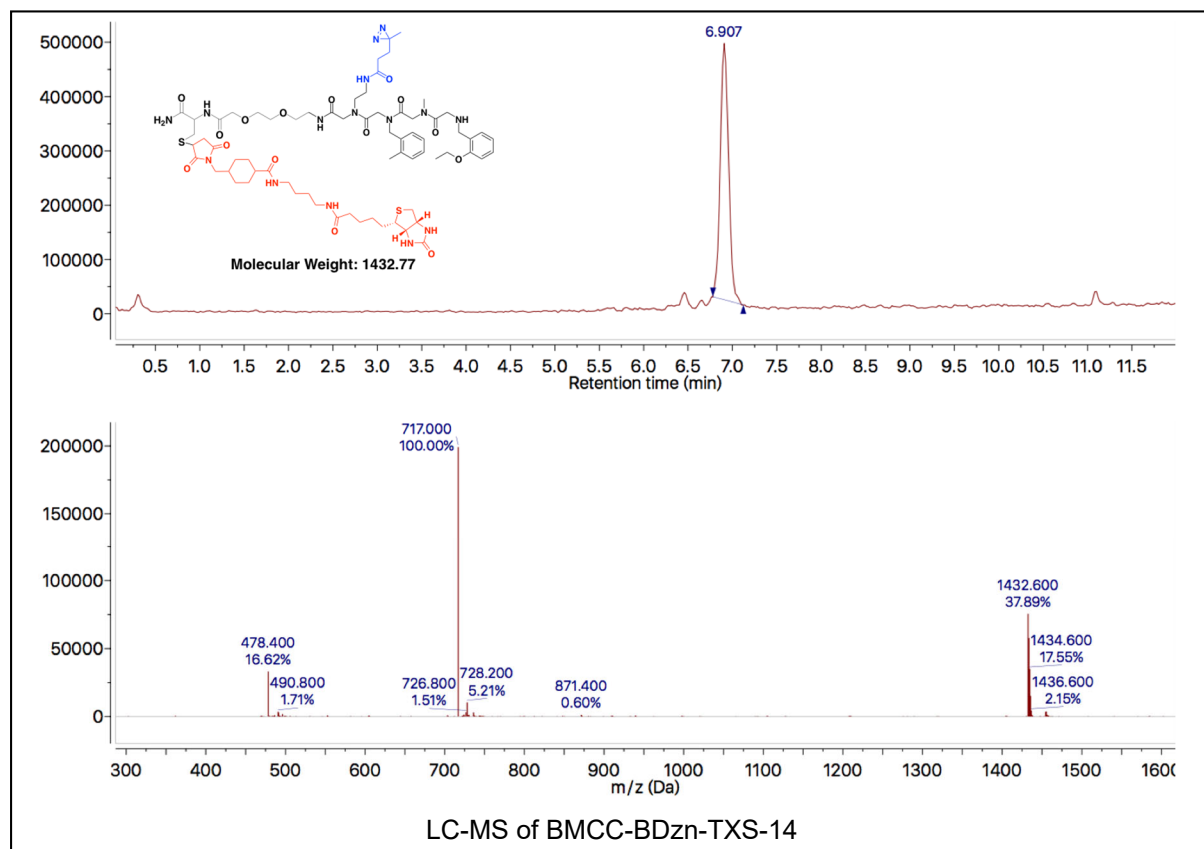
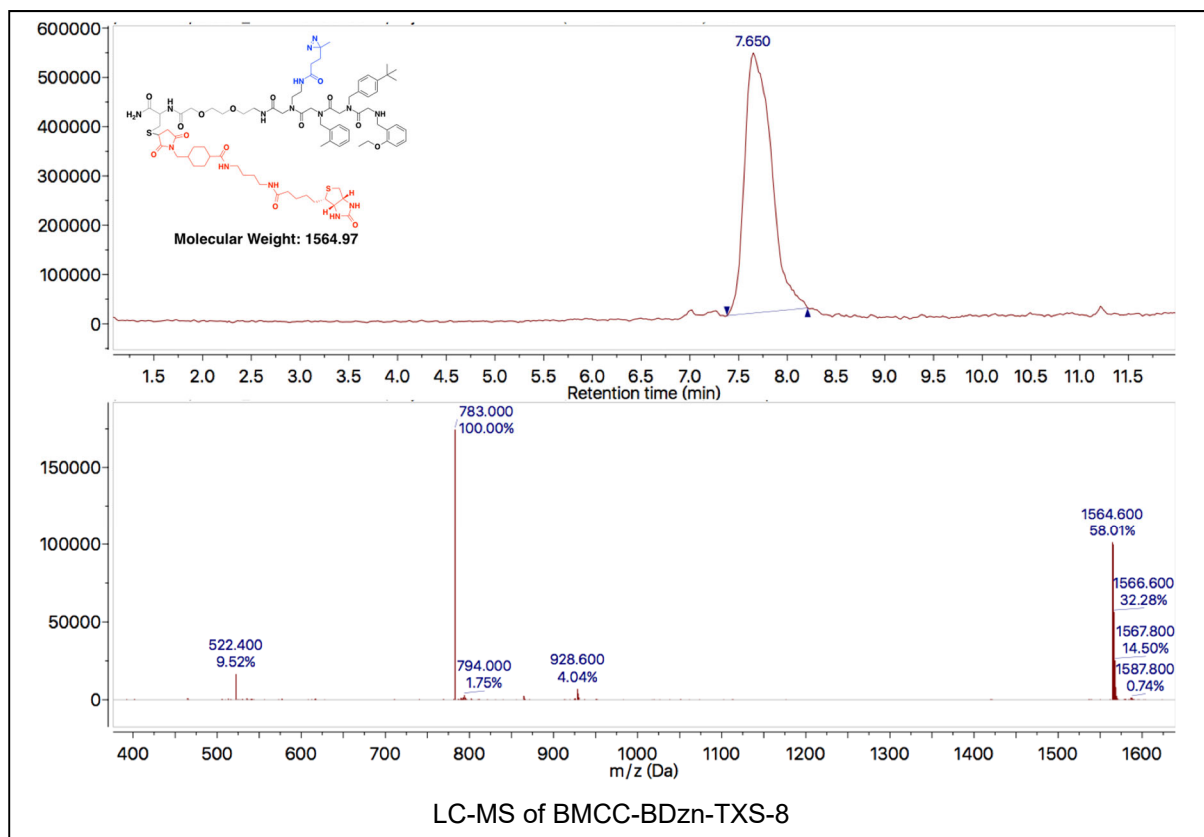
- (104) Zorba, A.; Nguyen, C.; Xu, Y.; Starr, J.; Borzilleri, K.; Smith, J.; Zhu, H.; Farley, K. A.; Ding, W.; Schiemer, J.; Feng, X.; Chang, J. S.; Uccello, D. P.; Young, J. A.; Garcia-Irrizary, C. N.; Czabaniuk, L.; Schuff, B.; Oliver, R.; Montgomery, J.; Hayward, M. M.; Coe, J.; Chen, J.; Niosi, M.; Luthra, S.; Shah, J. C.; El-Kattan, A.; Qiu, X.; West, G. M.; Noe, M. C.; Shanmugasundaram, V.; Gilbert, A. M.; Brown, M. F.; Calabrese, M. F. Delineating the Role of Cooperativity in the Design of Potent PROTACs for BTK. *Proceedings of the National Academy of Sciences* **2018**, *115* (31), E7285–E7292. <https://doi.org/10.1073/pnas.1803662115>.

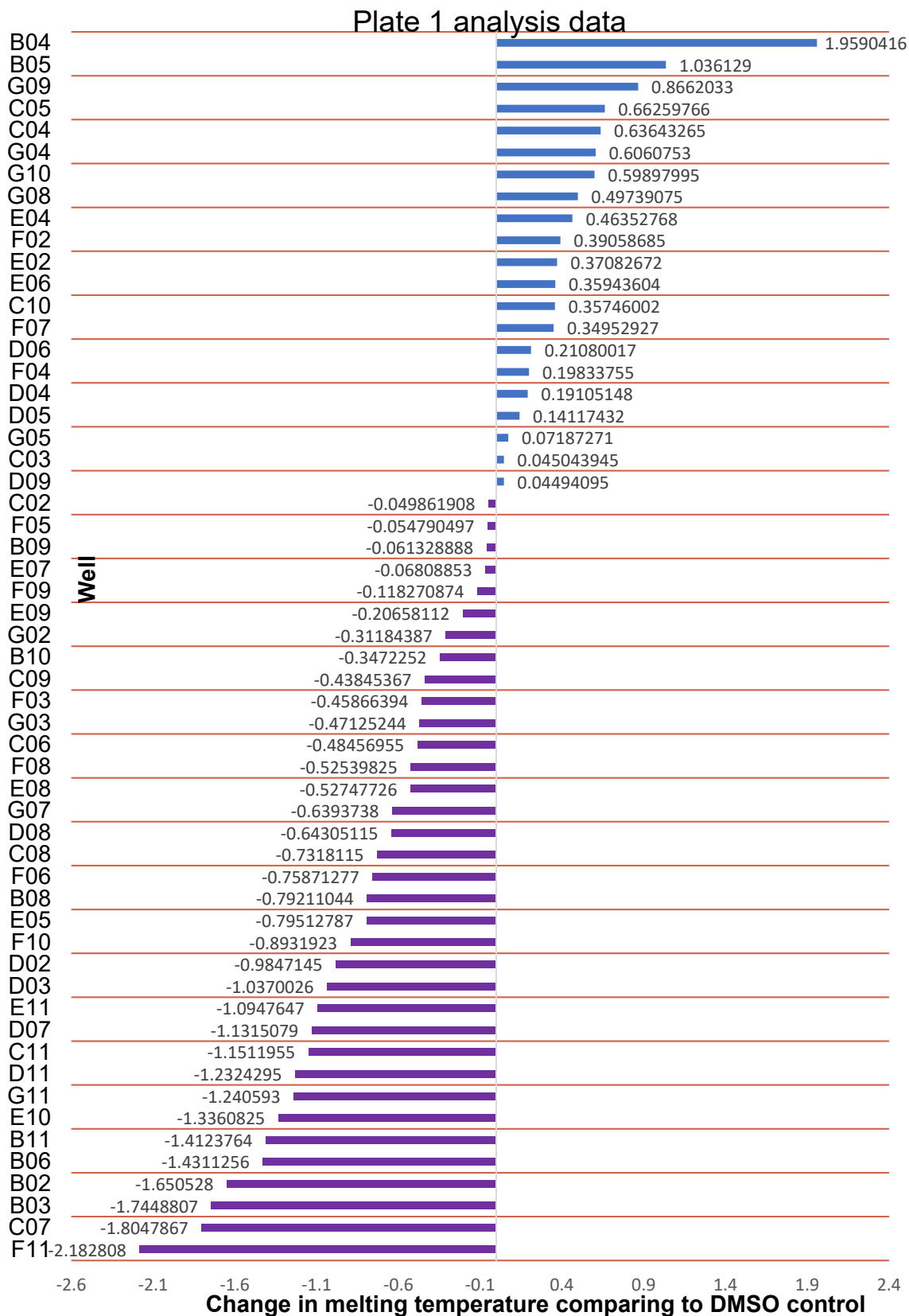
## APPENDIX A. MASS SPEC DATA

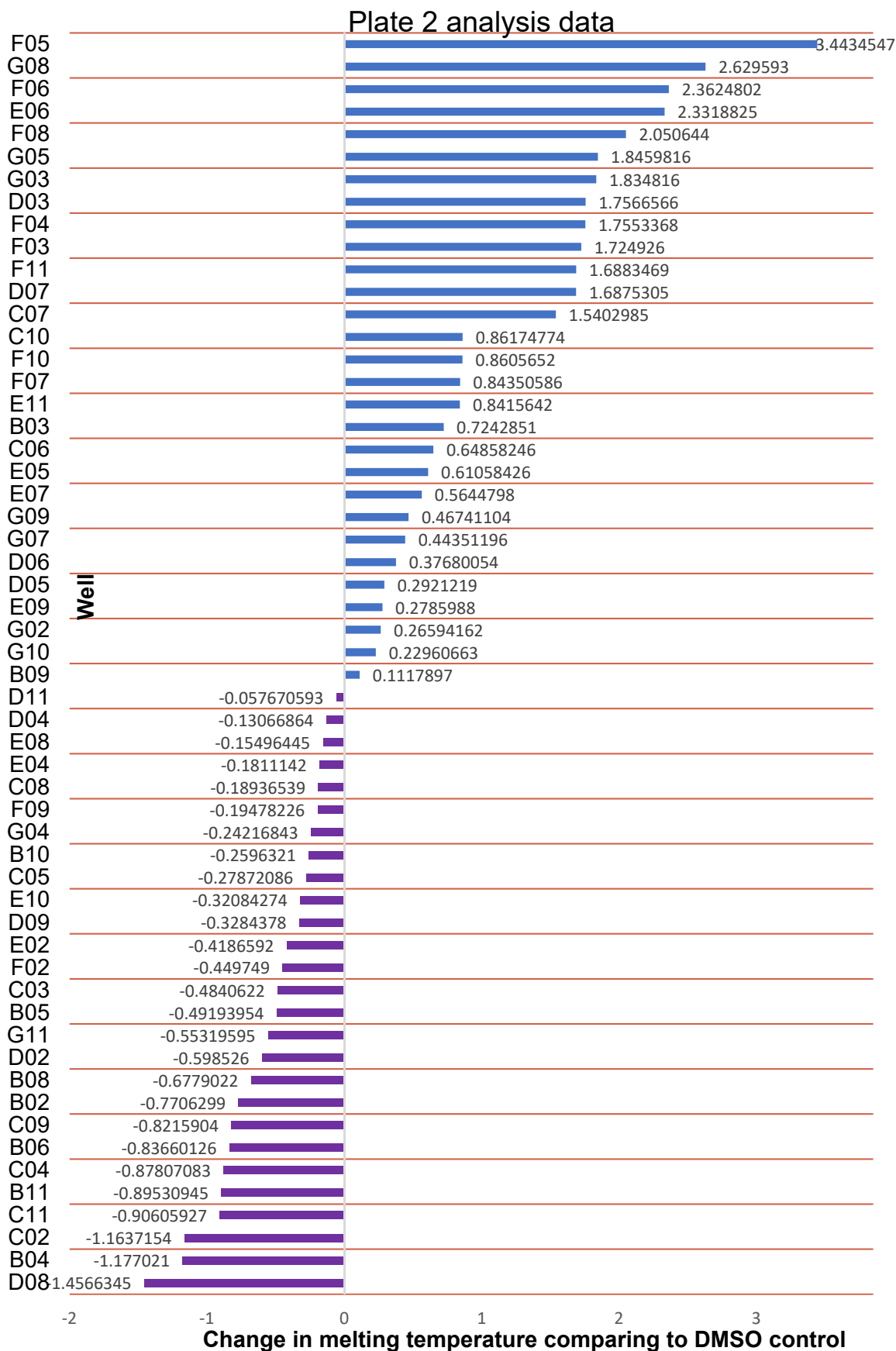
### A) LC-MS data for compounds

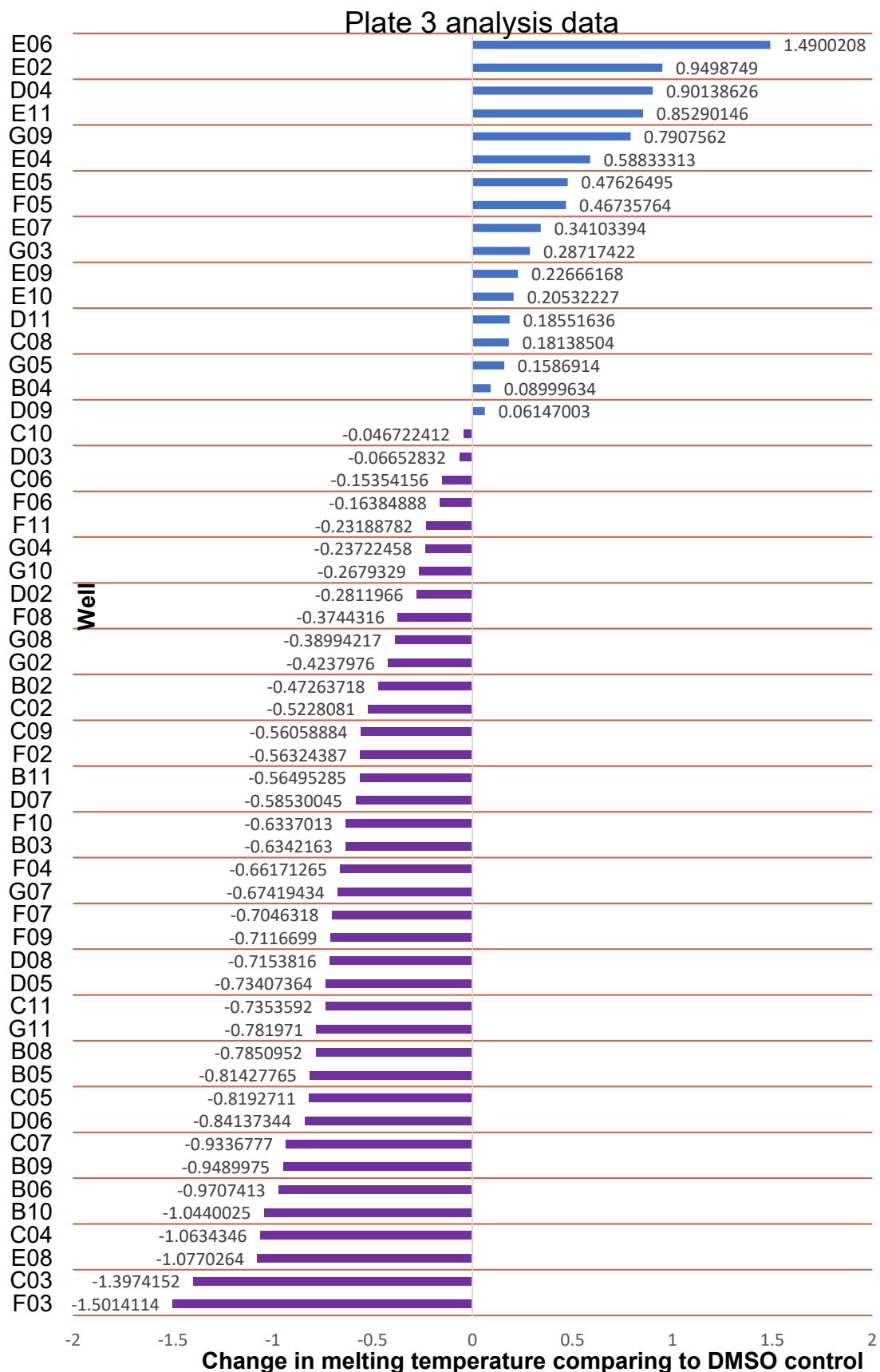


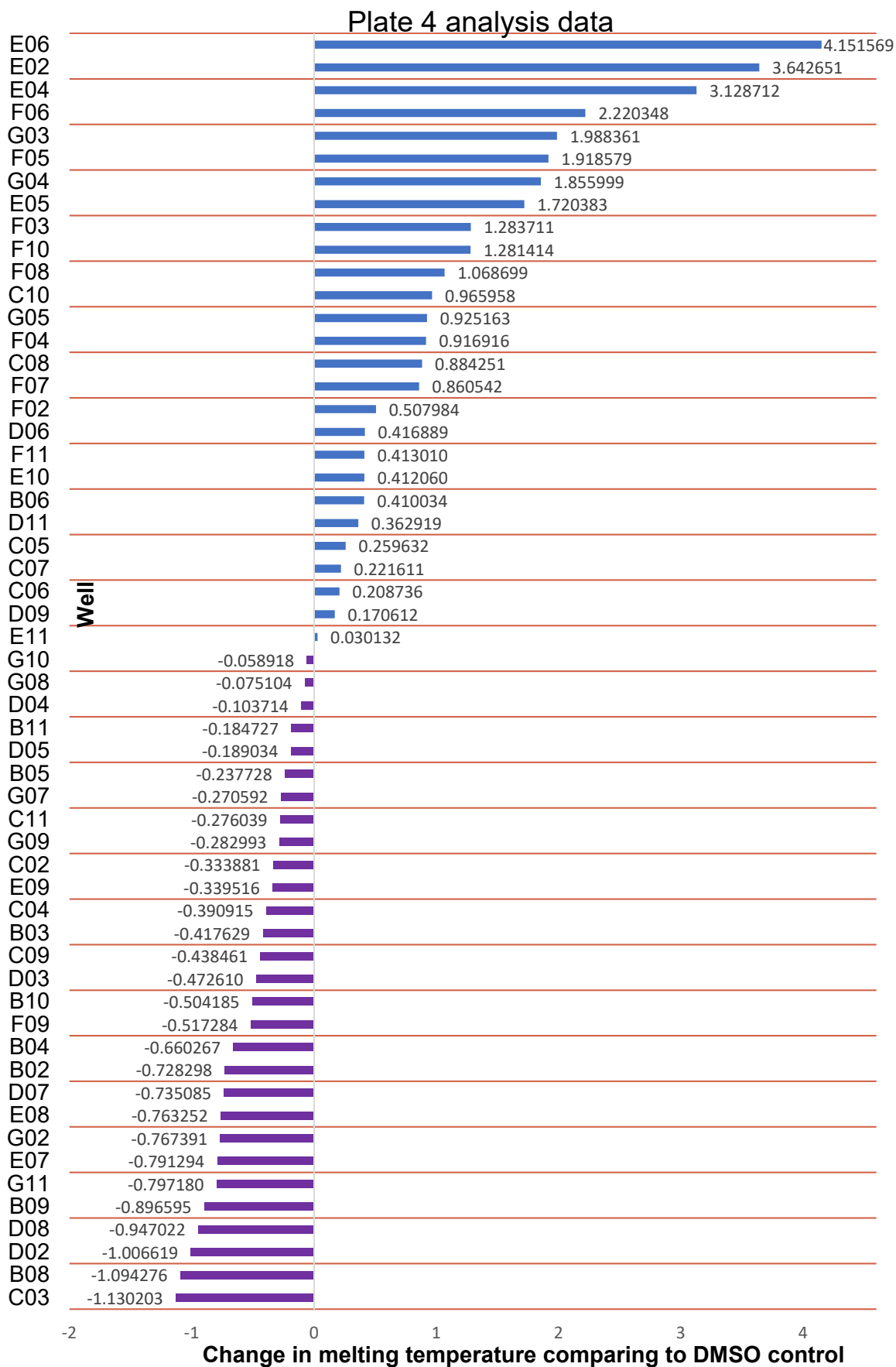




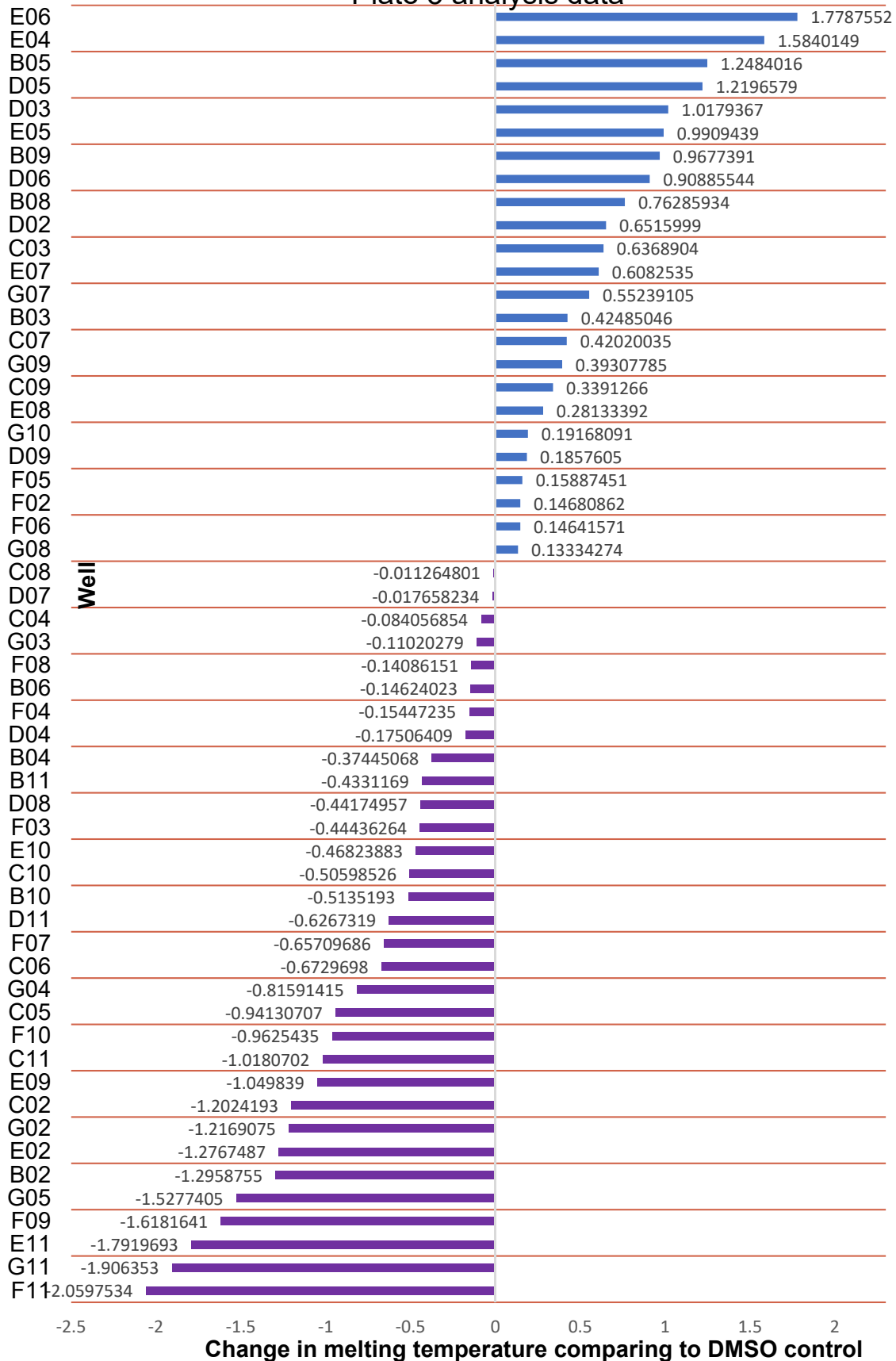


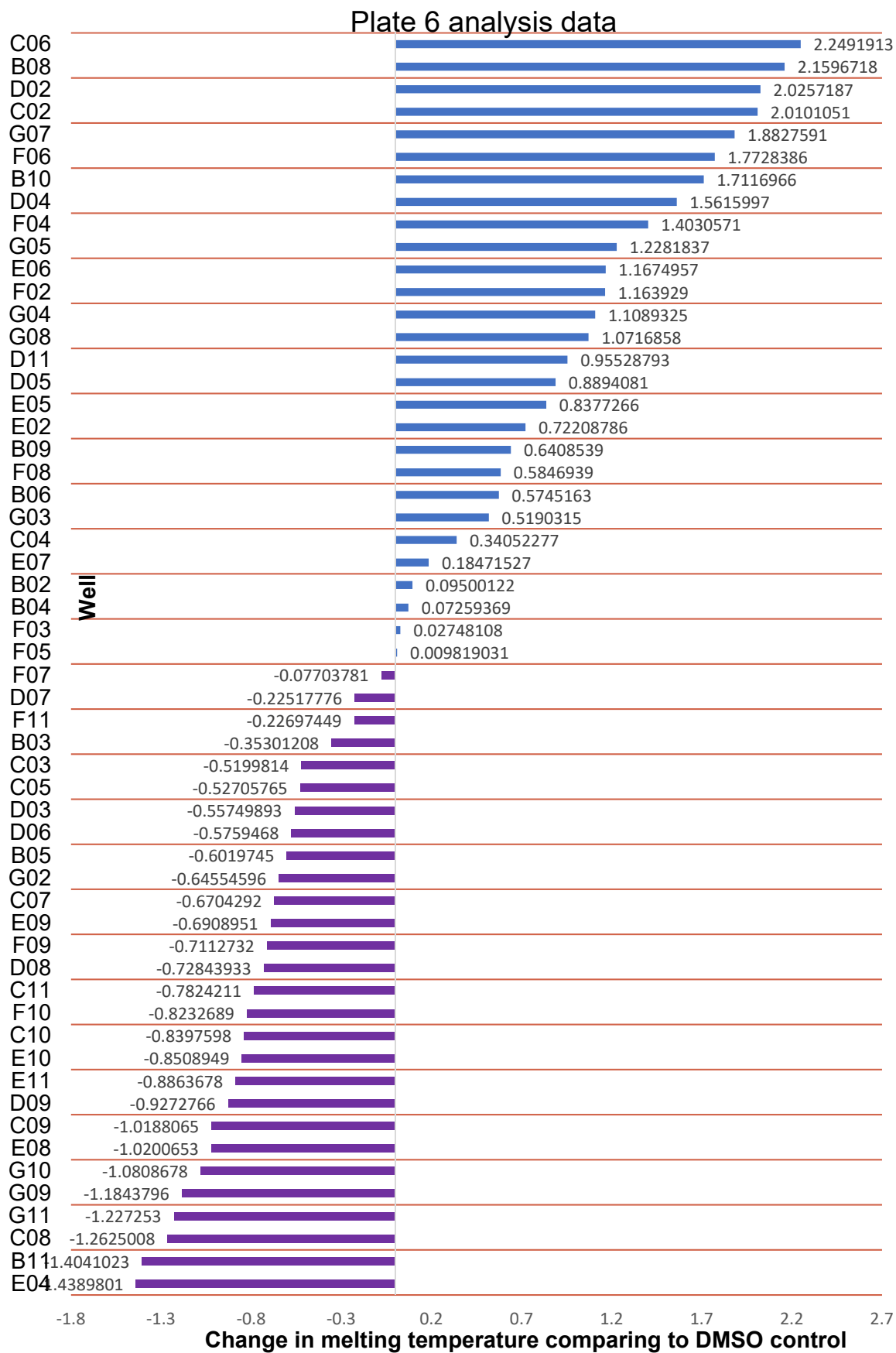


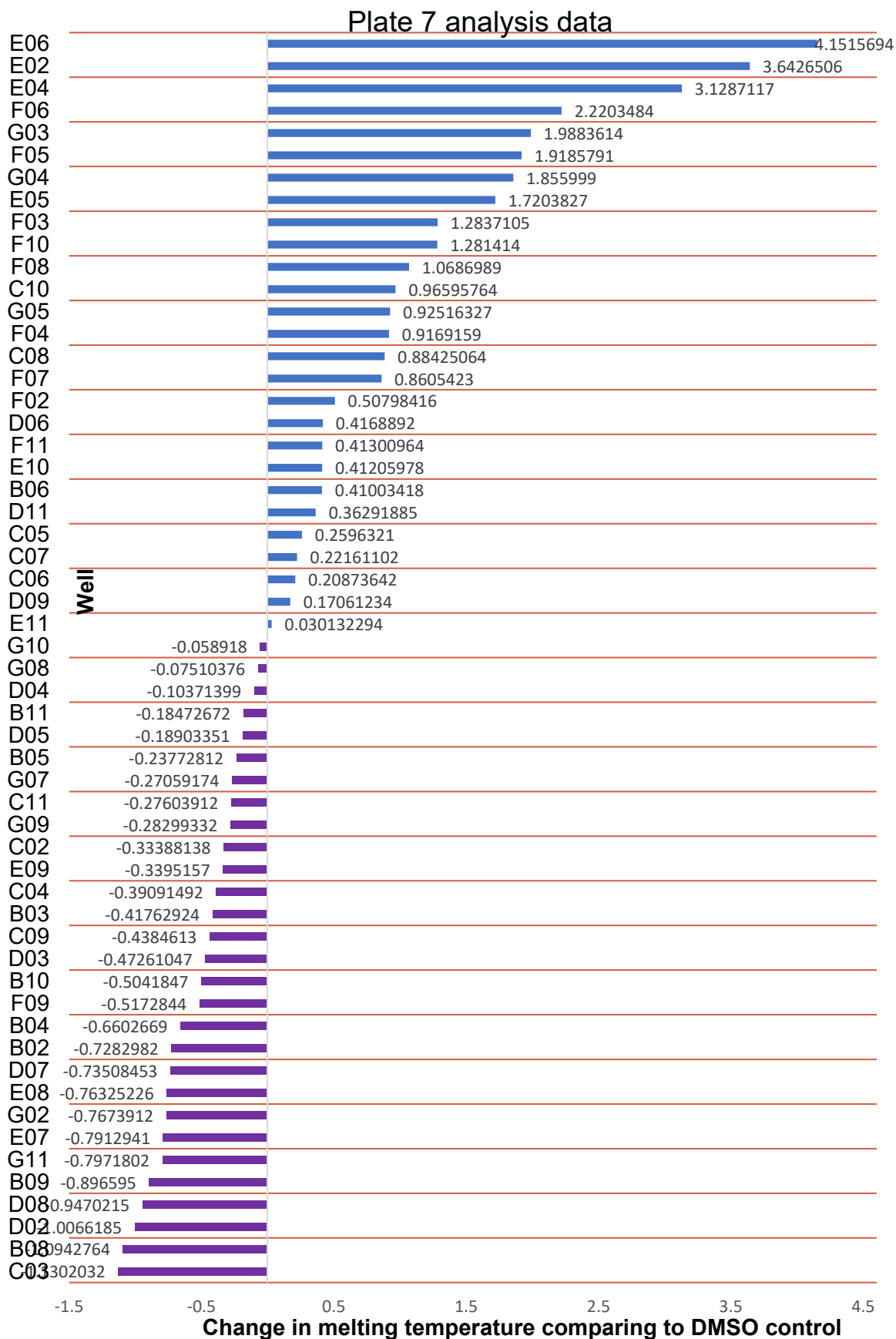




# Plate 5 analysis data







Hits from TSA:

Plate 1: B4

Plate 2: C7, D3, D7, E6, F3, F4, F5, F6, F8, G3, G5, G8

Plate 3: E6

Plate 4: G4

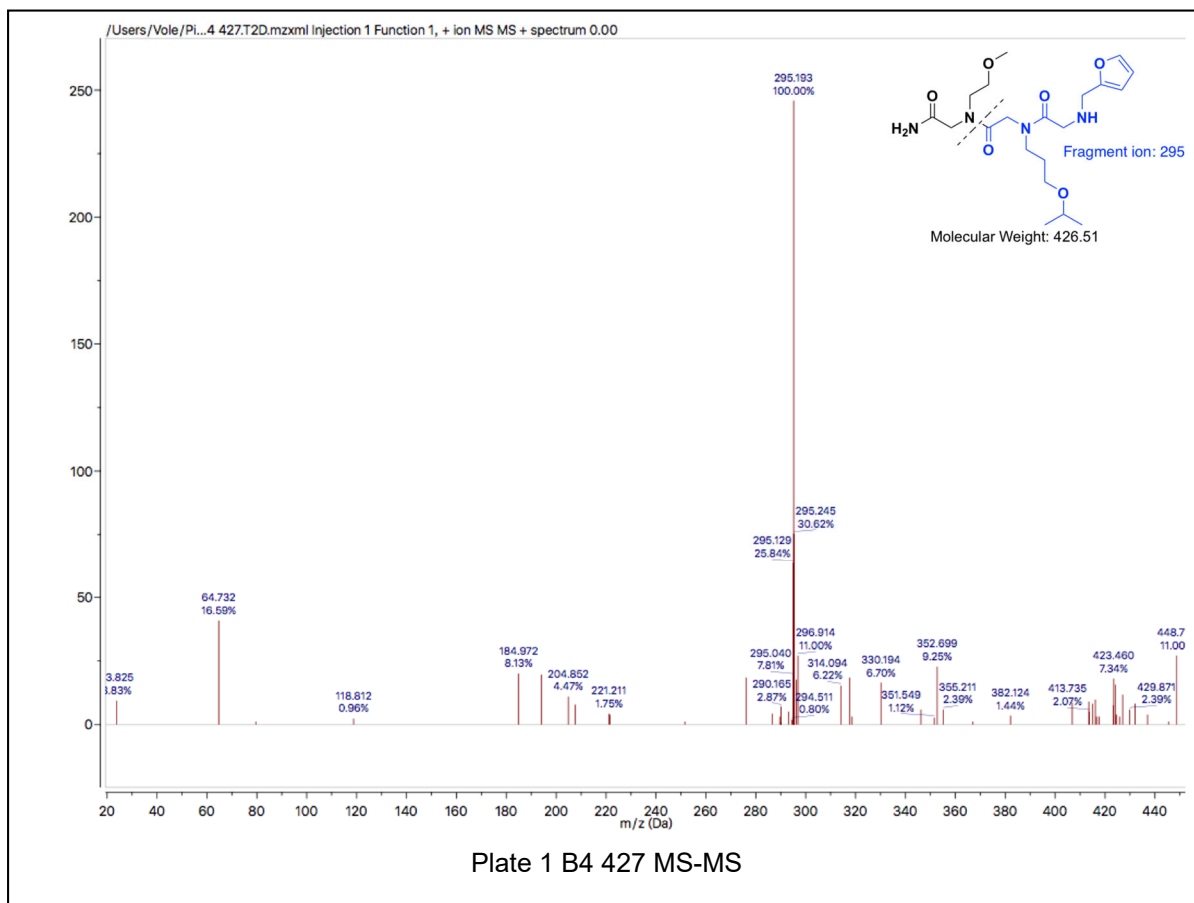
Plate 5: E6, E4

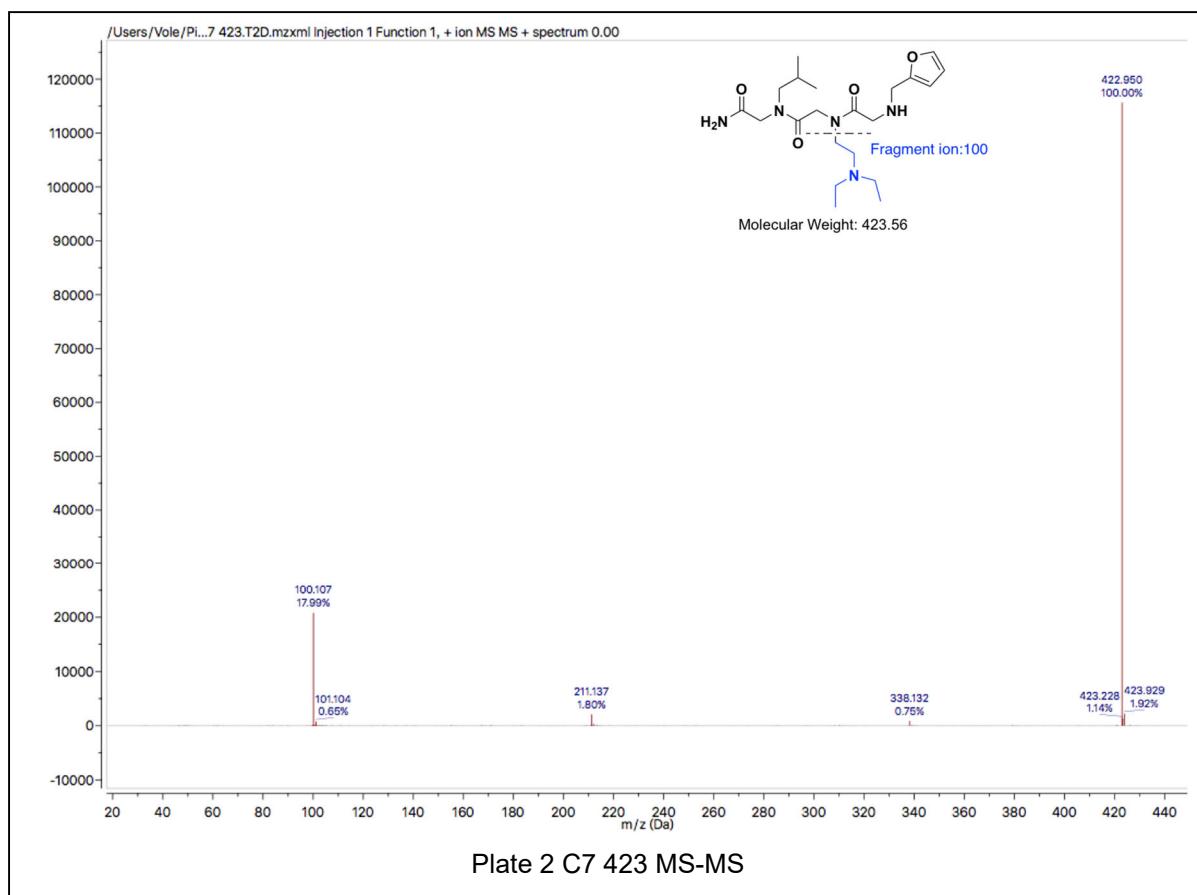
Plate 6: B8, B10, C2, C6, D2, D4, D6, G7

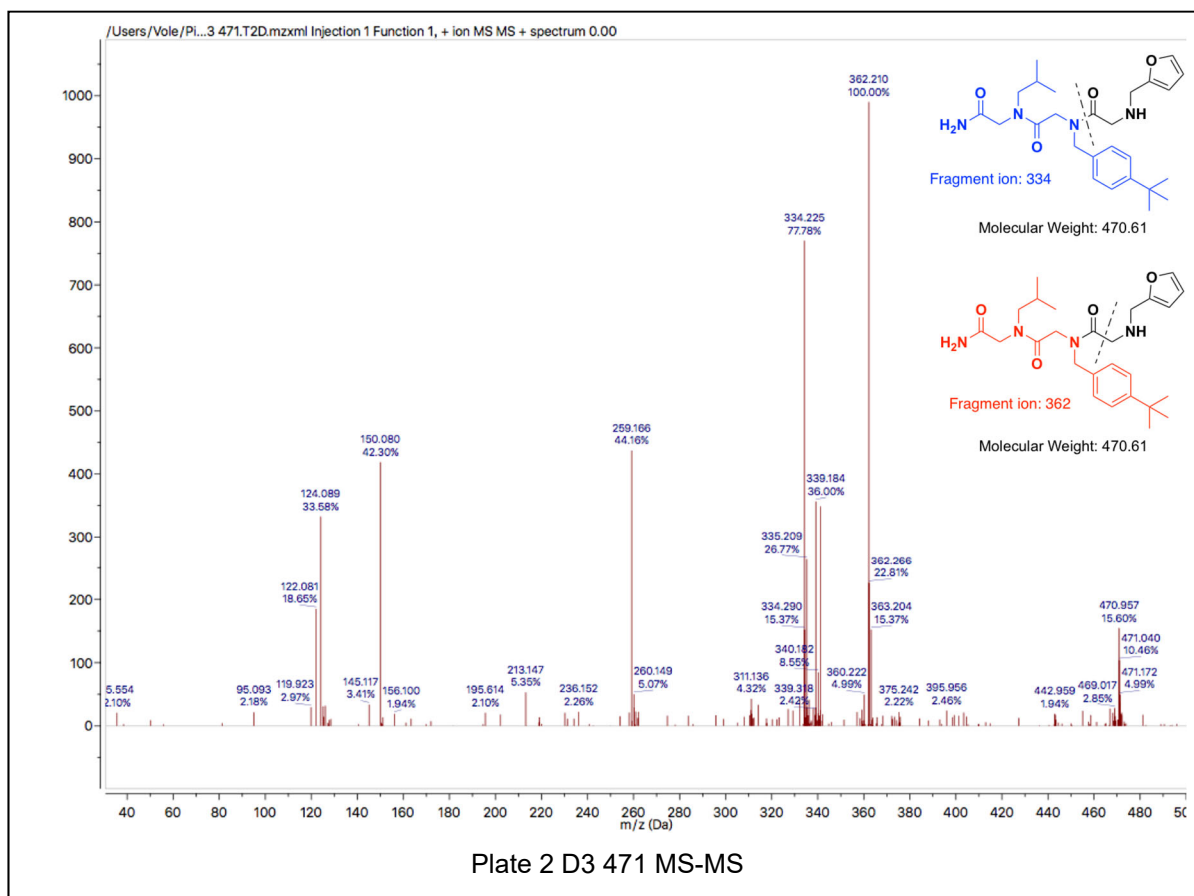
Plate 7: E2, E4, E5, E6, F5, F6, G3, G4

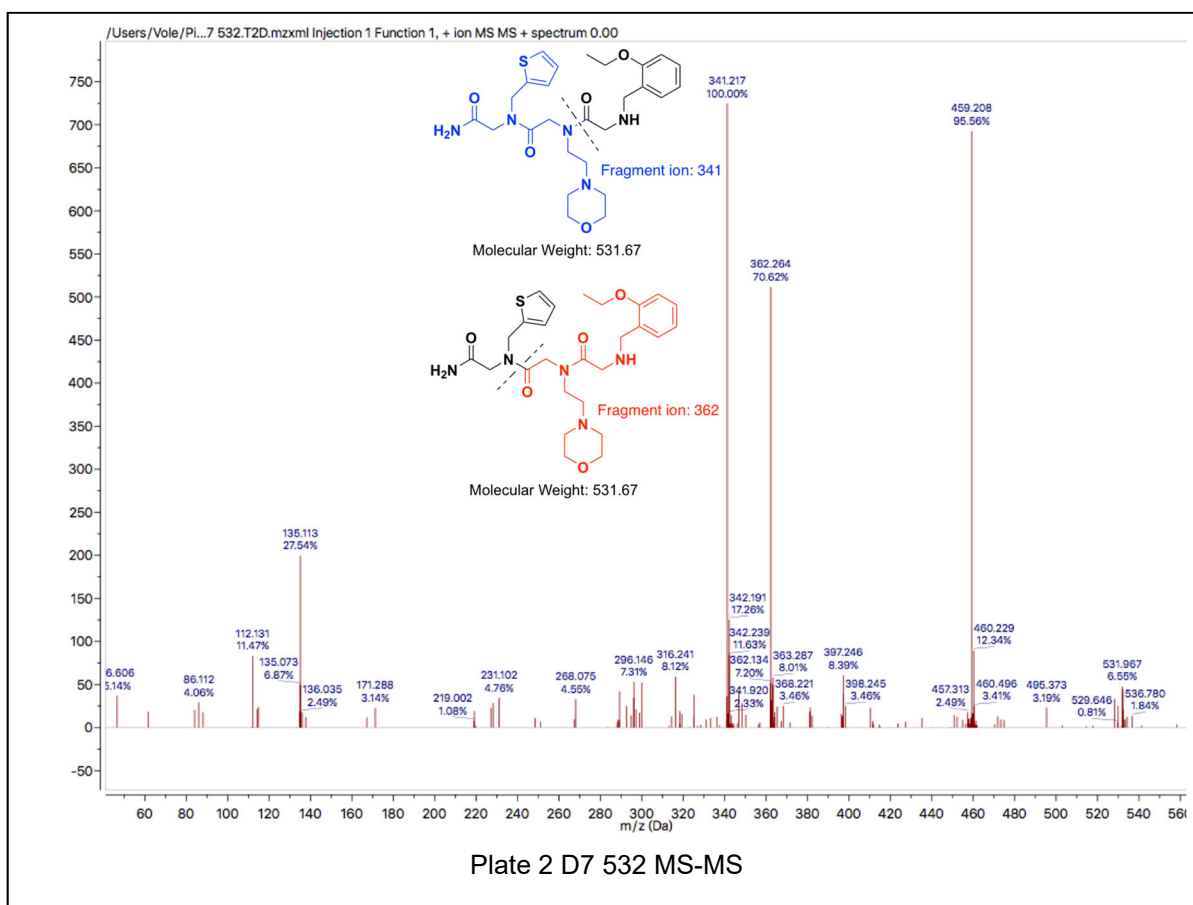
In total, 33 compounds were identified as hits through TSA. However, we could not obtain either MS or MS-MS from plate 2 F3, plate 7 E2, plate 7 E4, and plate 7 F6. We were also not confident of the amine composition of plate 2 G3 and plate 6 D2.

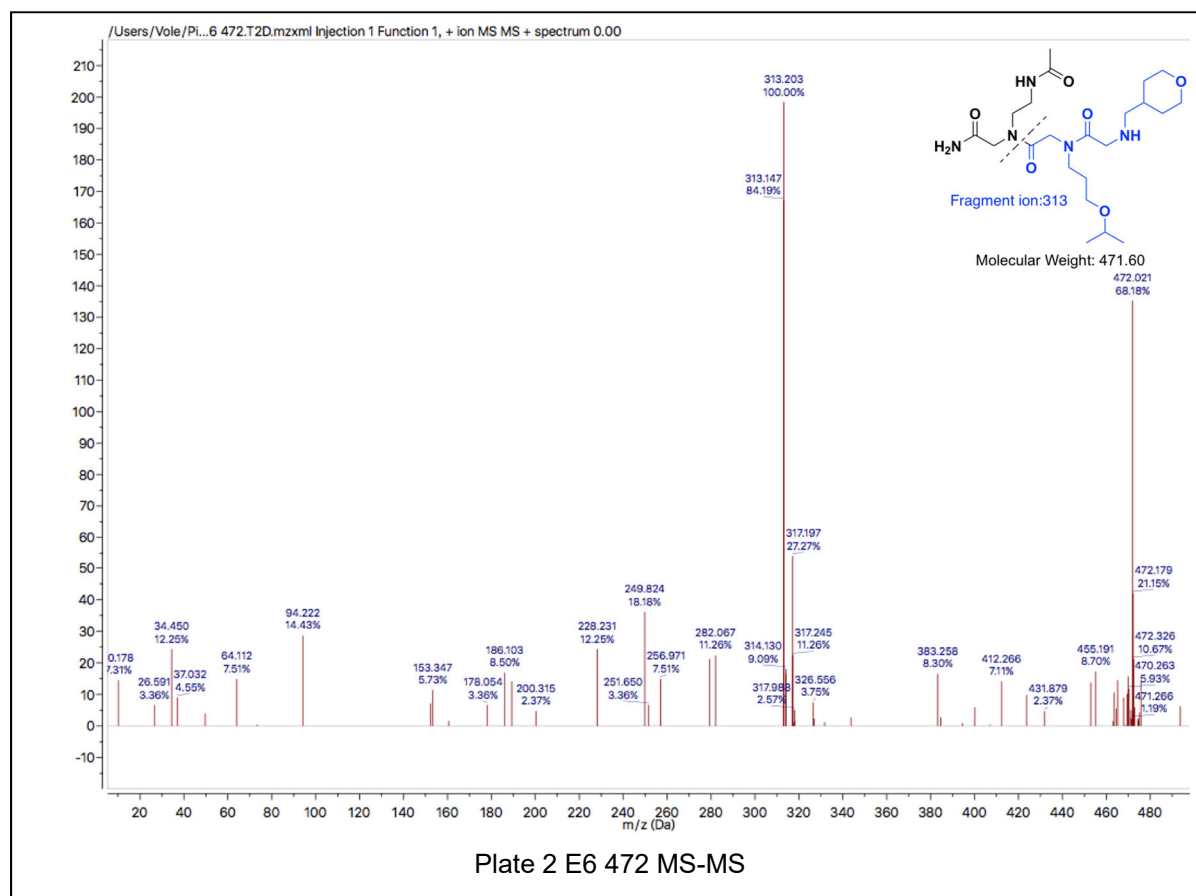
## B) MALDI-TOF MS/MS data of peptoid hits from screen

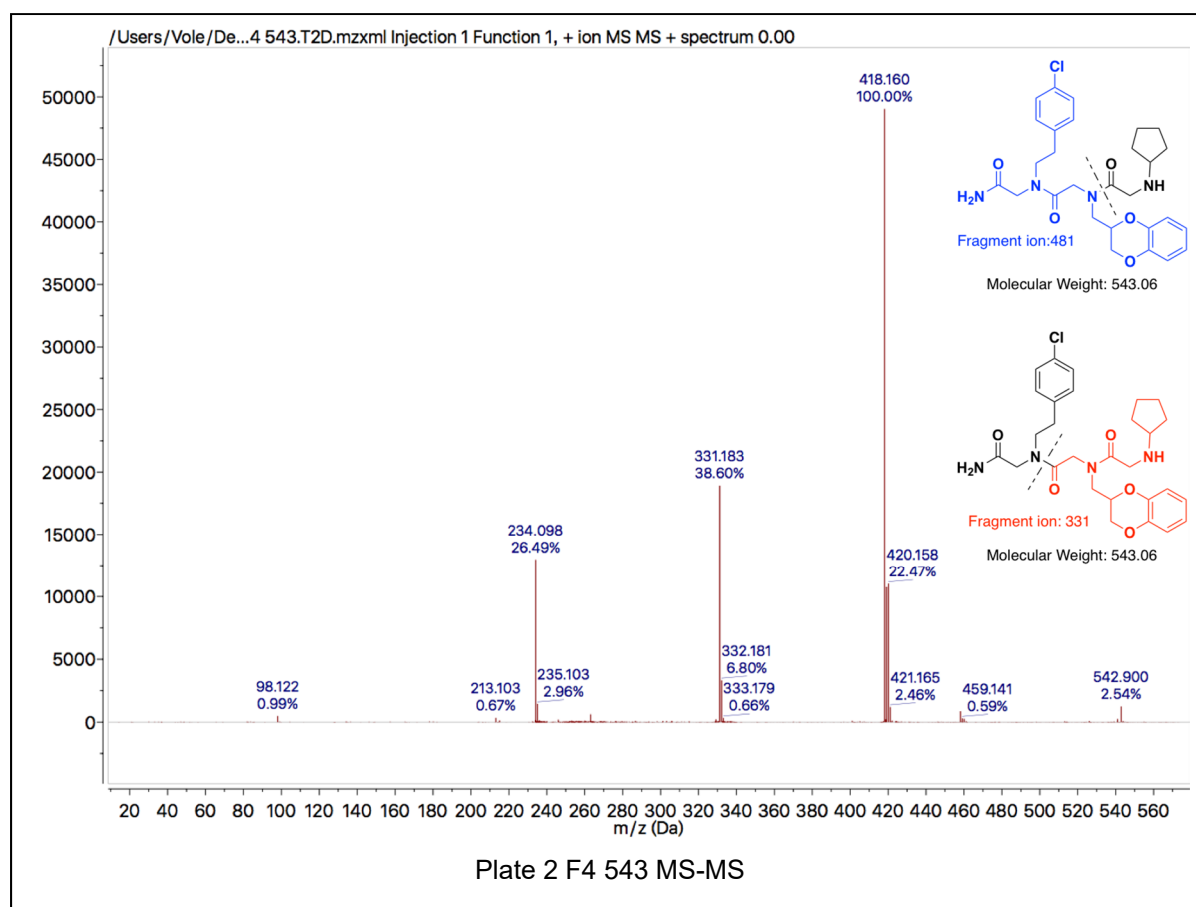


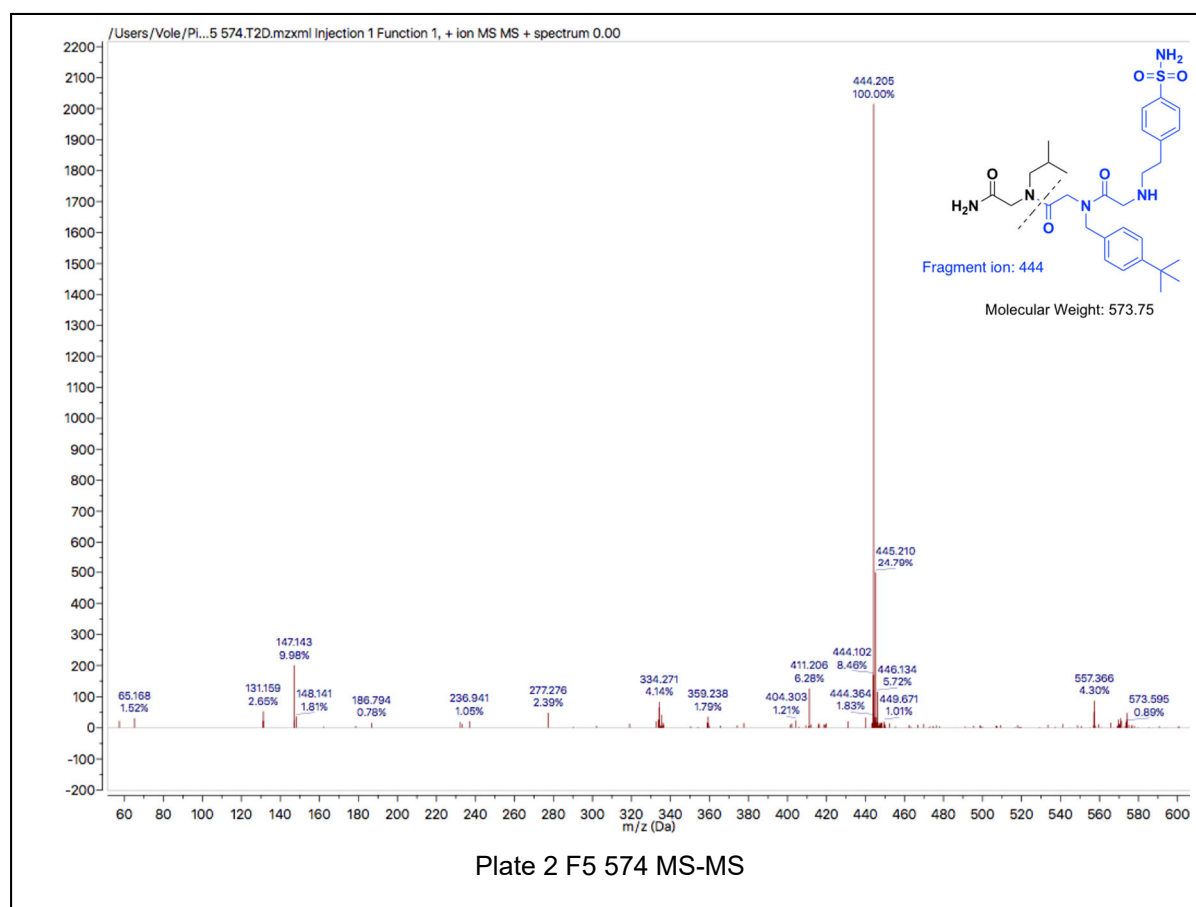


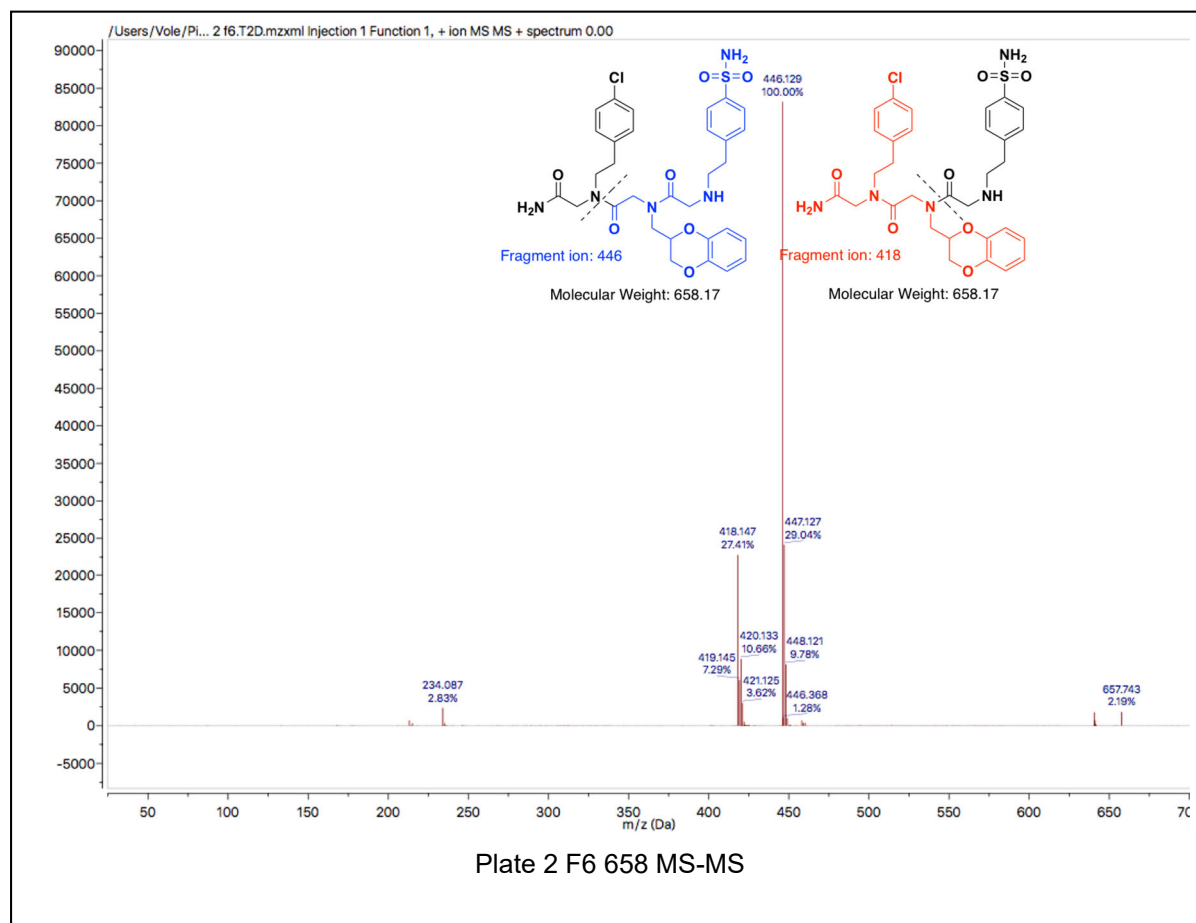


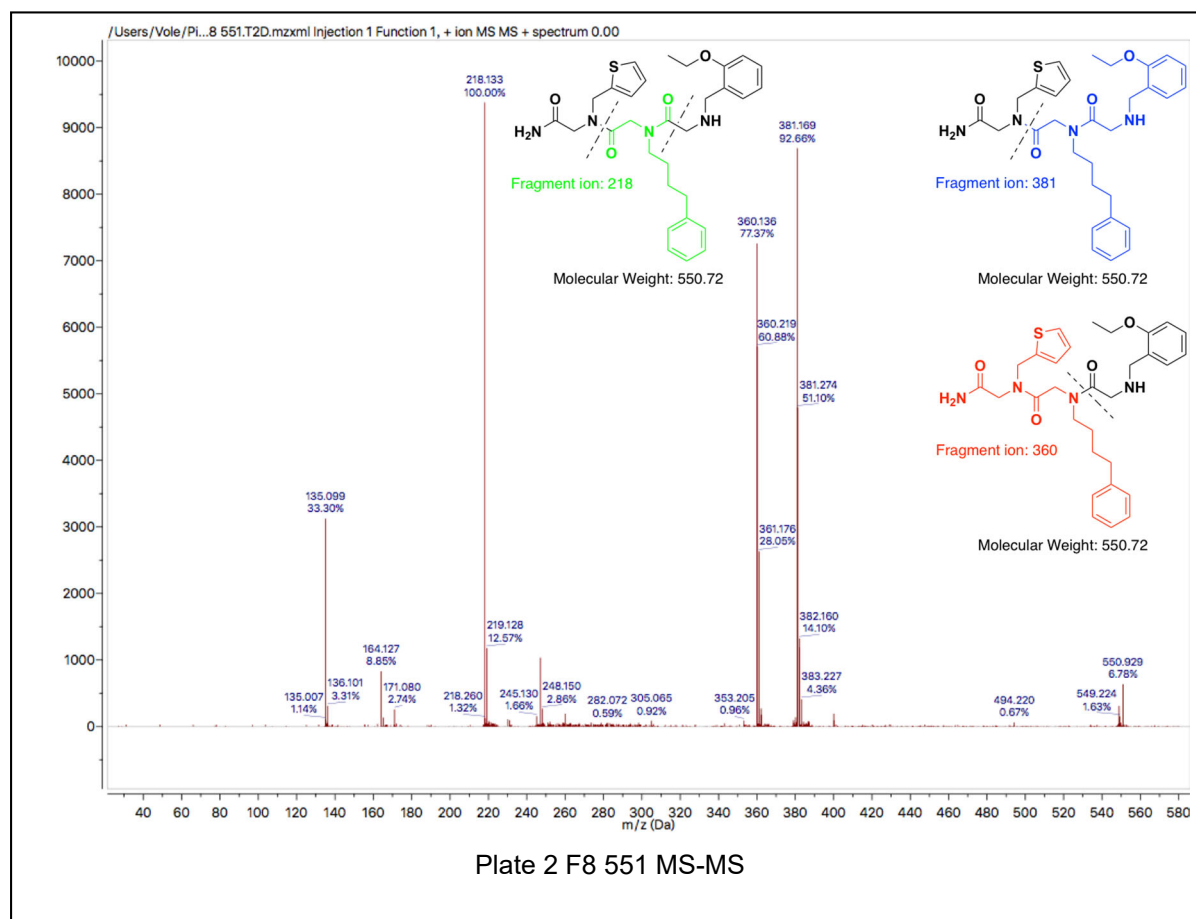


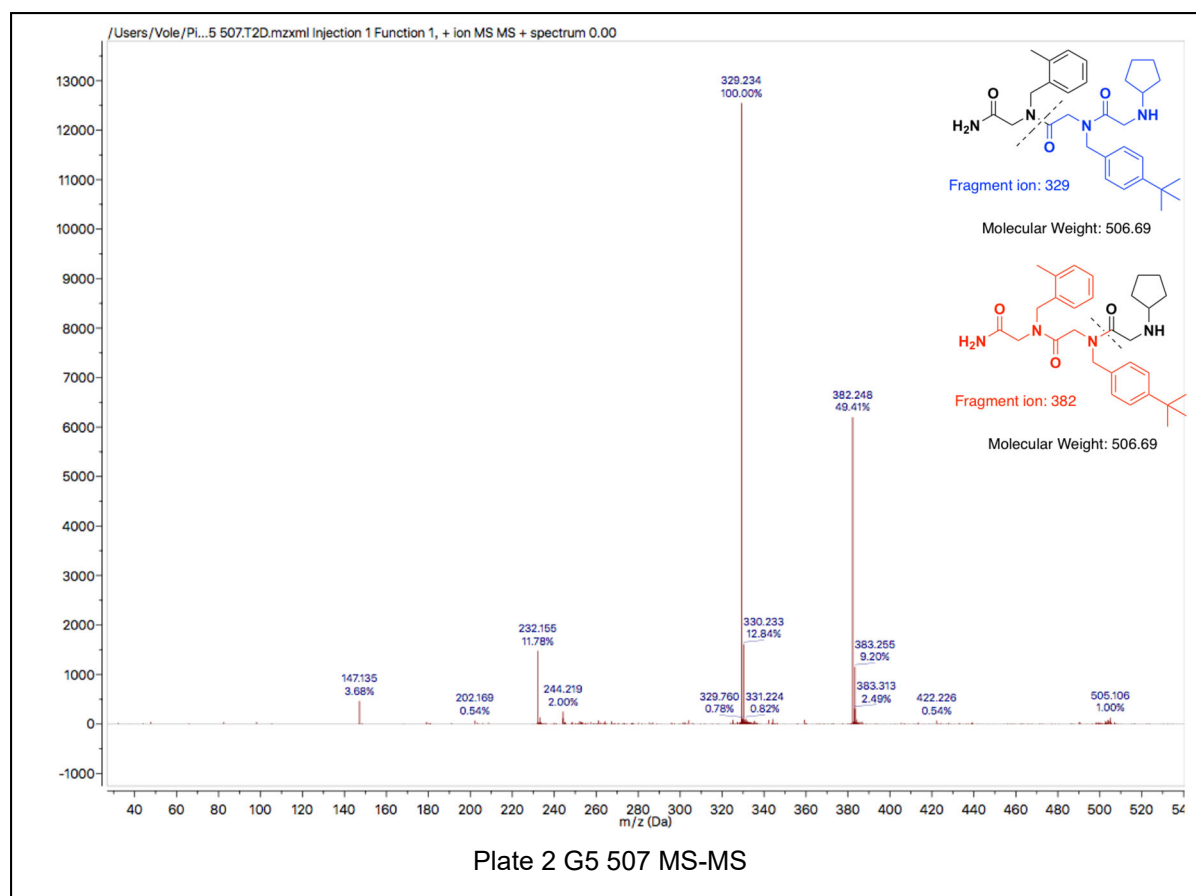


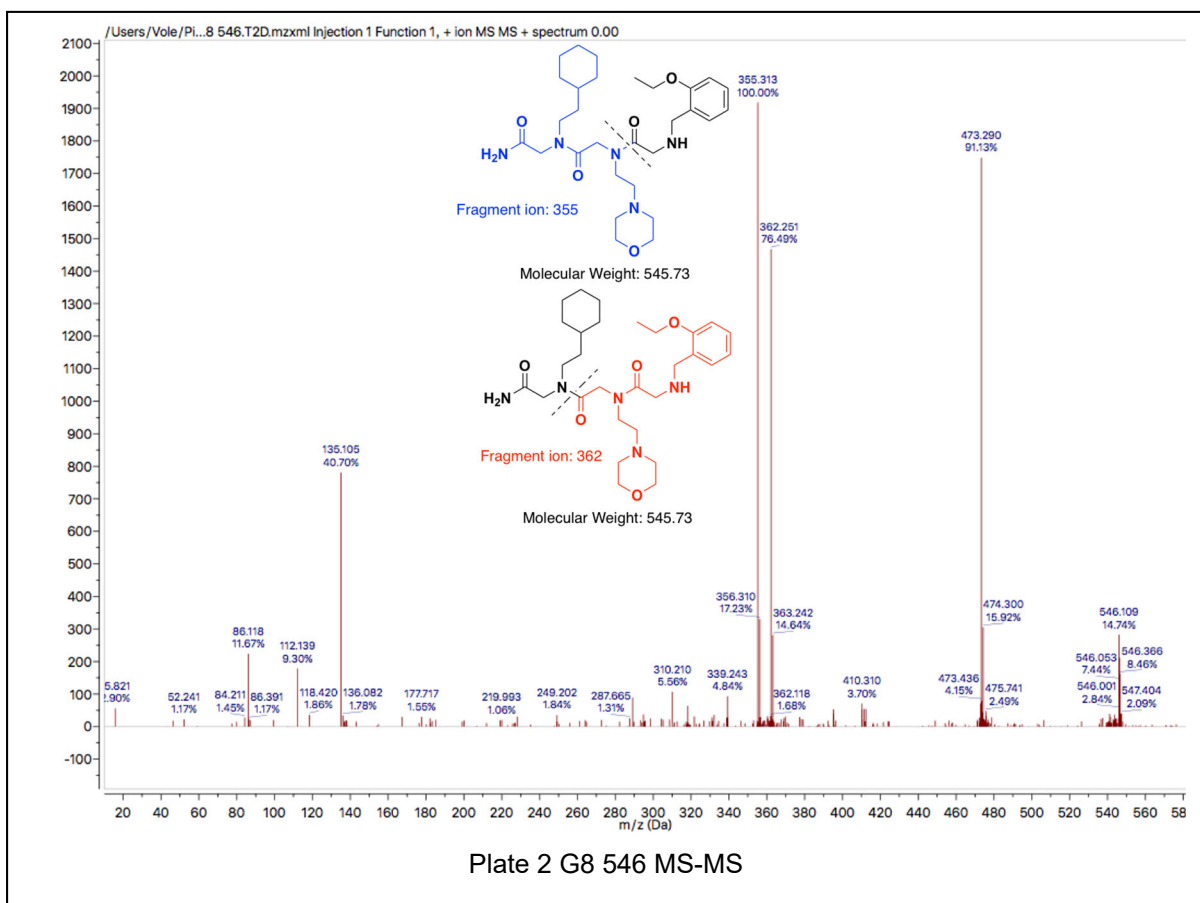


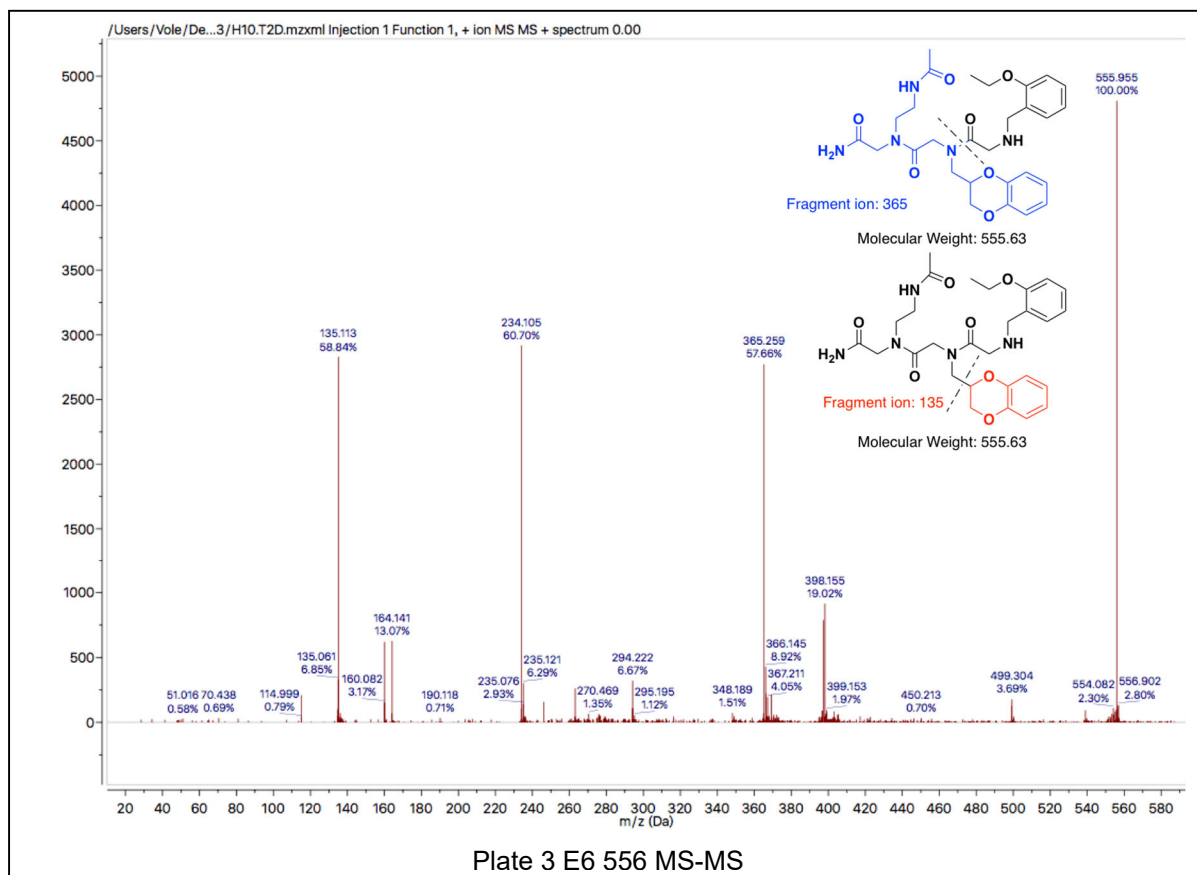


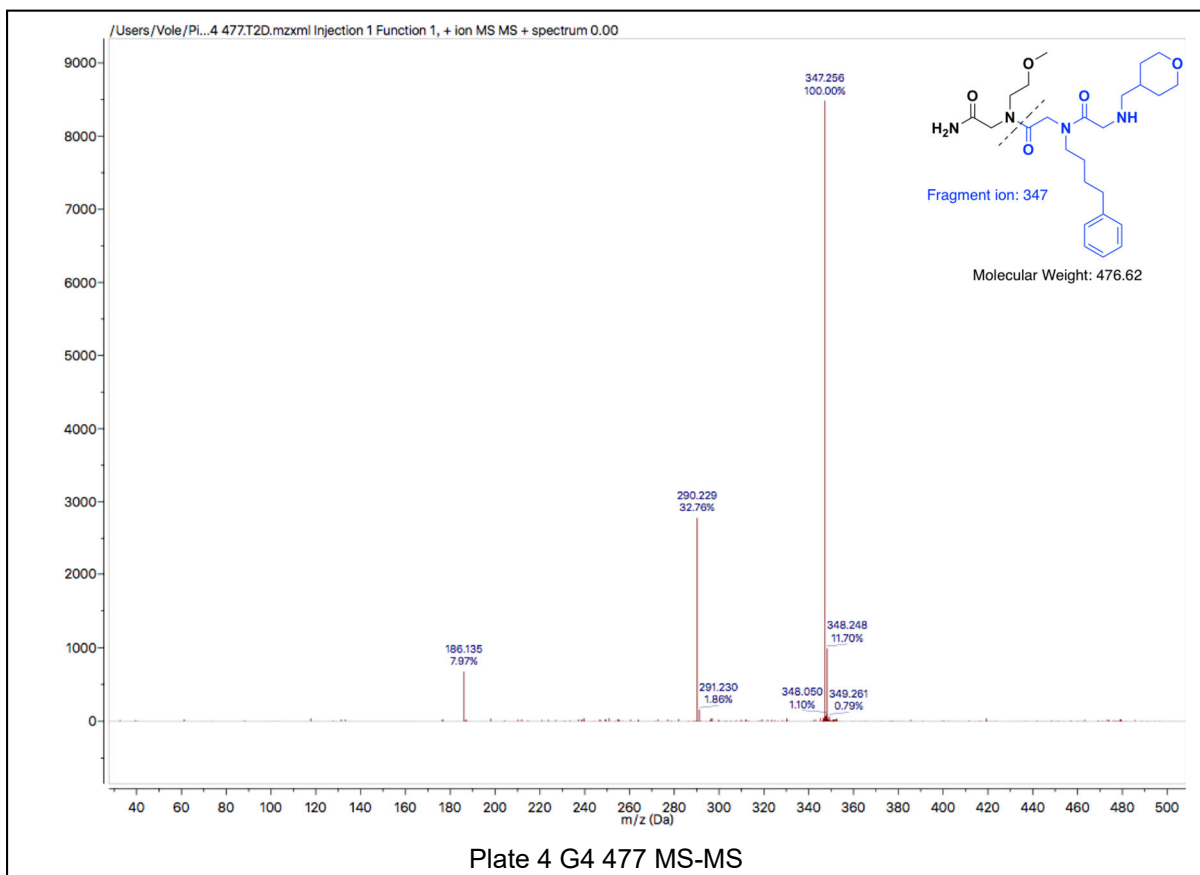


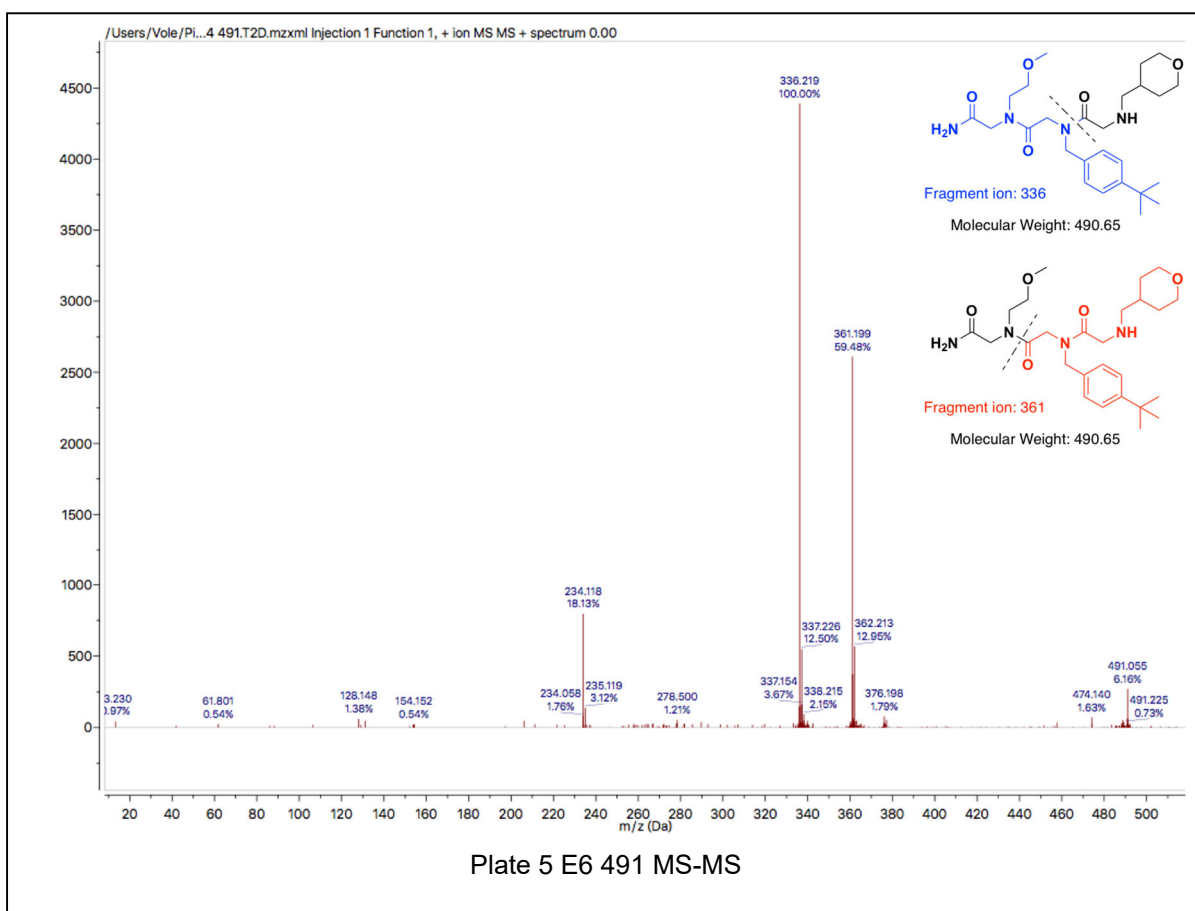


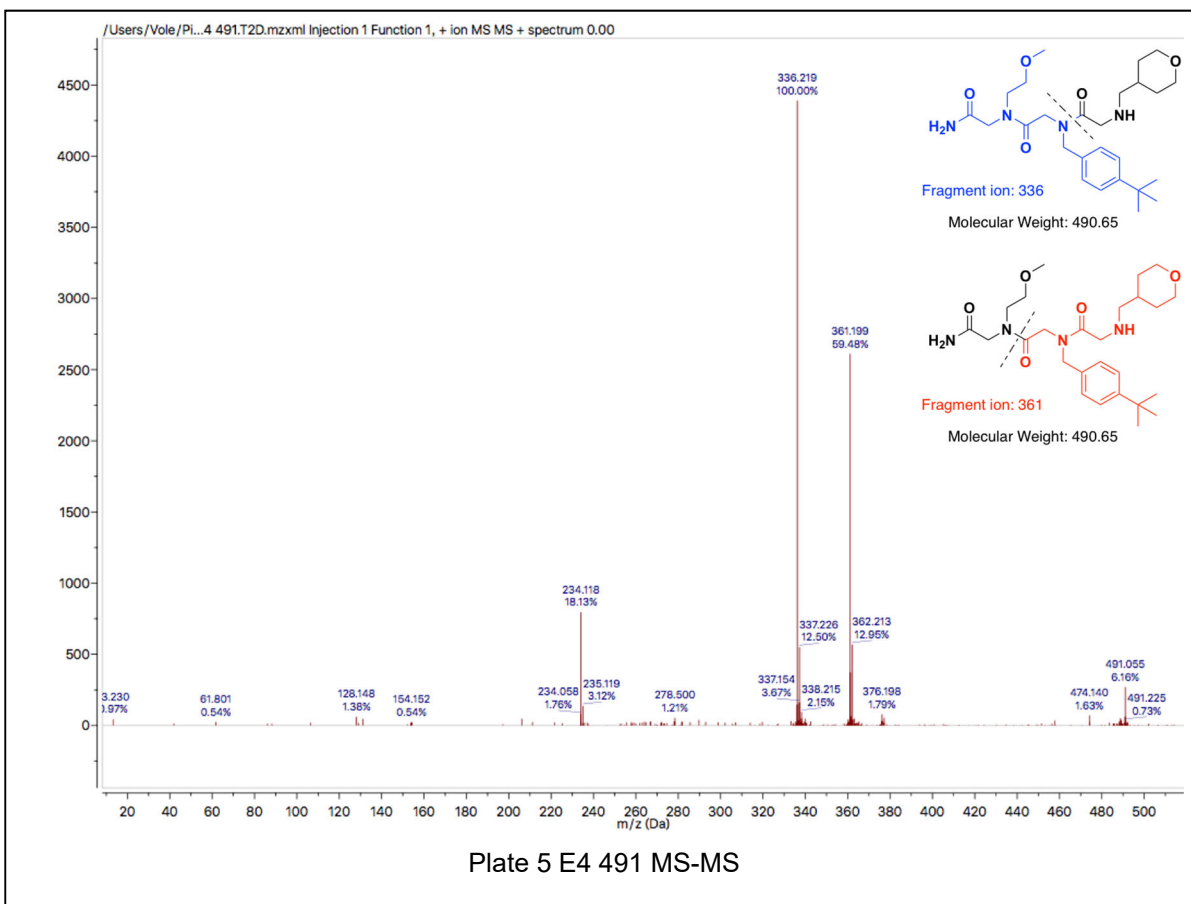


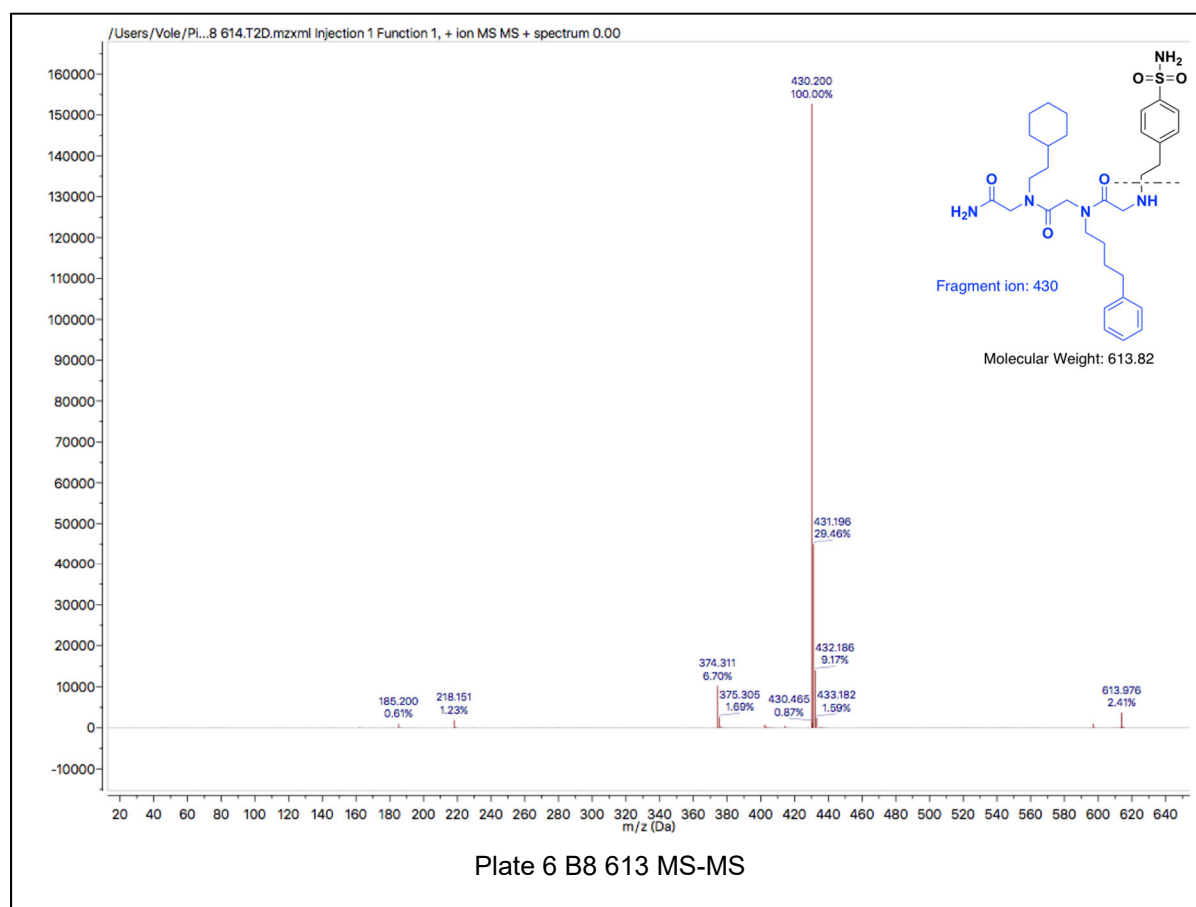


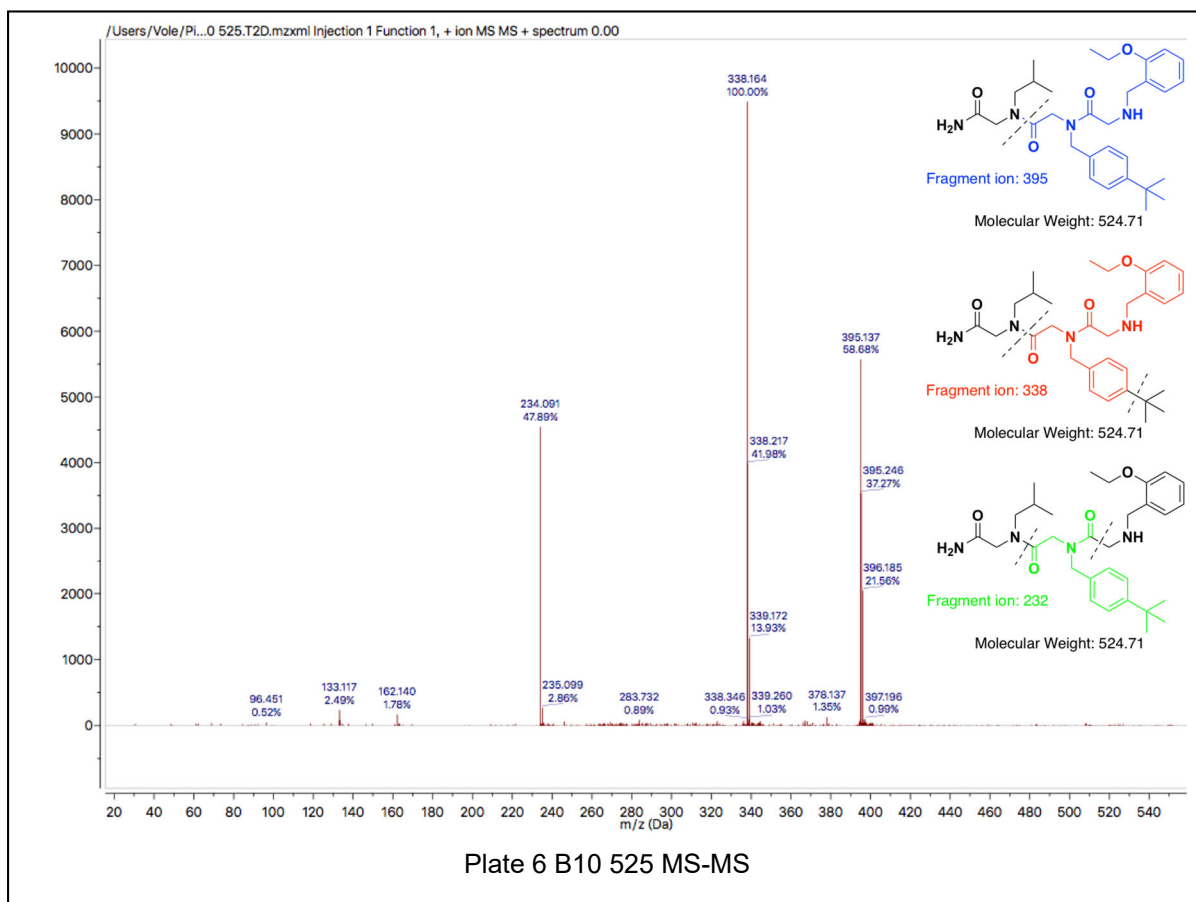


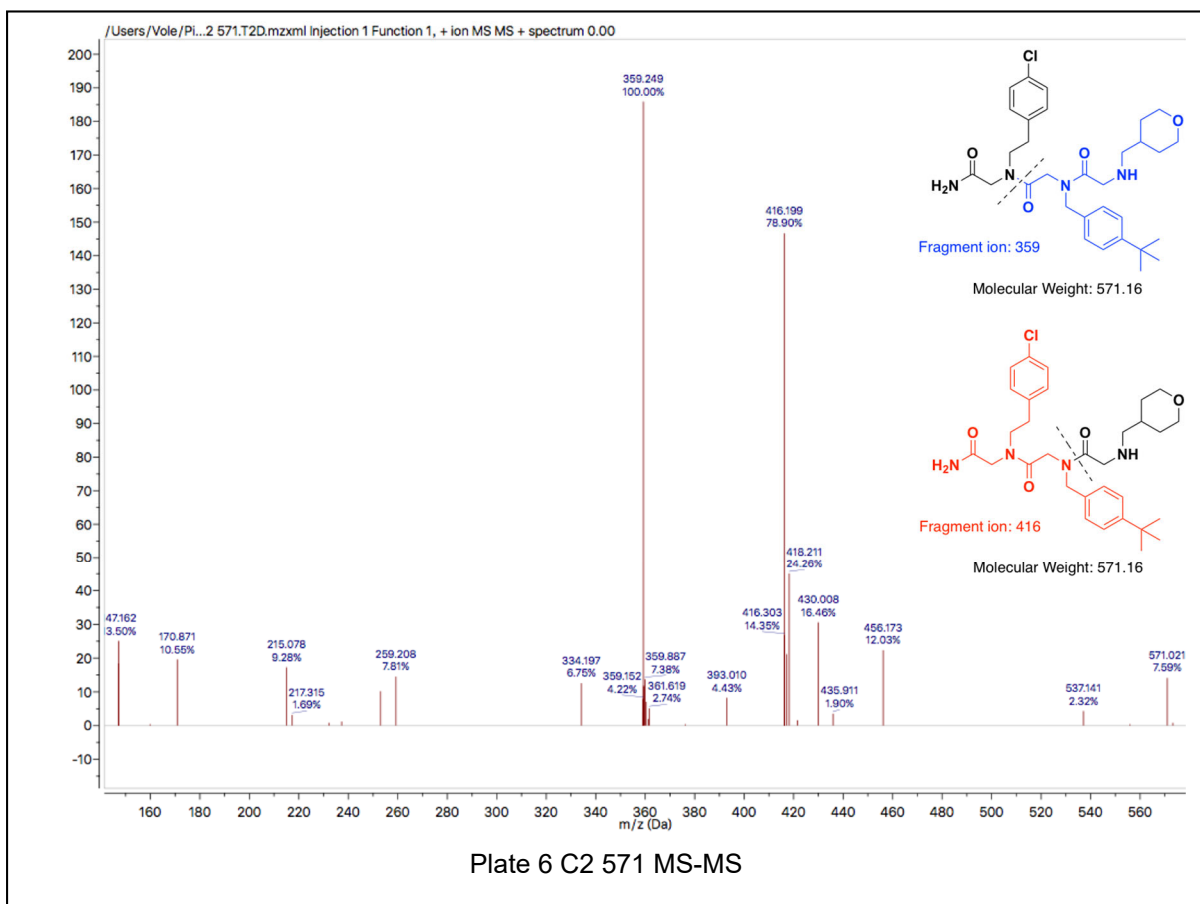


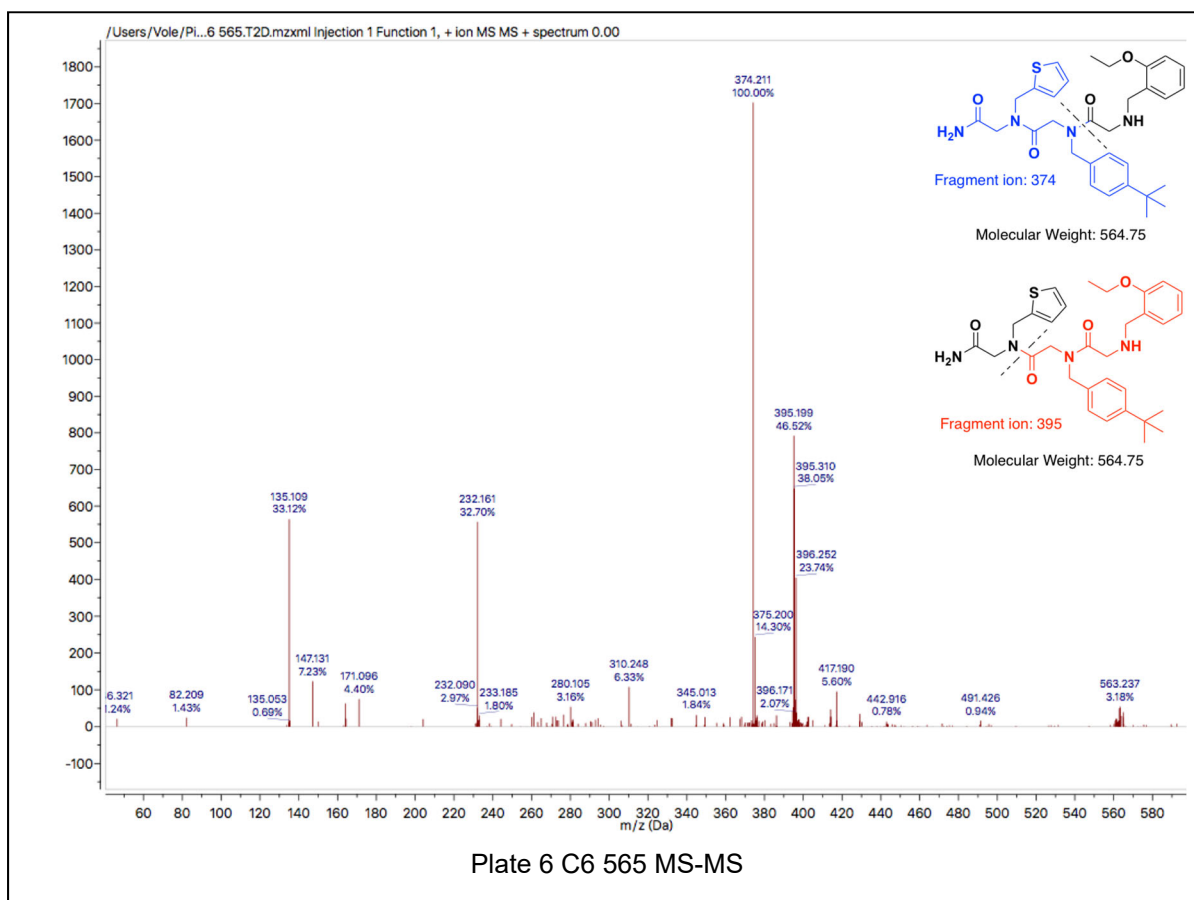


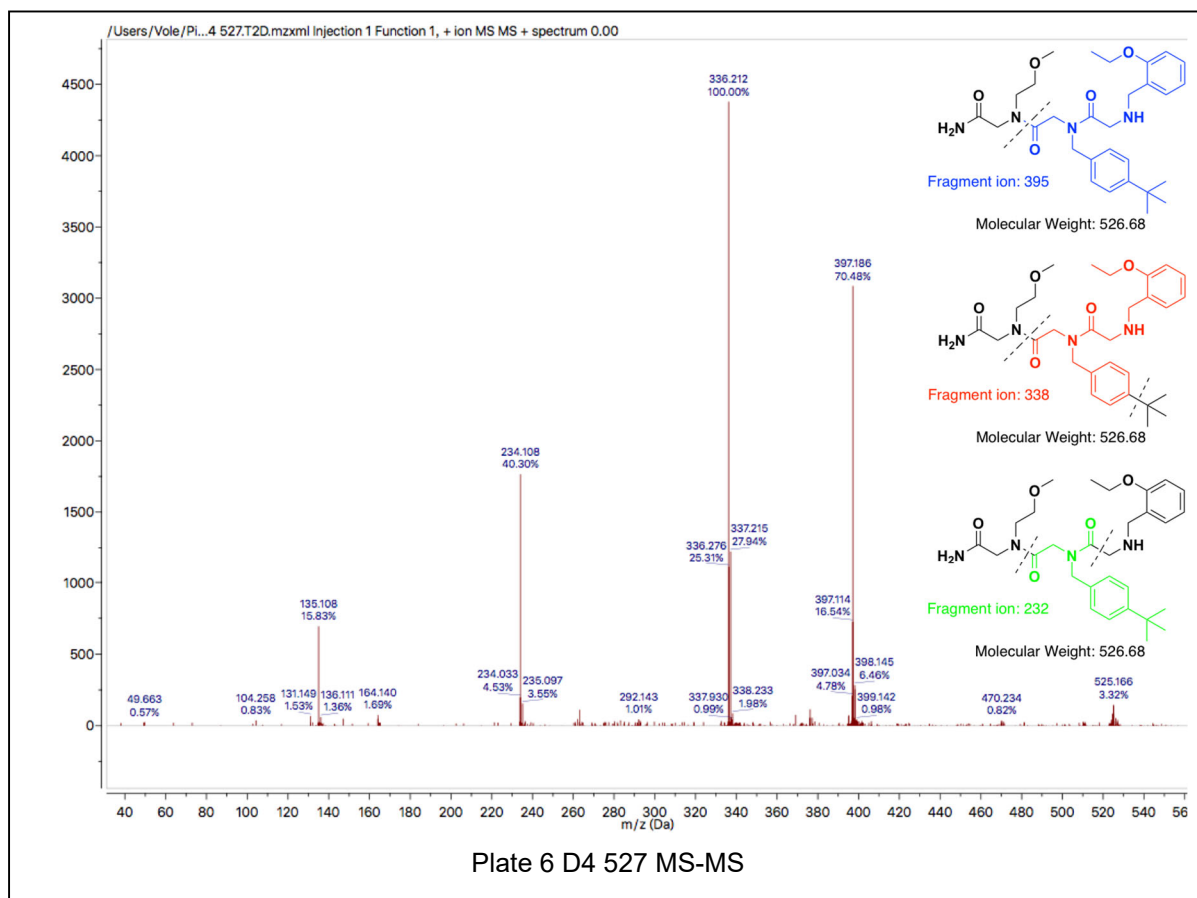


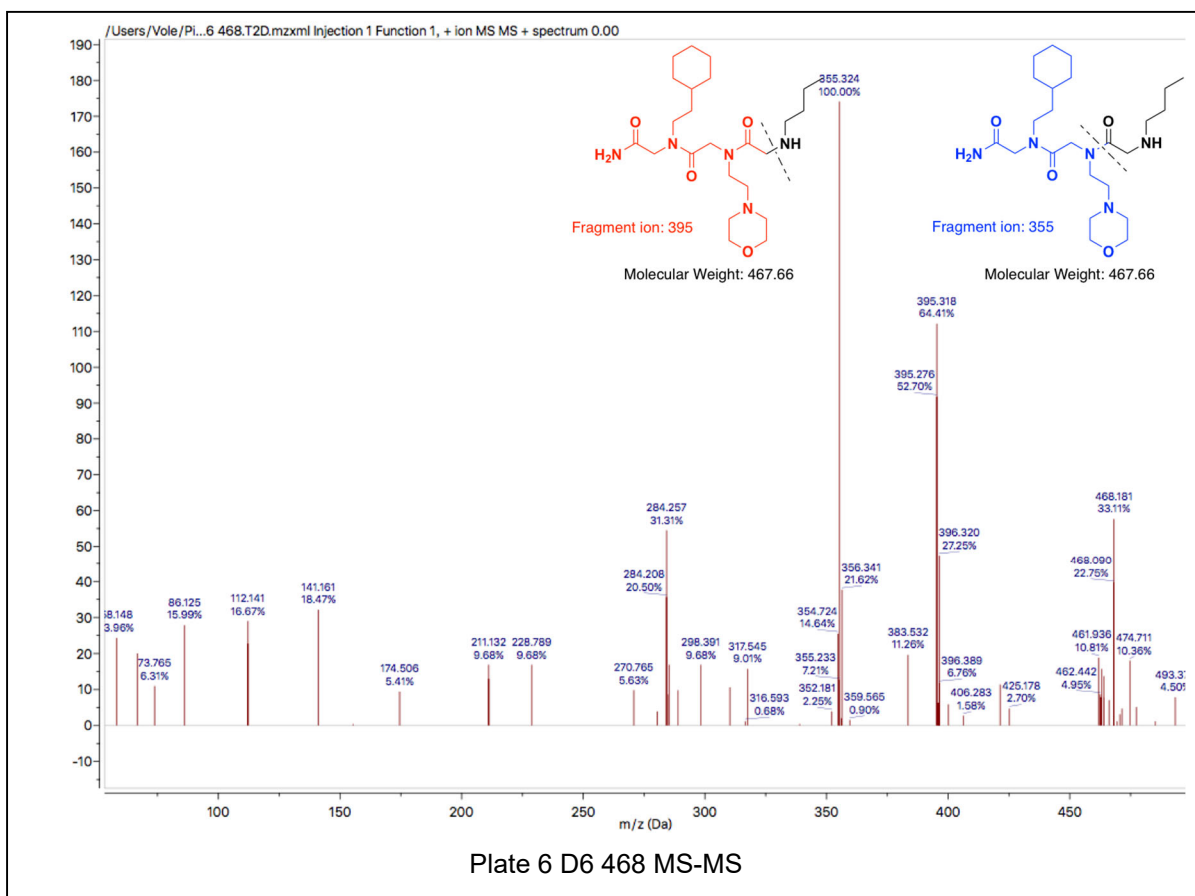


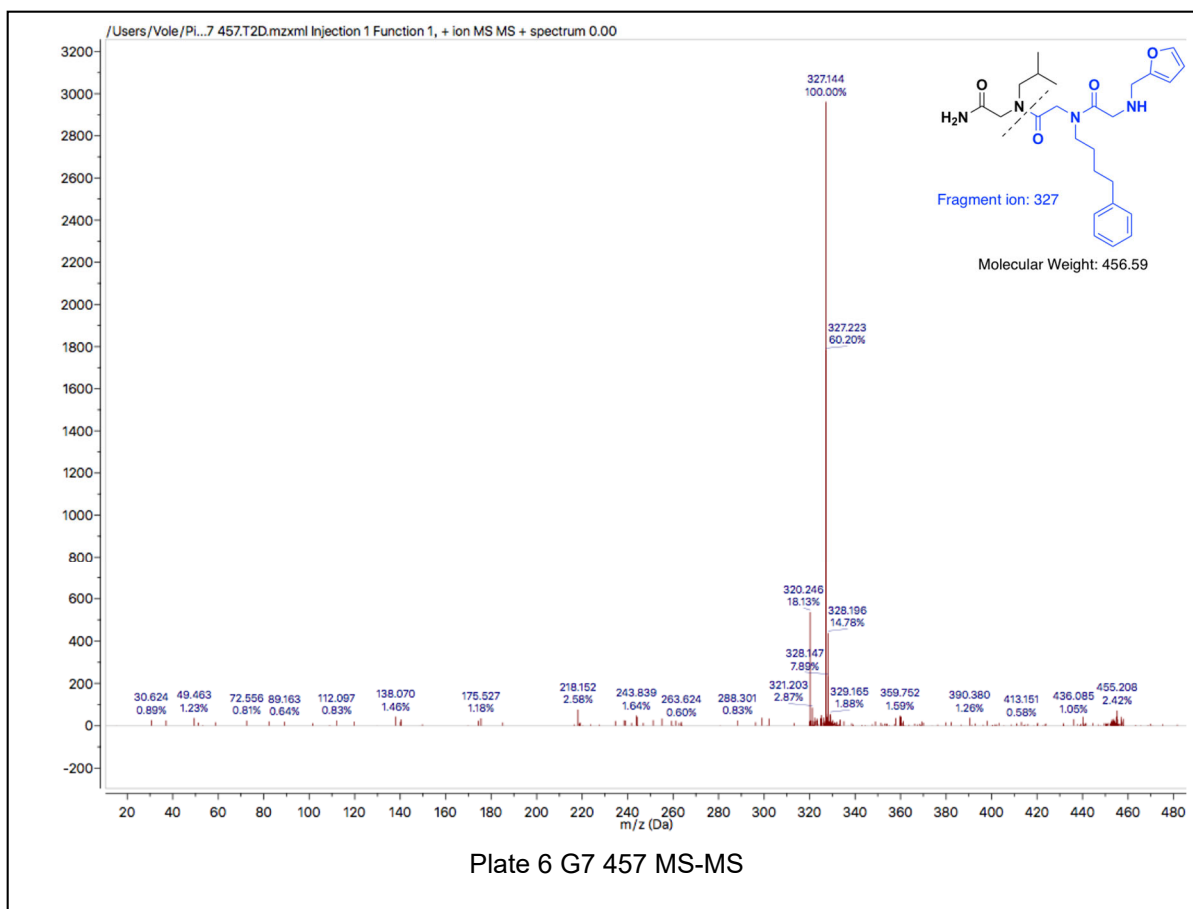


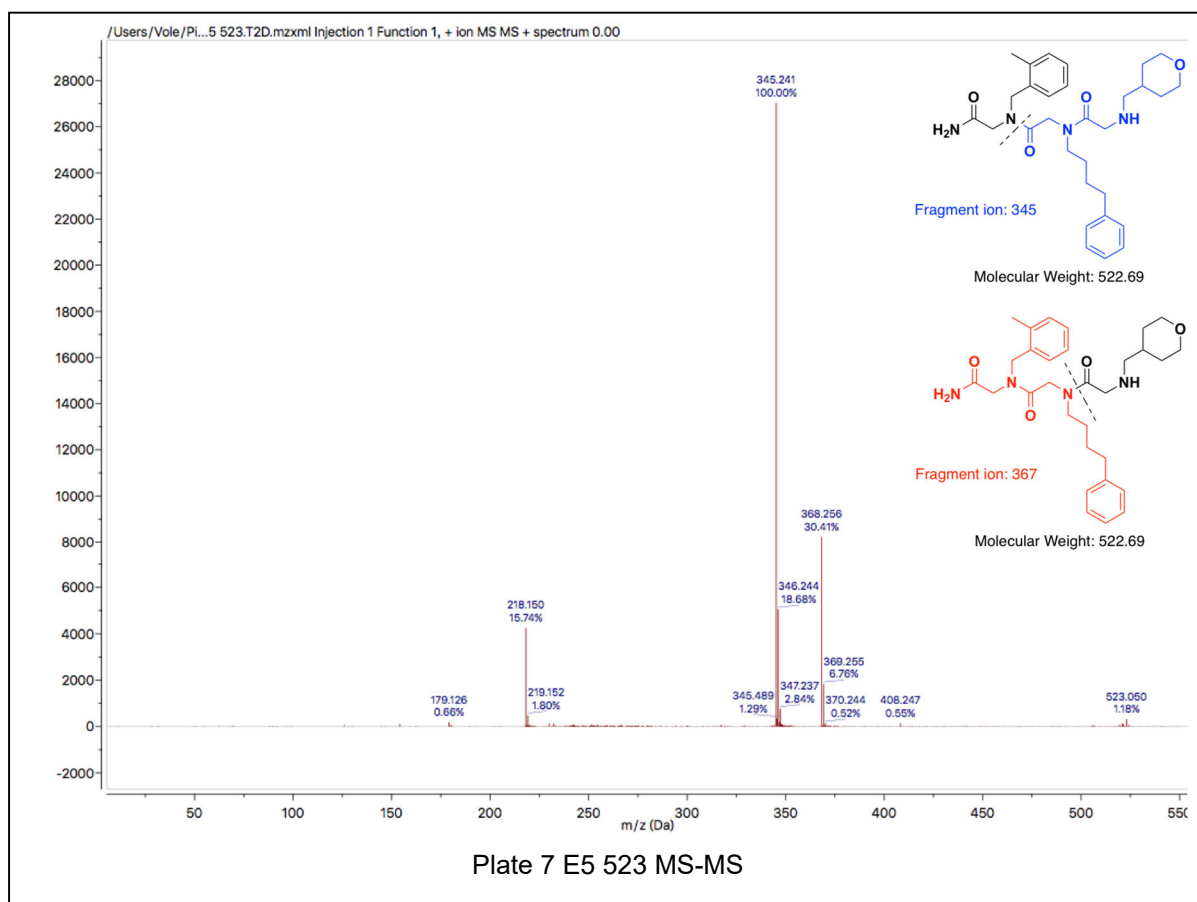


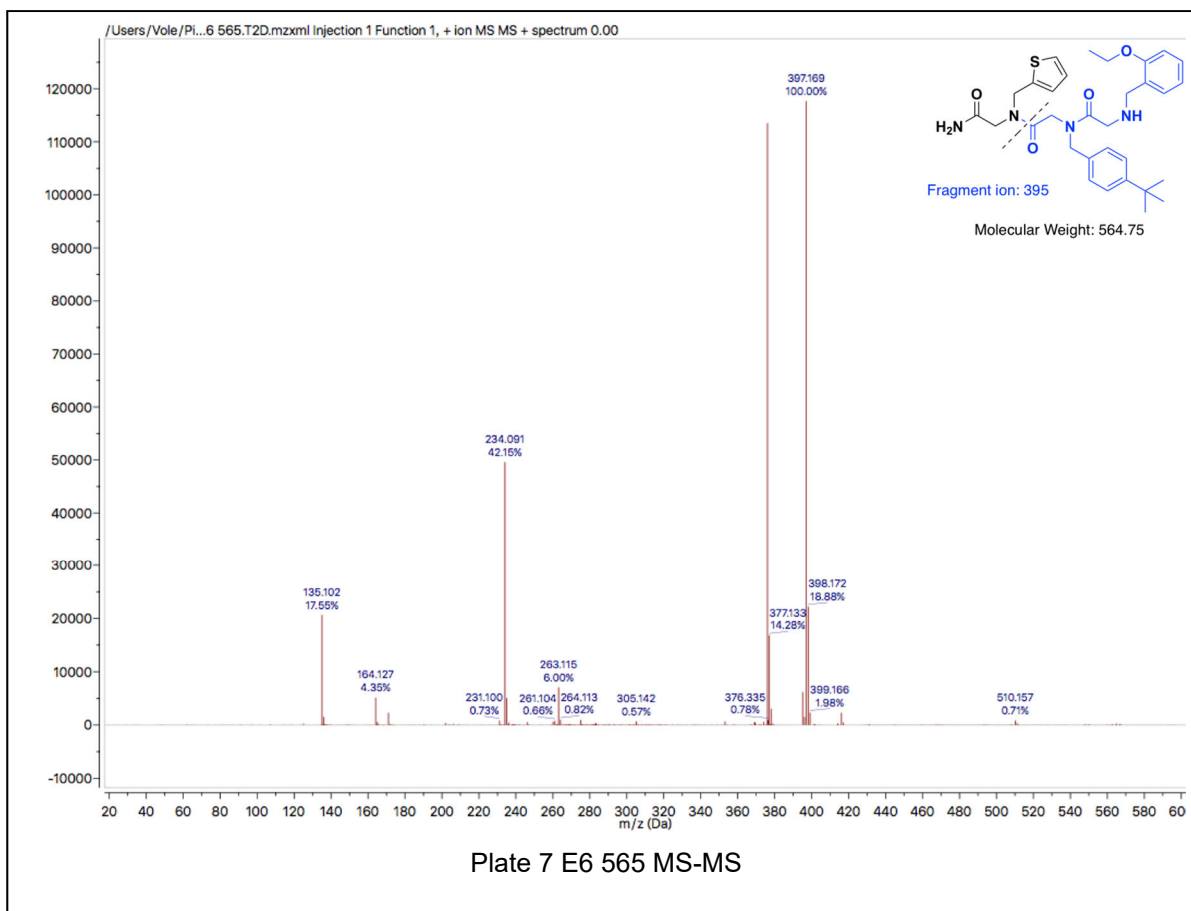


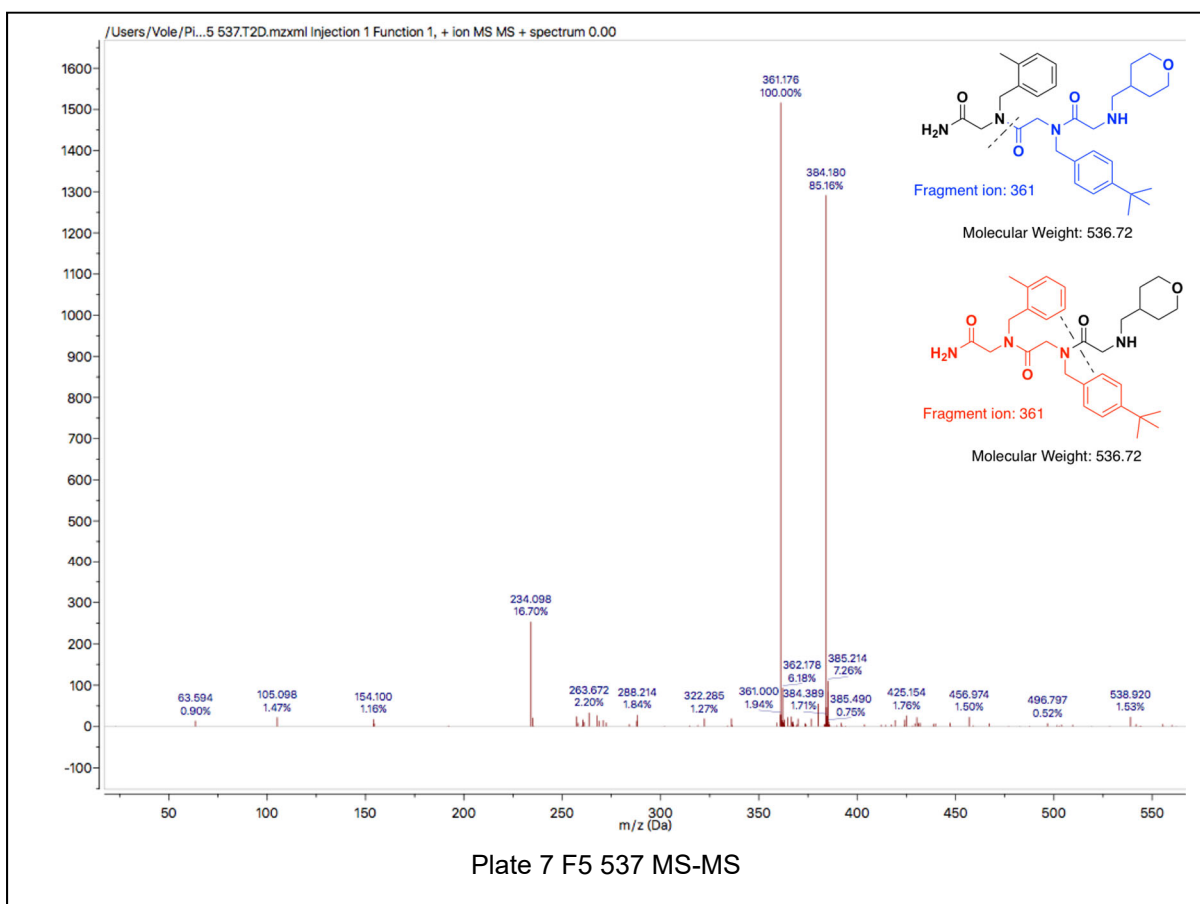


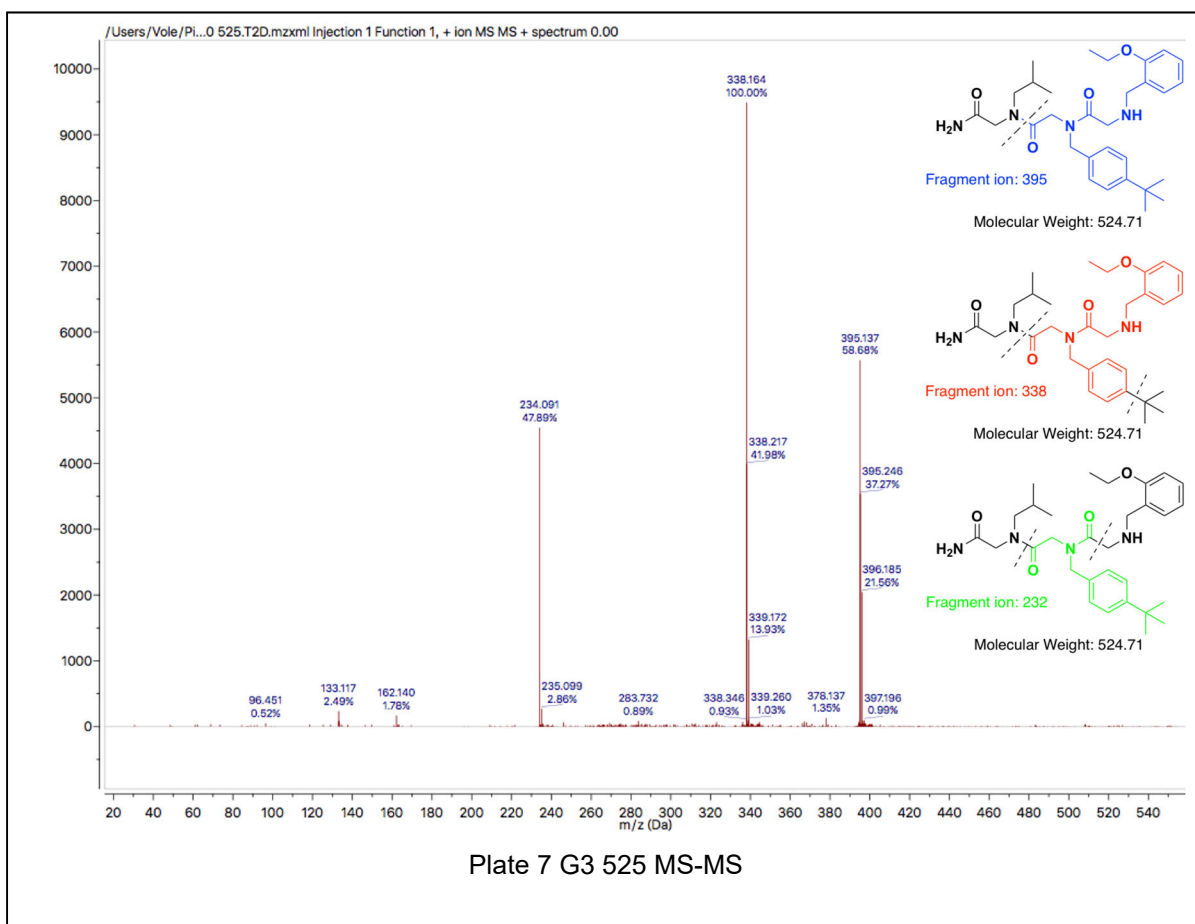


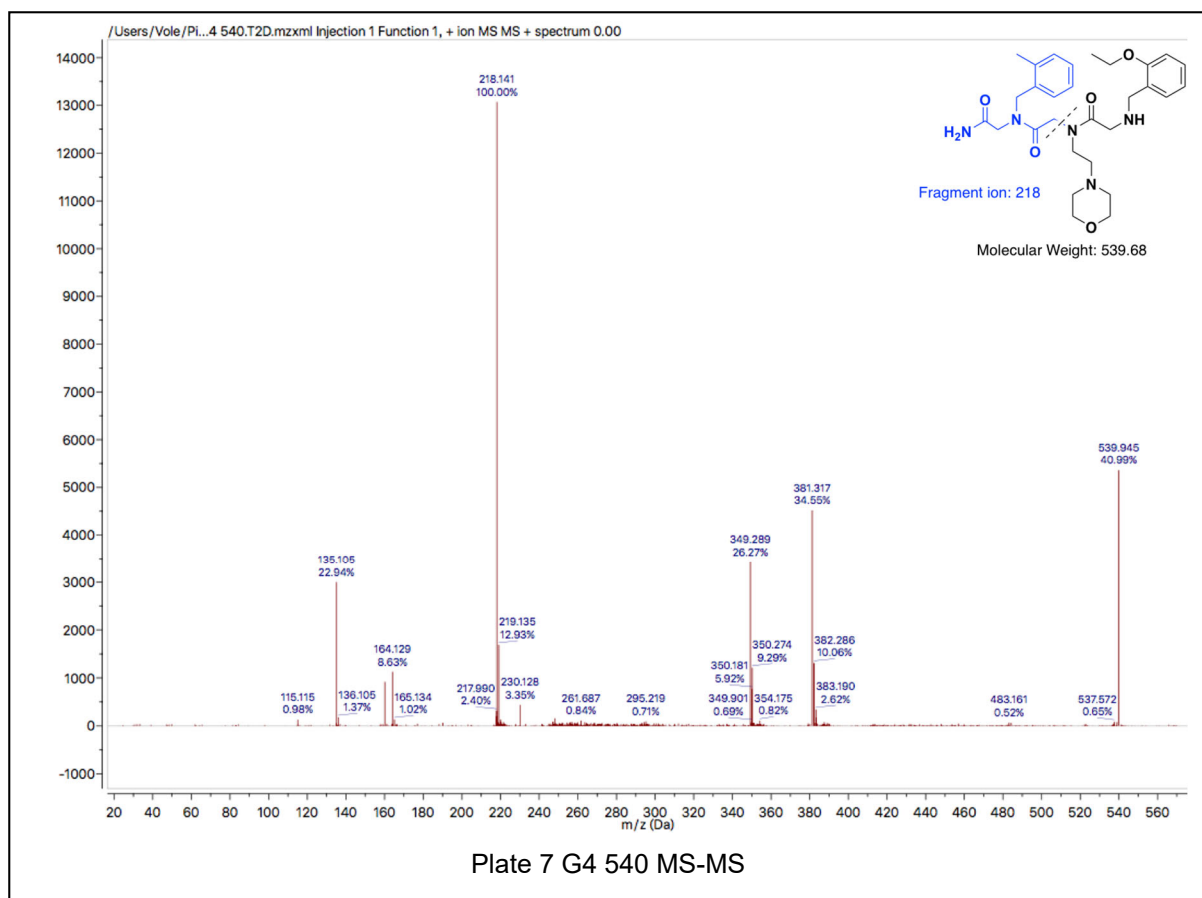












## APPENDIX B. COPYRIGHT PERMISSION

### Reusing Wiley content

If you're reusing Wiley content in your thesis or dissertation, rights will be granted at no cost to you if the content meets these requirements:

- **Your thesis or dissertation is not being used for commercial purposes.** This means that you're submitting it only for graduation requirements. You don't currently have a deal with a commercial publisher, and you won't otherwise be benefitting financially from the publication of your thesis.
- **Wiley is the rights holder of the content you are seeking to reuse.** Usually, Wiley holds the rights to our content, but occasionally the rights holder will be an author or sponsoring organization. In those cases, Wiley cannot guarantee free reuse.

While Wiley does grant free reuse of content in thesis and dissertation projects, we do still require a record of use so that we can issue you a license agreement.

If you publish your thesis or dissertation through a commercial publisher in the future, you will need to reapply for commercial reuse licenses. The legal rights granted for content reuse in non-commercial publications, such as a thesis or dissertation, are different from the rights required by commercial publishers to legally republish third-party content.

## American Chemical Society's Policy on Theses and Dissertations

If your university requires you to obtain permission, you must use the RightsLink permission system.  
See RightsLink instructions at <http://pubs.acs.org/page/copyright/permissions.html>.

This is regarding request for permission to include **your** paper(s) or portions of text from **your** paper(s) in your thesis. Permission is now automatically granted; please pay special attention to the **implications** paragraph below. The Copyright Subcommittee of the Joint Board/Council Committees on Publications approved the following:

### Copyright permission for published and submitted material from theses and dissertations

ACS extends blanket permission to students to include in their theses and dissertations their own articles, or portions thereof, that have been published in ACS journals or submitted to ACS journals for publication, provided that the ACS copyright credit line is noted on the appropriate page(s).

### Publishing implications of electronic publication of theses and dissertation material

Students and their mentors should be aware that posting of theses and dissertation material on the Web prior to submission of material from that thesis or dissertation to an ACS journal may affect publication in that journal. Whether Web posting is considered prior publication may be evaluated on a case-by-case basis by the journal's editor. If an ACS journal editor considers Web posting to be "prior publication", the paper will not be accepted for publication in that journal. If you intend to submit your unpublished paper to ACS for publication, check with the appropriate editor prior to posting your manuscript electronically.

**Reuse/Republishing of the Entire Work in Theses or Collections:** Authors may reuse all or part of the Submitted, Accepted or Published Work in a thesis or dissertation that the author writes and is required to submit to satisfy the criteria of degree-granting institutions. Such reuse is permitted subject to the ACS' "Ethical Guidelines to Publication of Chemical Research" (<http://pubs.acs.org/page/policy/ethics/index.html>); the author should secure written confirmation (via letter or email) from the respective ACS journal editor(s) to avoid potential conflicts with journal prior publication\*/embargo policies. Appropriate citation of the Published Work must be made. If the thesis or dissertation to be published is in electronic format, a direct link to the Published Work must also be included using the ACS Articles on Request author-directed link – see <http://pubs.acs.org/page/policy/articlesonrequest/index.html>

\* Prior publication policies of ACS journals are posted on the ACS website at  
<http://pubs.acs.org/page/policy/prior/index.html>

If your paper has not yet been published by ACS, please print the following credit line on the first page of your article: "Reproduced (or 'Reproduced in part') with permission from [JOURNAL NAME], in press (or 'submitted for publication'). Unpublished work copyright [CURRENT YEAR] American Chemical Society." Include appropriate information.

If your paper has already been published by ACS and you want to include the text or portions of the text in your thesis/dissertation, please print the ACS copyright credit line on the first page of your article: "Reproduced (or 'Reproduced in part') with permission from [FULL REFERENCE CITATION.] Copyright [YEAR] American Chemical Society." Include appropriate information.

**Submission to a Dissertation Distributor:** If you plan to submit your thesis to UMI or to another dissertation distributor, you should not include the unpublished ACS paper in your thesis if the thesis will be disseminated electronically, until ACS has published your paper. After publication of the paper by ACS, you may release the entire thesis (**not the individual ACS article by itself**) for electronic dissemination through the distributor; ACS's copyright credit line should be printed on the first page of the ACS paper.

10/10/03, 01/15/04, 06/07/06, 04/07/10, 08/24/10, 02/28/11

## VITA

Wenzhi Tian is the son of Li Liu and Qinghua Tian. He was raised in Chengdu, Sichuan, China and received his Bachelor of Science in Chemistry in May of 2016 from Sichuan University, China. During his time in Sichuan University, he completed an independent research study with his thesis titled, “The total synthesis of D/L-isocitric acid” under the supervision of Dr. Jason J. Chruma. He then enrolled in Purdue University Medicinal Chemistry and Molecular Pharmacology Program in the August of 2016. He joined Dr. Darci J. Trader’s lab in January of 2017 and conducted research on proteasomal subunit Rpn-6. Wenzhi received several awards during his graduate study including the Jenkins/Knevel Award for Excellence Research and a travel award from Purdue Center of Cancer Research.

## PUBLICATIONS

1. Tian, W.; Muli, C. S.; Trader, D. J. Development of selective probe for proteasome caspase-like, trypsin-like subunits and discovery of a potential small molecule proteasome activity stimulator. *In Press*.
2. Tian, W.; Maresh, M.; Trader, D. J. Approaches to Evaluate the Impact of a Small Molecule Binder to a Non-catalytic Site of the Proteasome. *ChemBioChem* **2021**, 22, 1961-1965. <https://doi.org/10.1002/cbic.202100023>
3. Tian, W.; Trader, D. J. Discovery of a Small Molecule Probe of Rpn-6, an Essential Subunit of the 26S Proteasome. *ACS Chemical Biology* **2020**, 15 (2), 554–561. <https://doi.org/10.1021/acscchembio.9b01019>
4. Muli, C. S.; Tian, W.; Trader, D. J. Small-Molecule Inhibitors of the Proteasome's Regulatory Particle. *ChemBioChem* **2019**, cbic.201900017. <https://doi.org/10.1002/cbic.201900017>.